Technical Report CHL-97-24
September 1997

US Army Corps of Engineers
Waterways Experiment Station

1990 DELILAH Nearshore Experiment: Summary Report

by William A. Birkemeier, Cinde Donoghue, Charles E. Long, Kent K. Hathaway, Clifford F. Baron

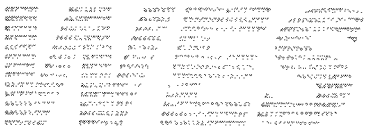

Prepared for Headquarters, U.S. Army Corps of Engineers
and Office of Naval Research

Technical Report CHL-97-24
September 1997

1990 DELILAH Nearshore Experiment: Summary Report

by William A. Birkemeier, Cinde Donoghue, Charles E. Long,
Kent K. Hathaway, Clifford F. Baron

U.S. Army Corps of Engineers
Waterways Experiment Station
3909 Halls Ferry Road
Vicksburg, MS 39180-6199

Final report

Approved for public release; distribution is unlimited

Prepared for U.S. Army Corps of Engineers
Washington, DC 20314-1000
and Office of Naval Research
800 N. Quincy Street, Arlington, VA 22217

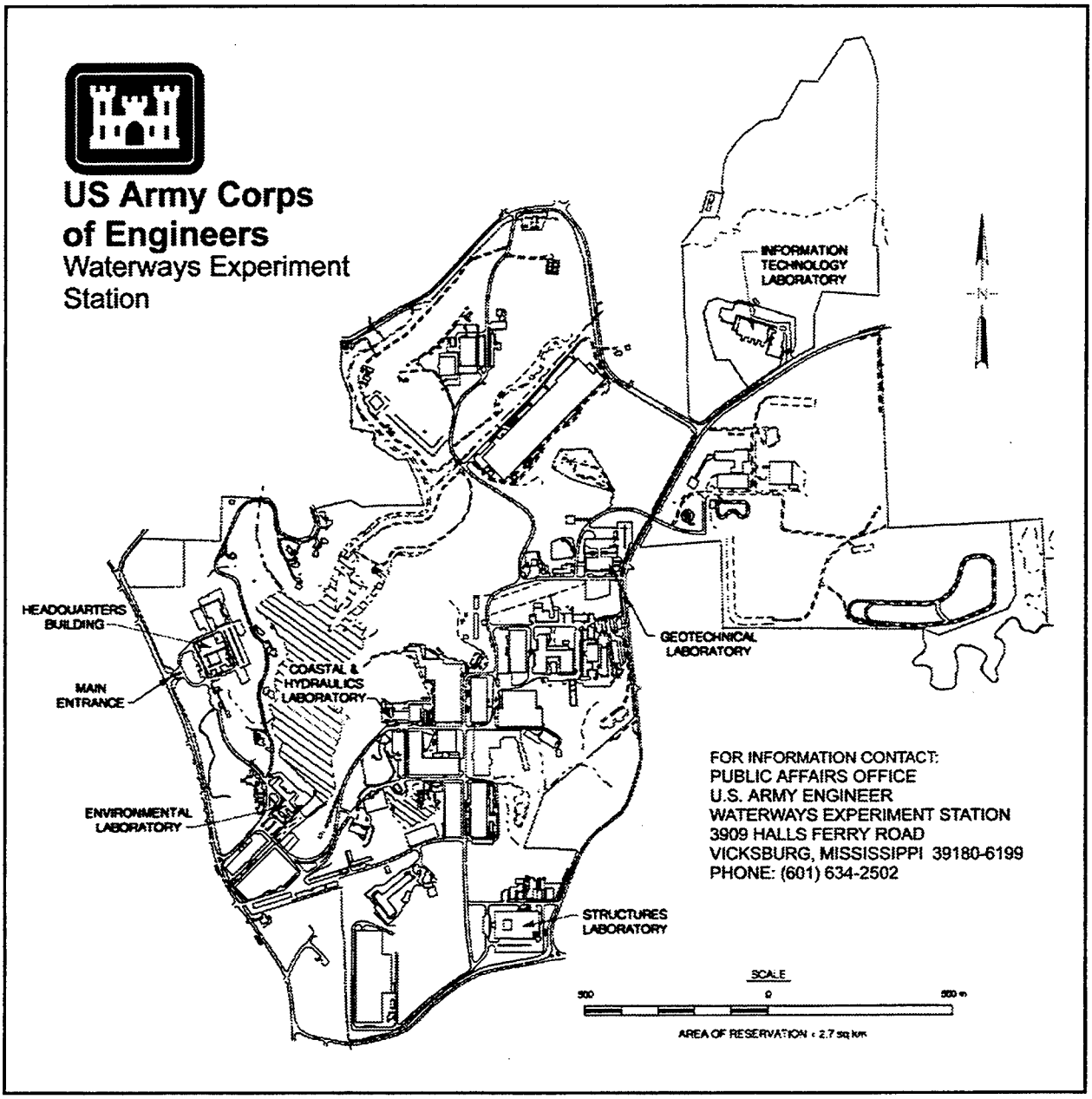

Waterways Experiment Station Cataloging-in-Publication Data

1990 DELILAH Nearshore Experiment : summary report / by William A. Birkemeier ... [et al.] ; prepared for U.S. Army Corps of Engineers and Office of Naval Research.
213 p. : ill. ; 28 cm. — (Technical report ; CHL-97-24)
Includes bibliographic references.
1. Ocean currents — Research. 2. Ocean waves — Research. 3. Coastal zone management. I. Birkemeier, William A. (William Allen), 1951- II. United States. Army. Corps of Engineers. III. U.S. Army Engineer Waterways Experiment Station. IV. Coastal and Hydraulics Laboratory (U.S. Army Engineer Waterways Experiment Station) V. United States. Office of Naval Research. VI. Series: Technical report (U.S. Army Engineer Waterways Experiment Station) ; CHL-97-24.
TA7 W34 no.CHL-97-24

Contents

Preface

This report summarizes the primary data sets collected during the DELILAH nearshore experiment held in October 1990 at the Field Research Facility (FRF), Coastal and Hydraulics Laboratory (CHL), U.S. Army Engineer Waterways Experiment Station (WES). DELILAH investigated the physics of the nearshore zone using a large array of stationary and mobile instruments, video cameras, radar systems, and precision surveys. This report was prepared to document and publicize the DELILAH data set following a waiting period agreed to by the scientists and sponsors. This report complements a growing series of technical papers, reports, theses, dissertations, and other results based on DELILAH data. These data are available electronically on-line or via other media such as CD-ROM.

The data presented here would not have existed without the combined efforts of the principal investigators, their students, technicians, and assistants. The staff of the FRF (Messrs. Eugene Bichner, William Grogg, Kent Hathaway, Clifford Baron, Charles Long, Herman C. Miller, Michael Leffler, Brian Scarborough, and Mrs. Dawn Miller) deserve special recognition. As hosts, they provided their time, commitment, and considerable field experience to ensure DELILAH's success. Dr. Jane Smith contributed to Appendix F, "Instrumented Sled." Mr. Kevin Kremkau helped to edit and prepare the final copy of the manuscript. Dr. Edward Thornton of the Naval Postgraduate School provided a technical review of the final version of this report.

DELILAH was sponsored by the U.S. Army Corps of Engineers (USACE), the Office of Naval Research and by the Naval Research Laboratory. This report was prepared under the Field Research Facility Analysis work unit USACE Civil Works Coastal Engineering Research and Development Program. Technical monitors were Messrs. John H. Lockhart, Jr., Charles Chesnutt, and Barry W. Holliday. CHL Program Manager was Mrs. Carolyn Holmes. Additional support was provided by the Coastal Dynamics program of the Office of Naval Research, Dr. Thomas Kinder; Program Manager.

The report was prepared under the direct supervision of Mr. Thomas W. Richardson, Chief, Engineering Development Division, CHL. General supervision was provided by Dr. James R. Houston and Mr. Charles C.Calhoun, Jr., Director and Assistant Director, CHL, respectively. Director of WES was Dr. Robert W. Whalin. Commander was COL(P) Bruce K. Howard, EN.

1 Introduction

During the fall of 1990, DELILAH, The *Duck Experiment on Low-frequency and Incident-band Longshore and Across-shore Hydrodynamics*, was conducted at the U.S. Army Engineer Waterways Experiment Station, Coastal and Hydraulics Laboratory's, Field Research Facility (FRF) located in Duck, North Carolina (Figure 1). This experiment was conceived as an outgrowth of SAMSON, *The Sources of Ambient MicroSeismic Oceanic Noise* experiment which also occurred that fall. DELILAH was developed to take advantage of the directional wave information being obtained from the instruments installed and data gathered during SAMSON. These experiments deployed 87 instruments from the shoreline out to the 13-m depth contour, and collected a vast amount of data useful to many coastal research efforts. This report will first briefly describe SAMSON, but its purpose is to summarize the investigations and data collected only during DELILAH.

SAMSON

This experiment, sponsored by the Office of Naval Research, was an investigation into the causes of ocean bottom microseisms (very small fluctuations which can create significant noise in underwater acoustic transmissions). In order to monitor these microseisms, a number of different arrays of instruments were deployed. To measure the directional wave field and to monitor nonlinear pressure fluctuations at depth, which may excite the microseisms, the Scripps

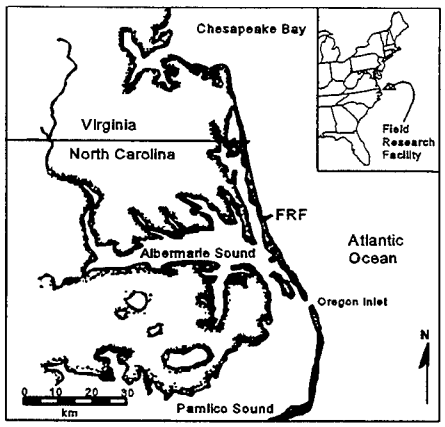

Figure 1. Location of the Field Research Facility

Institution of Oceanography deployed an array of 24 pressure sensors and 1 current meter at a depth of 13 m. This array covered an area 300 m by 300 m and is referred to as the "13-m array" throughout the remainder of the report (Figure 2). This effort was conducted by Dr. Robert Guza and Dr. Thomas Herbers with assistance from Dr. Steven Elgar and Dr. Joan Oltman-Shay. The 13-m array was deployed in August 1990 and operation began in September 1990. Although SAMSON officially ended at the end of November, the 13-m array continued to collect data until June 1991.

The 13-m array was operated in conjunction with the existing FRF directional wave array located directly landward in 8 m of water, and henceforth referred to as the "8-m array." This array, operated by Dr. Charles Long, consisted of a cross of pressure sensors with nine sensors located in a shore-parallel line and six in a cross-shore line (Figure 2).

Three additional arrays were deployed to measure the microseisms. Dr. Tok Yamamoto (University of Miami) deployed an array of five Ocean Bottom Seismometers (OBS) along the same 13-m depth contour as the Scripps' array. These not only recorded the microseisms but could also be used to measure the directional wave field. A large array of land-based seismometers was deployed across the state of North Carolina by Dr. John Nabelek (Oregon State University) and another OBS array was deployed in deeper water across the continental shelf.

Although data collected from the 8-m and 13-m arrays discussed above provided useful directional wave information for DELILAH, there was a separate array deployed closer to shore, referred to from here on as the "DELILAH array." This array and the DELILAH experiment are summarized in the remainder of this report.

DELILAH

The idea for DELILAH originated during the later planning stages of SAMSON. Simultaneous collection of wave and current data from 8-m and 13-m depths led to the suggestion that similar inshore data would provide information necessary to characterize the entire surf zone. Experience with earlier experiments, such as DUCK85[1] and SUPERDUCK,[2]helped to refine the objectives, instrumentation plan, required equipment, and general logistics for

---

[1]Mason, C., Birkemeier, W. A., and Howd, P.A. (1987). "An Overview of DUCK85, a Nearshore Processes Experiment." *Proceedings of the Coastal Sediments '87 Conference*, American Society of Civil Engineers.

[2]Crowson, R. A., Birkemeier, W. A., Klein, H. M., and Miller, H. C. (1988). "SUPERDUCK Nearshore Processes Experiment: Summary of Studies, CERC Field Research Facility," Technical Report CERC-88-12, U.S. Army Engineer Waterways Experiment Station, Vicksburg, MS.

DELILAH. The objectives were:

a. To measure the wave and wind forced three-dimensional nearshore dynamics with specific emphasis on infragravity waves, shear waves, mean circulation, setup, runup, and wave transformation.

b. To monitor the bathymetric response to these processes.

Investigators

The DELILAH investigators, their organizations at the time of the experiment, and general areas of scientific interest are listed below.

U.S. Army Engineer Waterways Experiment Station, Coastal and Hydraulics Laboratory:

William Birkemeier - Morphology.
Kent Hathaway - Runup, infragravity waves, morphology, remote sensing.
Charles Long - Incident and reflected directional wave spectra.
Nicholas Kraus - Longshore currents.
Jane Smith - Vertical current profile, 2-D circulation.
Todd Walton - Runup.
Edward Thompson - Surf beat modeling.

Naval Postgraduate School:

Edward Thornton - Mean circulation, shear waves, rip currents.

Naval Research Lab:

Dennis Trizna - Radar measurements of waves and currents.

Oregon State University:

Rob Holman - Morphology, runup, shear waves, infragravity waves, video remote sensing.
Peter Howd - Infragravity waves, morphology.
Tom Lippman - Morphology, infragravity waves, video remote sensing.
Todd Holland (also with the U.S. Geological Survey) - Runup, cusp formation.

Scripps Institution of Oceanography:

Robert Guza - Cross-shore and longshore currents, infragravity waves, wave transformation (also SAMSON Principal Investigator).

Quest Integrated Inc.:

Joan Oltman-Shay - Shear waves, infragravity waves (also SAMSON Principal Investigator)

Washington State University:

Steve Elgar - Incident and reflected directional wave spectra (also SAMSON Principal Investigator).

Experiment plan

The DELILAH array consisted of four subarrays that were interdependent. The primary cross-shore sub-array contained nine current meters and nine pressure wave gauges situated approximately 500 m north of the pier. Two other sub-arrays were positioned longshore, perpendicular to the cross-shore sub-array. Each consisted of one gauge from the cross-shore array where the longshore arrays intersected it. Five additional current meters placed in the trough region, and four placed slightly seaward of the nearshore bar crest, completed these sub-arrays (Figure 2). A final instrument package was positioned between the two longshore arrays forming a secondary cross-shore sub-array approximately 100 meters south of the primary cross-shore sub-array. All of the instruments in the DELILAH array extended across the typical position of the nearshore bar and were designed to sample in conditions generated by incident waves with significant heights up to 1.5 m. Dr. Edward Thornton of the Naval Postgraduate School provided the design and instruments for the primary cross-shore array and, with help from Rob Wyland, Katie Scott, and others, collected all of the data from the DELILAH array. The instruments in the other subarrays were provided by Scripps Institution of Oceanography and by the FRF.

FRF and Oregon State University video cameras were mounted on the FRF's observation tower to record swash and other surf zone processes. Five radar systems operated by the Naval Research Laboratory monitored the waves, currents, and bathymetry. Daily surveys conducted by the FRF's Coastal Research Amphibious Buggy (CRAB) documented changes to the bathymetry in a small 550-m by 375-m gridded area that surrounded the DELILAH array. This region will be referred to as the "minigrid" throughout the remainder of this report. Analysis of the current and bathymetry data collected during the 1986 SUPERDUCK experiment[1] helped in designing the instrument array.

The 8-m,13-m, and DELILAH arrays are shown in Figure 2. As in previous Duck experiments, the minigrid was located north of the FRF pier, open to storm waves from the northeast, and in an area typically characterized by shore-parallel contours. The southern end of the minigrid was within the shadow zone of the FRF pier for waves approaching from the southeast.

DELILAH commenced in the final weeks of September 1990 when the instruments were mounted on pipes (Figures 3 and 4) and deployed from the CRAB (Figure 5). Current meters were positioned so as to be submerged during low tide and to remain above the highest expected bed level (Figure 6).

---

[1]Birkemeier, W.A., et. Al (1989). "SUPERDUCK Nearshore Processes Experiment Data Summary: CERC Field Research Facility," Miscellaneous Paper CERC-89-16, U.S. Army Engineer Waterways Experiment Station, Vicksburg, MS.

Stationary instrument measurements were supplemented by a vertical stack of five current meters, an anemometer, and two wave gauges located on the instrumented sled (Figures 7 and 8). This sled was towed out by the CRAB and retrieved toward shore, stopping at the same inshore distance as the stationary instruments.

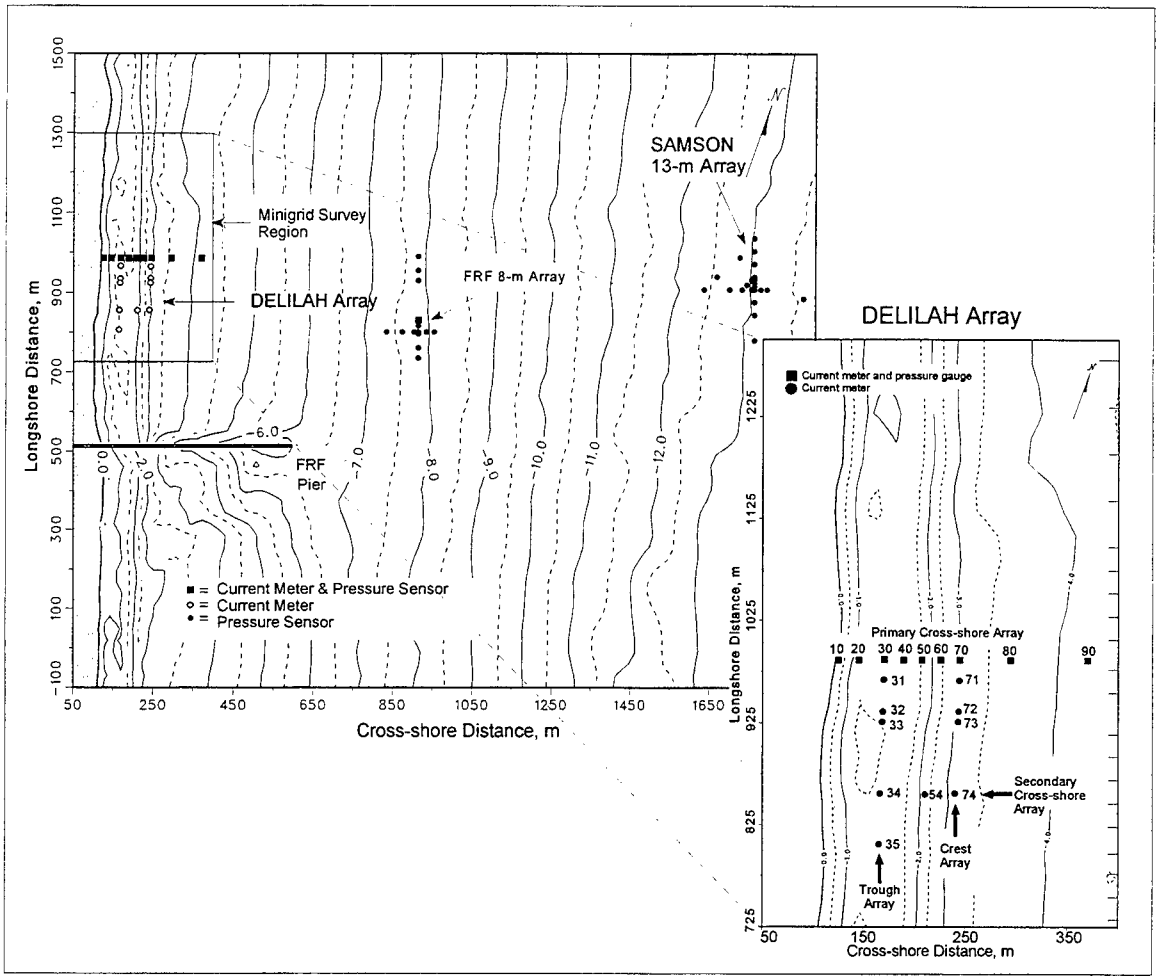

Figure 2. DELILAH and SAMSON instrument locations

Figure 3. Mr. Rob Wyland assembling the instrument pipes in the FRF parking lot

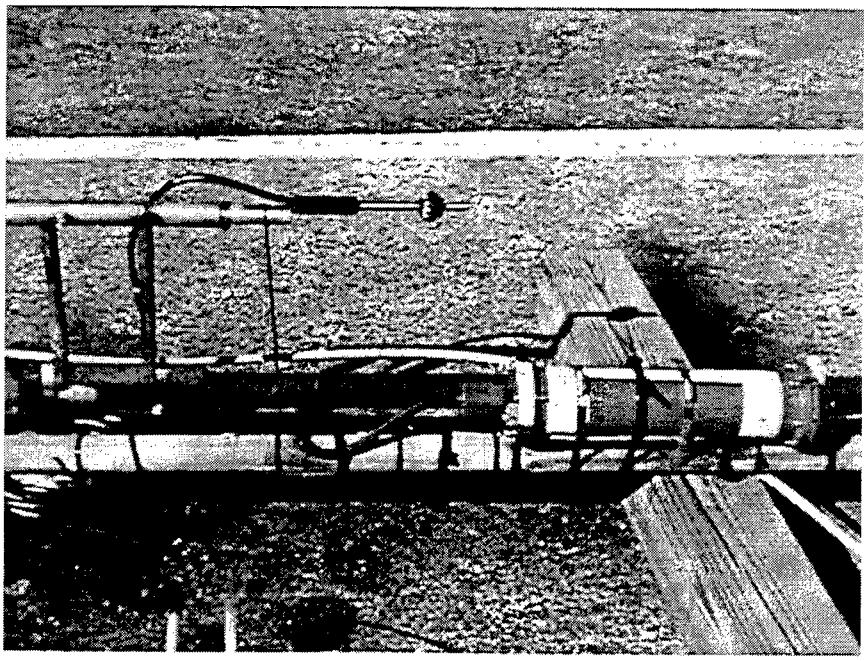

Figure 4. Closeup of assembled electronic package and sensor pipes. The Marsh-McBirney electromagnetic current meter is the small ball at the top center of the photograph

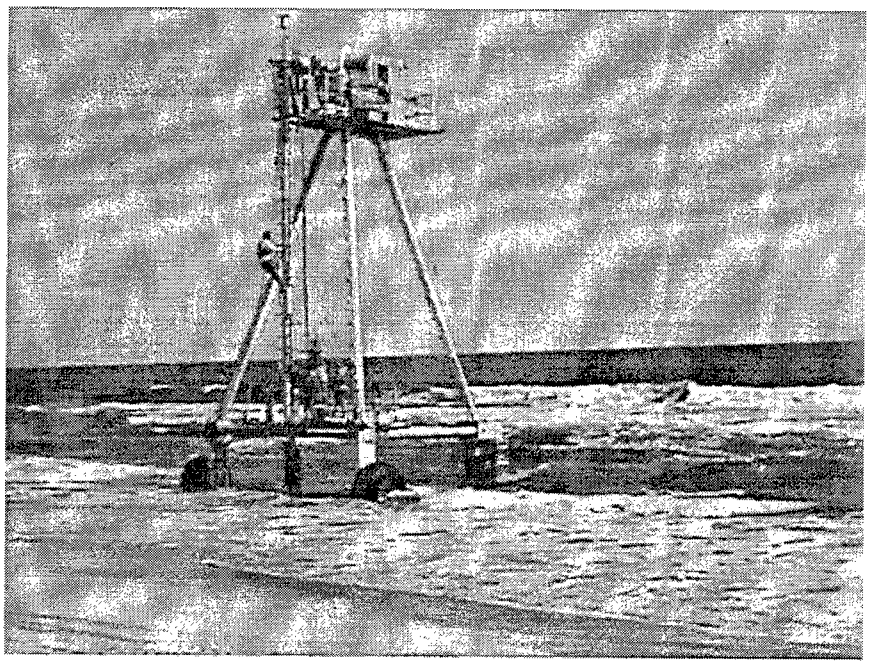

Figure 5. Instrument pipe being deployed from the CRAB

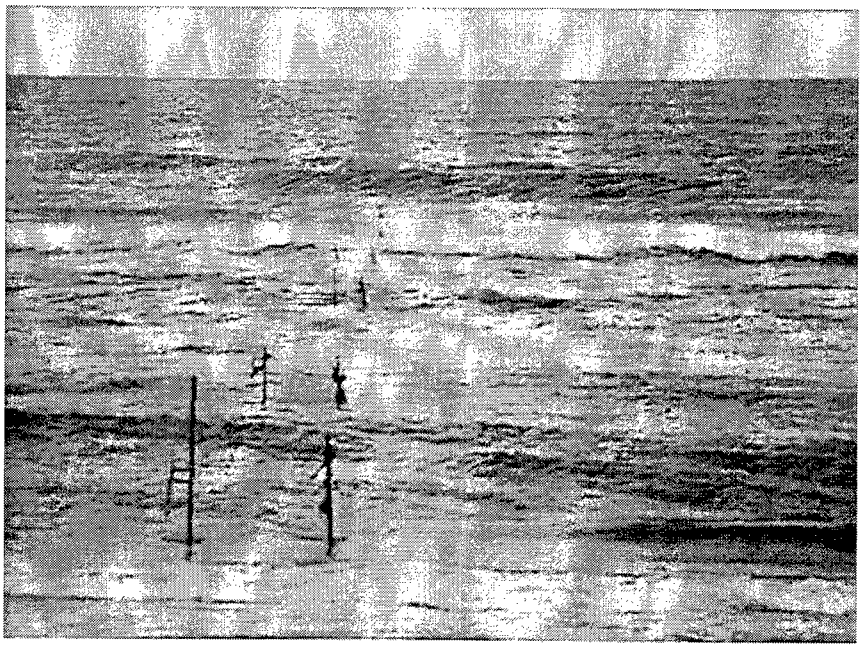

Figure 6. Cross-shore array after deployment. Current meter sensors were mounted on the left pipes, electronics and pressure gauges on the right pipes

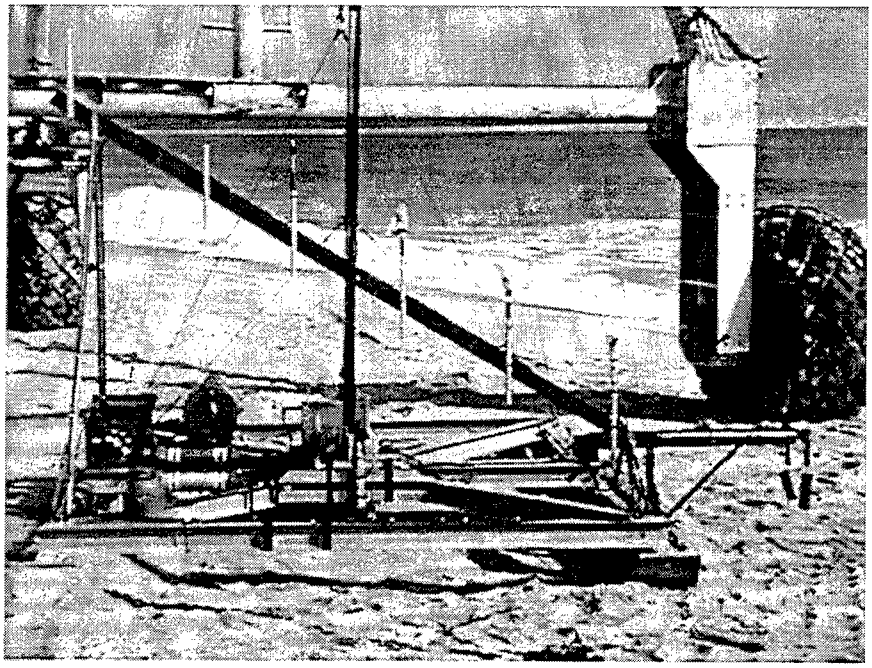

Figure 7. The instrumented sled prior to deployment. In this configuration it has five current meters, two wave gauges, and an anemometer

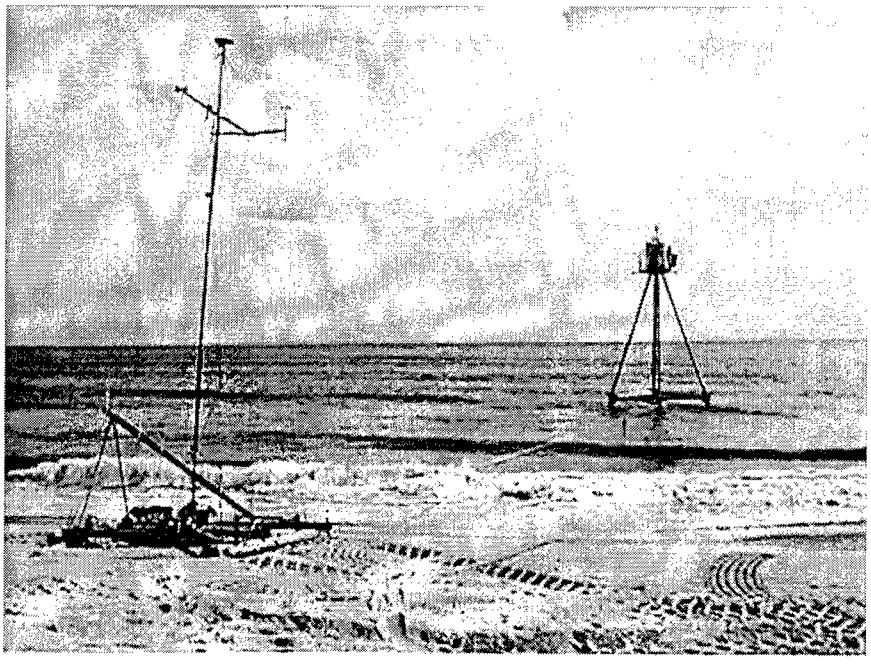

Figure 8. The sled being towed seaward by the CRAB

Experiment Conditions

During the 21 days of data collection, from 1 to 21 October 1990, a variety of conditions were encountered, as shown in Figure 9. This graph shows the wind, as measured at the end of the FRF pier (gauge 3932); the significant wave height, wave period, and wave direction measured in 8 m of water (gauge 3111); the longshore current in the inner bar trough (gauge 2342); and water level from gauge 1, relative to the National Geodetic Vertical Datum. After a short-duration wave event on 1-2 October, there was an extended period of low waves (< 1 m) until 9 October, when a "Southeaster" occurred, causing the wave height to build to nearly 2 m. There was initial concern that Hurricane Lili might interrupt the experiment, but Lili's passage brought only windless, long-period swell approximately 2.5 m in height on 13 October. Energetic waves ($H_{mo} > 1$ m) and longshore currents (> 1 m/s) continued until the end of the experiment.

As in each previous Duck experiment, significant changes occurred in the nearshore profile. Figure 10 illustrates four of the minigrid surveys with the current meter locations indicated by vertical lines. The topography was rhythmic in the longshore dimension through 9 October, when it began to become more linear. The topography was linear on 11 October and remained so until the end of the experiment. High longshore flows occurred frequently during the experiment; an example of one of the more energetic periods is given in Figure 11, which shows longshore currents greater than 1.5 m/sec concentrated along the nearshore trough, inshore of the longshore bar crest. A plot of the cross-shore currents from the sled (Figure 12) shows onshore flow only near the surface in the region of the bar crest and weak offshore flow elsewhere.

Instrument retrieval and cleanup began on 22 October. All pipes and cables were removed, with the last being recovered on 25 October.

The remainder of this report consists of a series of appendices which include details about specific DELILAH data sets. Appendix A contains the survey data; Appendix B tabulates the video and runup data; Appendix C provides summary information about the bottom sediments; Appendix D presents pre- and post-experiment current meter calibrations; Appendix E summarizes the locations of and data from the stationary instruments; Appendix F summarizes the data collected from the instrumented sled; and Appendix G provides addresses for the participants and lists publications which use DELILAH and SAMSON data.

This report summarizes the collected data. The actual data are available via electronic media including online access and CD-ROM. Connect through the World Wide Web to http://frf.usace.army.mil. Since this address may change, contact the US Army Engineer Waterways Experiment Station, Coastal and Hydraulics Laboratory at 3909 Halls Ferry Road, Vicksburg, MS 39180.

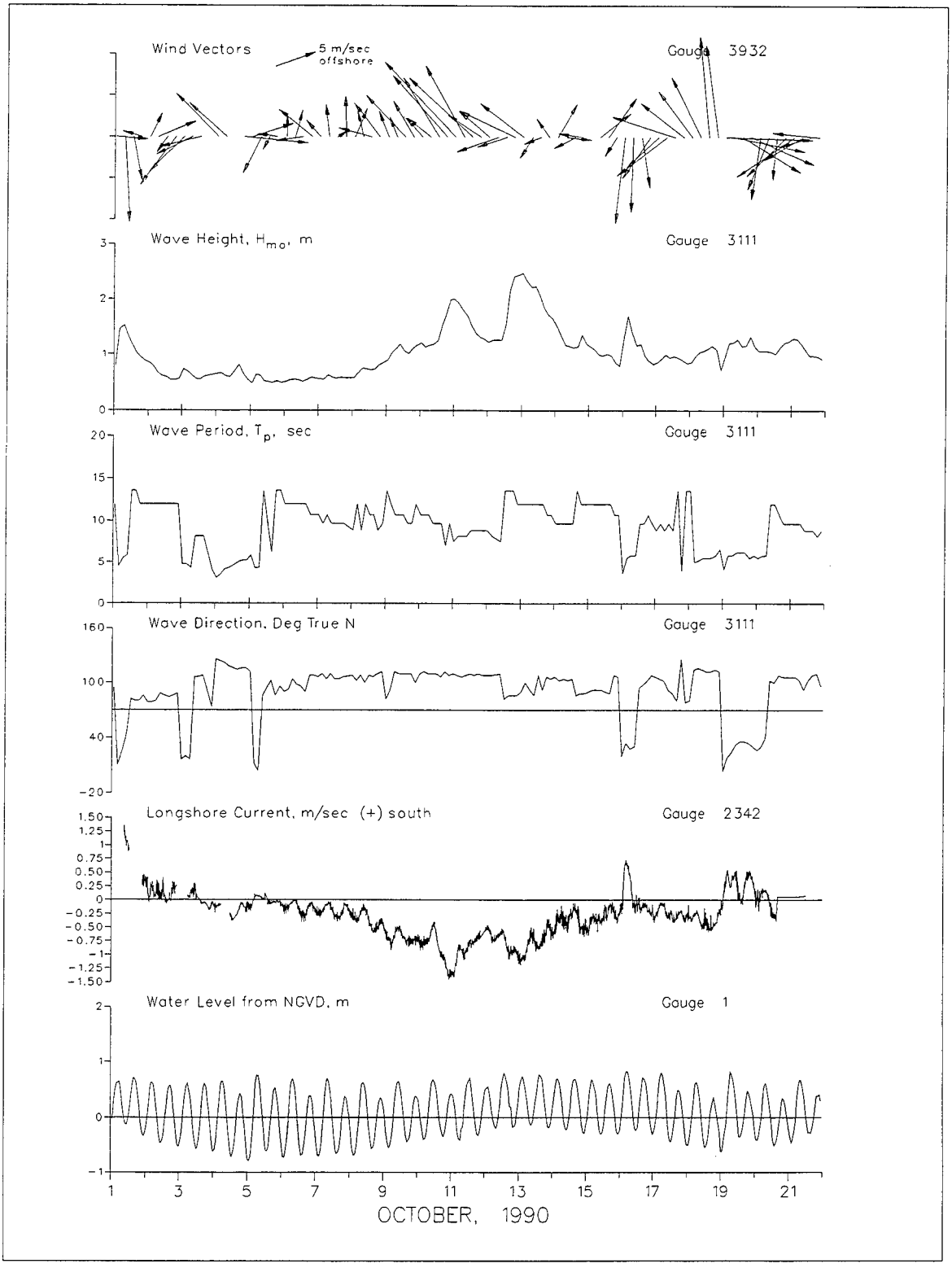

Figure 9. Conditions during the DELILAH experiment

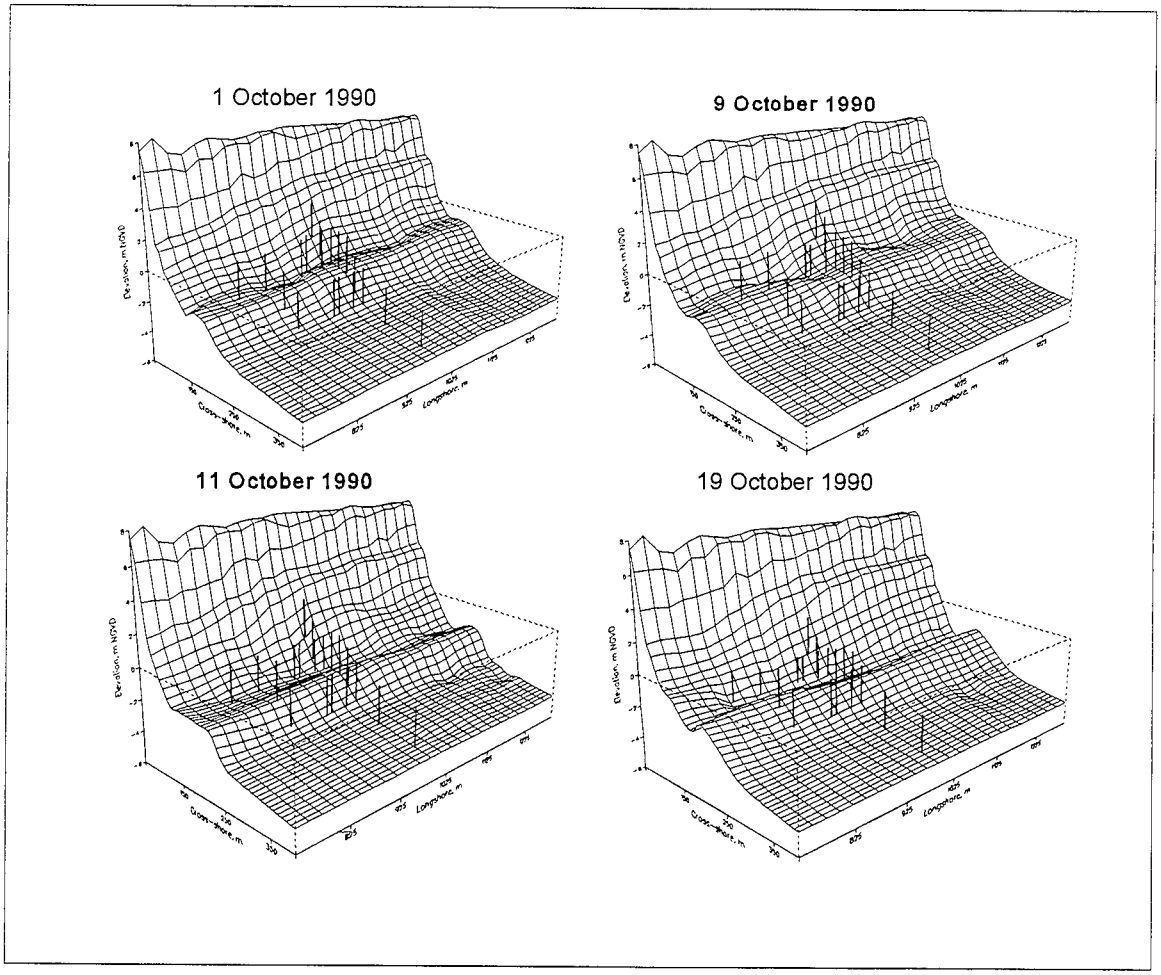

Figure 10. Four of the minigrid surveys showing bathymetric change over time

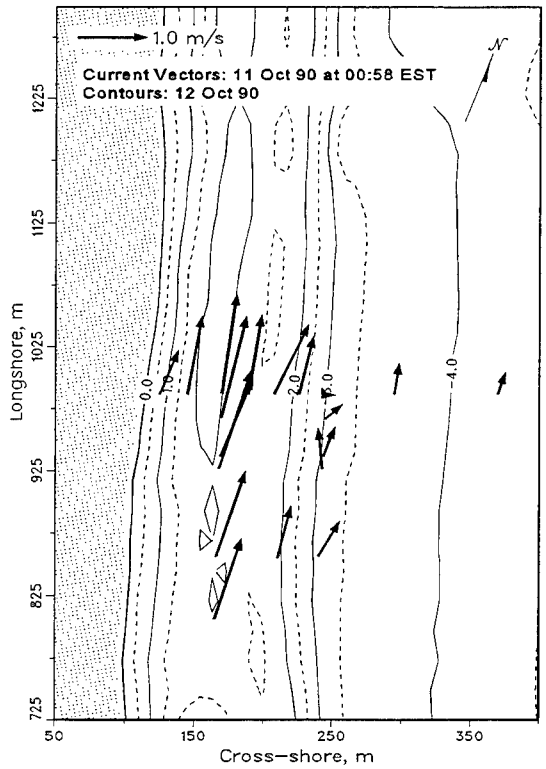

Figure 11. Current vectors during one of the energetic periods

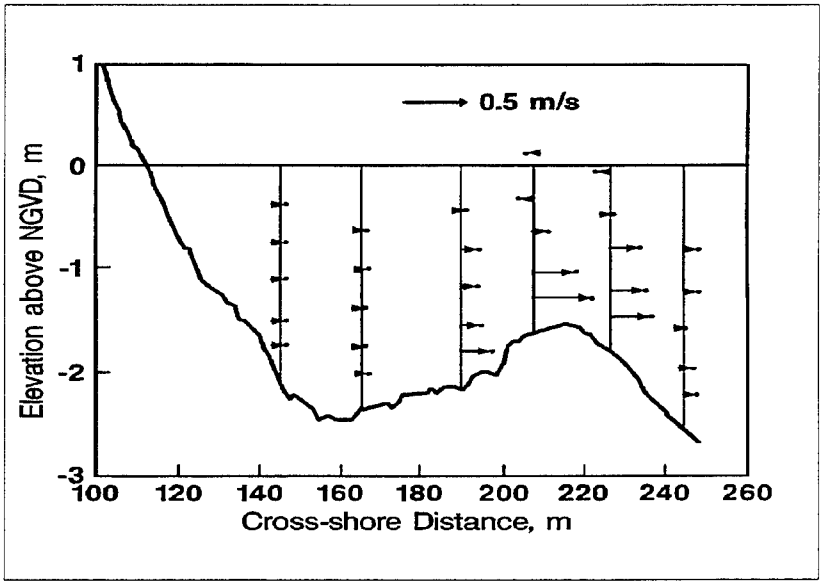

Figure 12. Sample cross-shore current data from the instrumented sled

Appendix A
Surveying

As in previous Duck experiments, surveying was a critical part of DELILAH. The CRAB was used to locate the instrument pipes and to survey the minigrid area. An additional survey was conducted of the bathymetry surrounding the FRF, out to a water depth of 13 m, using a combination of the CRAB and a survey sled. In this survey, referred to from here on as the "13-m-deep" survey, the sled was towed behind the FRF's amphibious Lighter Amphibious Resupply Cargo (LARC). Presentation of the data and descriptions of this survey and the minigrid surveys, as well as details about the survey equipment and sources of error follow.

Coordinate System

All survey data were collected relative to the FRF coordinate system, which has its origin located behind the duneline near the southern boundary of the FRF property. The baseline of this system (cross-shore distance = 0) is perpendicular to the FRF pier and is aligned 20 deg west of true north. Elevations were measured relative to the National Geodetic Vertical Datum (NGVD) of 1929. This datum is 0.42 m above Mean Low Water.

Survey Equipment

All DELILAH surveying was conducted with either a Zeiss Elta 2s ® total station or a Geotronics Geodimeter 140-T® auto-tracking total station. Problems developed with each of these instruments, and it is important to understand what the problems were and their impact before using the DELILAH survey data.

Zeiss Elta-2s

The Zeiss system incorporates in one compact unit a first-order electronic theodolite, distance meter, microprocessor, rechargeable power supply, and an interchangeable solid state memory module. The instrument is manually aimed at a reflecting prism and a collimated infrared beam measures the distance and

the electronic theodolite measures both horizontal and vertical angles. The microprocessor then uses these measurements plus the coordinates of the instrument to compute X, Y, and Z Cartesian coordinates of the prism (corrected for earth curvature).

The ELTA-2s was primarily used for positioning the instrumented sled, the instrument pipes, and for beach surveying. It is classed as a first-order survey instrument with 0.6-sec horizontal and vertical angle reading accuracy. Unfortunately, it began malfunctioning during the latter half of the experiment with some impact on the positioning of the instrumented sled. The errors resulted from a problem in the horizontal rotation of the instrument and were easily identified as inconsistent changes in horizontal position.

Geotronics Geodimeter 140-T

The Geodimeter 140-T (Figure A1) consists of an electronic theodolite, distance meter, tracker, joystick, and cables. The system is designed to track the position of a moving object with the aid of a servo unit, which permits automatic motorized rotation of the instrument in the horizontal and vertical directions. The angle and distance measuring unit is both mechanically and electronically connected to a top-mounted tracker unit. The initial aiming of the instrument is controlled by a joystick. Once locked onto the prism array mounted on the CRAB, the Geodimeter 140-T continues to follow it.

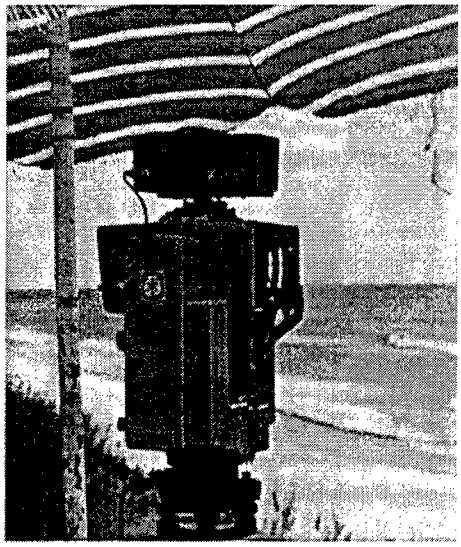

Figure A1. Geodimeter 140-T

With the auto-tracking ability of the Geodimeter 140-T, the CRAB was able to move continuously, obtaining position information every 2-3 m along the survey transect. Data were collected by a shore-based personal computer, and steering information was radioed to the driver. The Geodimeter was put into use at the FRF early in 1990 and the DELILAH surveys were the first real production surveys with the instrument.

A combination of unfamiliarity with the instrument and several unique quirks resulted in problems processing and interpreting some of the Geodimeter survey data, particularly the 13-m deep data. The problems affect elevation measurement. There were three types of problems.

One of the instrument errors of the Geodimeter results from the separation of the tracking unit and the angle measurement unit. For accurate vertical measurements, the two units must be parallel. Instead of attempting to fine adjust the parallelism, the angular error was computed based on targeting a

fixed prism of known elevation. This *vertical angle correction* was then applied to the measured vertical angle in the collection software. It wasn't learned until later that the correction angle changes during the day, especially on hot days. Although checks of the vertical angle correction were made, they were not made frequently enough to fully remove the error. This vertical error increases with distance from the instrument. Over a distance of 1,000 m, a 20-s angle error, if uncorrected for, would result in a vertical error of 10 cm (elevation checks were also made with the ELTA-2S, but there were no vertical problems with the Zeiss data) .

Another error associated with the vertical angle correction occurred when there was slight shifting of the instrument out of level (probably due to differential heating) during full days of surveying. Some of this movement is automatically compensated for by the Geodimeter, and it is designed to stop acquiring data if the instrument tilts outside the range of the internal compensator. However, it was determined well after DELILAH that this applies only for the horizontal compensation, not for the vertical. Consequently, even when tilted, the instrument continued to collect slightly erroneous vertical data with the only indication being an off-centering of the bubble level. Because the operator watches a computer screen, and not the bubble level, a tilted instrument could go undetected. From the beginning, this error was minimized by sheltering the Geodimeter with an umbrella or by setting it up in a "dome shelter" located on the roof of the FRF building. Unfortunately, during the first year of use, some of the out-of-level errors were wrongly corrected for by recomputing the vertical angle correction, thus compounding the error. This type of error manifests itself as an offset of the survey data that increases with distance from the instrument. In several cases, the survey data for one or more profile lines collected in sequence shifted during one survey and then unnaturally shifted back for the next and later surveys. When this shift was significant, the data were adjusted accordingly.

A further source of error was vertical oscillations of the Geodimeter which occurred because of an improperly adjusted tracker amplitude. This resulted in jagged data with an oscillatory amplitude of a few centimeters. Although the data follow the true profile shape, it is difficult to remove the oscillations since they are not centered on the true profile. At its worst, the tracker would drift completely away from the prism and temporarily lock onto a horizontal plane above the actual position of the moving prism for a short distance before reacquiring the prism center, resulting in a "step function" appearance to the data. These problems affect the nearshore data of some of the profile lines from the September 1990 CRAB survey that is part of the 13-m-deep survey data and affected several of the minigrid surveys. These errors were not a problem in most of the minigrid data and are not to be confused with the megaripples, which were reliably surveyed on many of the profile lines. Data affected by these oscillations are characterized by small oscillations along the entire profile line with no smooth regions. Major changes caused by the tracker drift were identified by overlaying all surveys of each profile line and

deleting points that fell outside the overall envelope or had a "step" shape to them when compared to subsequent surveys of the same line.

While these Geodimeter errors are unfortunate, their impact on the minigrid survey data is seldom $> \pm 15$ cm in the vertical and is typically $< \pm 10$ cm.

Because of the height of the prism, data affected by the tilt of the CRAB on steep parts of the profile (particularly the foreshore and the bar slopes) were adjusted using an iterative technique in the analysis. The measured slope was used as a first guess to adjust the data points both horizontally and vertically. A new slope was then determined and a second pass, if required, was made. On a 10° slope typical of the beachface, the tilt can result in a +20-cm vertical adjustment to the data.

13-m-Deep Survey

The first 13-m-deep survey was conducted on 1 May 1990, followed by subsequent surveys on 2, 8, and 27 August 1990. All of the surveys were conducted with the Geodimeter 140-T, which was located on the end of the FRF pier and which tracked the sled as it was towed behind the LARC.

The final 13-m deep bathymetry data were acquired on six different dates and include sled data from the three dates given above and CRAB survey data from the September FRF 26-line bathymetry survey and a preliminary minigrid survey on 19 September 1990. Unfortunately, the CRAB and sled data do not overlap well, resulting in discontinuities where the data sets meet. The difference is usually less than 20 cm, but the effect is quite pronounced on the bathymetric chart and on specific cross sections (an explanation for the discontinuities is given below). The most serious discontinuity, and the largest data gap, is around the 8-m pressure gauge array location. Neither the CRAB nor the sled were normally driven through the 8-m array. A special deepwater parallel pass was made alongside the array with the CRAB, but not until January 1991. In order to fill the data gaps in a reasonable way, a very large "search" area had to be defined in the gridding routine which was used to plot the data. This has the adverse effect of overly smoothing all of the data, particularly the irregular bottom found in the 10-to 13-m depth south of the pier.

Problems with the sled were also encountered. These resulted primarily from the sled tilting sideways while on a turn, or backward when under tow. During the surveys on 2 and 8 August, strong currents caused the sled to tilt sideways when it was under tow. Consequently, these surveys were not used in the final data set unless they provided the only coverage of an area. Sled tilt results in a vertical error, which can show up as either a bump or a hole. If the tilt occurred gradually, it was difficult to identify and correct.

Because of these problems, the data processing included rechecking and

recomputing the data points based on a reanalysis of the vertical angle correction data for each day (any out-of-level errors were not corrected for). Data with nearby coverage from the same or different days were overlaid and compared. The plan view and the cross-section view of each profile line were examined and suspect points, indicated by wide variations in depth between adjacent points, were removed. Where data from two surveys overlapped and didn't match well, data that best fit the rest of the data were retained. Confidence in a particular survey was determined by the overall smoothness of the data (no Geodimeter oscillation) and from the frequency and quality of the vertical angle error checks. Most of the data from the 1 May 1990 and the 27 August 1990 surveys were kept. Data were deleted if there was evidence of sled tilt. Finally, the large gap in the data at 1,280 m longshore and 900 m cross-shore was filled with data from 1,100 m in the longshore. To reduce the total number of points only the median depth value of every three data points along a line was kept (limited by a maximum allowable distance and vertical change). Still, the raw data file includes over 10,000 points. It should be noted that all of the errors described in the 13-m-deep survey section result in less than 30 cm vertical error at the outer edge of the survey region.

The 13-m deep survey data are shown in Figures A2 to A4. Figure A2 shows the tracklines of all the data points used with profile numbers marked.

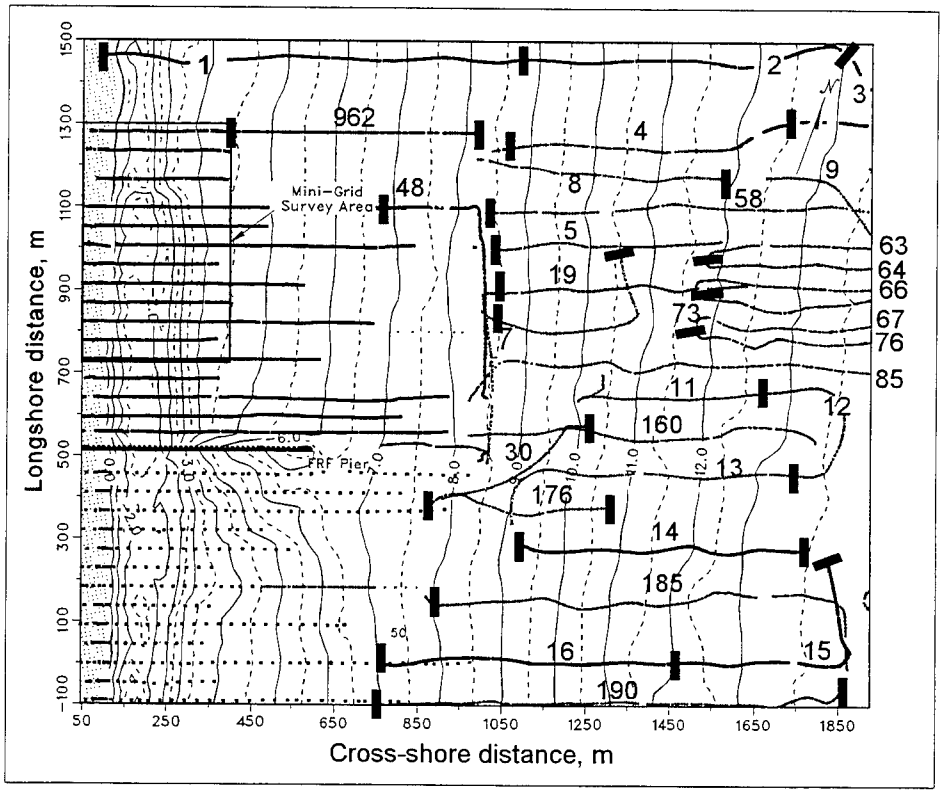

Figure A2. Sled tracklines from 13-m-deep survey. Numbers indicate profile lines surveyed; bold rectangles indicate end points

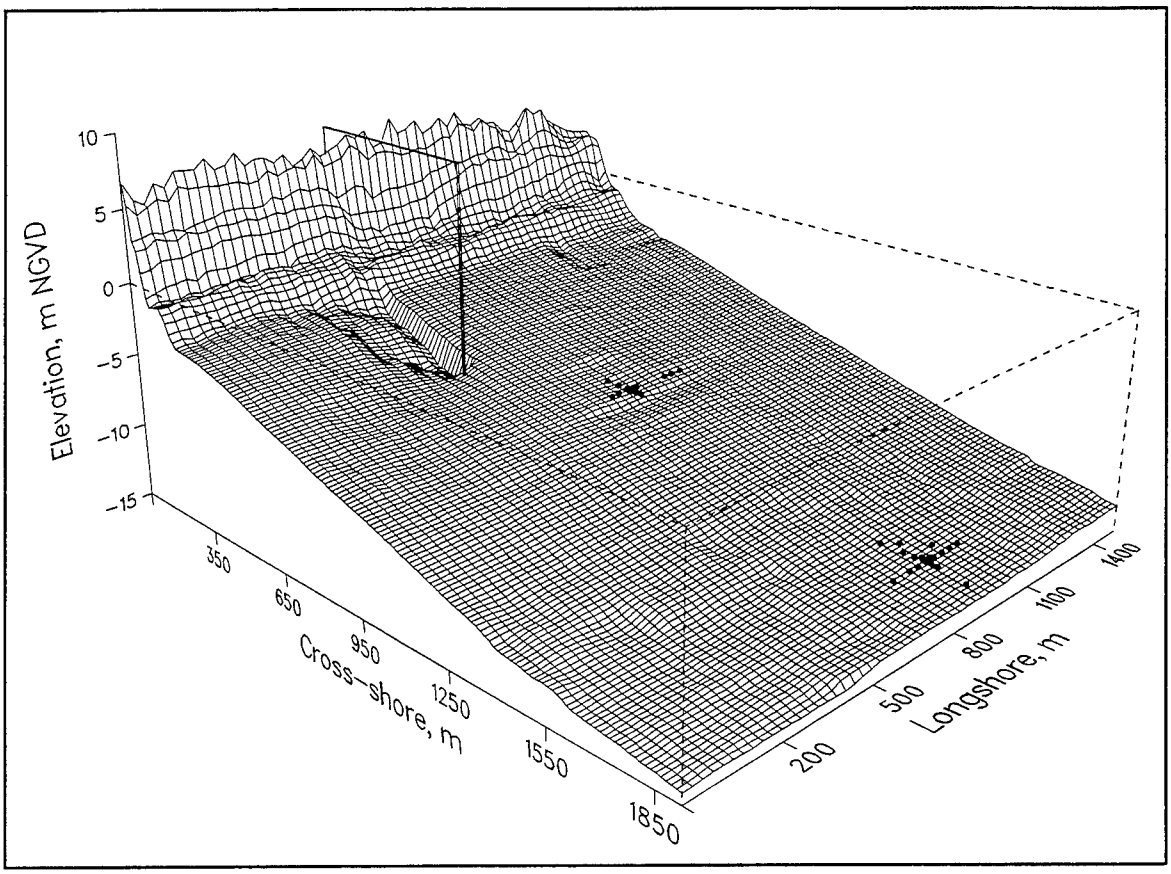

Figure A3. 13-m-deep survey showing the 13-m array, and the FRF's 8-m array

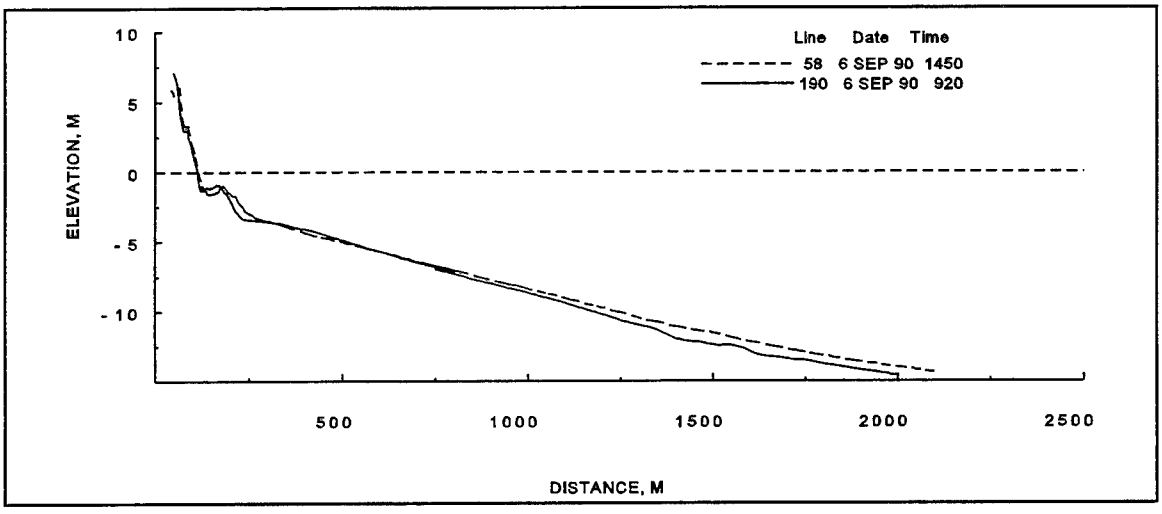

Figure A4. North (line 58) and south (line 190) transects from the 13-m-deep survey

The 1 May 1990 data used FRF profile numbers, but the later data used a sequential numbering system primarily dictated by software restrictions. As can be seen in Figure A3 and the transects shown in Figure A4, the bottom 580 m north of the pier (line 58), out to -13 m, is basically flat, while 516 m south of the pier (line 190), there are some interesting irregularities with cross-shore lengths of approximately 150 m, and vertical relief on the order of 1 m.

Minigrid Surveys

A series of 20 profile lines were surveyed every day during DELILAH beginning 1 October and continuing throughout the experiment. The lines were spaced approximately 25 m apart near the instruments and 50 m apart elsewhere. Profile lines, along with the locations of the nearshore instruments, are shown in Figure A5. All lines extended from the base of the dune to approximately 375 m offshore, except during the high wave period on 13 October 1990. The dune section of each profile line was only surveyed at the beginning of the experiment. To provide continuity between surveys, the dune data points were automatically added to each survey. The surveys were sequentially numbered. Unlike the 13-m-deep survey, a median smooth was not used to reduce the number of data points.

Most of the changes which occurred resulted from the offshore movement of the inner bar. This can be seen in Figure A6, which over-plots all the surveys for profile line 230, located just north of the cross-shore instrument line. The largest vertical changes occurred at approximately 160 m offshore and were

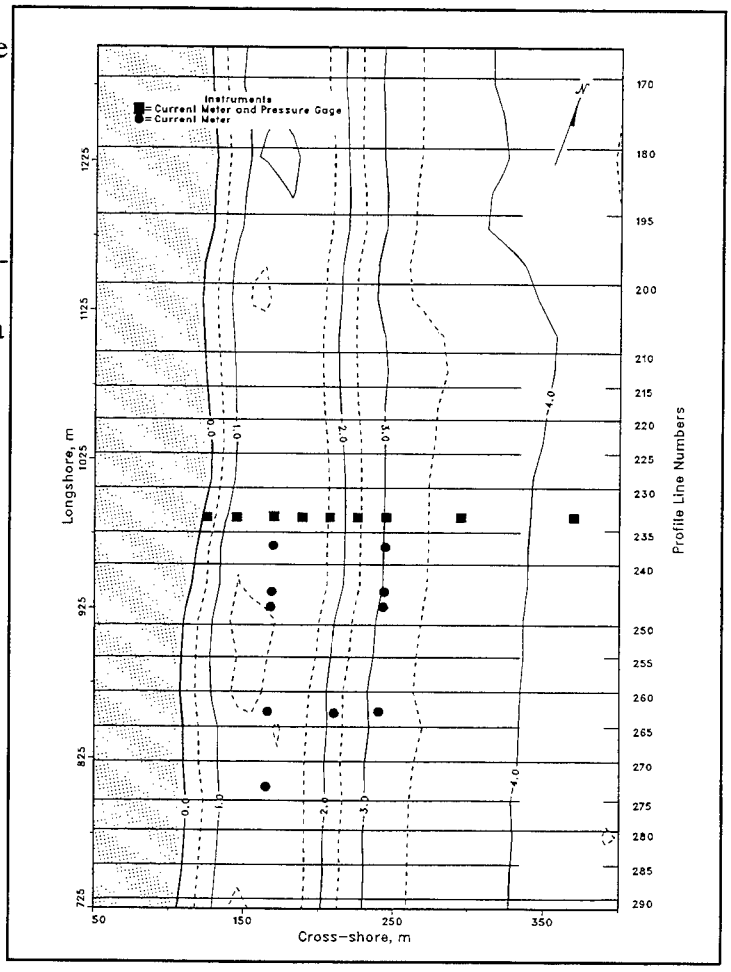

Figure A5. DELILAH minigrid profile lines

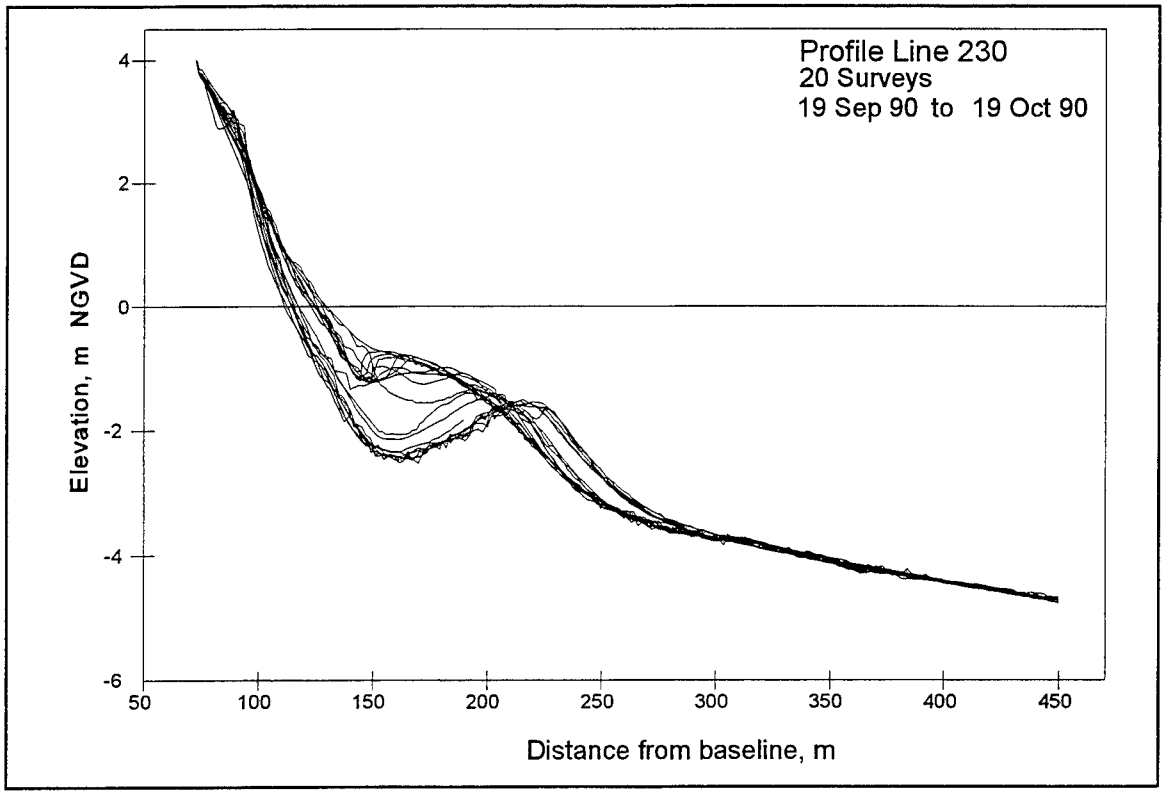

Figure A6. Envelope of all surveys of profile line 230

caused by the rapid development of the nearshore trough and the offshore movement of the bar. Seaward of 300 m, the bottom was stable and the influence of the errors previously discussed is more significant.

One interesting feature that was measured for the first time at the FRF was large bed forms, or megaripples, which developed along some of the profile lines in the nearshore trough and seaward of the bar (Figure A7). These features are large enough to be felt by the wheels of the CRAB and are reflected in the data (the CRAB surveys the average elevation between the two back wheels). Because they appeared repeatedly from day to day, and were observed by the CRAB operators, there is convincing evidence that these features are not the result of the Geodimeter oscillations described previously.

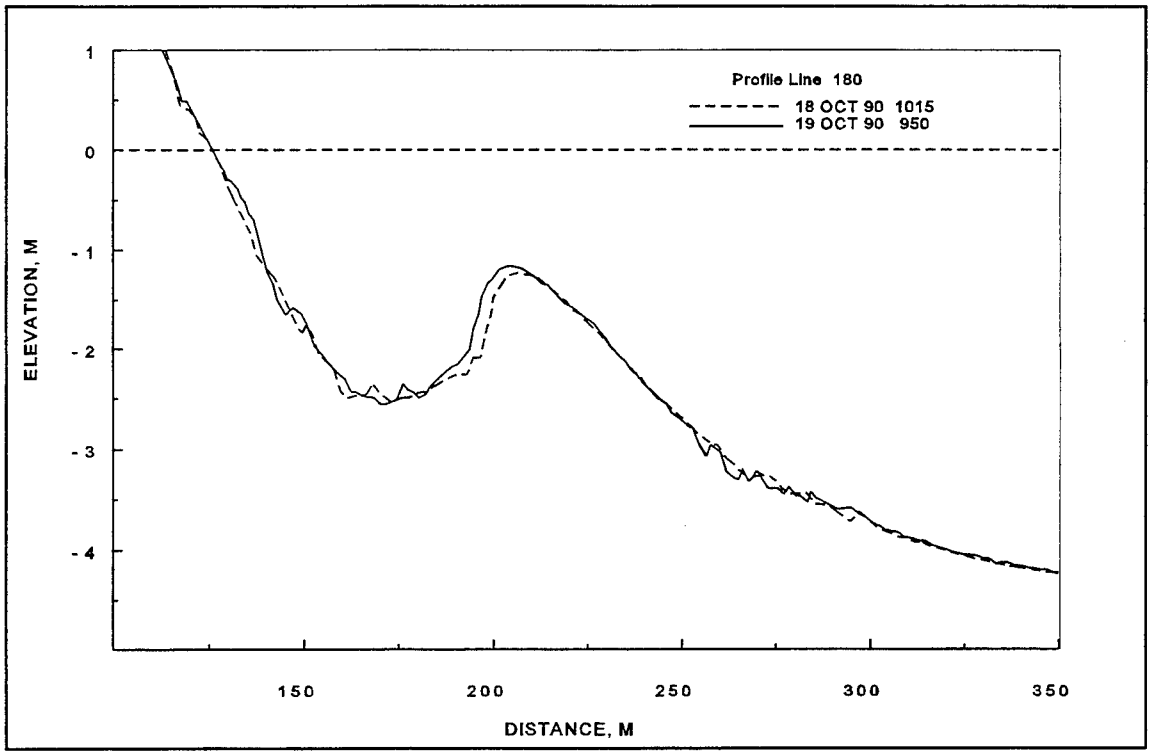

Figure A7. Megaripple features in the trough and offshore of the nearshore bar

Collection of the minigrid survey data under the changing DELILAH conditions was arduous. Some of the profile lines were perilously close to the instruments. Many individuals contributed to the survey data collection, most notably Messrs. Kimble Milliken, Doug Alden, and Brian Scarborough who drove the CRAB and Mr. Steve Blanchard who processed all of the data and assisted in its collection.

Table A1 provides a summary, by profile and survey number, of the data collected. Numbers in the table are of computed cross-section volume changes (m^3/m) between successive surveys. Surveys were conducted daily, but conditions limited the operation of the CRAB during 12-14 October 1990, when only the inshore portion of the lines could be surveyed and some of the lines had to be skipped completely. Following Table A1 are plots of the minigrid survey data, which are presented in two ways. First, the original cross-section data are displayed as comparison plots between successive surveys of all of the lines surveyed (Figures A8-A25). Then, contour and perspective plots are shown for each survey (Figures A26-A44).

Table A1
Summary of Profile Lines Surveyed and Net Volumetric Change Between Surveys

Profile Line Number	170	180	195	200	210	215	220	225	230	235	240	250	255	260	265	270	275	280	285	290	Average Total Volume Change m^3/m^{**}
Longshore Distance, m	1280	1234	1189	1143	1097	1074	1052	1029	1006	977	954	914	892	869	846	823	797	777	754	732	
Survey Date	Net Volume Change, m^3/m																				
19 Sep 90	0	0	0	0	0	0	0	0	0	--	0	0	0	0	0	0	0	--	--	--	0
1 Oct 90	6	19	31	-5	-17	11	-10	26	18	--	10	-6	14	-19	3	-18	8	0	0	0	5
2 Oct 90	15	-2	8	12	-4	-8	-4	-8	-8	0	-5	6	2	-2	-7	-3	-6	-3	1	2	0
3 Oct 90	-35	-25	-24	-20	-13	-13	-17	-13	-8	-7	-8	4	-10	-1	-10	-1	-11	1	-12	-2	-13
4 Oct 90	-4	-9	0	-2	8	-15	7	-14	10	-15	8	-10	1	-10	-1	-9	3	-6	6	-6	-3
5 Oct 90	9	-4	18	18	9	0	1	1	-2	3	5	-1	0	2	1	2	2	3	3	2	4
6 Oct 90	-18	2	--	2	1	9	9	5	2	6	8	1	11	*	4	-1	4	-6	-4	-6	2
7 Oct 90	15	6	0	-15	-19	10	-19	--	14	11	0	-5	-13	-8	-6	2	4	14	1	-6	-1
8 Oct 90	2	14	-2	-9	11	-10	9	-3	2	0	-6	-11	1	-4	7	-1	-1	-9	-5	-4	-1
9 Oct 90	13	-5	-16	3	8	9	20	11	4	-27	-23	10	*	12	-12	4	-21	-8	-30	2	-3
10 Oct 90	-5	-6	-14	-10	15	3	-10	-7	-25	-15	-7	-3	-6	-12	-2	-19	-10	-29	0	-6	-8
11 Oct 90	-21	-15	-7	24	*	-17	-25	*	-43	--	-32	--	-10	5	-1	0	-4	9	16	35	-5
12 Oct 90	-9	-20	-2	*	*	*	--	-24	-7	*	*	*	*	*	-8	-14	-8	-4	3	10	-5
13 Oct 90	*	*	*	*	*	--	*	--	*	--	*	*	--	*	--	*	--	*	--		0
14 Oct 90	19	0	*	*	-42	-19	*	*	-14	-70	*	*	-9	-17	-5	2	22	*	56	63	-3
15 Oct 90	-21	3	-26	-2	20	1	-35	-26	16	12	-33	-24	-14	*	-15	*	-8	41	-8	1	-6
16 Oct 90	14	-7	22	-7	-20	-11	17	-2	-18	1	1	-2	-2	0	-3	1	8	7	6	-5	0
17 Oct 90	2	-2	-2	-5	0	1	-5	2	22	7	-1	-7	10	-7	14	-3	9	-4	2	-16	1
18 Oct 90	-3	4	4	4	-15	5	-9	-11	-24	-11	4	-6	-4	0	-1	-3	2	2	-6	-5	-3
19 Oct 90	-6	6	-3	1	8	-19	-6	-2	-7	0	2	4	7	6	5	9	7	1	2	10	1
Cumulative Total***	-28	-42	-14	-10	-50	-62	-76	-65	-69	-106	-78	-50	-23	-54	-35	-52	1	10	31	69	-38

Net volume changes in m^3/m for the region between 70 m and 365-400 m offshore (actual surveys may extend further offshore than 400 m).
-- Profile line not surveyed.
* Profile line surveyed, but survey did not reach 365 m distance.
** Average volume change per meter alongshore, weighted by the distance between profile lines.
*** Cumulative change computed based only on surveys that reached 365-400 m offshore.

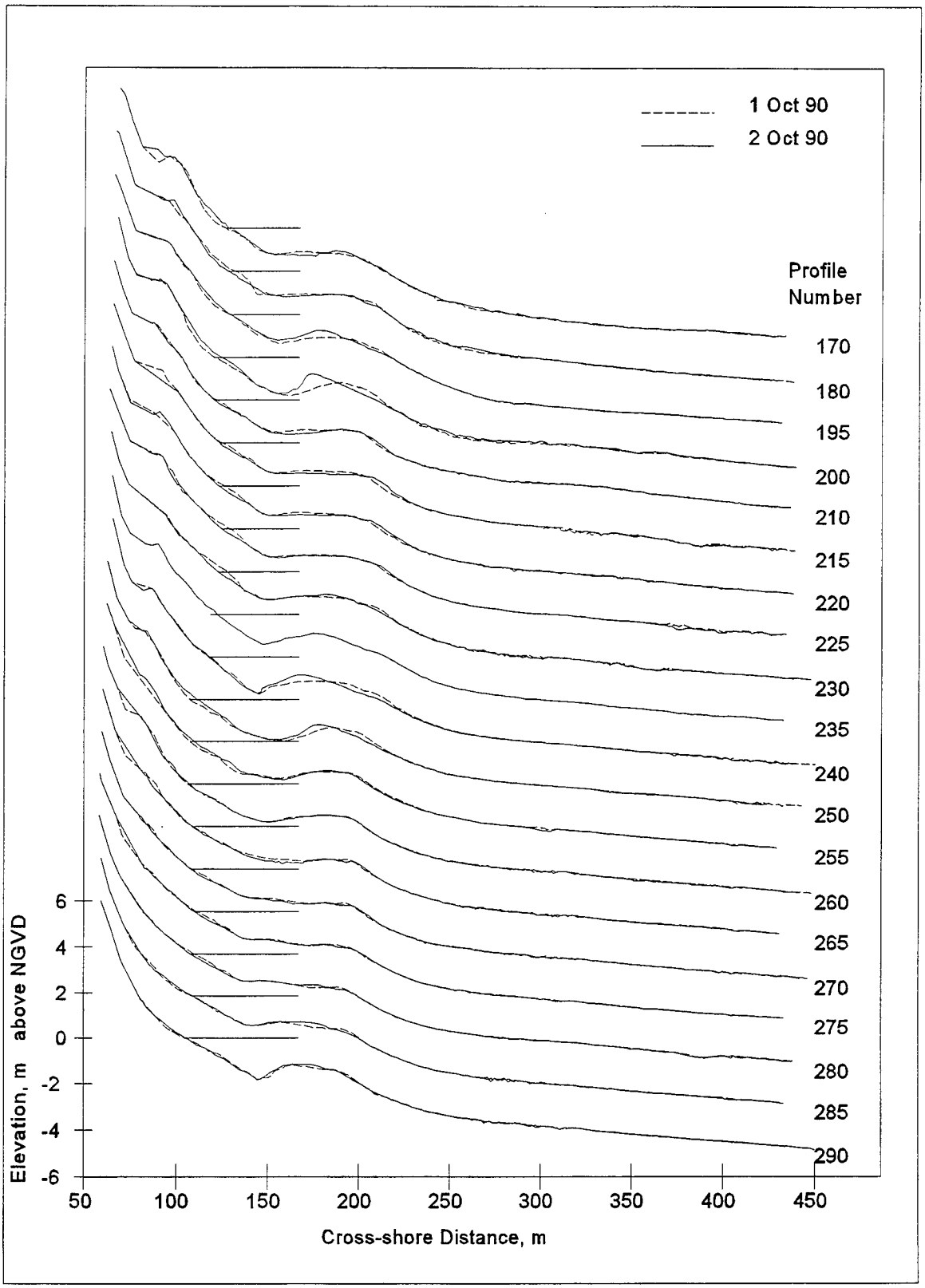

Figure A8. DELILAH profile line cross sections, 1-2 October 1990

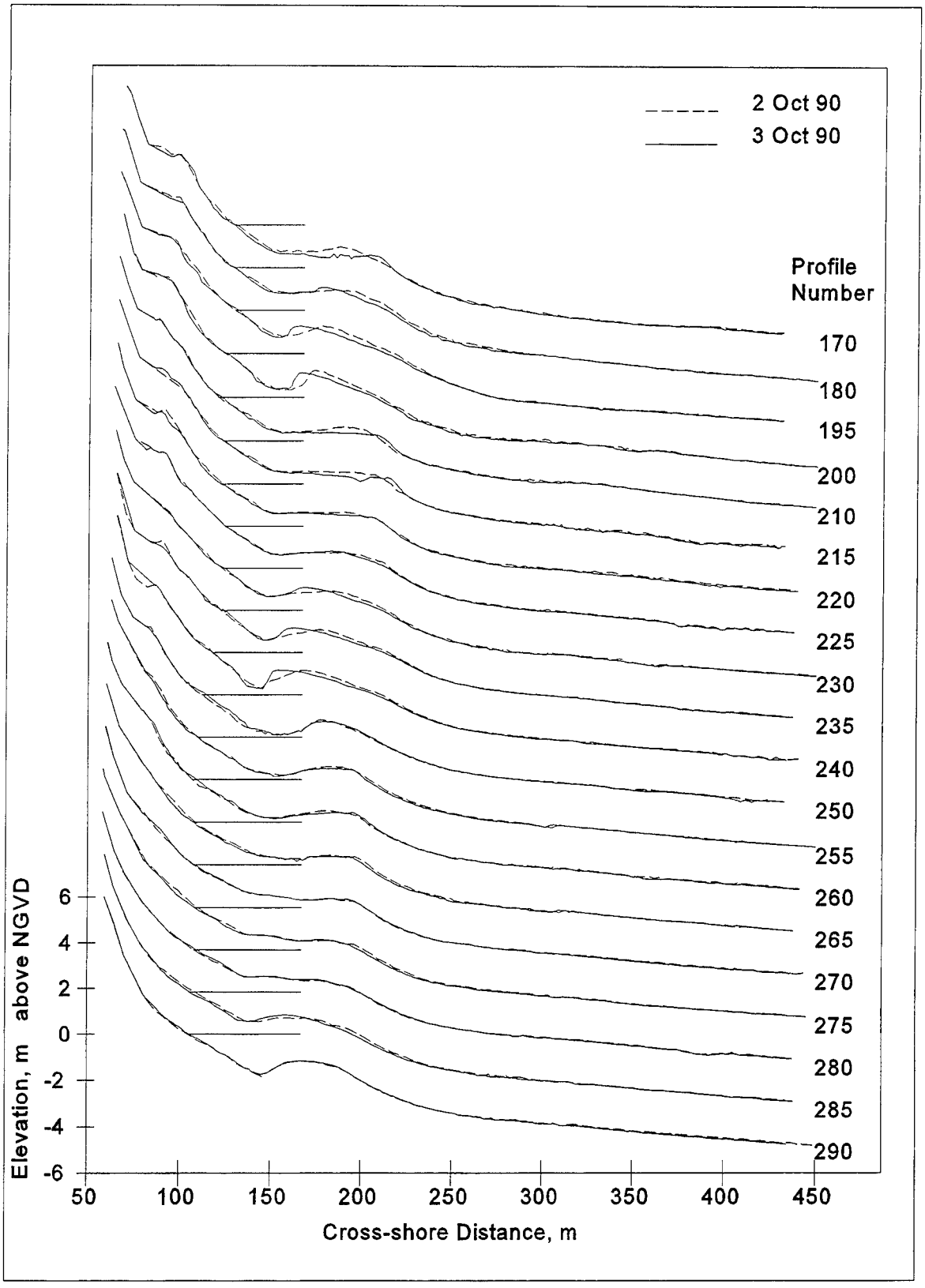

Figure A9. DELILAH profile line cross sections, 2-3 October 1990

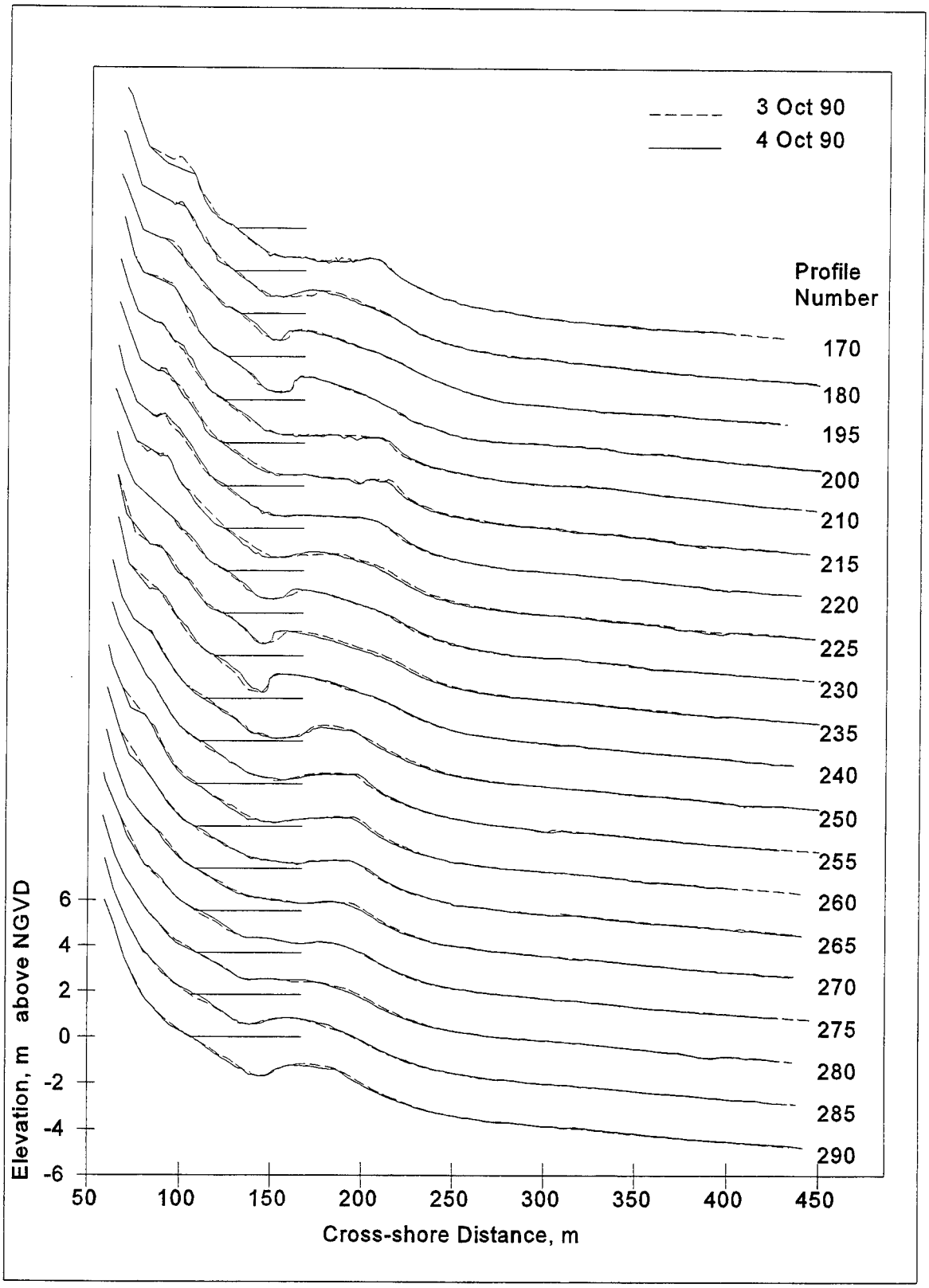

Figure A10. DELILAH profile line cross sections, 3-4 October 1990

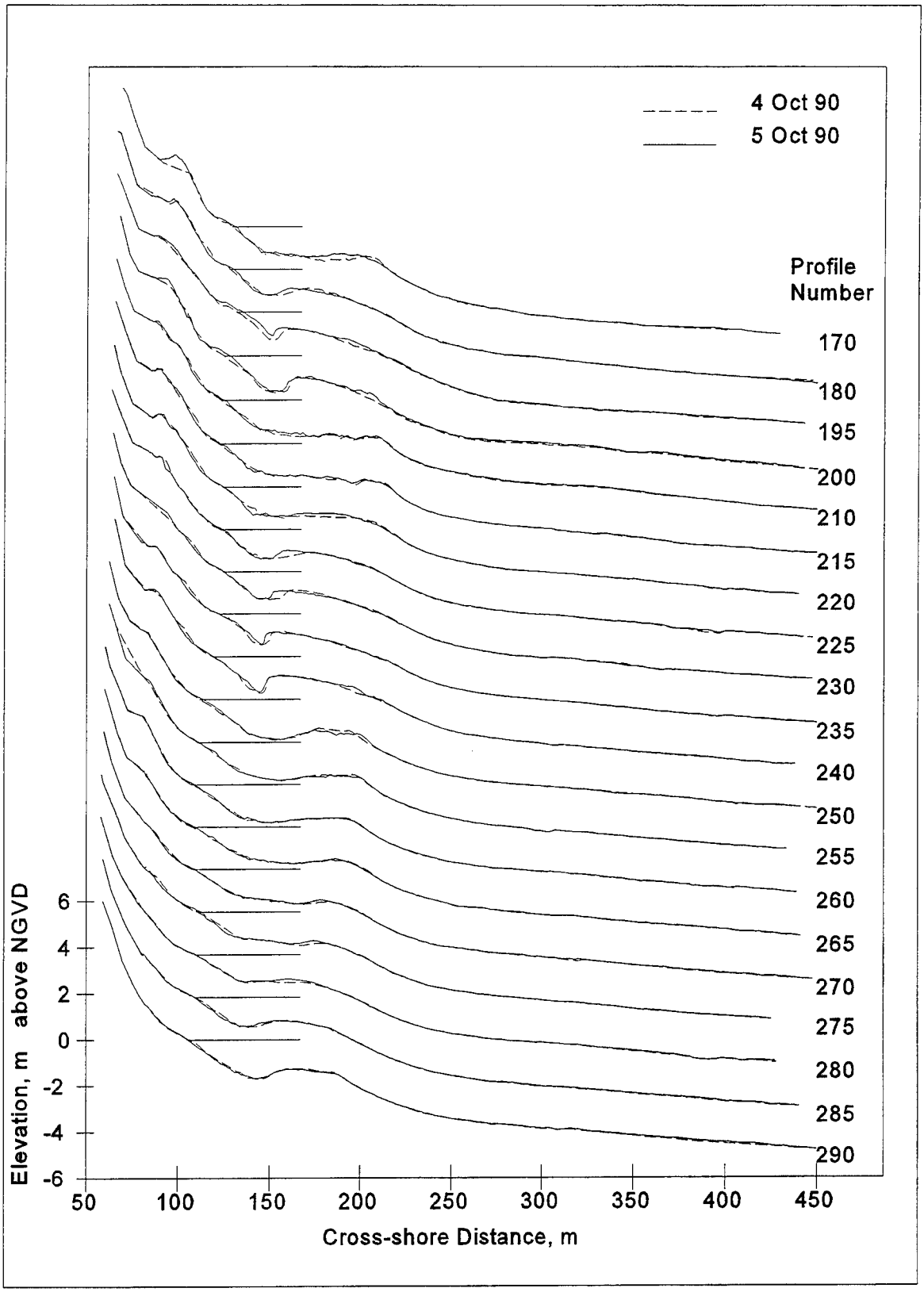

Figure A11. DELILAH profile line cross sections, 4-5 October 1990

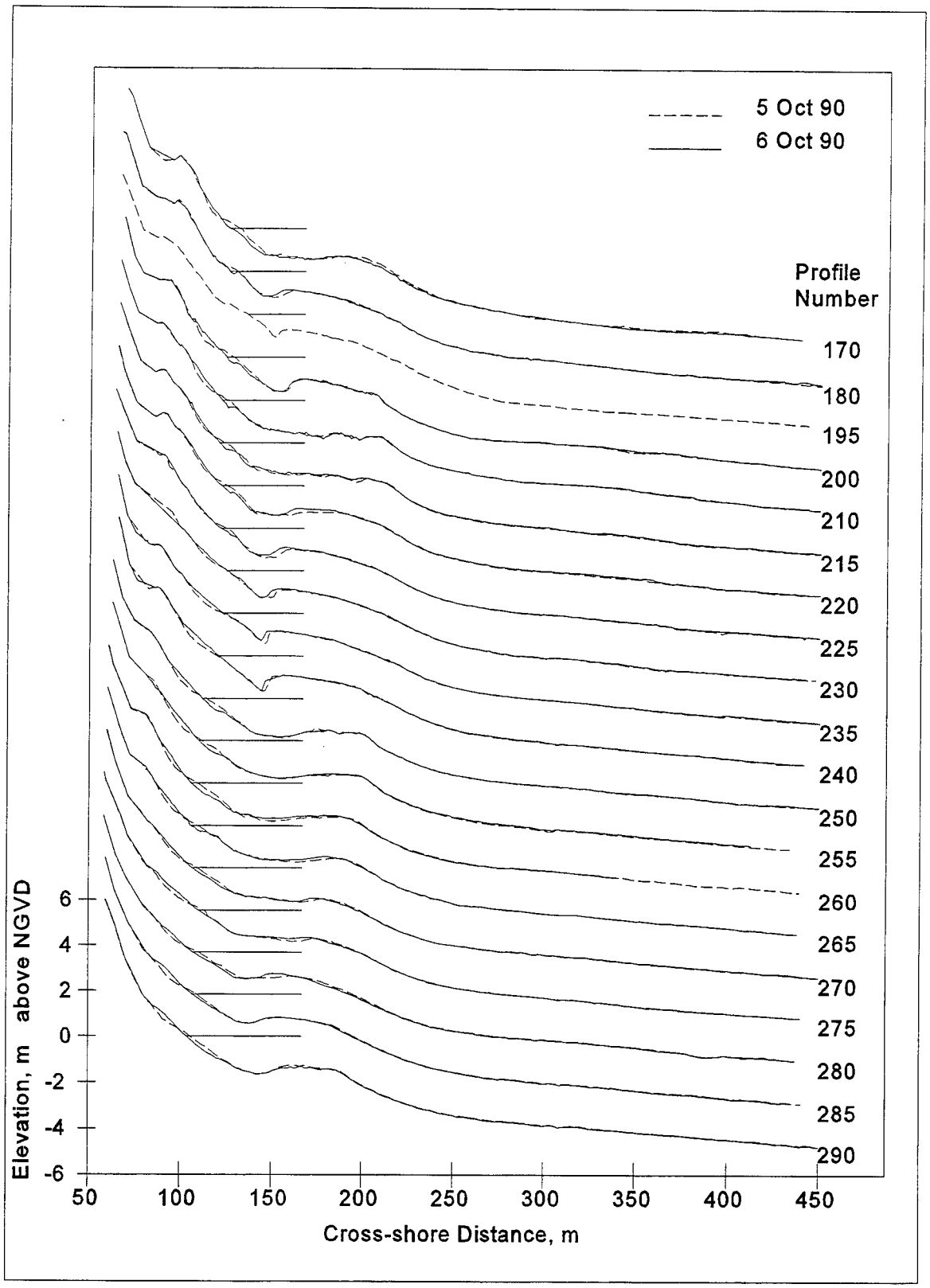

Figure A12. DELILAH profile line cross sections, 5-6 October 1990

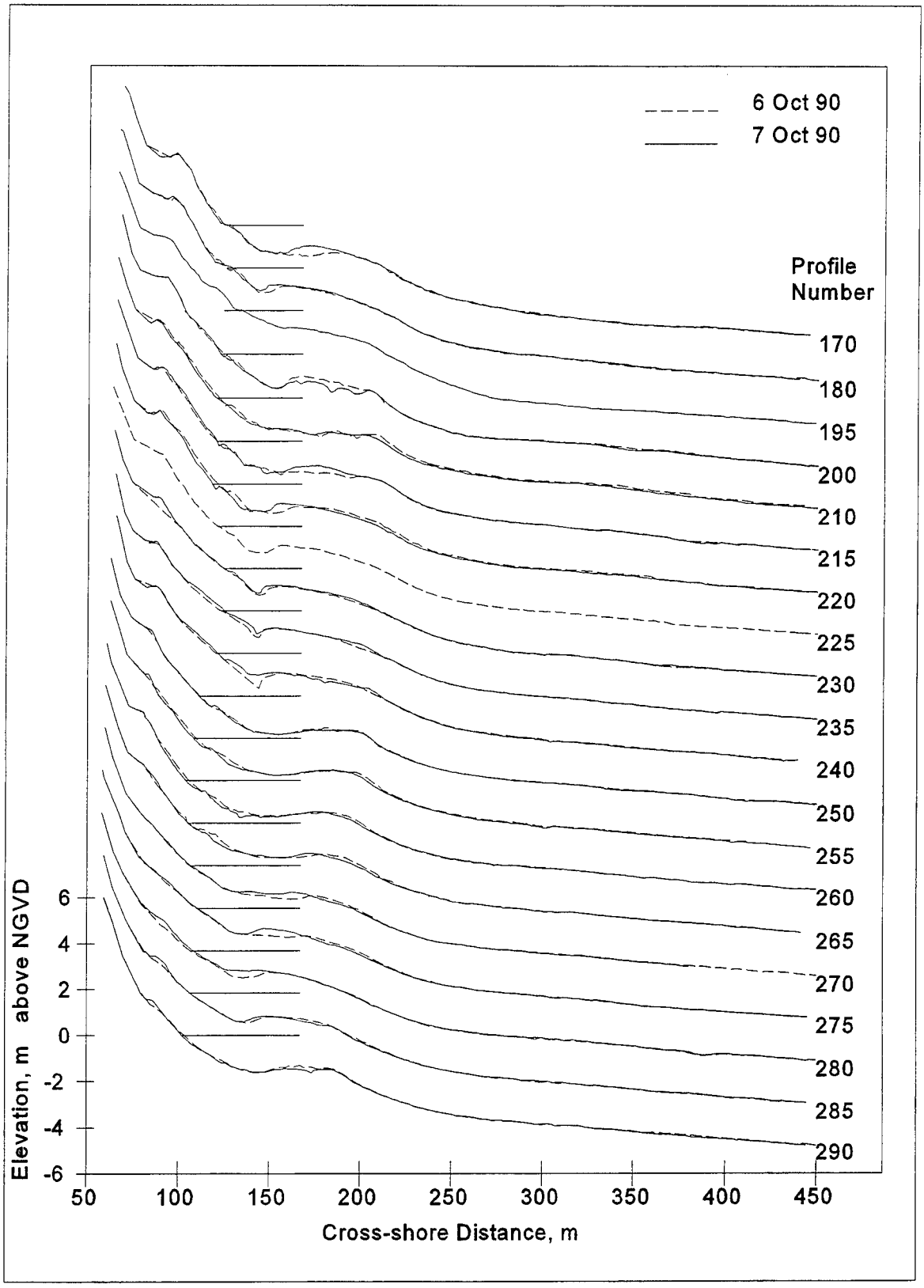

Figure A13. DELILAH profile line cross sections, 6-7 October 1990

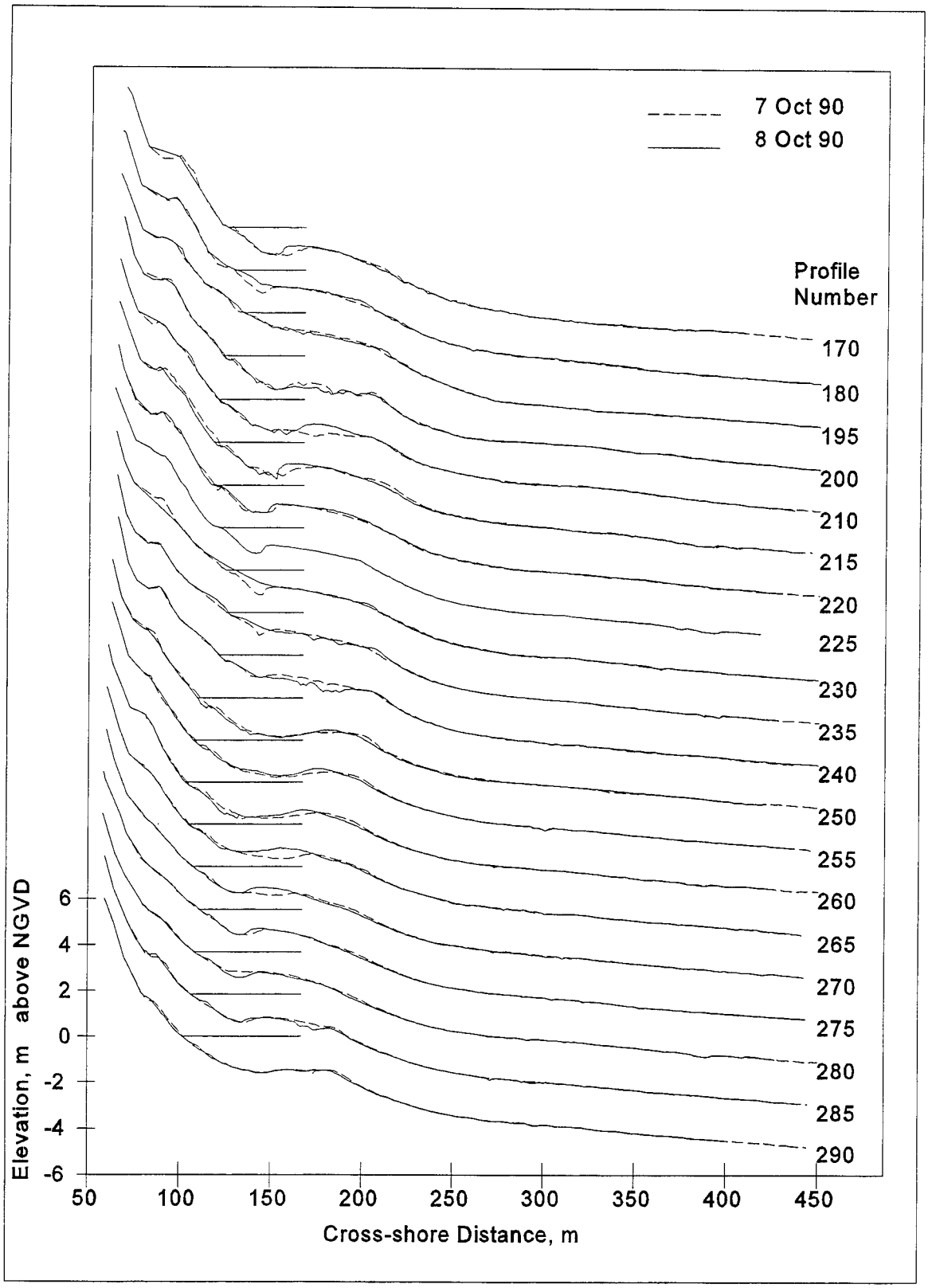

Figure A14. DELILAH profile line cross sections, 7-8 October 1990

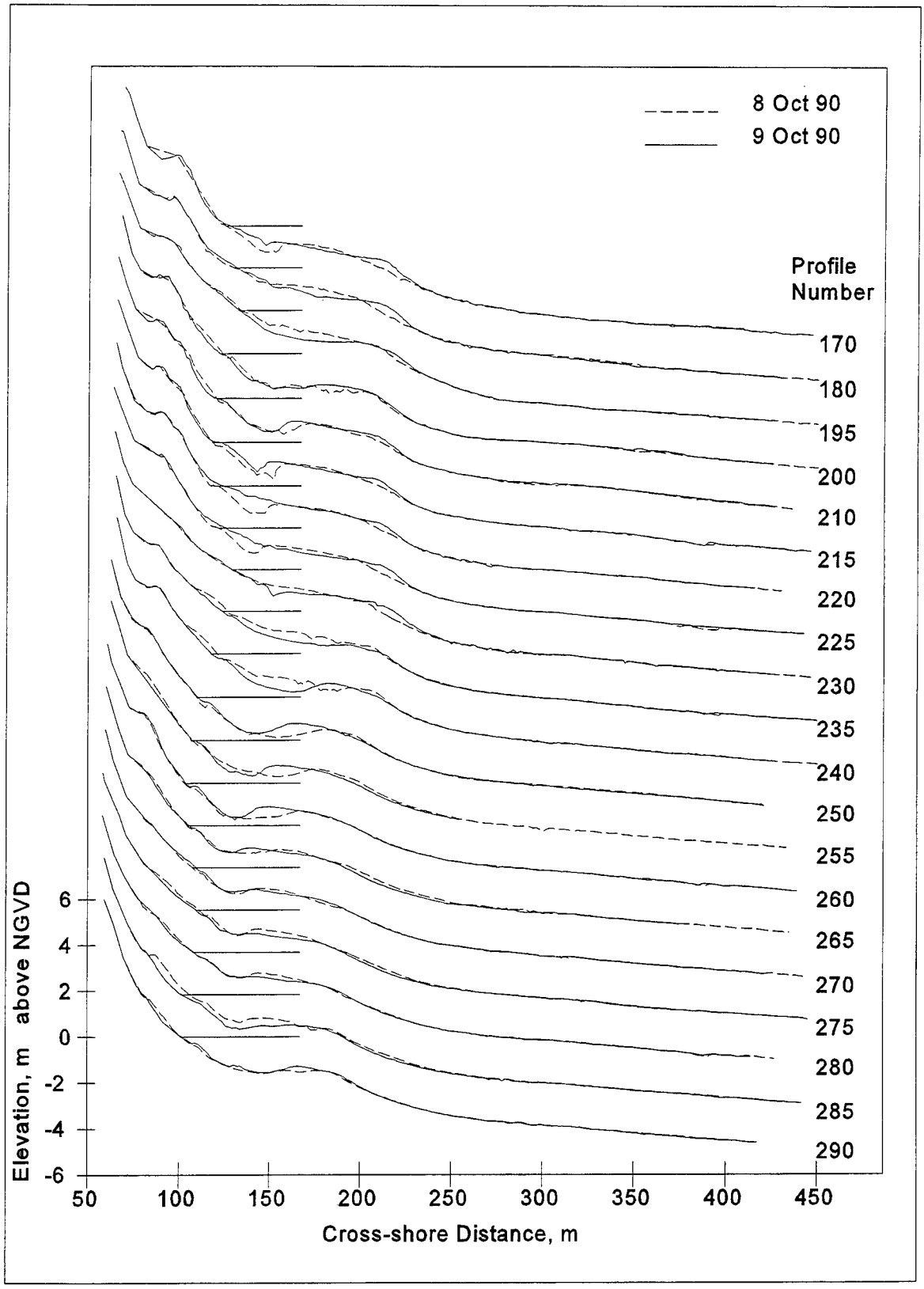

Figure A15. DELILAH profile line cross sections, 8-9 October 1990

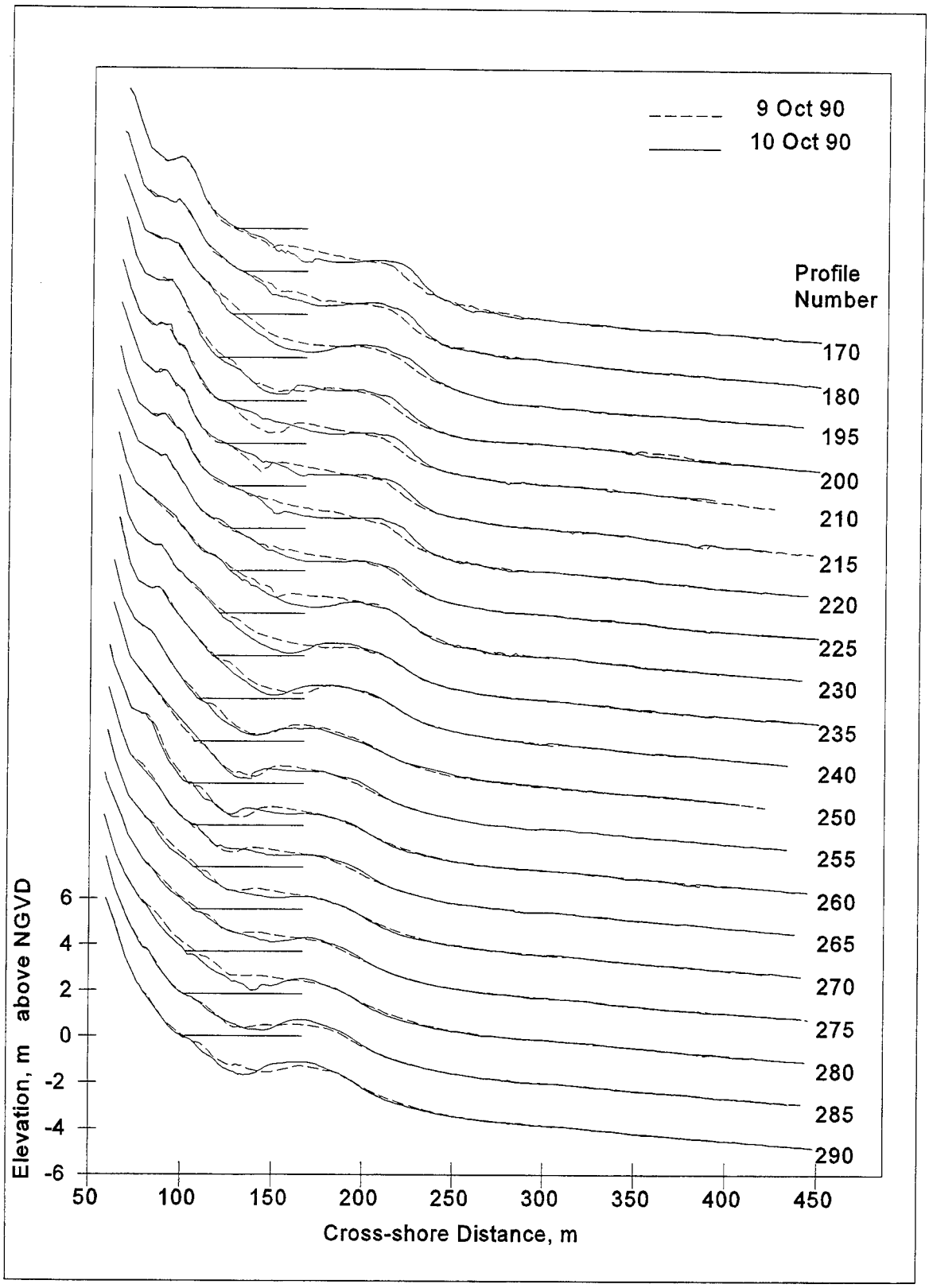

Figure A16. DELILAH profile line cross sections, 9-10 October 1990

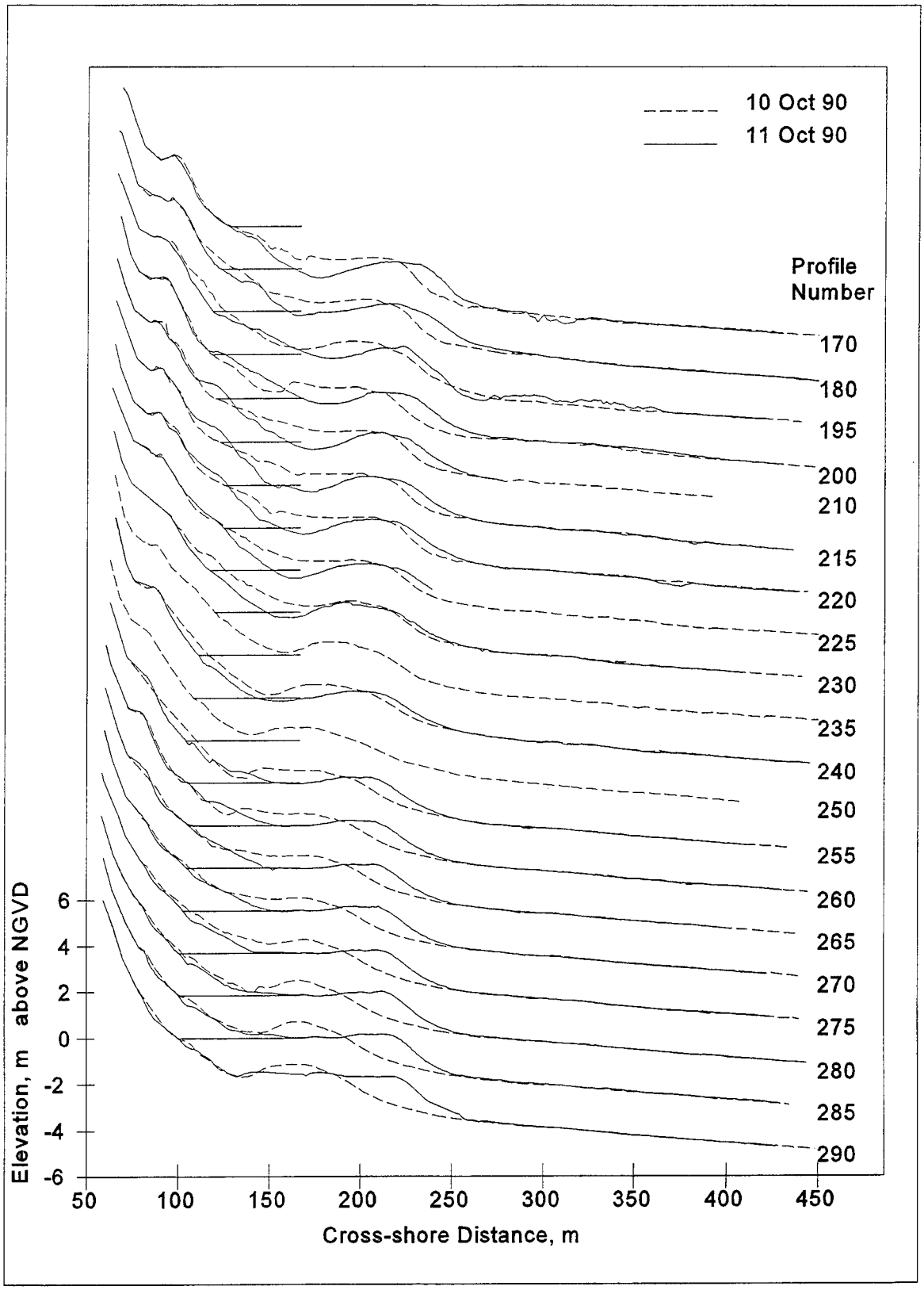

Figure A17. DELILAH profile line cross sections, 10-11 October 1990

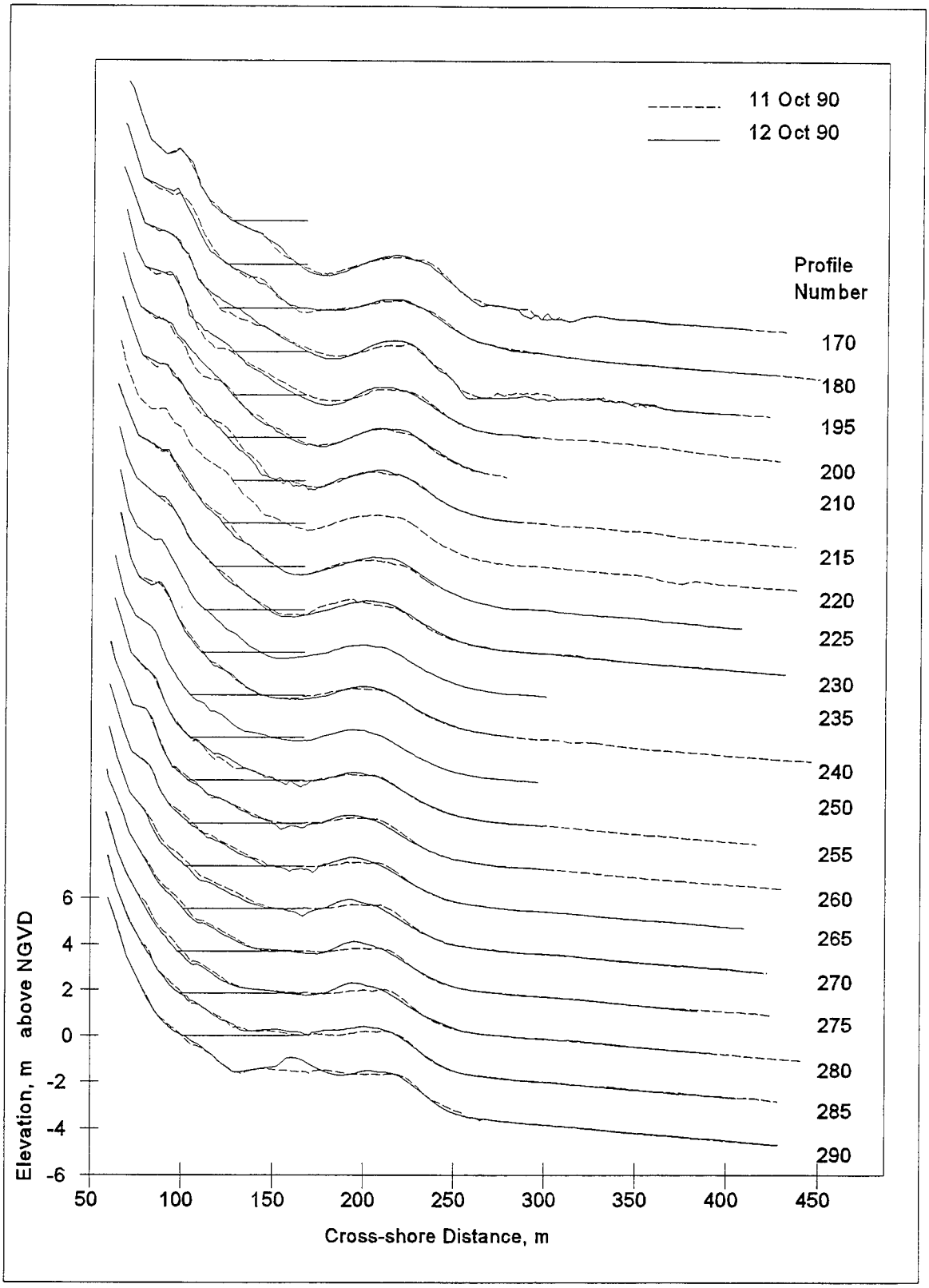

Figure A18. DELILAH profile line cross sections, 11-12 October 1990

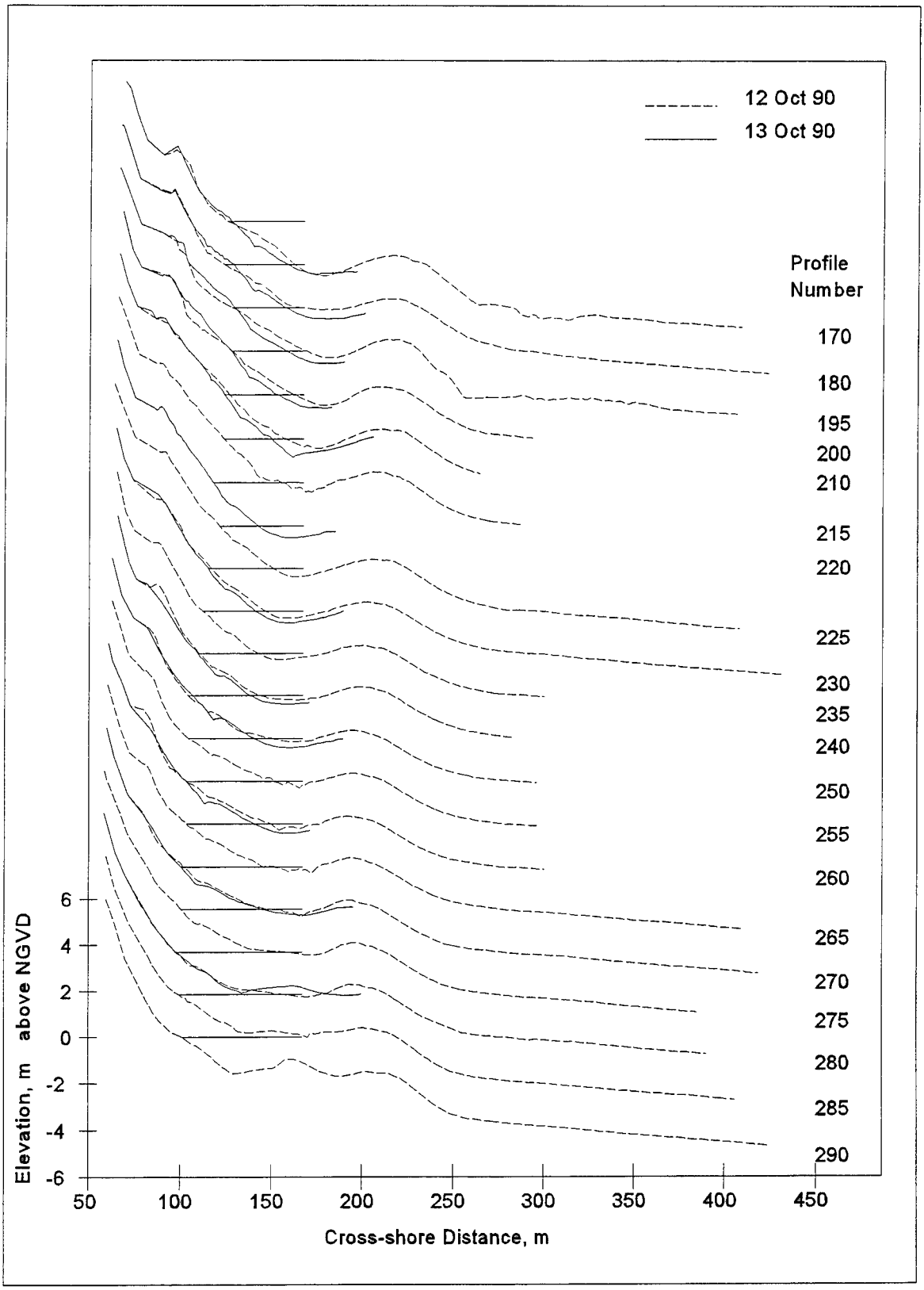

Figure A19. DELILAH profile line cross sections, 12-13 October 1990

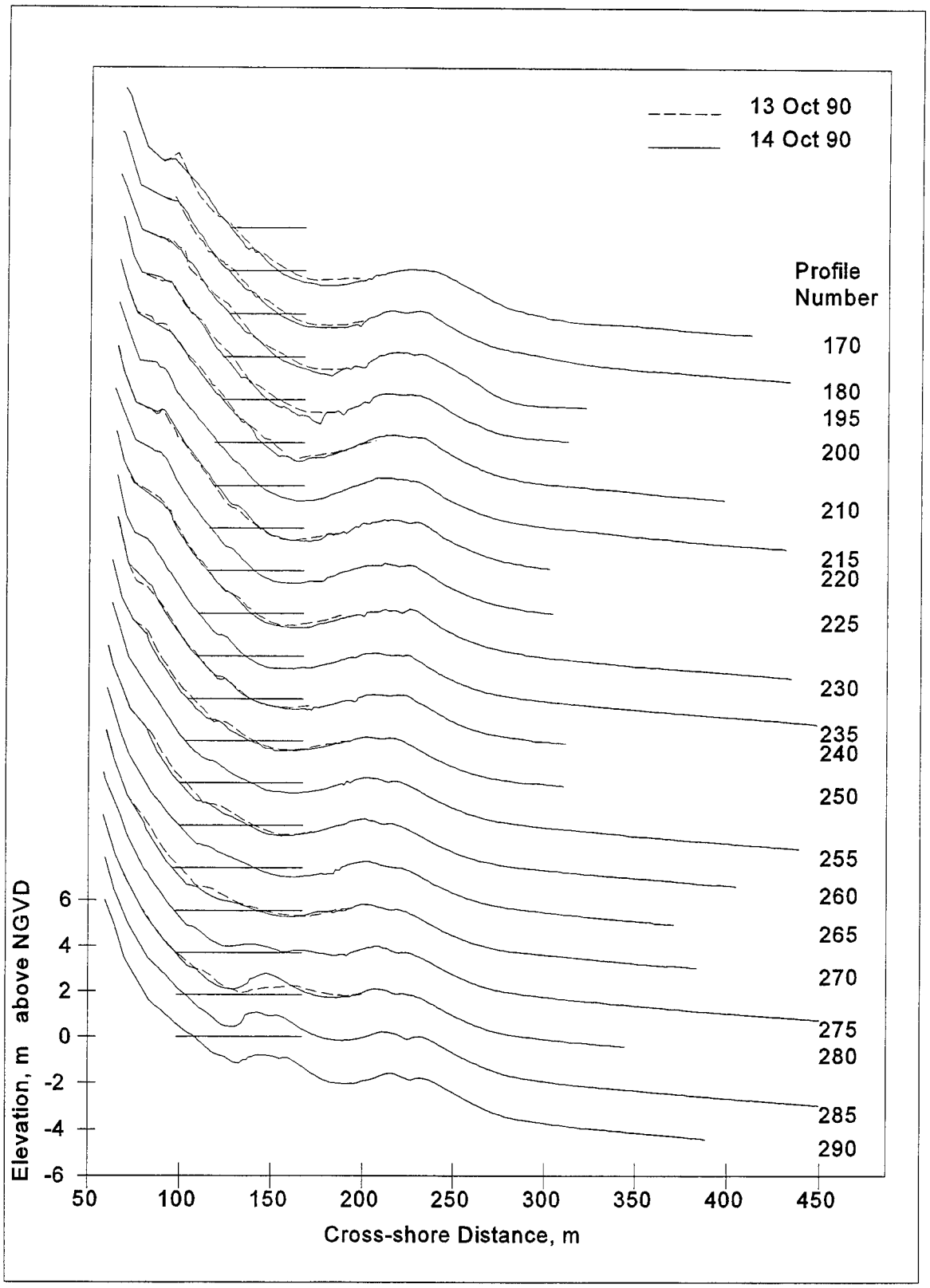

Figure A20. DELILAH profile line cross sections, 13-14 October 1990

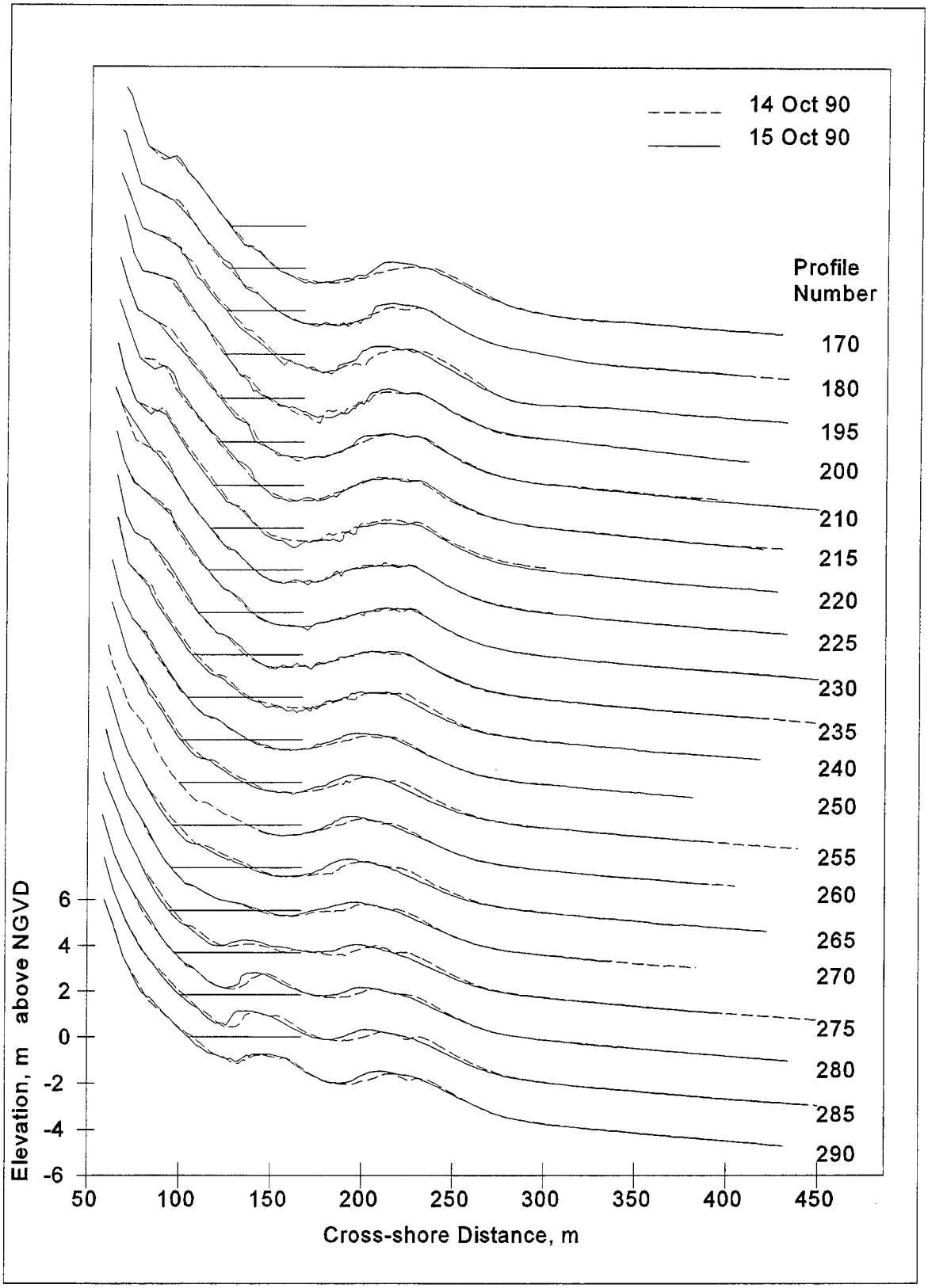

Figure A21. DELILAH profile line cross sections, 14-15 October 1990

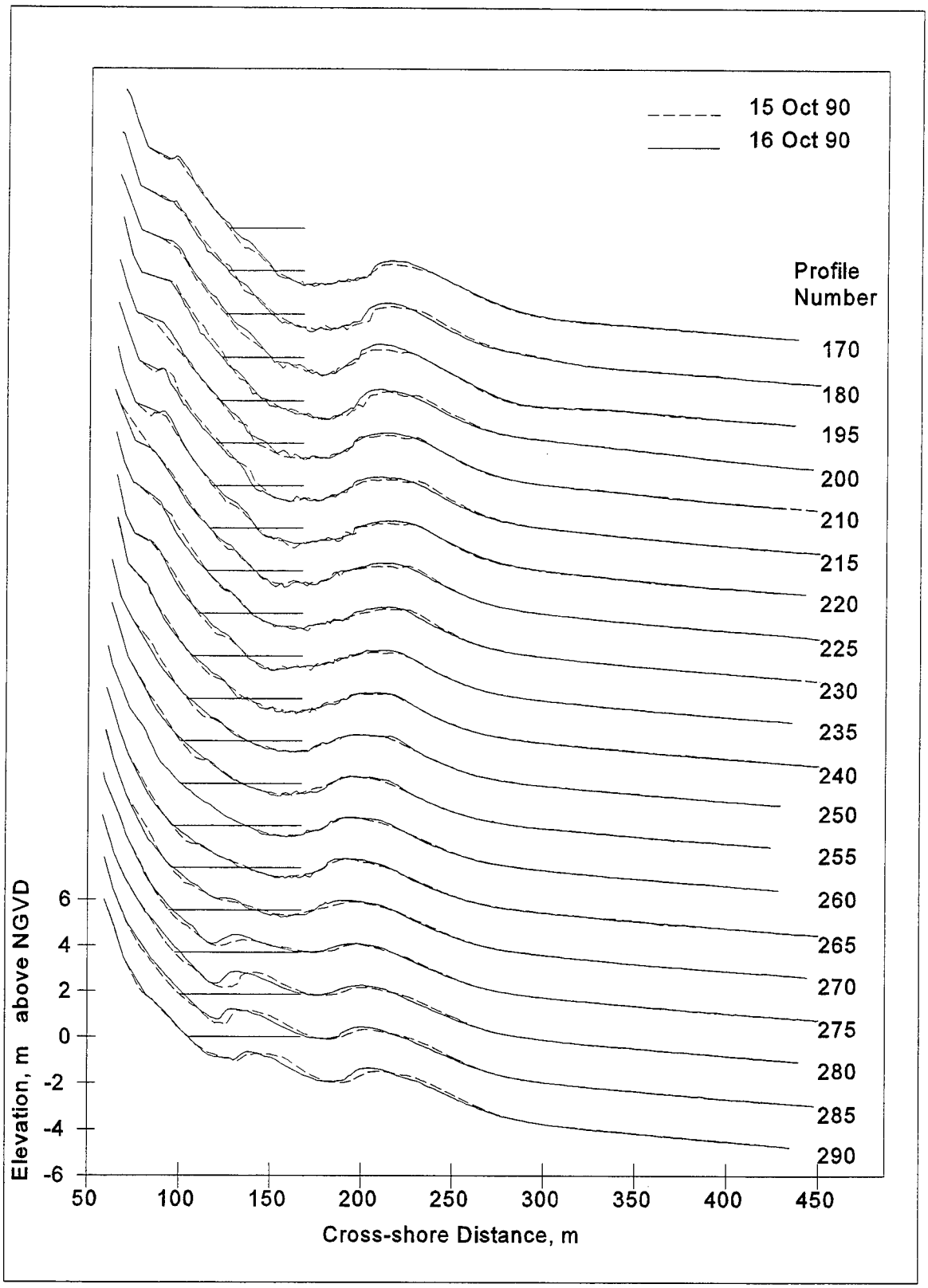

Figure A22. DELILAH profile line cross sections, 15-16 October 1990

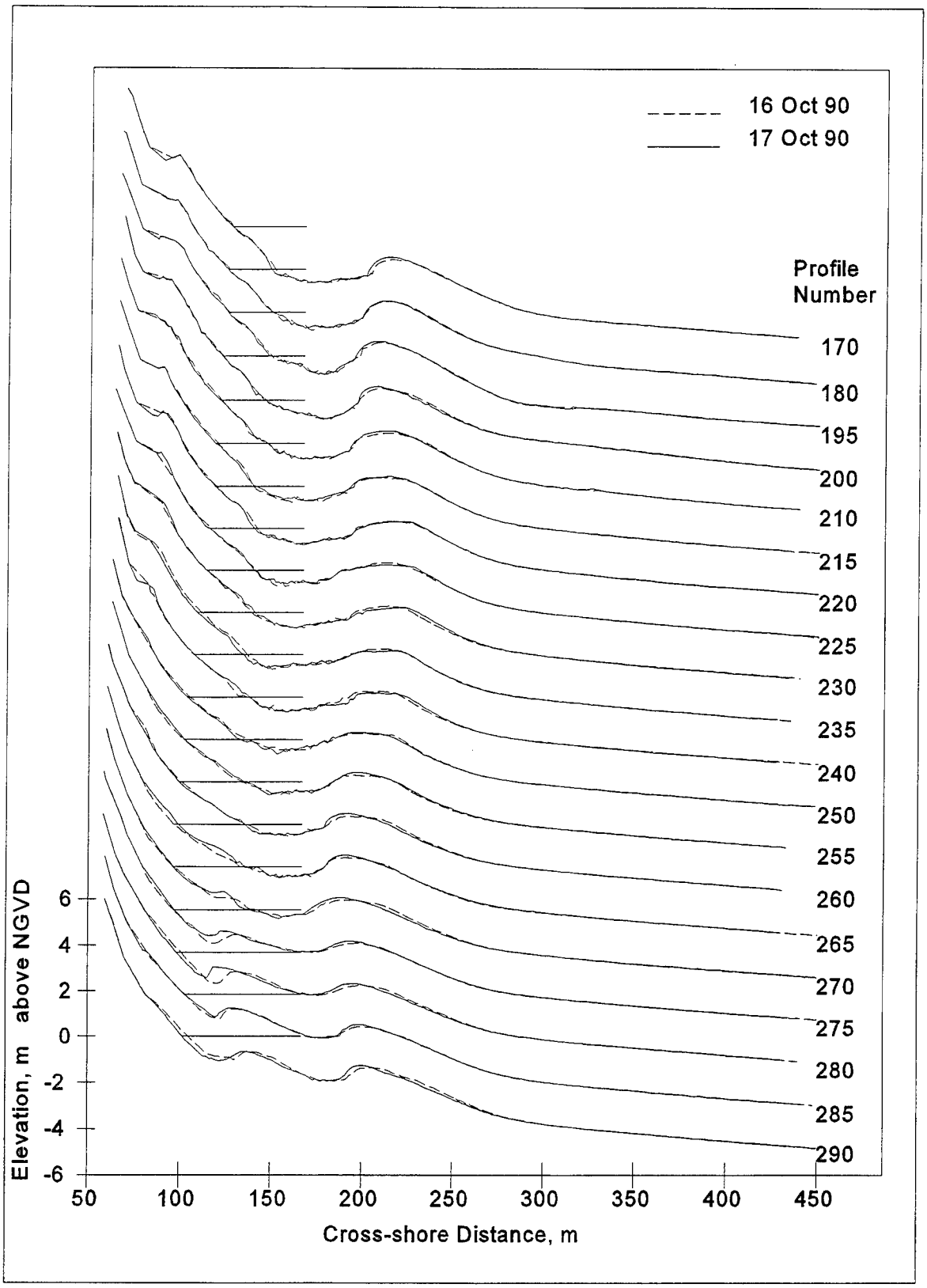

Figure A23. DELILAH profile line cross sections, 16-17 October 1990

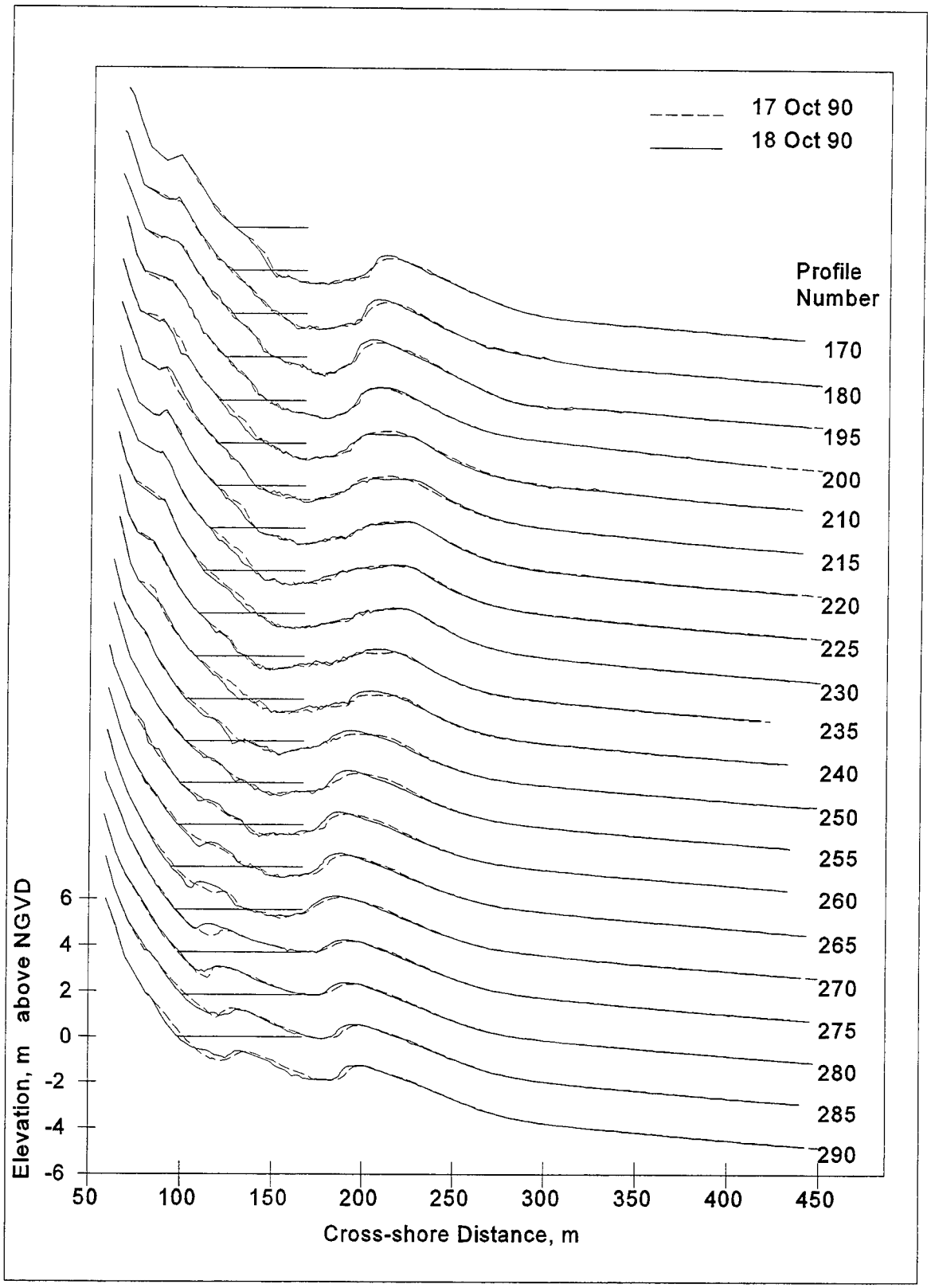

Figure A24. DELILAH profile line cross sections, 17-18 October 1990

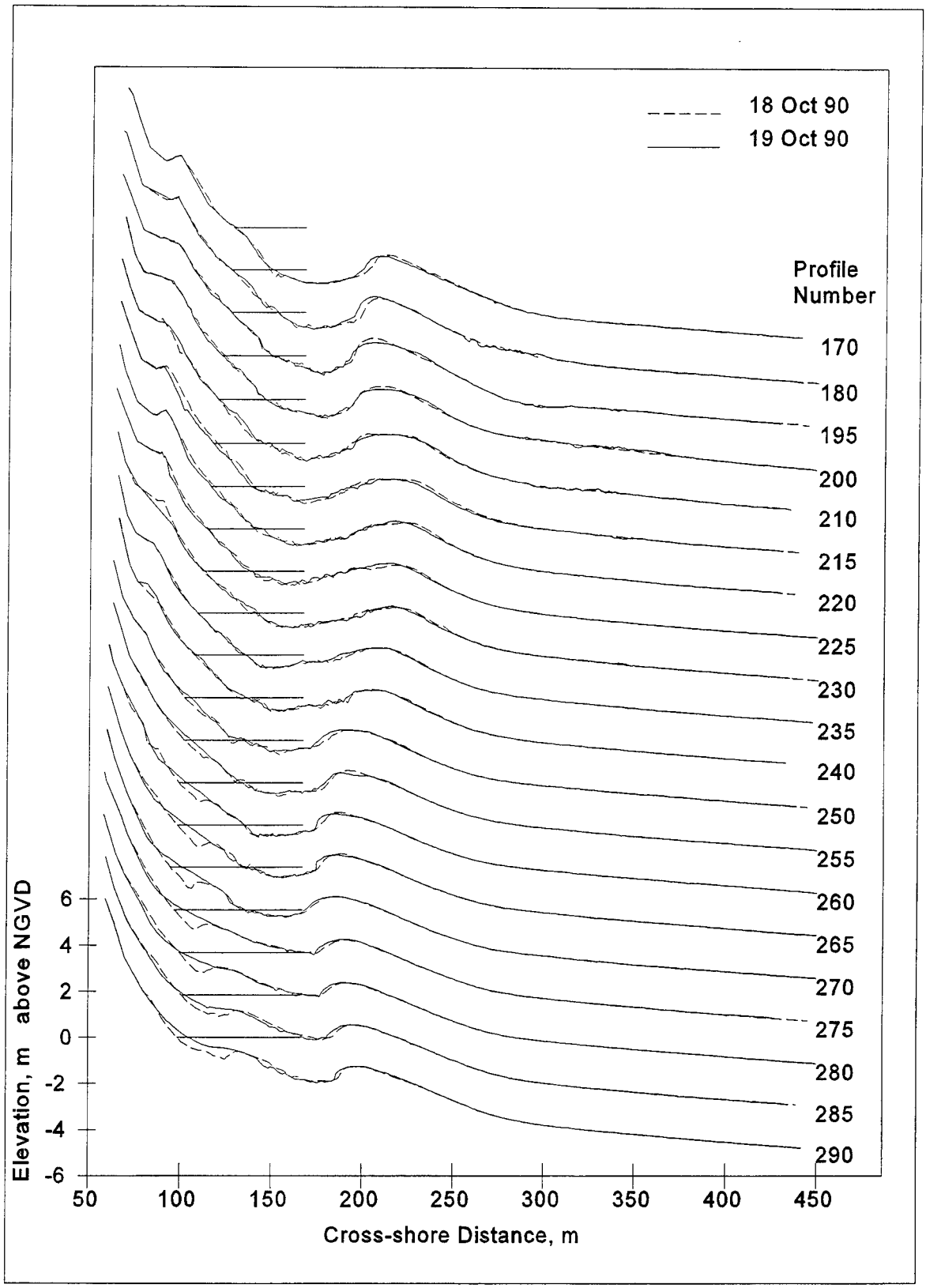

Figure A25. DELILAH profile line cross sections, 18-19 October 1990

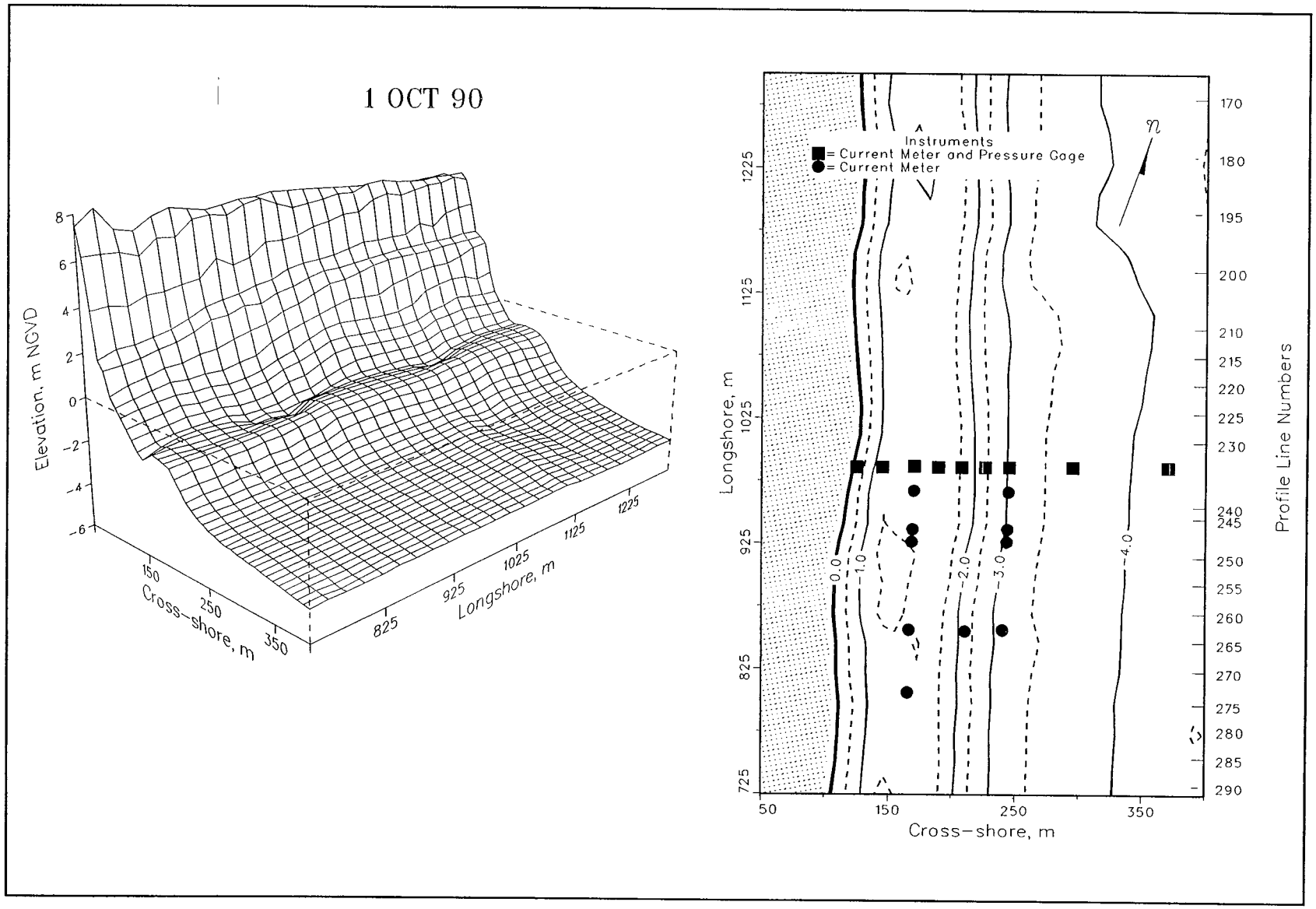

Figure A26. DELILAH Minigrid Survey, 1 October 1990

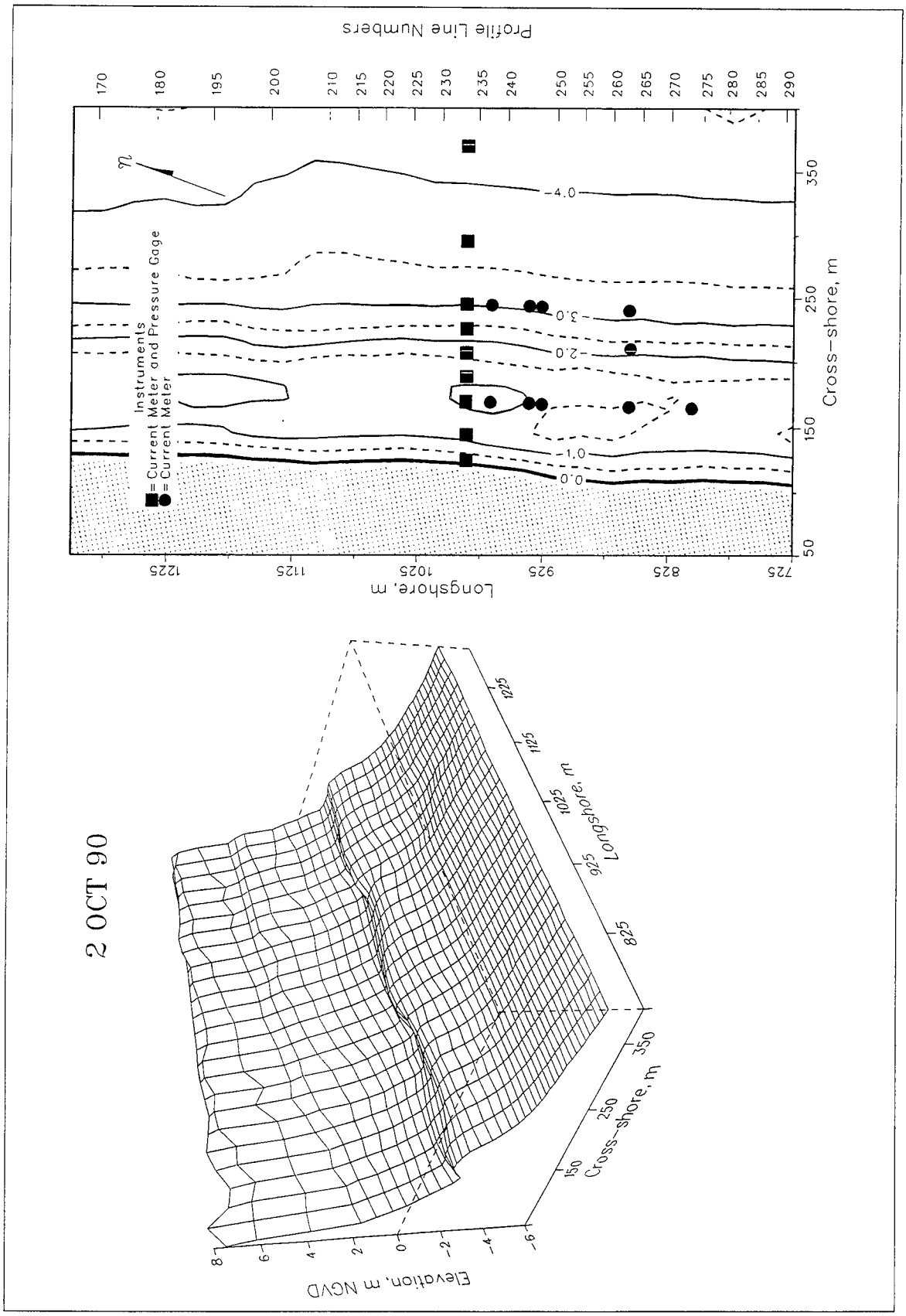

Figure A27. DELILAH Minigrid Survey, 2 October 1990

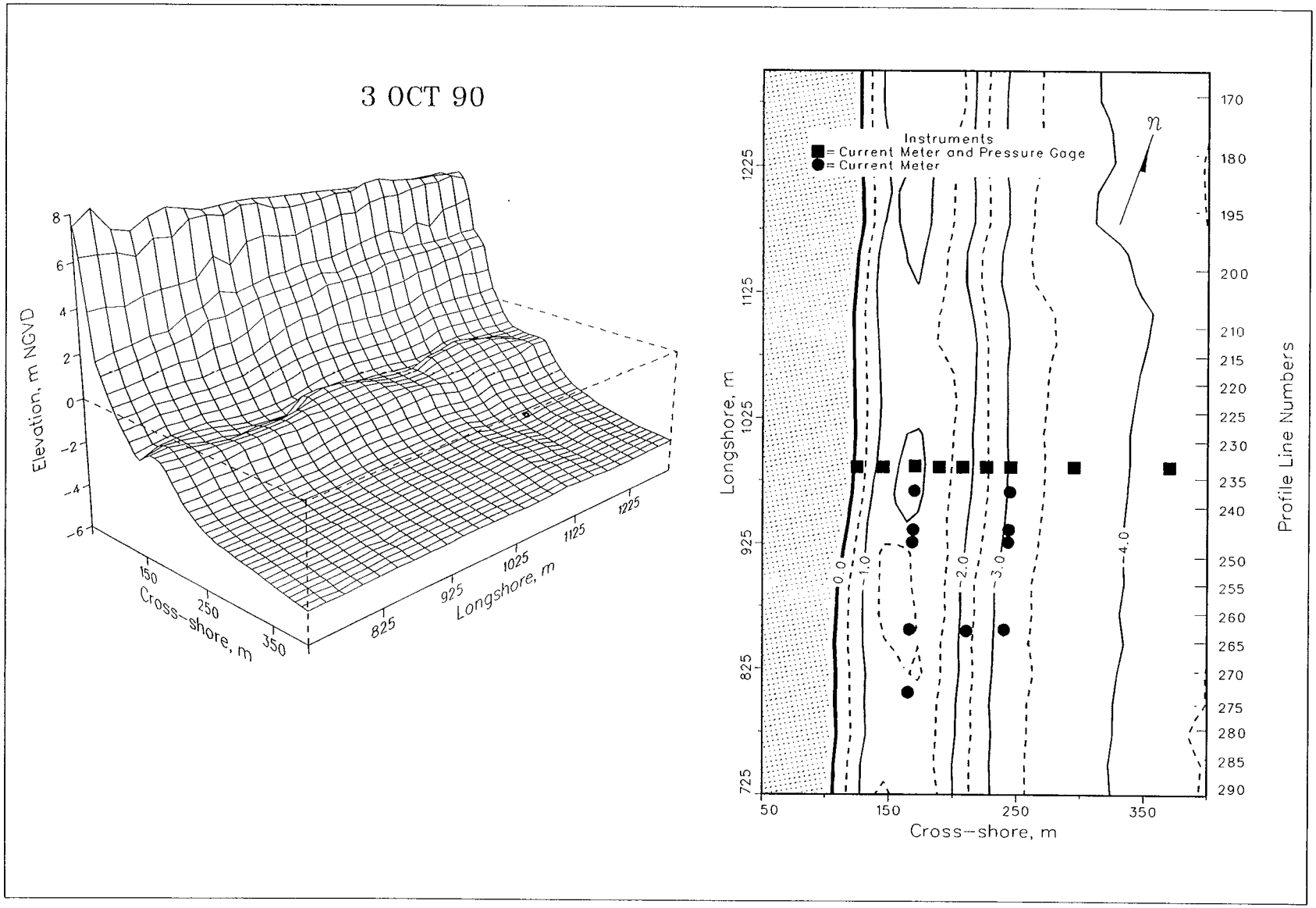

Figure A28. DELILAH Minigrid Survey, 3 October 1990

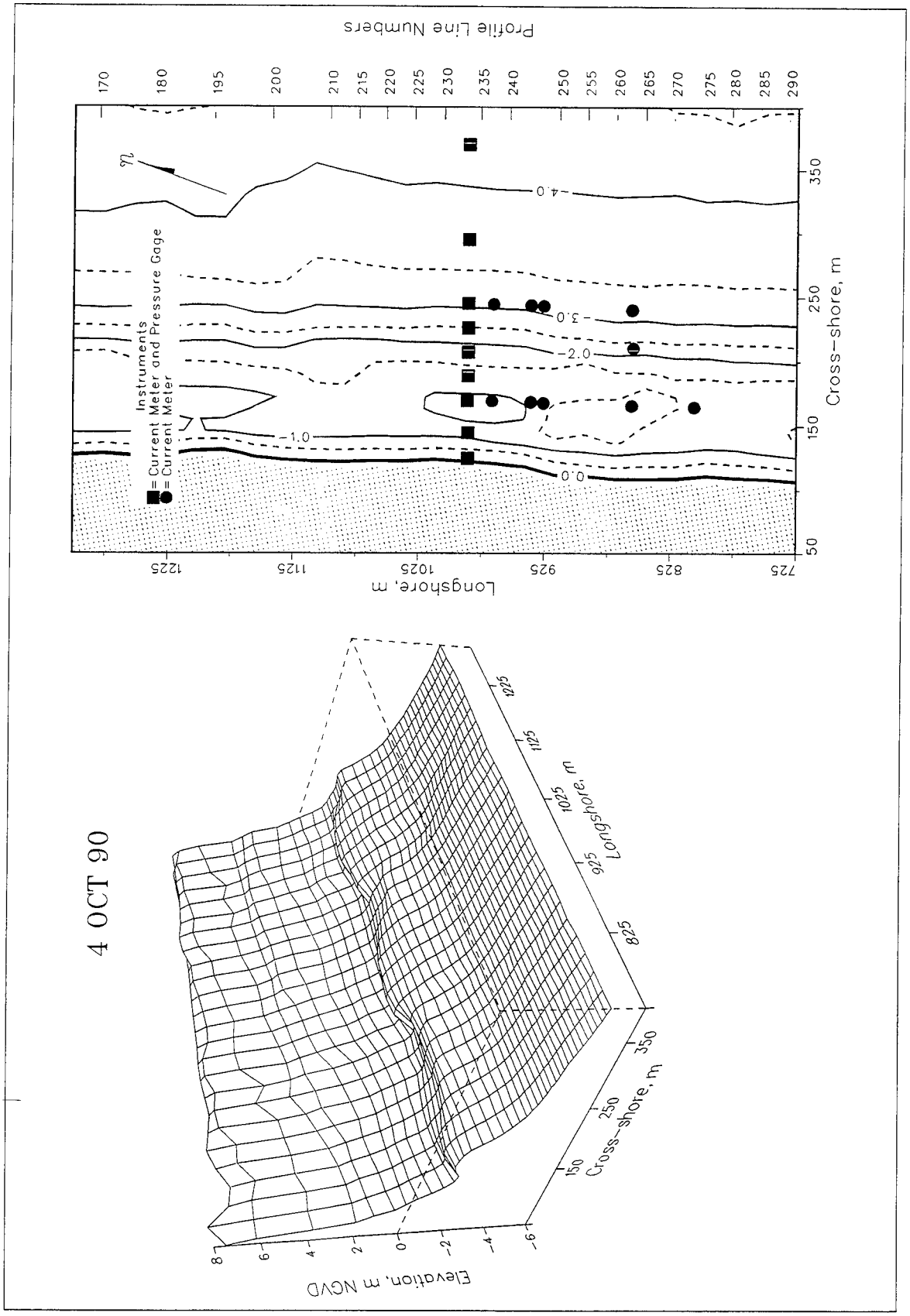

Figure A29. DELILAH Minigrid Survey, 4 October 1990

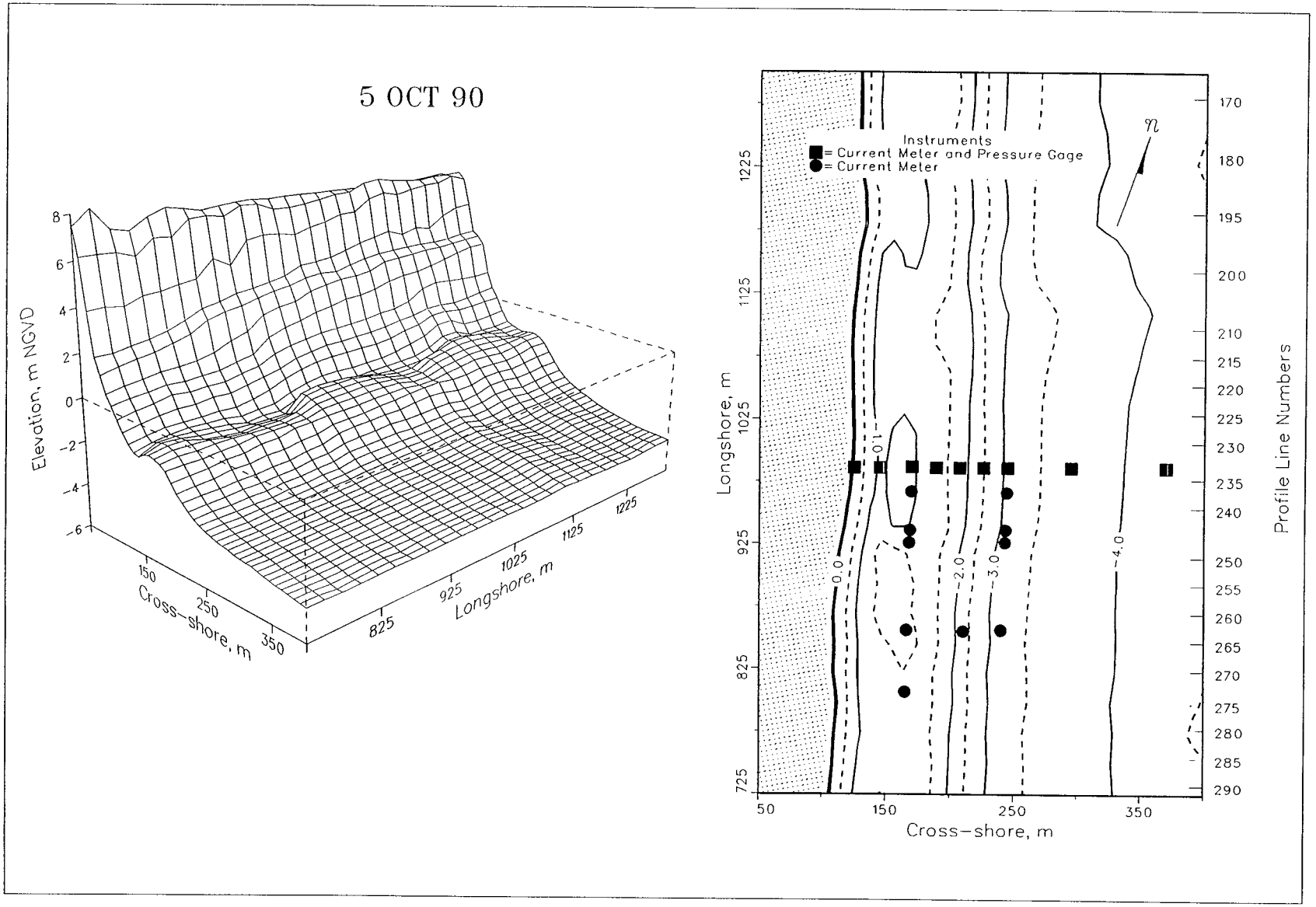

Figure A30. DELILAH Minigrid Survey, 5 October 1990

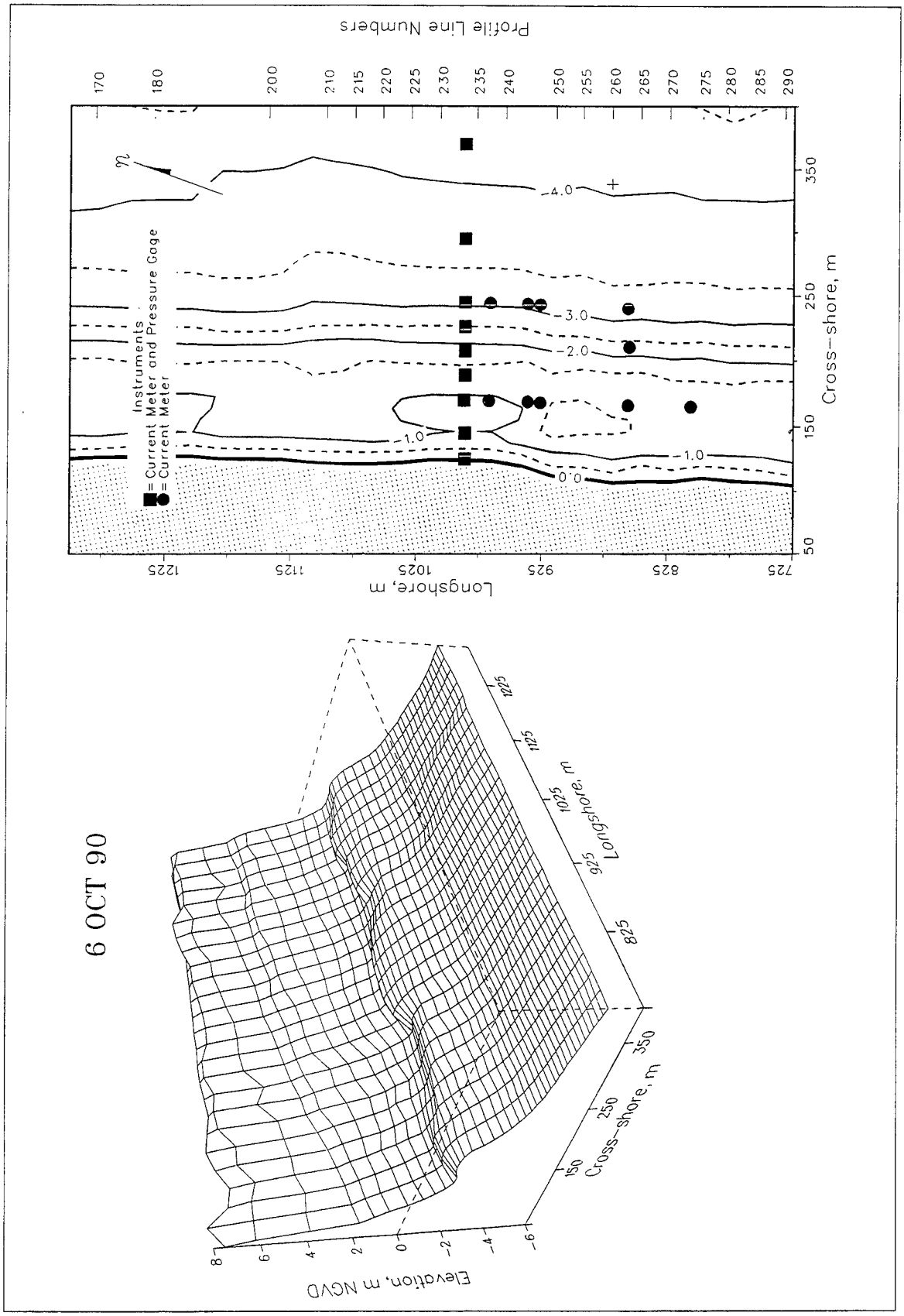

Figure A31. DELILAH Minigrid Survey, 6 October 1990 (crosses on right panel mark end of survey lines)

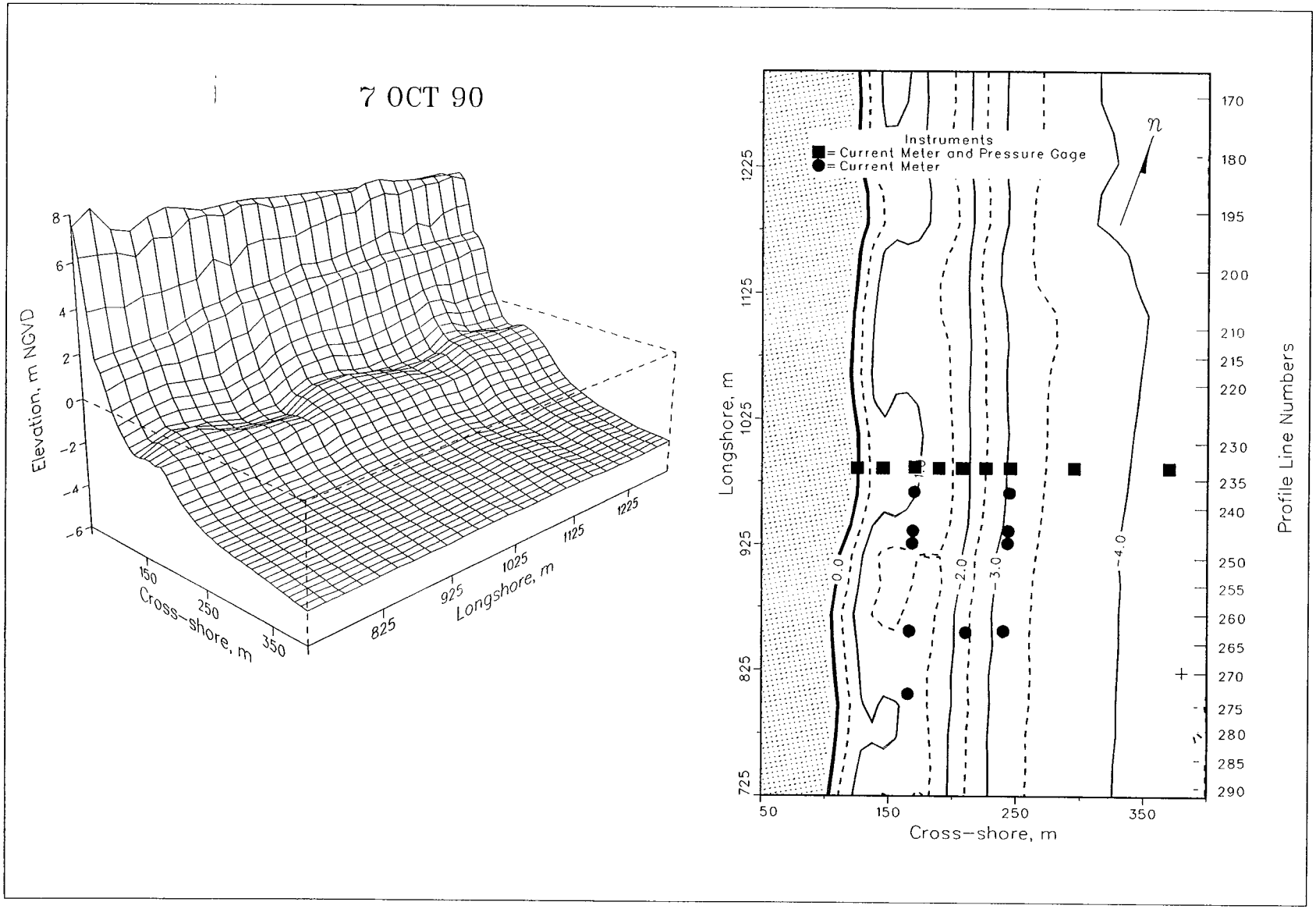

Figure A32. DELILAH Minigrid Survey, 7 October 1990 (crosses on right panel mark end of survey lines)

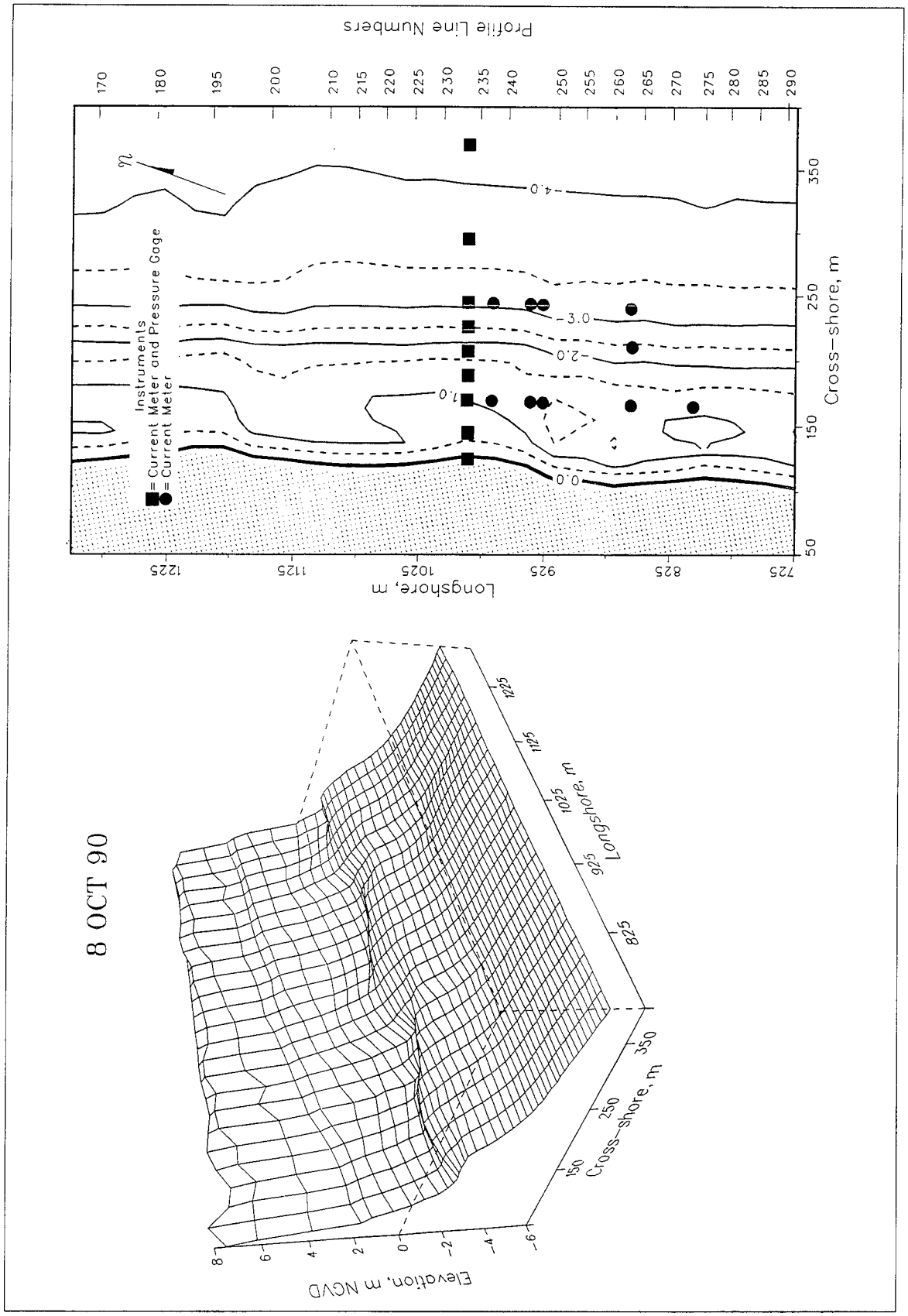

Figure A33. DELILAH Minigrid Survey, 8 October 1990

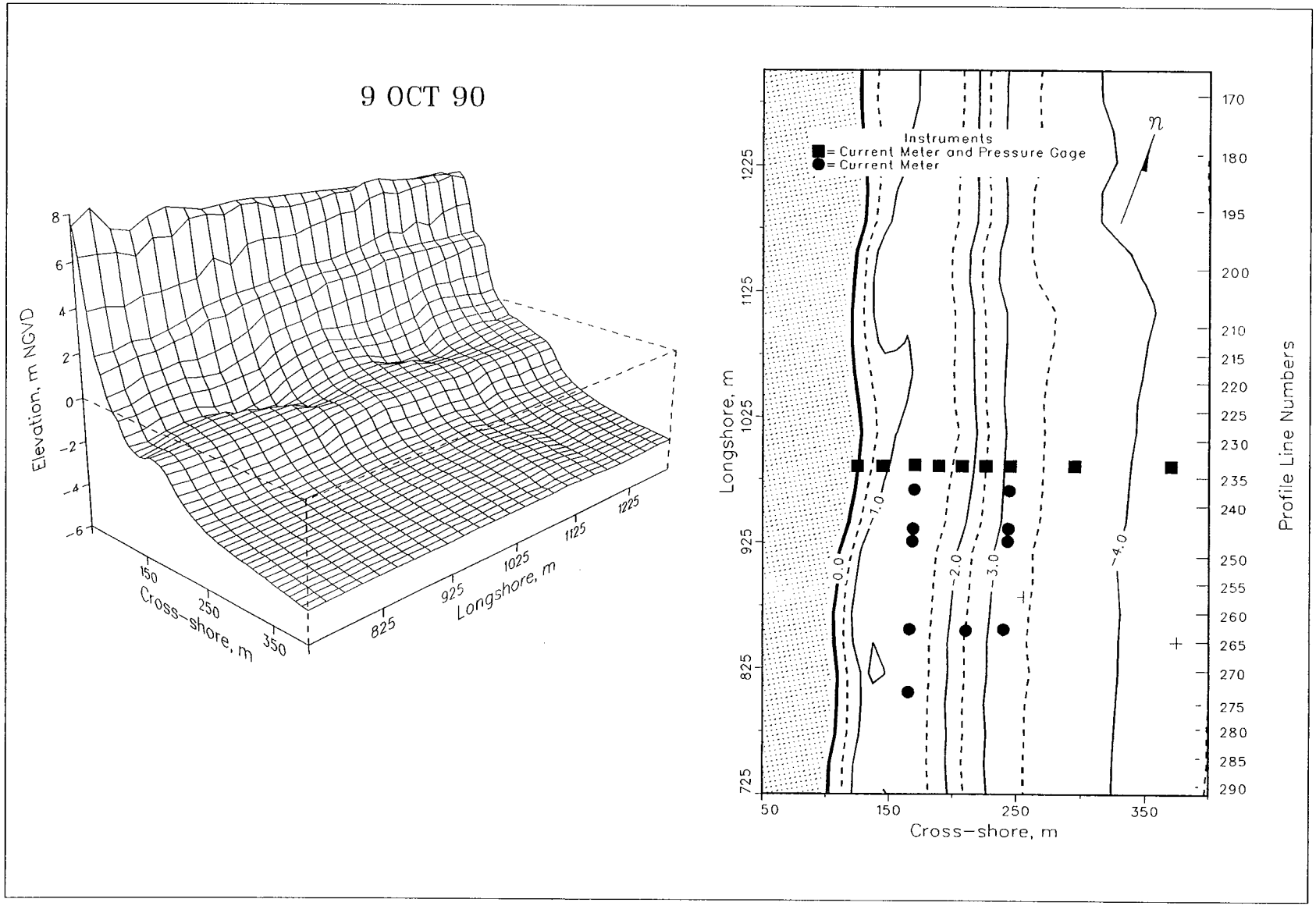

Figure A34. DELILAH Minigrid Survey, 9 October 1990 (crosses on right panel mark end of survey lines)

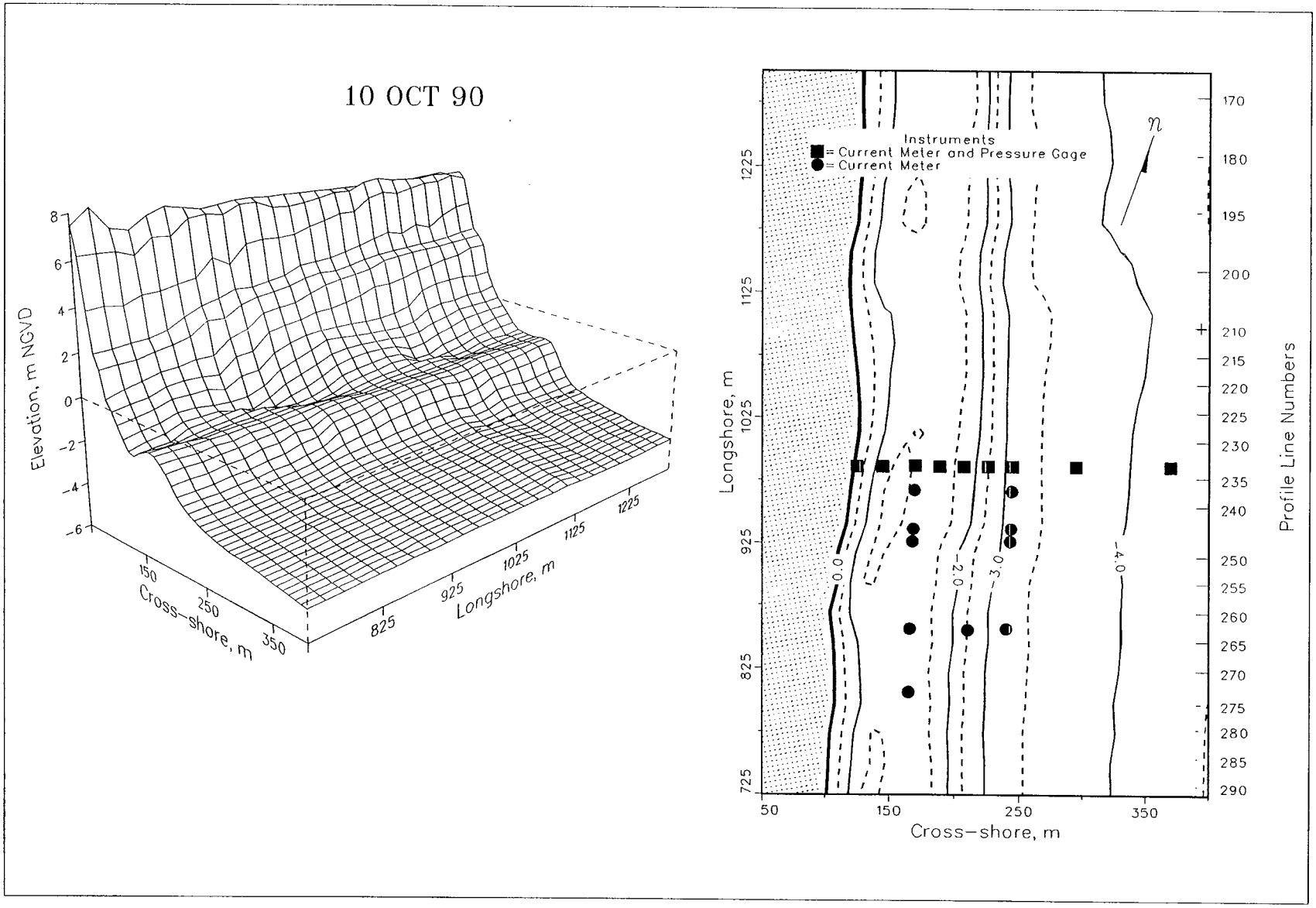

Figure A35. DELILAH Minigrid Survey, 10 October 1990

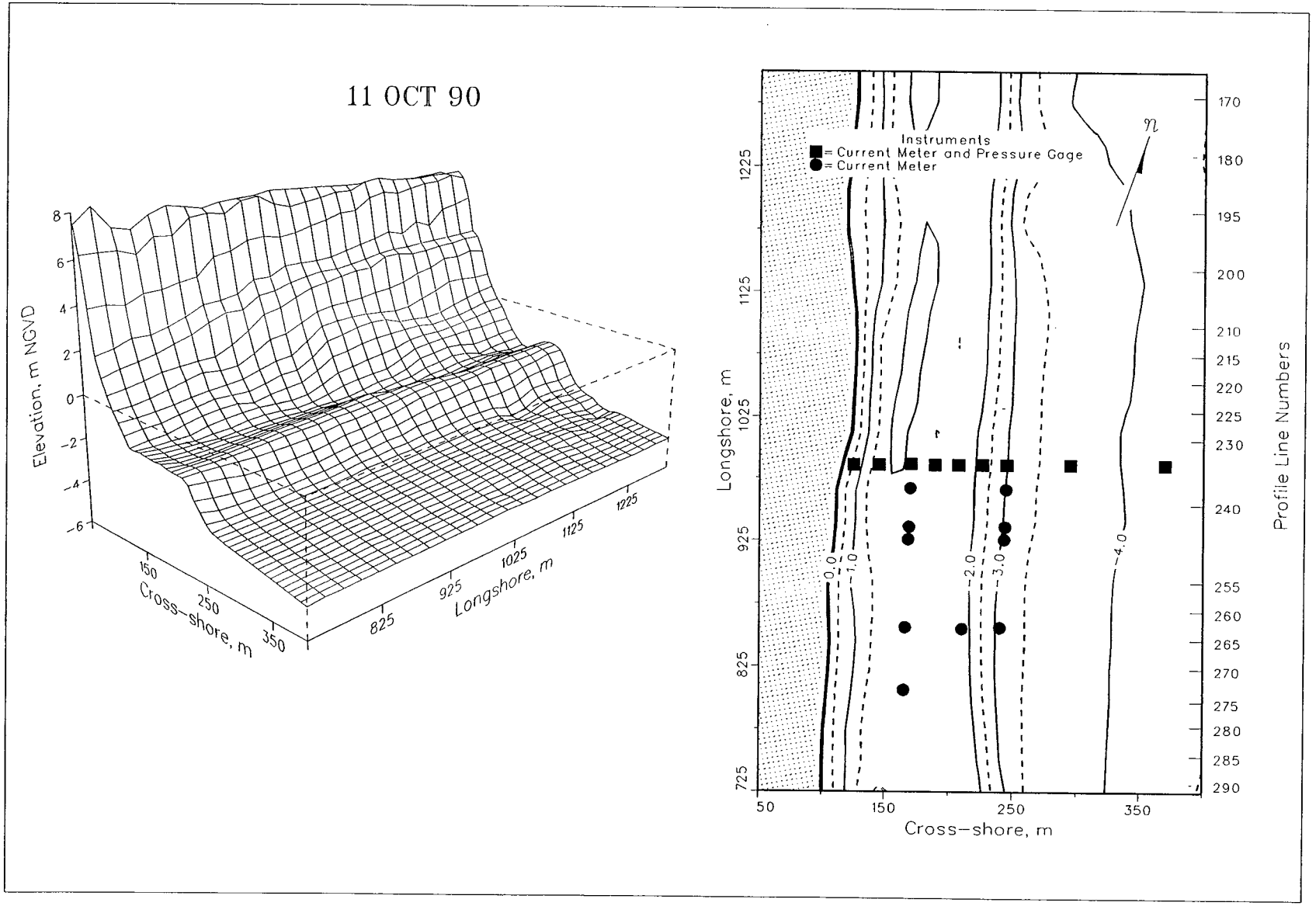

Figure A36. DELILAH Minigrid Survey, 11 October 1990

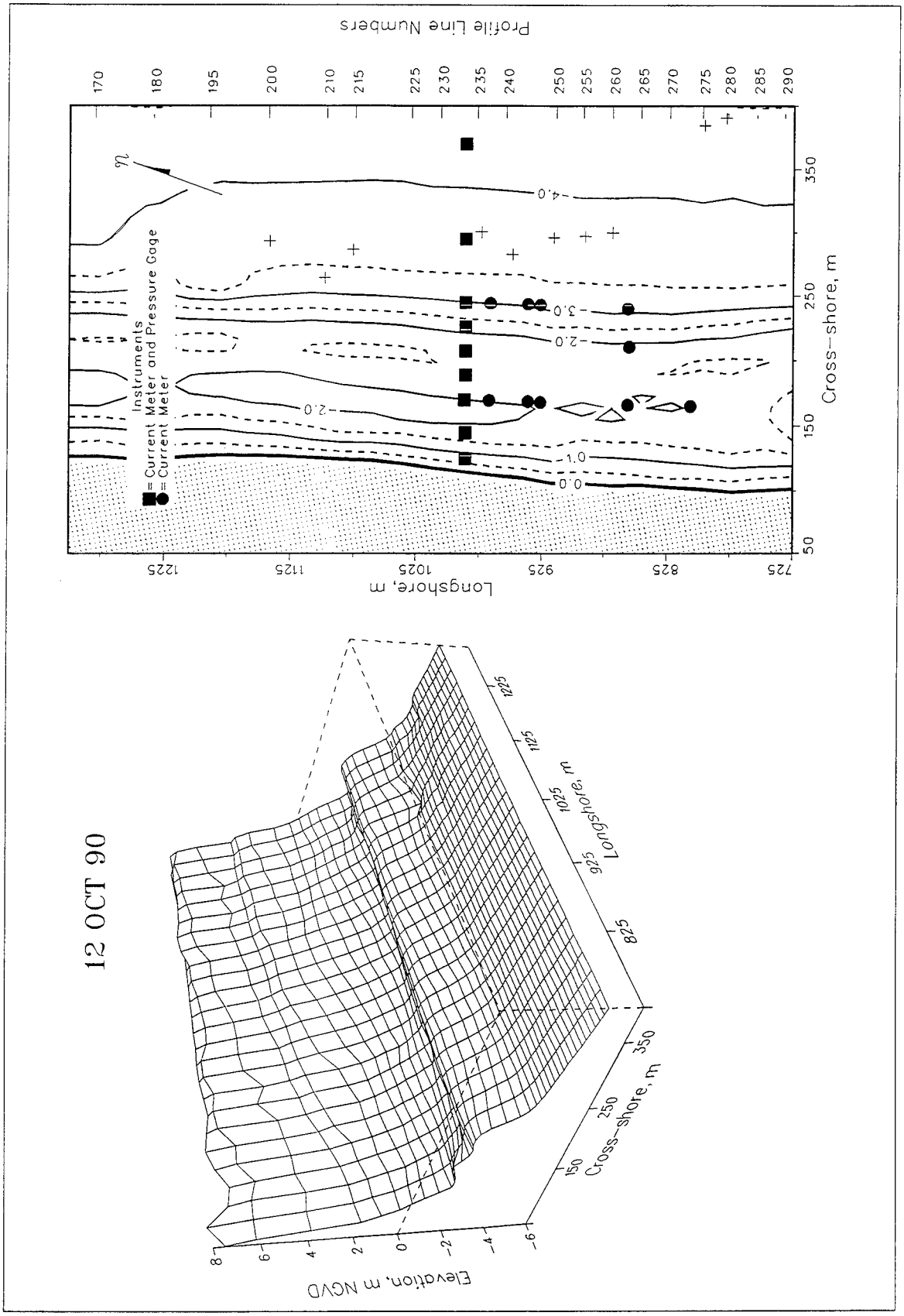

Figure A37. DELILAH Minigrid Survey, 12 October 1990 (crosses on right panel mark end of survey lines)

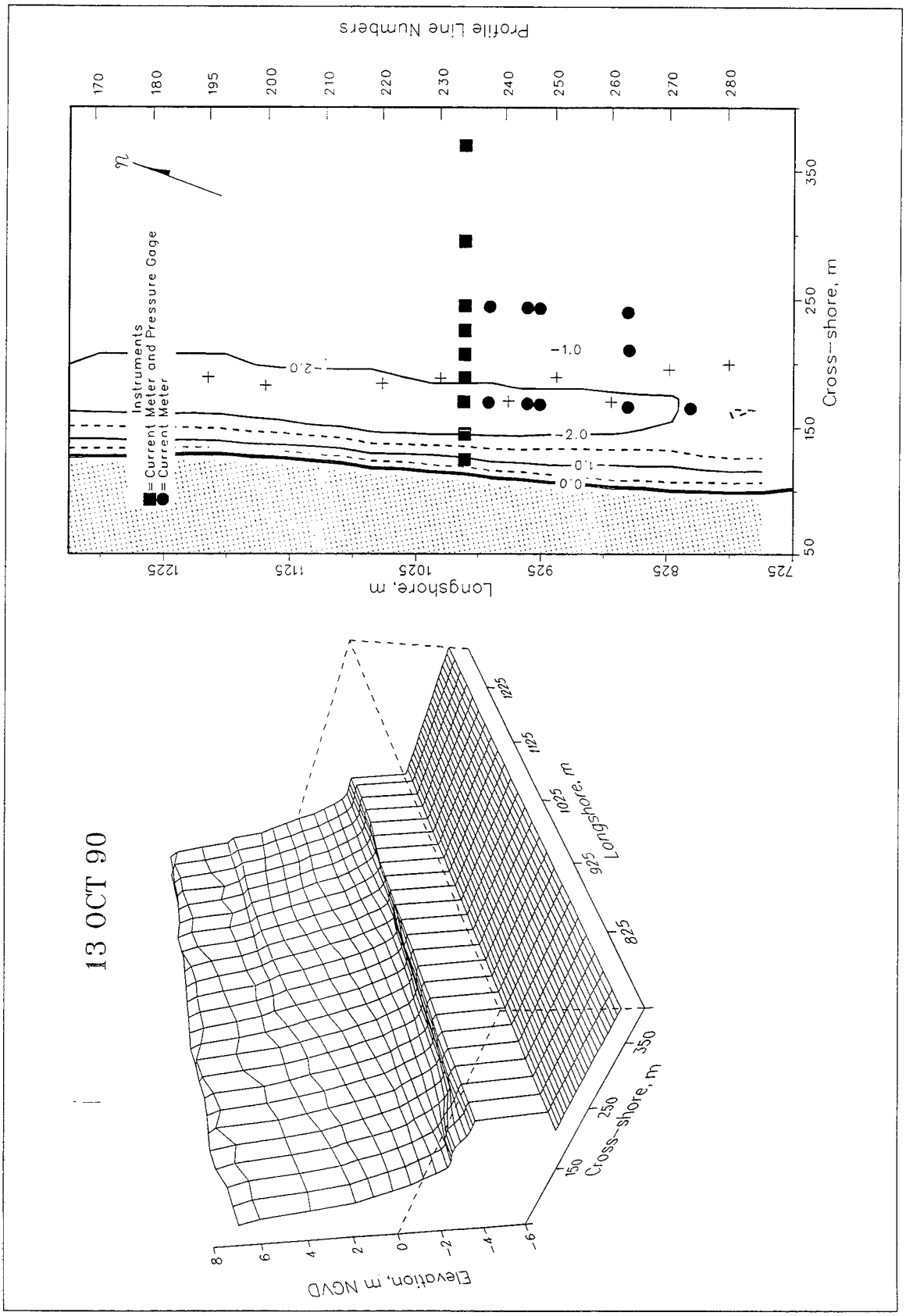

Figure A38. DELILAH Minigrid Survey, 13 October 1990 (crosses on right panel mark end of survey lines)

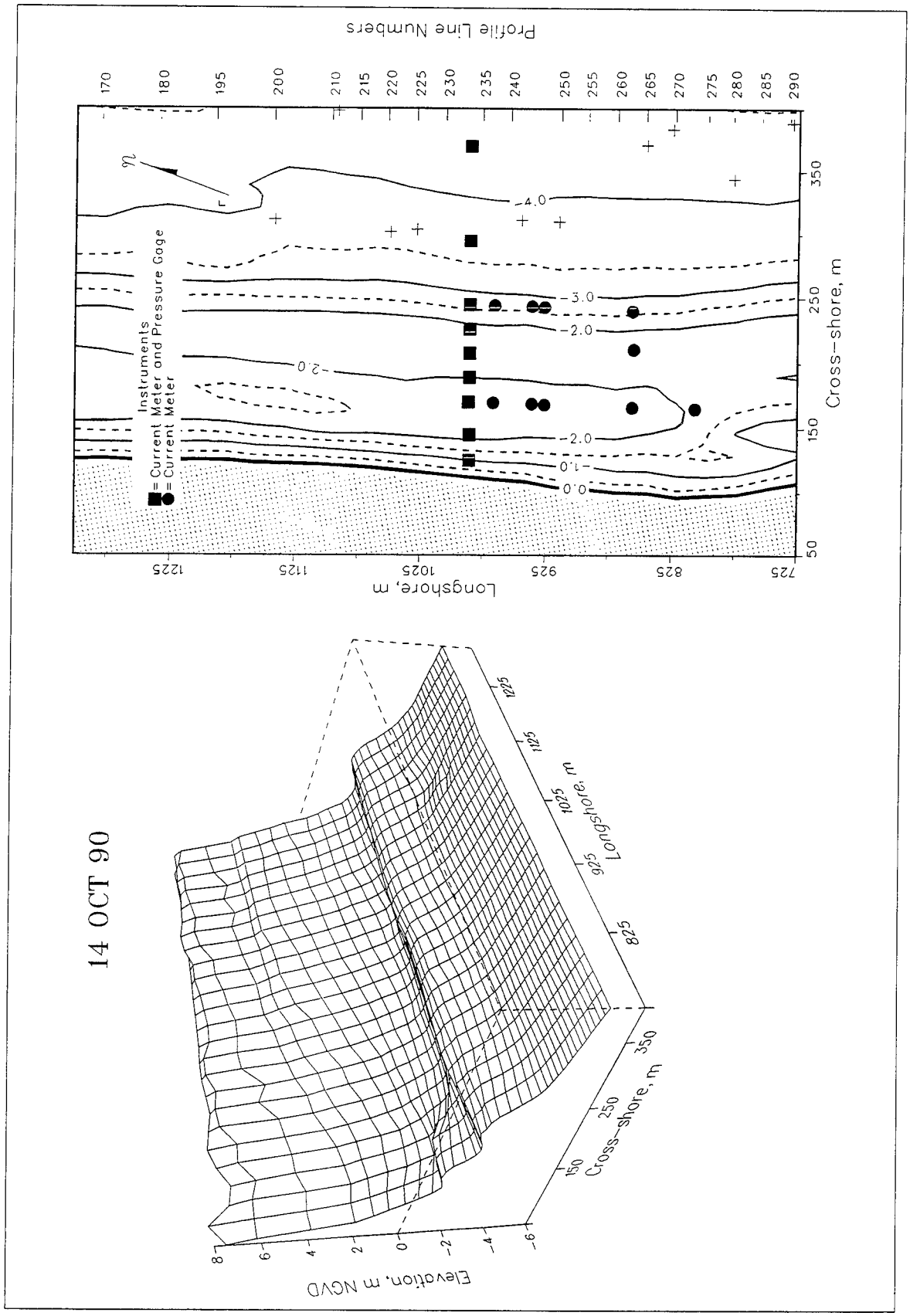

Figure A39. DELILAH Minigrid Survey, 14 October 1990 (crosses on right panel mark end of survey lines)

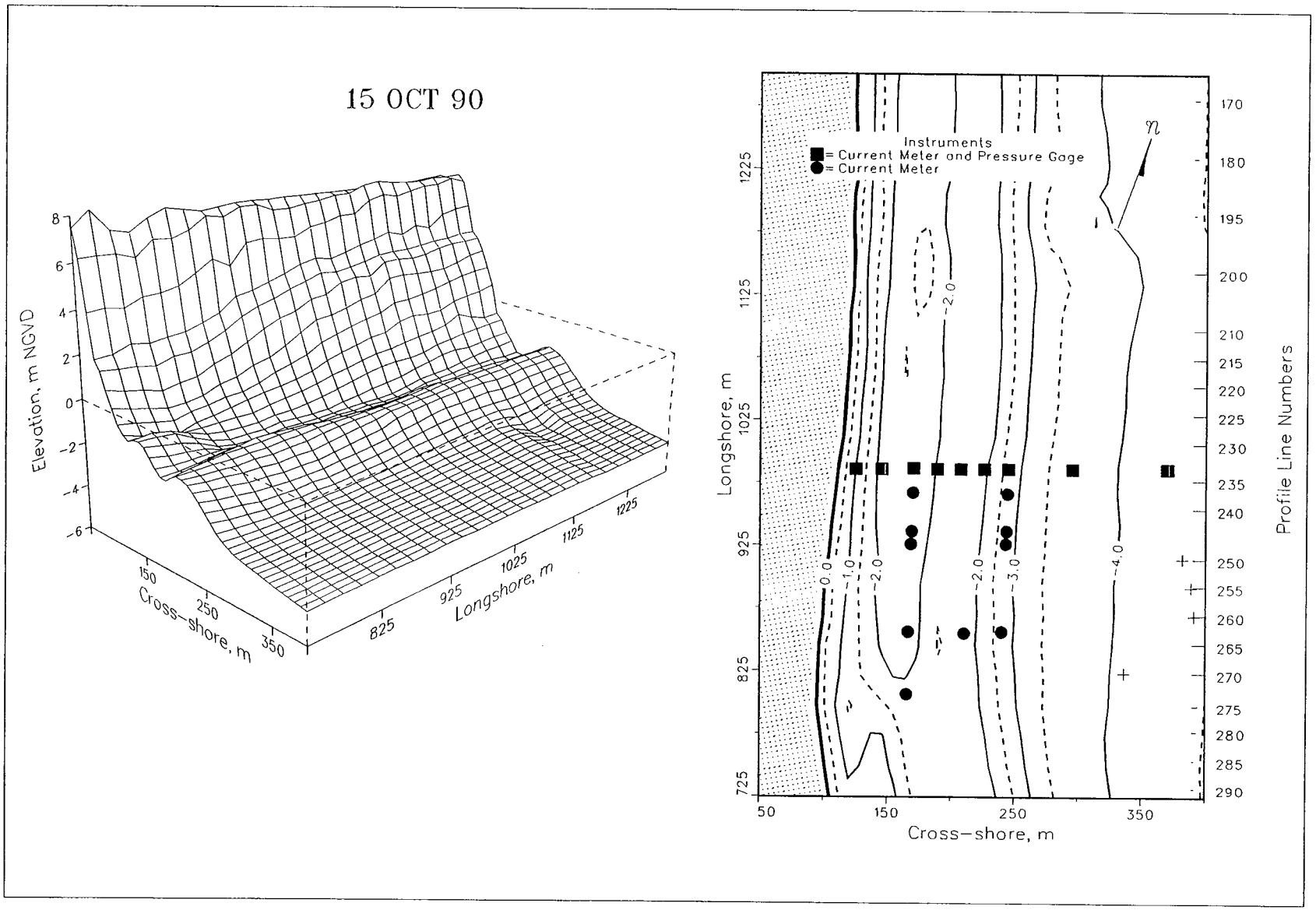

Figure A40. DELILAH Minigrid Survey, 15 October 1990 (crosses on right panel mark end of survey lines)

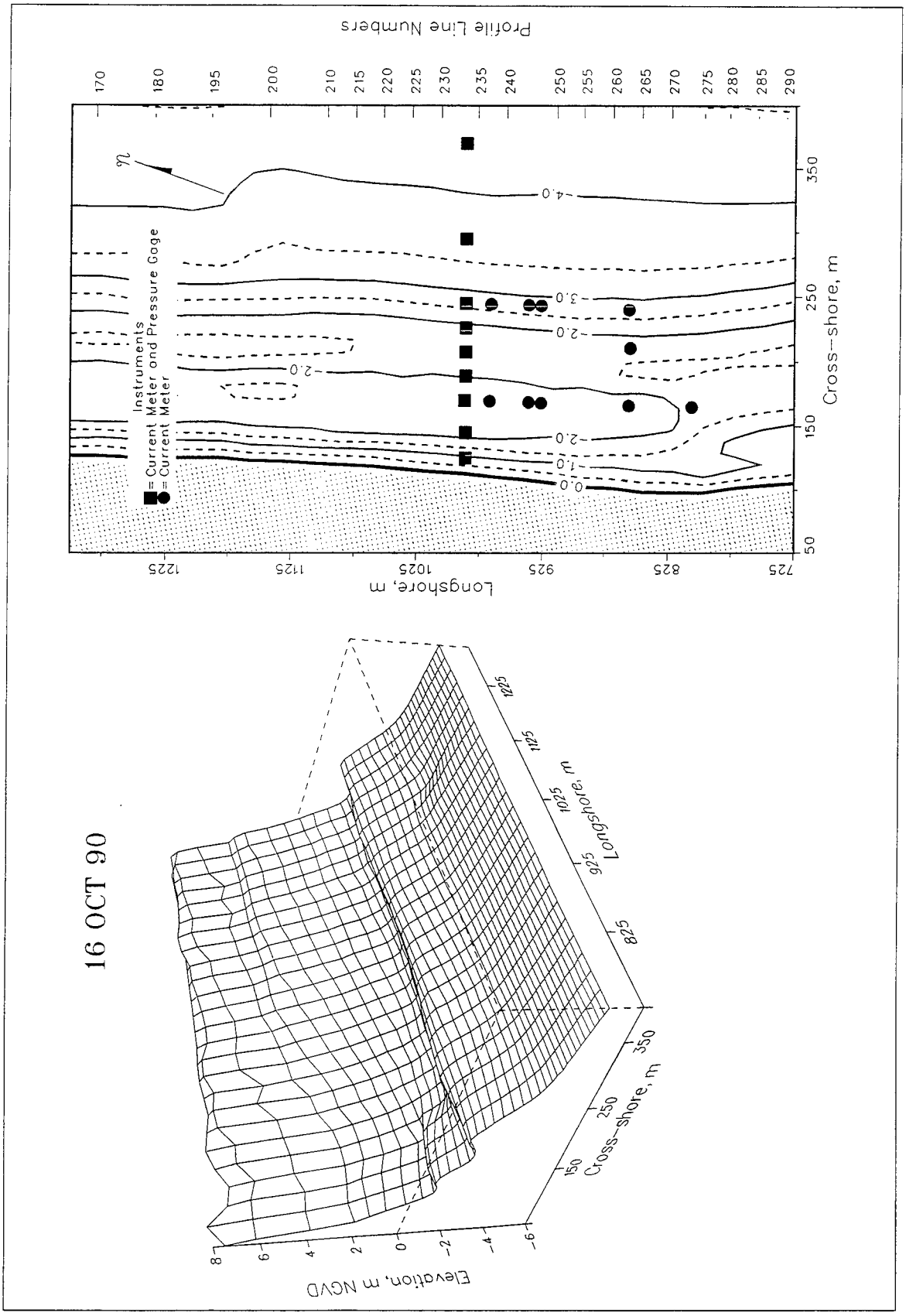

Figure A41. DELILAH Minigrid Survey, 16 October 1990

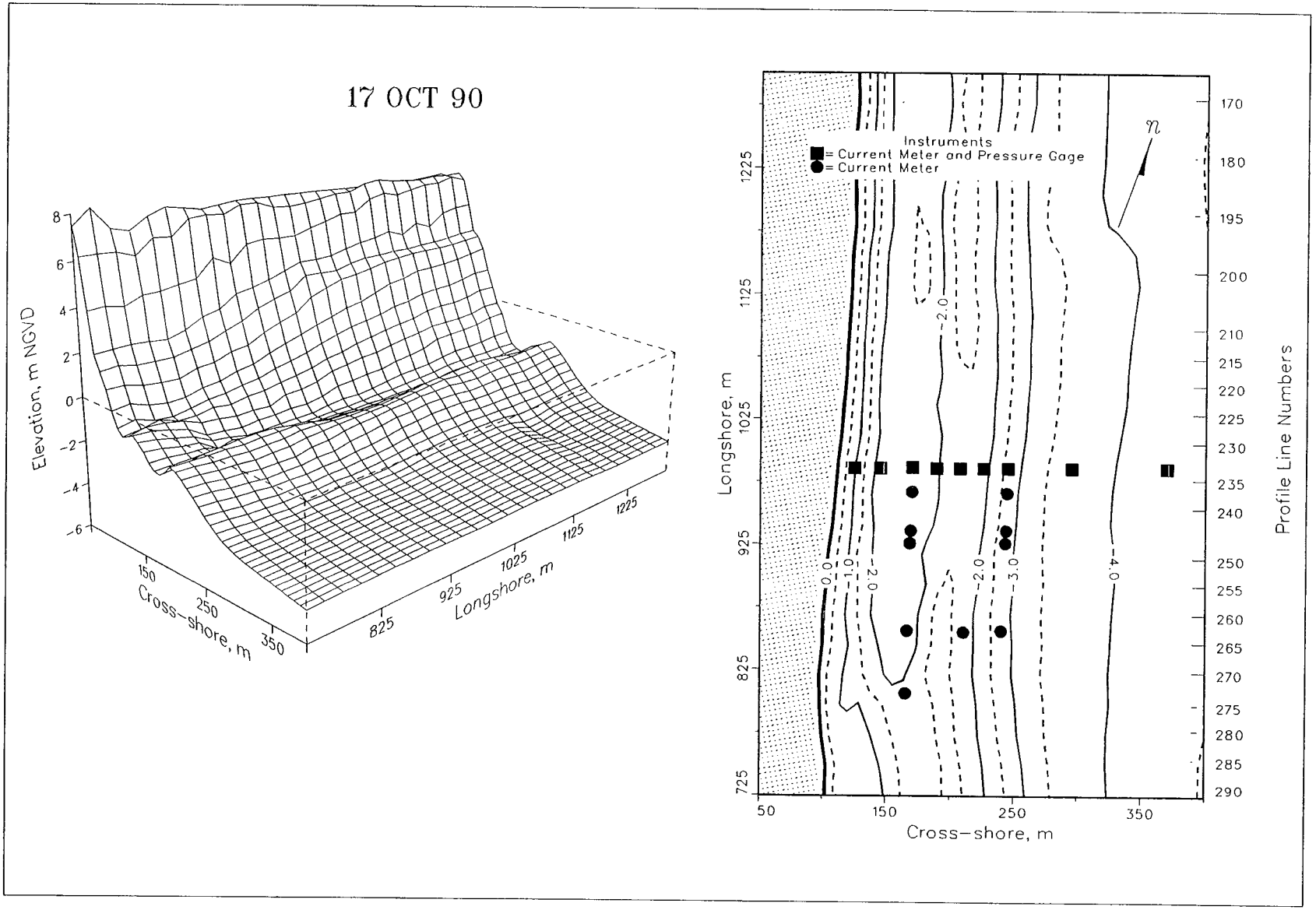

Figure A42. DELILAH Minigrid Survey, 17 October 1990

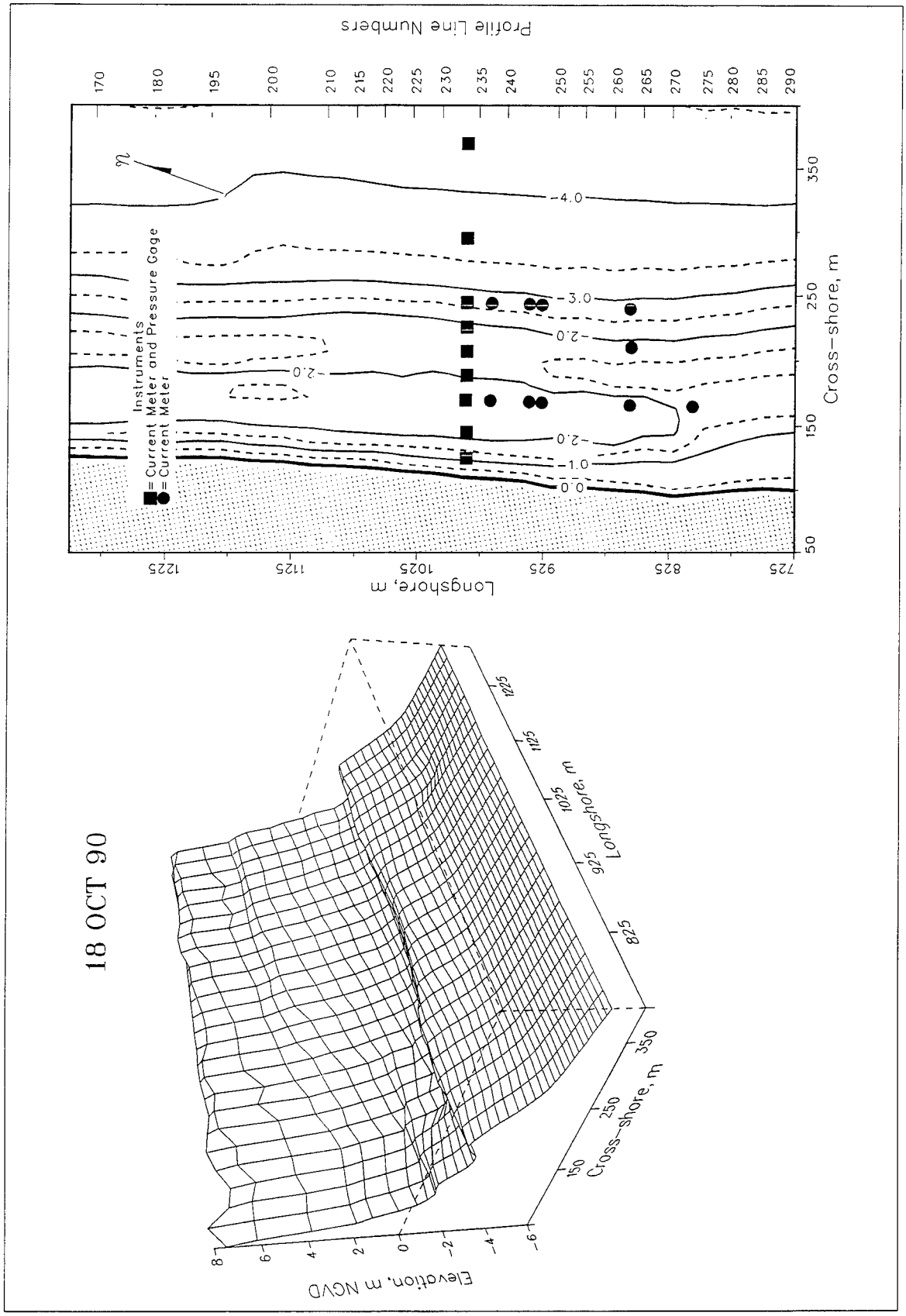

Figure A43. DELILAH Minigrid Survey, 18 October 1990

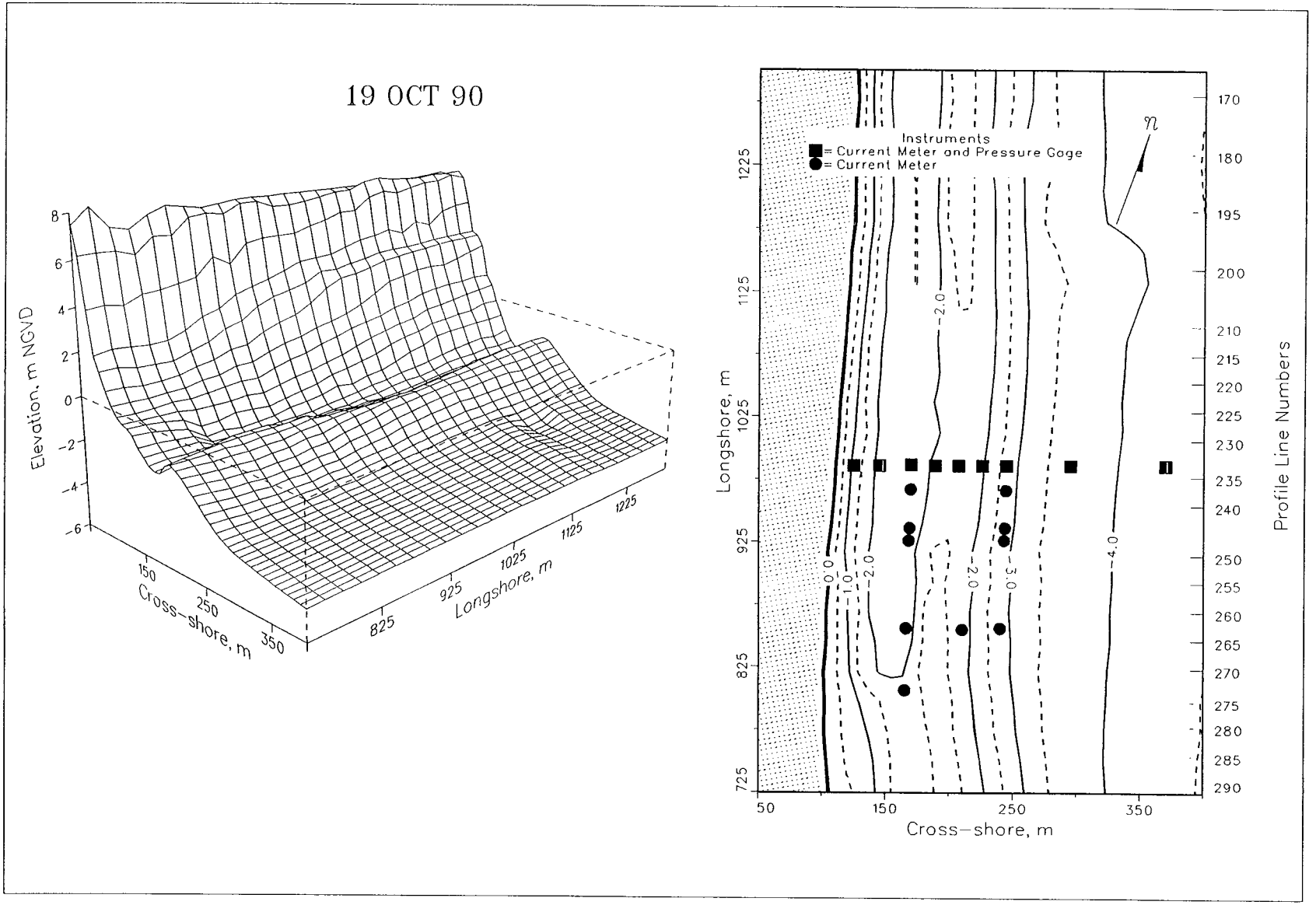

Figure A44. DELILAH Minigrid Survey, 19 October 1990

Appendix B
Video Data

Seven monochrome video cameras (Table B1) were mounted on the Field Research Facility's (FRF's) 42-m-tall tower (Figure B1) and aimed at the minigrid area. These cameras were used to monitor wave run-up and incident wave dissipation. Runup cameras (R1, R2, and R3) used telephoto lenses for improved spatial resolution and viewed different regions of the beach. Two dissipation cameras used wider angle lenses for greater spatial coverage of the minigrid area. One dissipation camera (DS) measured wave breaking over the main cross-shore array of instruments. The other dissipation camera (HU), with a wider field of view, monitored wave dissipation over a larger region and provided images of bar morphology using Time Exposures. An infrared camera (IR) was used for testing nighttime measurements of runup and wave dissipation. A remotely controlled pan-tilt camera (DO) provided additional coverage for special purposes and served as a backup camera. The camera view angles are shown in Figure B2.

Table B1
DELILAH Video Cameras

Camera	Number	Purpose	δ(deg)	R_{max} (m)	r_x (m)	r_y (m)
R1	1	Runup	17	300	0.17	1.17
R2	2	Runup	10	410	0.14	1.32
R3	3	Runup	6	675	0.14	2.16
DS	4	Dissipation	25	475	0.40	4.40
HU	5	Time exposure	40	500	0.68	7.77
IR	6	Night uses				
DO	6	Remote Control				

Where: δ = horizontal view angle in degrees
Rmax = maximum range in meters
r_x = horizontal cross-shore resolution in meters
r_y = horizontal longshore resolution in meters

Fundamental to the video measurements is the transformation between two-dimensional video images and three dimensional world coordinates, which requires a determination of camera geometry. This was accomplished with visually identifiable *ground control points* (GCP's) in the cameras' field of view. The 38 GCP's established during the experiment consisted primarily of white square signs or highway safety cones painted black and placed on the beach. Coordinates of the GCP's are listed in Table B2 and shown graphically in Figures B3 and B4. Many of those GCP's were temporary, with a select number positioned on any particular day. A few instrument pipes and the north property fence posts served as permanent GCP's throughout the experiment.

All video data, with the exception of time exposures, were collected on 12 Super-VHS video cassette recorders. Each VHS tape recorded two continuous hours, with 4 or 5 runs (8 to 10 hours) collected each day. The collection schedule is listed in Table B3. Several duplicate tapes were made between 16 and 19 October, with times staggered approximately 15 minutes, to ensure data redundancy and to obtain data in the time gaps between video runs. Data runs are sequentially numbered and include the camera designation. For example, run R101 refers to the first run of camera R1. Video tapes for each run had near-synchronous start times and a common SMPTE *(Society of Motion Picture and Television Engineers)* time code recorded on one of the audio tracks. All DELILAH tapes are in the possession of Dr. Robert Holman, who can be contacted regarding obtaining copies (see Appendix G).

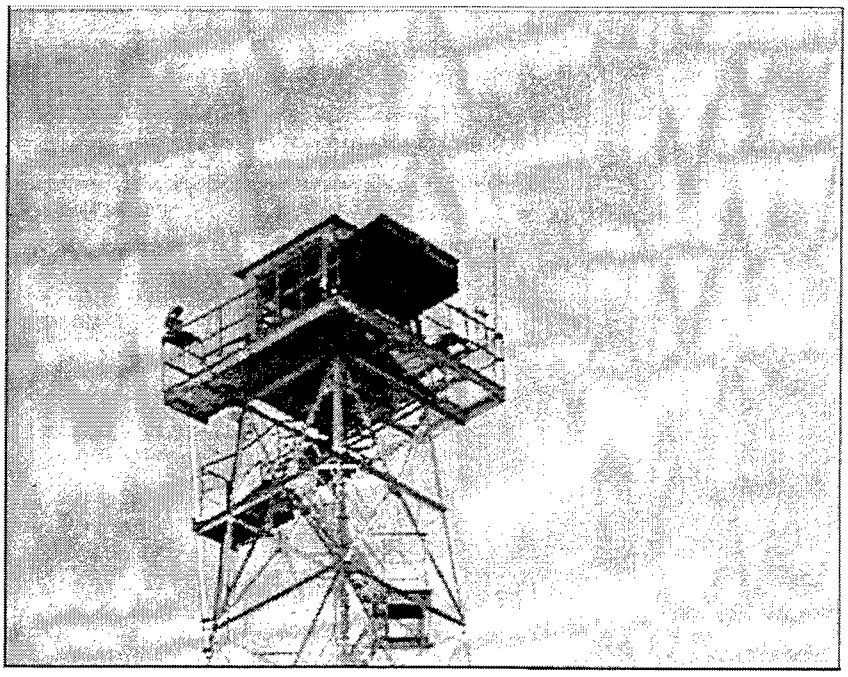

Figure B1. The FRF'S's 42-m-tall observation tower. The photo shows the housing for the fixed-look video cameras(the remote control camera is on the leftmost corner)

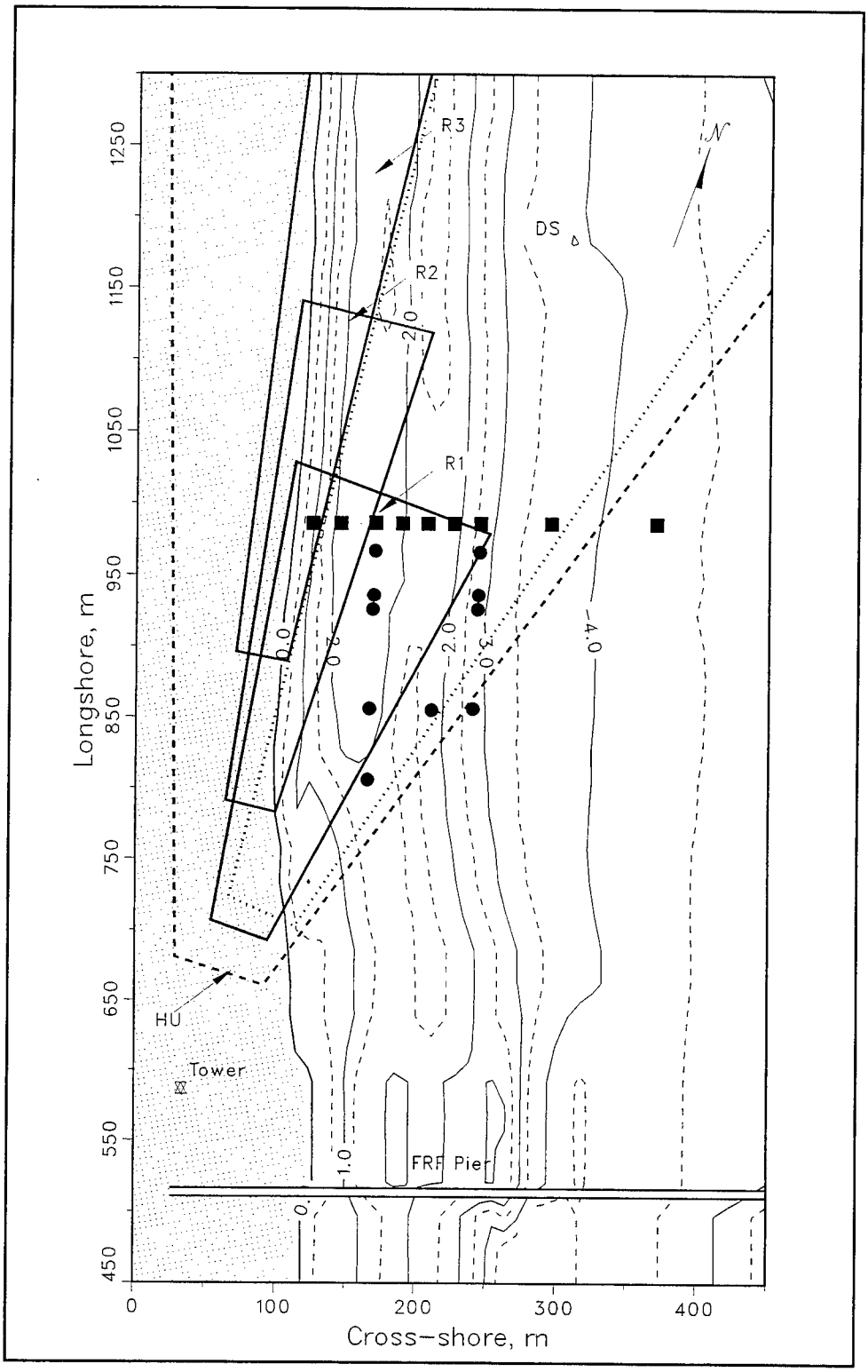

Figure B2. Video camera footprints

Table B2
DELILAH Cameras and Ground Control Points (GCPs)

Number	Description	Cross-shore, m	Longshore, m	Elevation, m NGVD
0	Camera R1	33.99	586.87	42.76
1	Camera R2	33.74	586.78	42.76
2	Camera R3	33.43	586.78	42.76
3	Camera DS	33.31	586.87	42.76
4	Camera HU	32.93	586.78	42.76
5	Cone #1 (southmost)	77.88	701.79	2.23
6	Top of temp cone, south	90.60	721.63	1.76
7	Cone #1A	78.42	724.99	2.03
8	Cone #2	78.30	743.28	2.05
9	Top of temp cone, north	94.39	787.78	1.80
10	Cone #3	77.47	812.04	2.52
11	Cone #4	78.80	879.01	2.88
12	Cone #5	79.64	933.90	2.96
13	Cone #6	83.56	988.57	2.92
14	Beach Sign #1 (center)	71.63	786.74	4.57
15	Beach Sign #2	88.67	962.57	4.63
16	Beach Sign #3	92.16	1002.42	4.36
17	Post #3	86.00	1008.07	4.76
18	Post #4	91.35	1005.92	4.58
19	Post #5	96.60	1004.01	4.91
20	Post #6	106.33	1001.92	4.33
21	Post #7	114.08	1001.03	3.50
22	Post #8	124.01	1000.08	2.69
23	CM10 pipe	124.65	985.80	1.02
24	Tom's W Sign	59.96	986.82	7.29
25	Tom's G Sign	58.29	987.27	6.99
26	Tom's B Sign	56.53	987.46	7.39
27	Tom's BWG Sign	55.77	813.29	7.97
28	Tom's BWG Sign	58.73	698.05	8.42
29	PVO Sign #7	52.48	914.19	8.91
30	PVO Sign #6	54.10	868.54	8.49
31	PVO Sign #5	50.38	822.61	8.28
32	PVO Sign #4	51.55	776.87	8.72
33	PVO Sign #3	49.88	731.13	8.31
34	PVO Sign #2	54.40	685.56	7.40
35	PVO Sign #1	62.09	662.55	8.44
36	Top of EP20.	144.99	984.65	0.16
37	Top of CM32	168.77	936.06	0.32
38	Water Sign #4	169.86	966.10	0.74
39	Water Sign #3	167.45	935.98	2.04
40	Water Sign #2	164.93	856.14	1.82
41	Water Sign #1	163.39	806.20	1.75

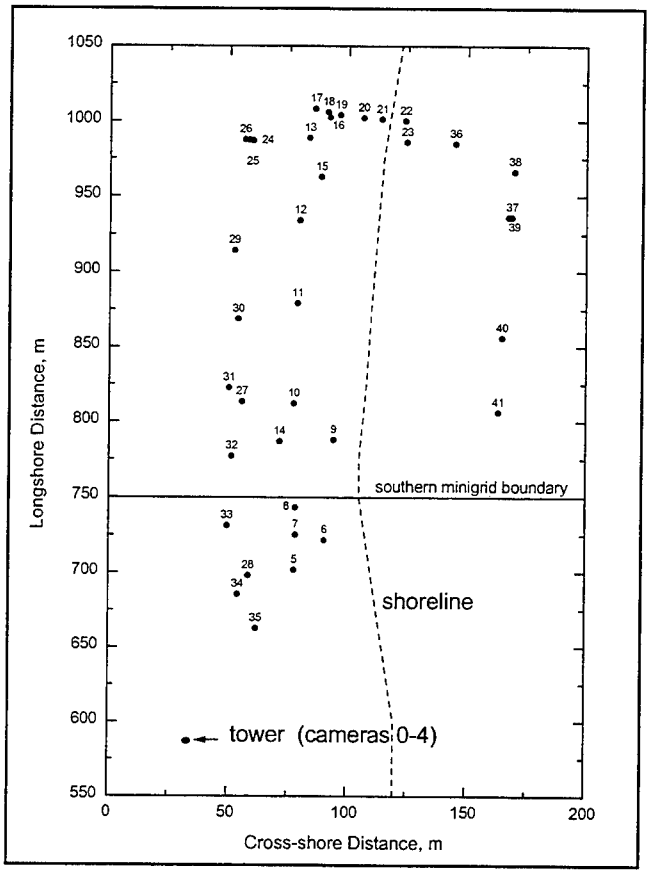

Figure B3. Plan view of ground control point (GCP) positions

Figure B3. Ground Control Points as viewed from the FRF Tower.

Table B3
DELILAH Video Log

Start Time	VCR #1	VCR #2	VCR #3	VCR #4	VCR #5	VCR #6	Tide, m NGVD	WAVES Hmo m	WAVES Tp s	WAVES θp deg	WIND speed m/s	WIND Dir. true N
901003.1340	R101	R201	R301	DS01			-0.40	0.6	8.2	-36	5.1	173
901004.0820	R102	R202	R302	DS02			0.50	0.6	4.3	-48	9.1	73
901004.1132	R103	R203	R303	DS03			-0.47	0.7	5.0	-46	9.1	73
901004.1355	DS04						-0.59	0.8	5.0	-46	9.3	63
901004.1608	R104	R204	R304	DS05			-0.03	0.8	5.0	-46	9.3	63
901005.0823	R105	R205	R305	DS06			0.70	0.7	4.2	68	4.2	-149
901005.1300	R106	R206	R306	DS07			-0.54	0.5	6.2	-32	3.1	153
901005.1537	DS08						-0.35	0.5	6.2	-32	3.1	153
901006.0714	R107	R207	R307	DS09			0.68	0.6	12.	-34	2.2	38
901006.0917	R108	R208	R308	DS10			0.62	0.5	12.	-28	2.4	-177
901006.1235	R109	R209	R309	DS11			-0.34	0.5	12.	-26	5.2	153
901006.1437	R110	R210	R310	DS12			-0.67	0.5	12.	-26	6.4	129
901006.1635	DS13						-0.41	0.5	10.	-36	6.4	129
901007.0728	R111	R211	R311	DS14			0.58	0.6	10.	-38	5.3	66
901007.0930	R112	R212	R312	DS15			0.72	0.6	10.	-40	3.5	47
901007.1143	DS16						0.24	0.6	9.7	-38	3.8	118
901007.1357	R113	R213	R313	DS17			-0.46	0.6	9.7	-38	3.8	118
901007.1604	R114	R214	R314	DS17			-0.59	0.6	9.7	-38	6.4	90
901008.0813	R115	R215	R315	DS18			0.51	0.8	10.	-38	4.0	66
901008.1022	R116	R216	R316	DS19			0.65	0.7	10.	-40	3.4	84
901008.1211	DS20						0.36	0.7	10.	-38	4.0	146
901008.1330	R117	R217	R317	DS21			-0.02	0.7	10.	-38	4.0	146
901008.1532	R118	R218	R318	DS22			-0.47	0.7	10.	-38	6.1	113
901008.1940	IR01						-0.01	0.8	9.7	-42	4.8	112
901009.0426	IR02						-0.53	1.0	10.	-38	2.4	93
901009.0900	R119	R219	R319	DS23			0.47	1.2	10.	-40	6.9	112
901009.1107	R120	R220	R320	DS24			0.67	1.2	10.	-40	6.9	112
901009.1330	R121	R221	R321	DS25	DO01		0.32	1.1	10.	-42	7.2	115
901009.1537	R122	R222	R322	DS26	DO02		-0.22	1.0	10.	-40	6.8	106
901009.2157	IR03						0.30	1.1	10.	-40	5.3	93
901010.0723	R123	R223	R323	DS27	DO03		-0.19	1.2	10.	-38	4.6	128
901010.0924	DS62	DO22	IR12	RD02			0.37			-10	5.0	120
901010.0954	R124	R224	R324	DS28	DO04		0.51	1.2	9.7	-40	5.9	119
901010.1213	R125	R225	R325	DS29	DO04		0.70	1.3	10.	-40	9.5	105
901010.1523	RD01	DS30	O05	IR04			0.17	1.5	9.7	-38	9.1	114
901010.1725	IR05						-0.22	1.7	7.0	-40	9.1	114
901011.0630	R126	R226	R326	DS31	DO06		-0.37	1.8	8.2	-38	10.7	99
901011.0847	R127	R227	R327	DS32	DO07		-0.17	1.8	8.2	-38	10.3	100
901011.1055	R128	R228	R328	DS33	DO08		0.40	1.7	8.9	-40	10.3	100
901011.1305	R129	R229	R329	DS34	DO08		0.63	1.5	8.9	-40	10.1	110
901011.1514	R130	R230	R330	DS35	DO09		0.47	1.4	9.7	-40	7.1	110
901012.0718	R131	R231	R331	DS35	DO10		-0.17	1.3	8.2	-38	6.0	-168
901012.0930	R132	R232	R332	DS36	DO11		-0.02	1.3	8.2	-38	6.0	-168
901012.1226	R133	R233	R333	DS36	DO11		0.65	1.5	15.	-20	4.3	140
901012.1538	R134	R234	R334	DS37	DO12		0.72	2.2	13.	-16	6.7	142

(Continued)

Table B3 (Concluded)

Start Time	VCR #1	VCR #2	VCR #3	VCR #4	VCR #5	VCR #6	Tide, m NGVD	WAVES Hmo m	WAVES Tp s	WAVES θp deg	WIND speed m/s	WIND Dir. true N
901013.0645	R135	R235	R335	DS38	DO13		0.09	2.4	12.0	-16	1.0	161
901013.0901	R136	R236	R336	DS39	DO14		-0.17	2.4	12.0	-16	1.0	161
901013.1116	R137	R237	R337	DS40	DO01		0.08	2.1	10.7	-38	2.1	-170
901013.1339	R138	R238	R338	DS41	DO02		0.67	2.1	10.7	-38	2.1	-170
901013.1553	R139	R239	R339	DS42	DO03		0.75	1.9	10.7	-22	1.6	161
901014.0800	R140	R240	R340	DS43	DO04		0.01	1.2	9.7	-32	3.3	-35
901014.1011	R141	R241	R341	DS44	DO05		-0.22	1.2	9.7	-34	3.0	-108
901014.1330	R142	R242	R342	DS45	DO06		0.37	1.1	9.7	-22	3.2	-156
901014.1545	R143	R243	R343	R443	DS46	DO07	0.72	1.1	10.7	-18	3.1	159
901015.0712	R144	R244	R344	R402	DS47	DO08	0.38	1.0	10.7	-22	5.5	28
901015.0929	R145	R245	R345	R403	DS48	DO09	-0.23	1.0	10.7	-20	1.6	-42
901015.1141	R146	R246	R346	R404	DS49	DO10	-0.29	1.0	10.7	-20	1.6	-42
901015.1351	R147	R247	R347	DS50	DO11		0.12	1.0	10.7	-20	3.8	-144
901015.1601	R148	R248	R348	DS51	DO11	DO15	0.58	1.0	10.7	-20	3.8	-144
901016.0728	R149	R249	R349	DS52	DO12		0.65	1.6	5.8	42	8.0	112
901016.0743	R149	R249	R349	DS52	DO12		0.65	1.6	5.8	42	8.0	112
901016.0937	R150	R250	R350	DS53	DO13		0.09	1.2	9.7	40	6.4	-104
901016.0952	R150	R250	R350	DS53	DO13		0.09	1.2	9.7	40	6.4	-104
901016.1148	R151	R251	R351	DS54	DO14		-0.25	1.2	9.7	40	6.4	-104
901016.1203	R151	R251	R351	DS54	DO14		-0.25	1.2	9.7	40	6.4	-104
901016.1358	R152	R252	R352	DS55	DO15		-0.02	1.2	9.7	22	6.1	-107
901016.1414	R152	R252	R352	DS55	DO15		-0.02	1.2	9.7	22	6.1	-107
901016.1606	R299						0.50	1.0	9.7	40	5.6	-130
901016.2111	IR06						0.08	0.8	9.7	-14	5.7	-163
901016.2312	IR07						-0.35	0.9	9.7	-16	5.8	-156
901017.0710	R153	R253	R353	DS56	DO16	IR08	0.65	1.0	9.7	0	6.5	-179
901017.0725	R153	R253	R353	DS56	DO16	IR08	0.65	1.0	9.7	0	6.5	-179
901017.0934	R154	R254	R354	DS57	DO17	IR09	0.21	1.0	9.7	-2	7.7	140
901017.0918	R154	R254	R354	DS57	DO17	IR09	0.21	1.0	9.7	-2	7.7	140
901017.1129	R155	R255	R355	DS58	DO18	IR10	-0.36	1.0	9.7	-2	7.7	140
901017.1145	R155	R255	R355	DS58	DO18	IR10	-0.36	1.0	9.7	-2	7.7	140
901017.1338	R156	R256	R356	DS59	DO19	IR11	-0.34	1.0	9.7	-28	7.0	139
901017.1354	R156	R256	R356	DS59	DO19	IR11	-0.34	1.0	9.7	-28	7.0	139
901017.1550	R157	R257	R357	DS60	DO20		0.09	1.0	9.7	-26	8.7	137
901017.1604	R157	R257	R357	DS60	DO20		0.09	1.0	9.7	-26	8.7	137
901018.0700	R158	R258	R358	DS61	DO21		0.62	1.0	5.2	-48	8.9	90
901018.0720	R158	R258	R358	DS61	DO21		0.62	1.0	5.2	-48	8.9	90
901018.1116	R159	R259	R359	DS63	DO23		-0.30	1.1	5.5	-44	11.5	80
901018.1311	R160	R260	R360	DS64	DO24		-0.56	1.1	5.8	-42	11.7	79
901018.1507	R161	R261	R362	DS65	DO25		-0.38	1.2	6.2	-46	11.2	76
901018.1544	R161	R261	R362	DS65	DO25		-0.38	1.2	6.2	-46	11.2	76
901019.0710	R162	R262	R362	DS66	DO26		0.83	1.2	6.6	44	8.2	-32
901019.0726	R162	R262	R362	DS66	DO26		0.83	1.2	6.6	44	8.2	-32
901019.0919	R163	R263	R363	DS67	DO27		0.56	1.3	7.6	38	8.6	-45
901019.0935	R163	R263	R363	DS67	DO27		0.56	1.3	7.6	38	8.6	-45
901019.1213	R164	R264	R364	DS68	DO28	IR13	-0.18	1.2	7.0	24	9.2	-51
901019.1229	R164	R264	R364	DS68	DO28	IR13	-0.18	1.2	7.0	24	9.2	-51
901019.1423	R165	R265	R365	DS69	DO29	IR14	-0.34	1.2	7.0	24	9.2	-51
901019.1438	R165	R265	R365	DS69	DO29	IR14	-0.34	1.2	7.0	24	9.2	-51
901019.1802	IR15						0.27	1.3	5.5	36	6.6	-89

Video Time Exposures

Table B4 summarizes the video tape data collected and used to compute the video time exposures. These data were recorded on a Video-8 format VCR. Copies of daily time exposures are shown in Figures B5 to B24. These were taken with the HU camera and are the result of averaging 10 min of video images at a rate 1 frame per second.

Table B4
Time Exposure Video Log

Date.time	Tape #	Min.	Tide
901000.1504	T006		
901002.1630	vtest1	15	high
901003.1523	T001	12	low
901004.1157	T001	10	low
901004.1550	T001	11.5	rising
901004.1622	T001	11	rising
901004.1636	T001	10	rising
901004.1702	T001	13	rising
901004.1742	T001	10	high
901005.0847	T001	10	high
901005.1200	T001	12	mid
901005.1330	T001	12	low
901005.1552	T002	10	rising
901005.1703	T002	10:15	rising
901006.0705	T002	30	
901006.0800	T002	11	high
901006.1115	T002	11	mid
901006.1400	T002	11	low
901006.1652	T002	10.5	rising
901007.0645	T002	20+	mid
901007.0855	T003	13	high
901007.1155	T003	10	mid
901007.1525	T003	10	low
901007.1705	T003	11.5	mid
901008.0820	T003	20	high
901008.0820	T003	12	falling
901008.1312	T003	14	mid
901008.1623	T003	10	low
901009.0853	T003	10	mid
901009.1105	T003	11	high
901009.1235	T004	11	falling
901009.1314	T004	10	falling
901009.1405	T004	11	mid
901009.1515	T004	10	falling
901009.1720	T004	10	low

(Sheet 1 of 3)

Table B4 (Continued)

Date.time	Tape #	Min.	Tide
901010.0729	T004	12	rising
901010.0916	T004	11	mid
901010.1213	T004	12	high
901010.1501	T004	13	mid
901010.1650	T004		falling
901011.0630	T005	10	low
901011.0921	T005	13	mid
901011.1245	T005	10	high
901011.1424	T005	10	falling
901011.1648	T005		mid
901012.0854	T006		mid
901012.0856	T005	10	low
901012.1027	T005	10	rising
901012.1100			mid
901012.1151	T007		rising
901012.1200			rising
901012.1300			rising
901012.1400			high
901012.1500			falling
901012.1600			falling
901013.0710	T008	10	falling
901013.0710	T009	4 HRS	low
901013.0800	T008	10	rising
901013.0900	T008	10	rising
901013.1000	T008	10	rising
901013.1100	T008	10	rising
901013.1154	T010	4 HRS	mid
901013.1203	T008	10	rising
901013.1216	T008	10	rising
901013.1300	T008	10	rising
901013.1400	T008	10	rising
901013.1500	T008	10	high
901013.1600	T008	10	falling
901013.1700	T008	10	falling
901014.0600	T011	10	falling
901014.0700	T011	10	mid
901014.0800	T011	10	falling
901014.0900	T011	10	falling
901014.1000	T011	10	low
901014.1100	T011	10	rising
901014.1140	T012	6 HRS	mid
901014.1202	T011	10	rising
901014.1404	T011	10	rising
901014.1500	T011	10	rising
901015.0700	T011	10	falling
901015.0711	T013	6 HRS	falling
901015.0800	T014	10	mid
901015.0900	T014	10	falling
901015.1000	T014	10	falling
901015.1100	T014	10	low
901015.1200	T014	10	rising
901015.1300	T014	10	rising
901015.1400	T014	10	mid
901015.1500	T014	10	rising
901015.1600	T014	10	rising

(Sheet 2 of 3)

Table B4 (Continued)			
Date.time	**Tape #**	**Min.**	**Tide**
901016.0638	T015		falling
901016.0800	T016	10	falling
901016.0900	T016	10	falling
901016.1000	T016	10	falling
901016.1100	T016	10	low
901016.1200	T016	10	rising
901016.1300	T016	10	rising
901016.1400	T016	10	mid
901016.1429	T017		rising
901017.0709	T018	6 hr	
901017.1513	T019	10	
901018.0600	T019	10	
901018.0700			
901018.0703	T020	6 hr	
901018.0800			
901018.0900			
901018.1000			
901018.1100			
901018.1200			
901018.1300			
901018.1326	T021	6 hr	
901018.1400			
901018.1500			
901018.1600			
901018.1700			
901019.0600	T023	10	
901019.0634	T022	6hr	
901019.0700			
901019.0800			
901019.0900			
901019.1000			
901019.1100			
901019.1200			
901019.1200			
901019.1300			
901019.1345	T024	6hr	
901019.1400			
901019.1500			
901019.1600			
901019.1700			
901020.0600	T025	10	

(Sheet 3 of 3)

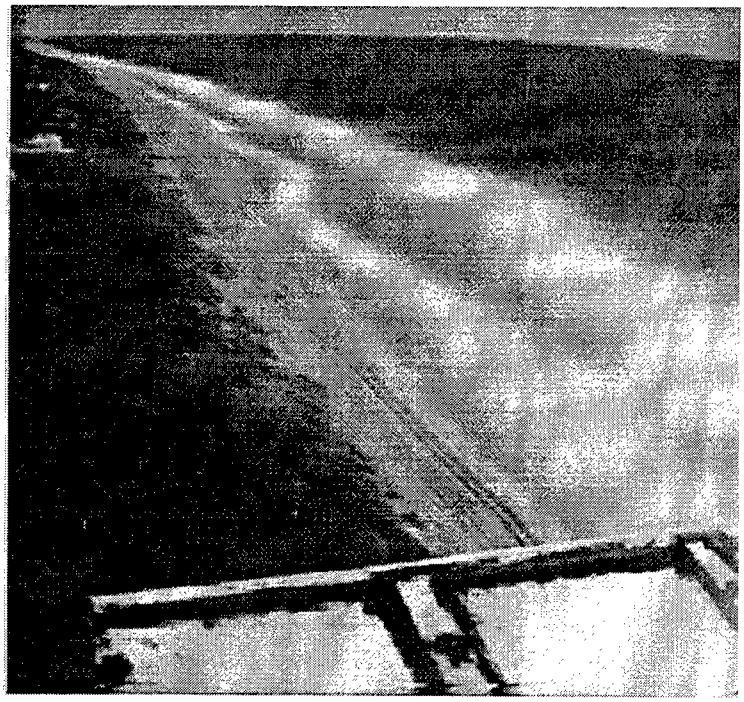

Figure B5. 1 October 1990 at 1504 EST

Figure B6. 2 October 1990 at 1630 EST

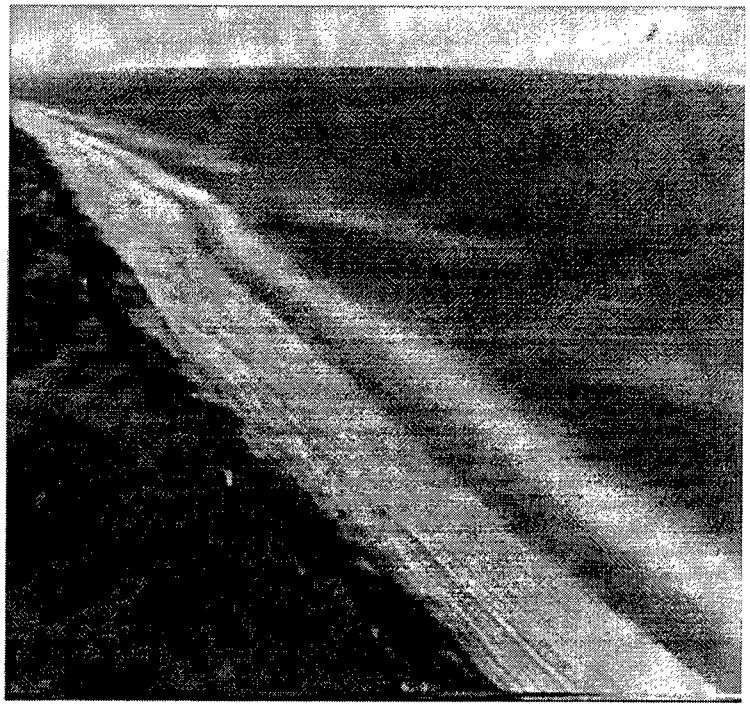

Figure B7. 3 October 1990 at 1523 EST

Figure B8. 4 October 1990 at 1157 EST

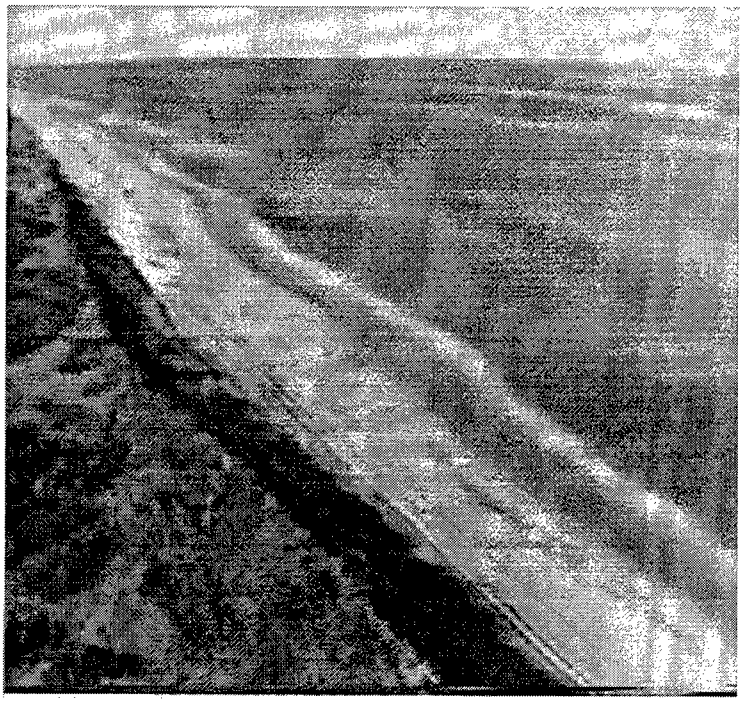

Figure B9. 5 October 1990 at 1330 EST

Figure B10. 6 October 1990 at 1990 EST

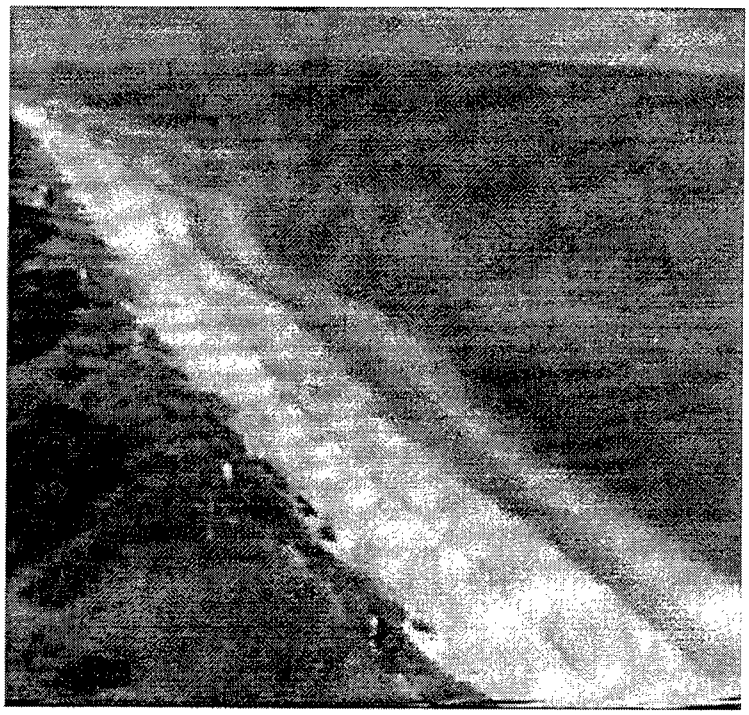

Figure B11. 7 October 1990 at 1400 EST

Figure B12. 8 October 1990 at 1525 EST

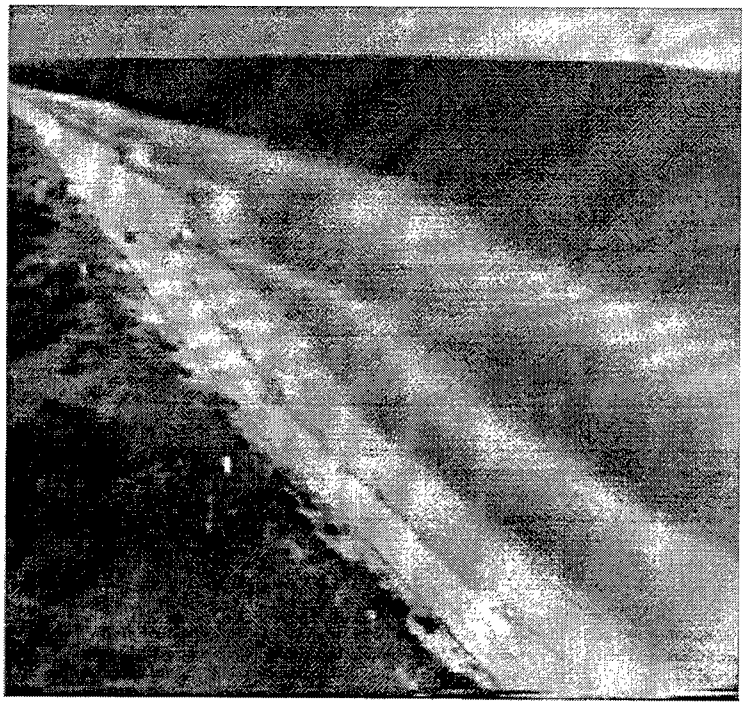

Figure B13. 9 October 1990 at 1720 EST

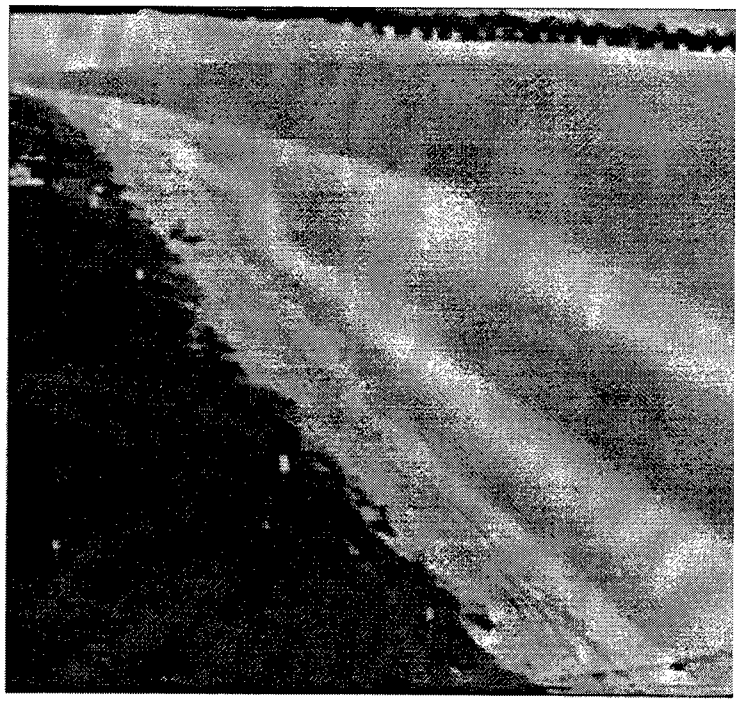

Figure B14. 10 October 1990 at 1650 EST

Figure B15. 11 October 1990 at 0630 EST

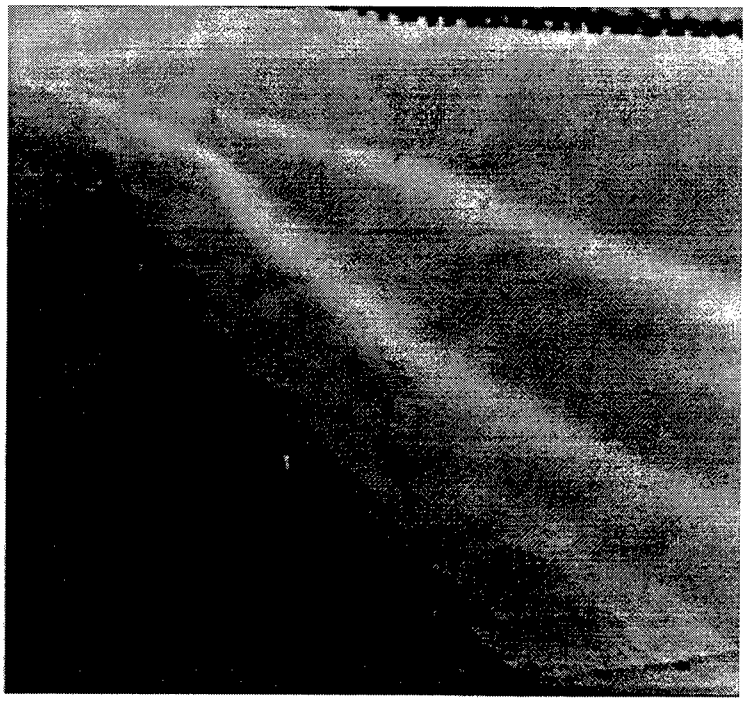

Figure B16. 12 October 1990 at 0921 EST

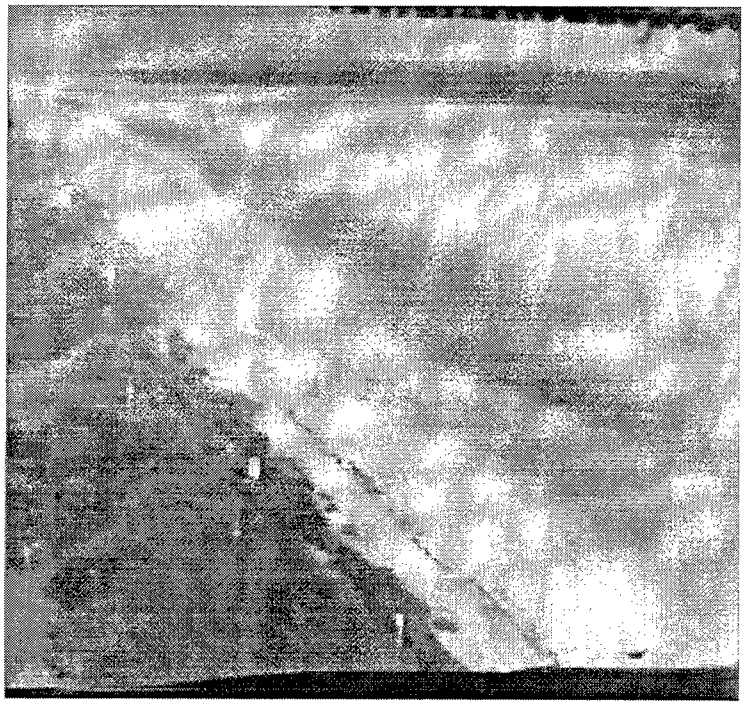

Figure B17. 13 October 1990 at 0900 EST

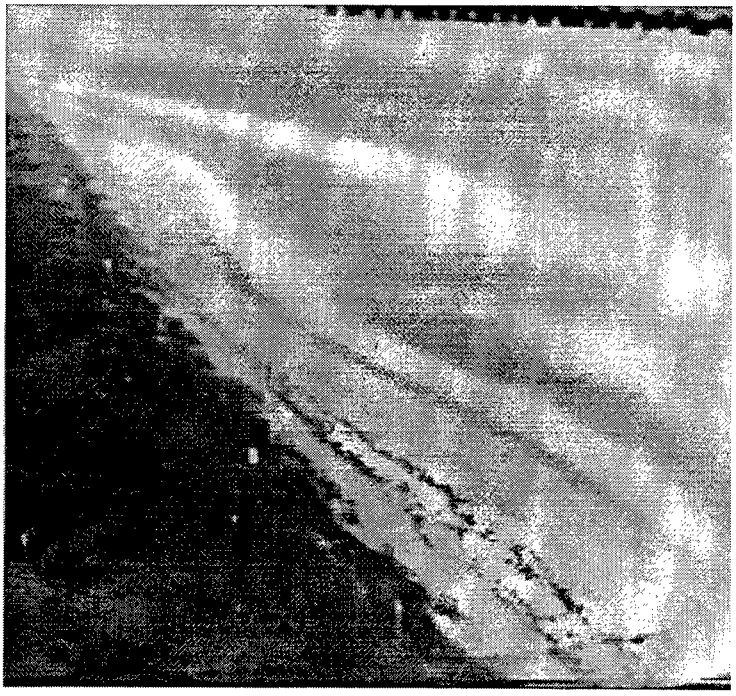

Figure B18. 14 October 1990 at 1000 EST

Figure B19. 15 October 1990 at 1000 EST

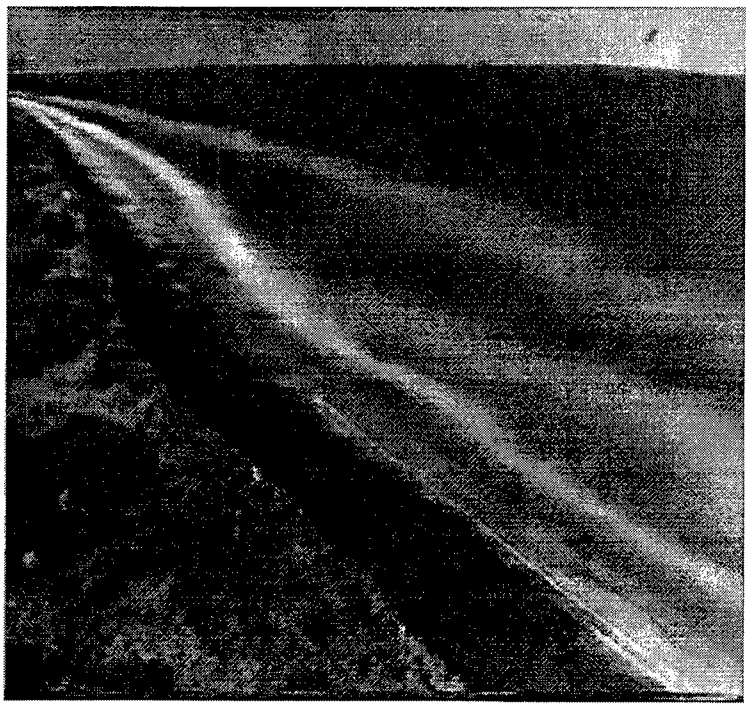

Figure B20. 16 October 1990 at 1000 EST

Figure B21. 17 October 1990 at 1300 EST

Figure B22. 18 October 1990 at 1300 EST

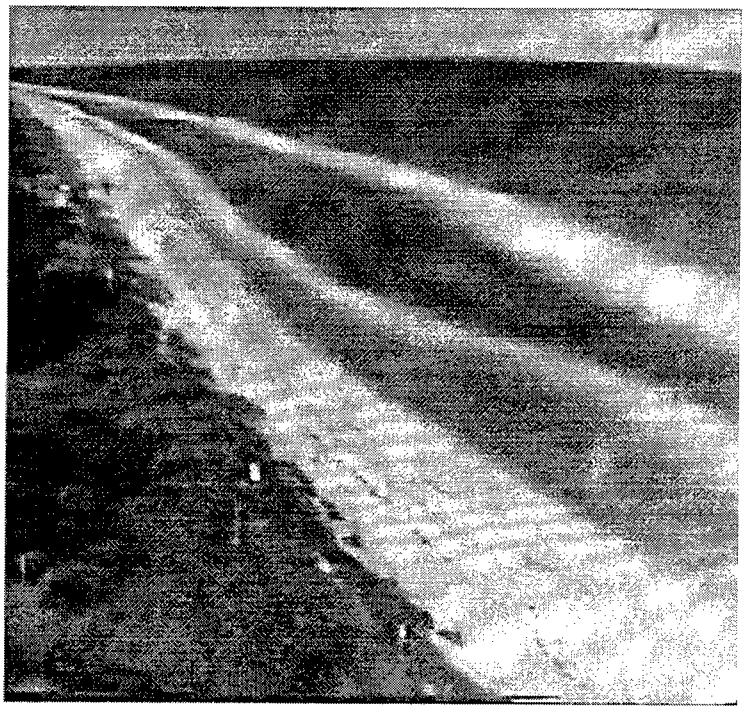

Figure B23. 19 October 1990 at 1400 EST

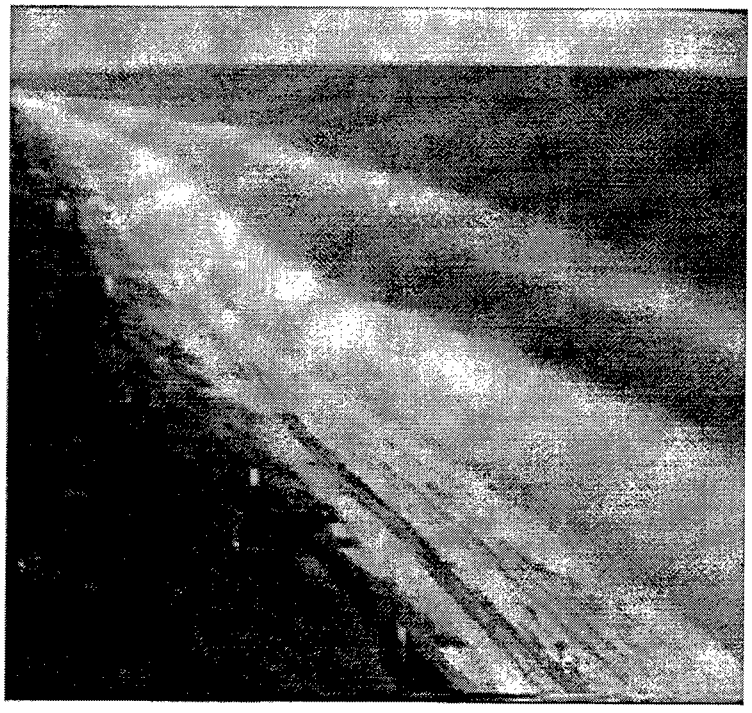

Figure B24. 20 October 1994 at 0600 EST

Video Analysis of Runup

Wave runup data were obtained using an Imaging Technology Incorporated video image processing system (model ITI-151) interfaced to a Sun host computer. By using the GCP's as control and knowing the profile coordinates, time series of wave runup were generated from the video. Runup was measured along one beach profile line located near the primary cross-shore array, at longshore coordinate 986 m. Beach profiles were surveyed once per day near low tide. Camera geometries were computed for each runup collection.

Runup time series was performed by the Coastal Imaging Laboratory at the Oregon State University, Corvallis, OR. The runup analysis technique is based on the "timestack" method described by Aagaard and Holm (1989).[1] A timestack is created by digitizing every fifth video frame (6 Hz) and recording the pixel intensities in the image that correspond to the profile line location. These pixel values are then "stacked" in a matrix and saved on disk. This results in a matrix of pixel intensities with one axis being the pixel position, directly related to the distance across the structure, and the other axis being time. In a typical timestack (Figure B25) the runup is clearly visible as a sharp change in pixel intensity, between the darker beach on the left, and the whiter foam of the runup on the right.

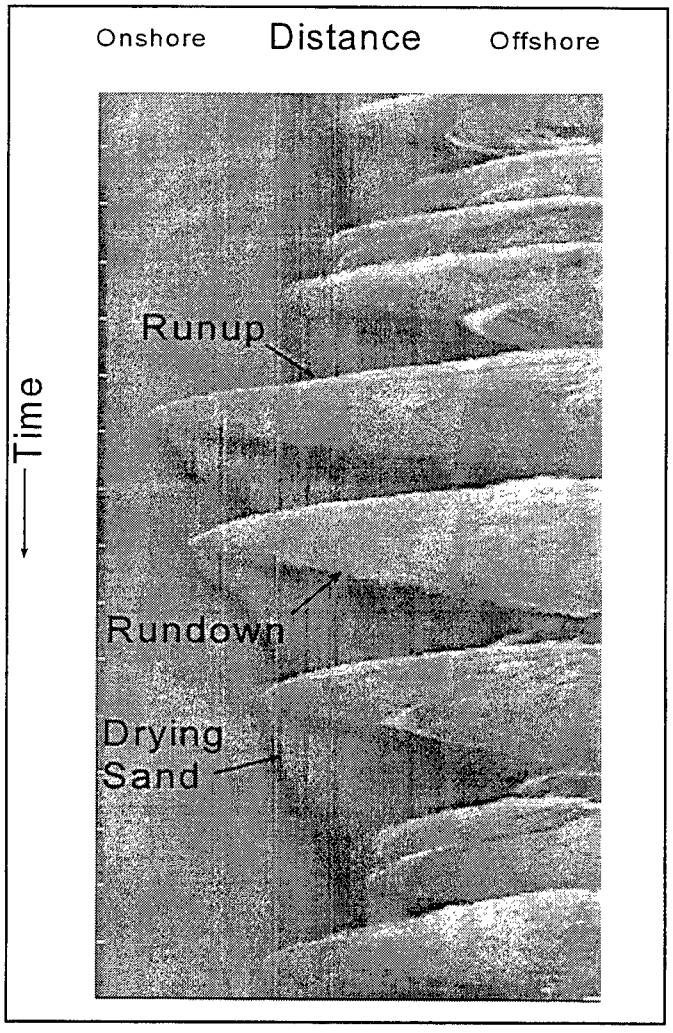

Figure B25. Example segment of a runup timestack

The cross-shore position of the runup is determined from the runup edge position in the timestack image. Image

[1] Aagaard, T., and Holm, J. (1989). "Digitization of wave run-up using video records," *Journal of Coastal Research* 5, 547-551.

coordinates of the edge are directly related to a time series of vertical runup excursion. Runup position in the timestack is found using edge detection algorithms combined with manual refinements when edge detection fails. After the edge detection is completed, image coordinates of the runup edge are transformed to a time series of vertical runup elevations. The 6-Hz timestack was decimated and saved as a 2-Hz time series. Standard Fourier wave analysis techniques were used to compute vertical runup spectra, runup wave height (R_{mo}), and peak period. Total record lengths were typically 119 min and processed in 4096-point (2,048-s) segments that overlapped 50 percent. The resulting spectra were smoothed in frequency with a 7-point band average, resulting in spectra with frequency resolution of 0.0034 Hz. Runup spectra were analyzed at the FRF.

The wave runup spectra were divided into three wave frequency classifications; infragravity (0.005 to 0.04 Hz), swell (0.04 to 0.15 Hz), and sea (0.15 to 0.5 Hz). These divisions are not necessarily definitive. Infragravity waves, for example, can sometimes fall within the swell frequency range. Total significant runup wave height (R_{mo}) is computed from the sum of energy from all three wave bands (0.005 to 0.5 Hz). Record length, runup wave height, period, and percentage distribution of wave energy in the three categories is presented in Table B5 and plotted in Figure B26.

The cross-shore range of runup was determined from each time series and is shown in Figure B27 superimposed on the daily beach profile. Mean runup position, mean water level recorded at the end of the FRF pier, and incident wave H_{mo} measured at the 8-m array are also listed in the figure. Beach slopes (β) in Figure B27 were computed between the two cross-shore positions on the profile that were ± 20 cm vertically from the mean runup position. This beach slope and incident wave conditions were used to determine a dimensionless surf-similarity parameter, the Irribaren number ξ_o, as a measure of the dissipative/reflective nature of the beach. The Irribaren numbers shown in Figure B27 were computed as:

$$\xi_o = \frac{\beta}{\left(\frac{H_o}{L_o}\right)^{1/2}}$$

where

H_o = incident deepwater significant wave height

L_o = deepwater wavelength

Table B5
Video Runup Data

Date & time	Rec length(s)	R_{mo} (m)	Tp (s)	% IG energy	%Swell energy	% Sea energy
901005 0824	7200	1.0	13.6	15	82	3
901005 1300	7200	0.4	16.7	24	71	5
901006 0713	7020	1.1	11.9	12	85	3
901006 0917	7200	0.8	11.9	28	70	2
901006 1235	6900	0.5	11.9	32	65	3
901007 0728	6902	0.8	10.6	29	67	4
901007 0930	7200	0.9	13.6	39	58	3
901008 0813	7200	0.7	23.3	45	53	2
901008 1023	7200	0.7	21.6	47	50	3
901008 1330	6900	0.4	23.3	62	37	1
901009 0900	7200	0.9	20.1	48	50	2
901009 1107	7200	0.9	21.6	47	50	3
901009 1330	7200	0.7	23.3	53	46	1
901010 0954	7200	1.0	23.3	51	47	2
901011 0630	7200	0.8	20.1	39	59	2
901011 0847	7200	1.1	17.7	37	61	2
901011 1055	7200	1.3	20.1	39	58	3
901011 1305	7200	1.4	15.8	29	67	4
901012 0719	7200	1.3	21.6	28	69	3
901012 1226	7200	2.2	16.7	16	82	2
901012 1538	7200	2.4	14.9	28	71	2
901013 0645	7200	1.7	12.4	35	63	2
901013 0901	7200	1.7	13.0	32	66	2
901013 1116	7200	2.3	11.4	22	76	3
901013 1339	7199	2.6	11.9	17	80	3
901013 1554	5400	2.6	11.9	19	78	3
901014 0800	7200	1.2	10.2	22	73	6
901014 1011	7200	1.2	10.6	26	70	4
901014 1330	7200	2.1	13.0	22	75	3
901014 1545	6000	2.5	14.2	16	82	2
901015 1141	7200	1.5	11.4	18	79	3
901015 1351	7200	2.2	11.9	17	80	4
901016 0728	7200	1.4	12.4	23	75	3
901016 0937	7200	1.0	9.9	30	67	3
901016 1148	7200	1.0	14.2	27	70	4
901016 1606	5400	1.8	10.6	20	78	2
901017 0710	7200	1.4	13.6	20	77	3
901017 0919	7200	1.0	16.7	22	75	3
901017 1129	7200	0.8	14.2	20	77	3
901017 1338	7200	0.9	14.9	20	77	3
901017 1550	6000	1.2	14.9	19	78	3
901018 0700	7200	1.6	13.6	11	85	4
901018 1116	6824	1.2	16.7	12	83	5
901018 1311	6840	1.2	16.7	16	79	5
901019 0710	7200	1.3	14.2	13	82	5
901019 0919	7200	1.4	14.2	14	81	4
901019 1213	7200	1.1	14.9	21	76	3
901019 1423	7200	1.1	13.6	19	79	3

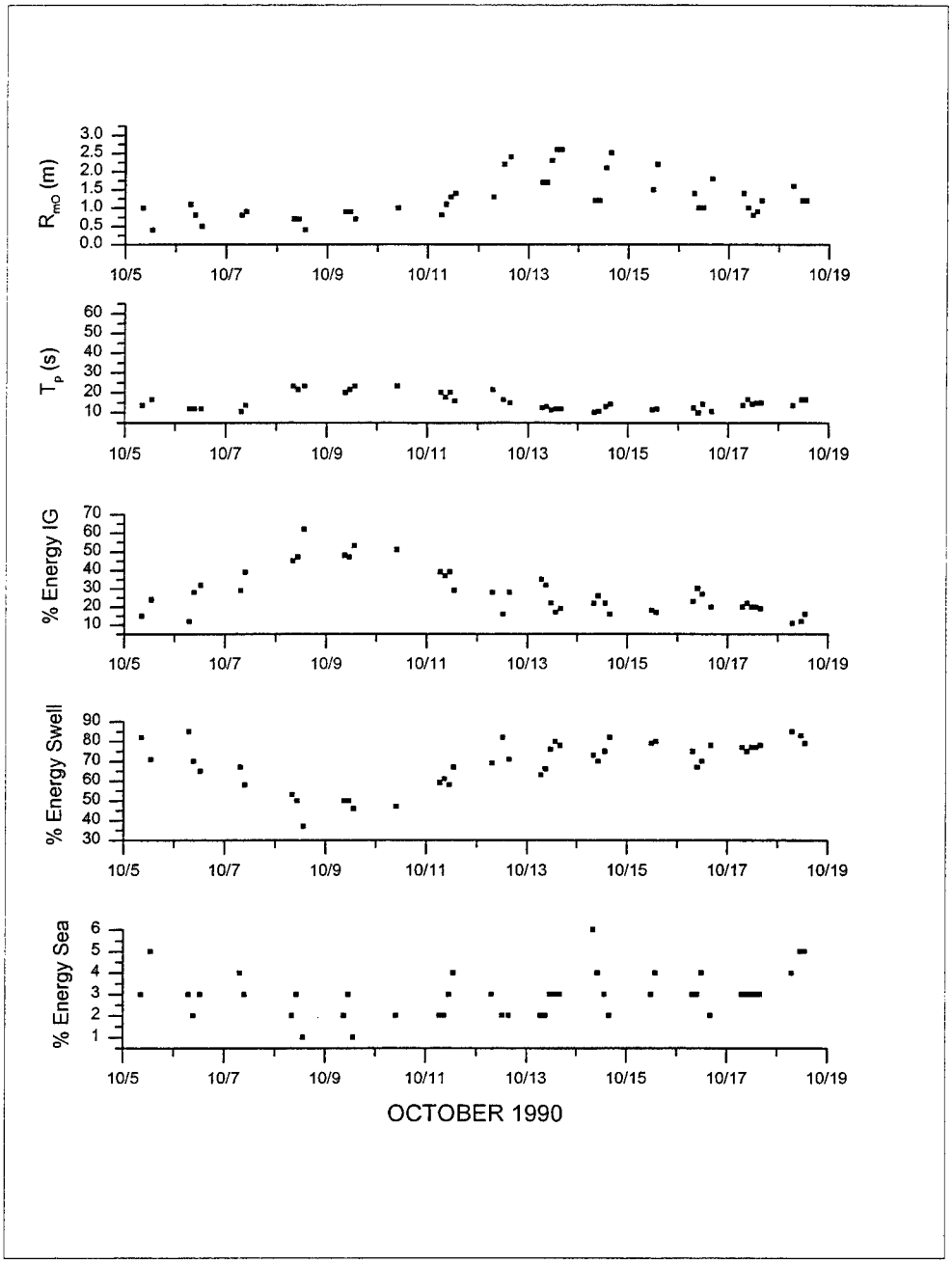

Figure B26. Time series of wave height, period and energy derived from DELILAH runup videos

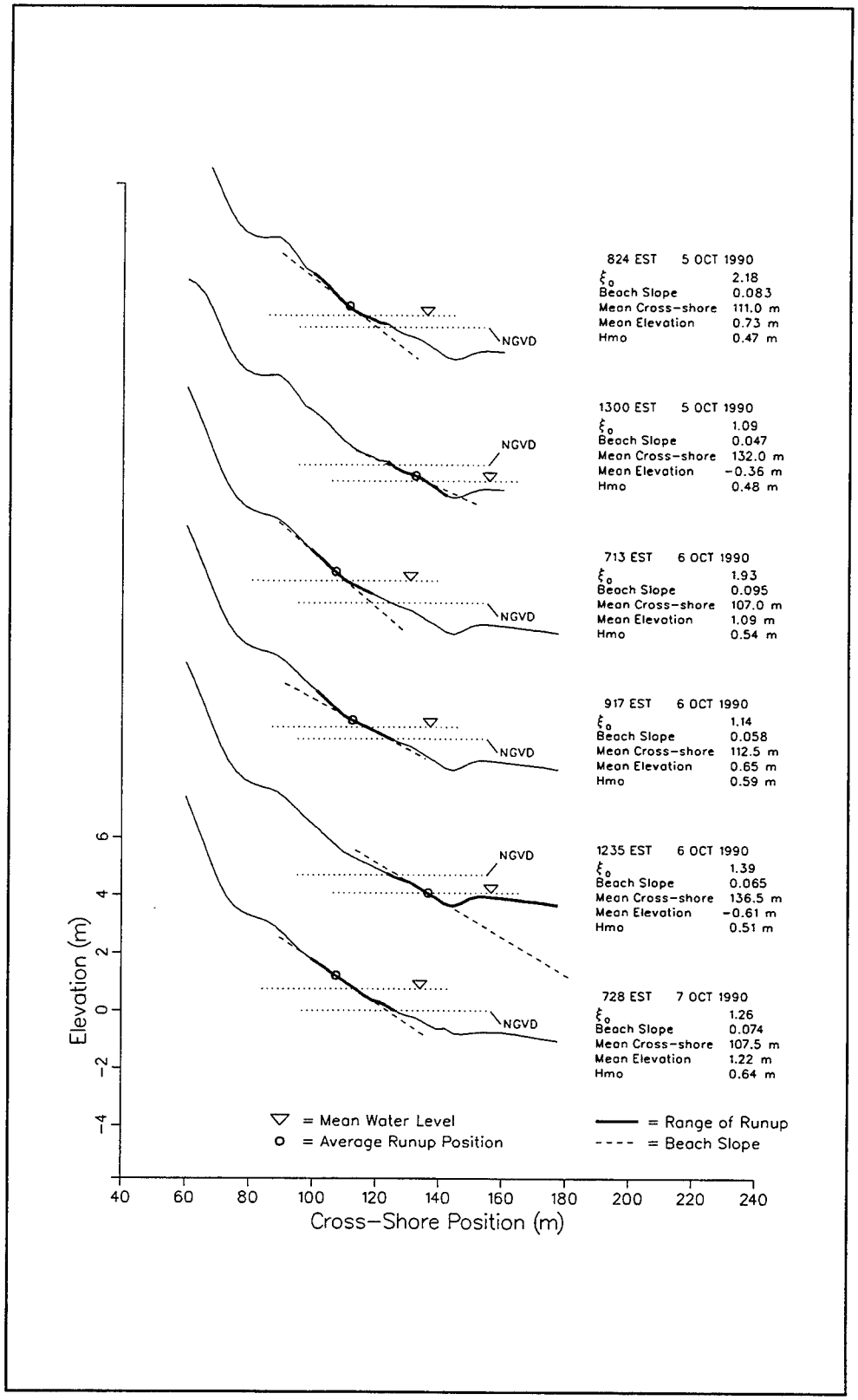

Figure B27. Runup excursion on beach profiles (Sheet 1 of 8)

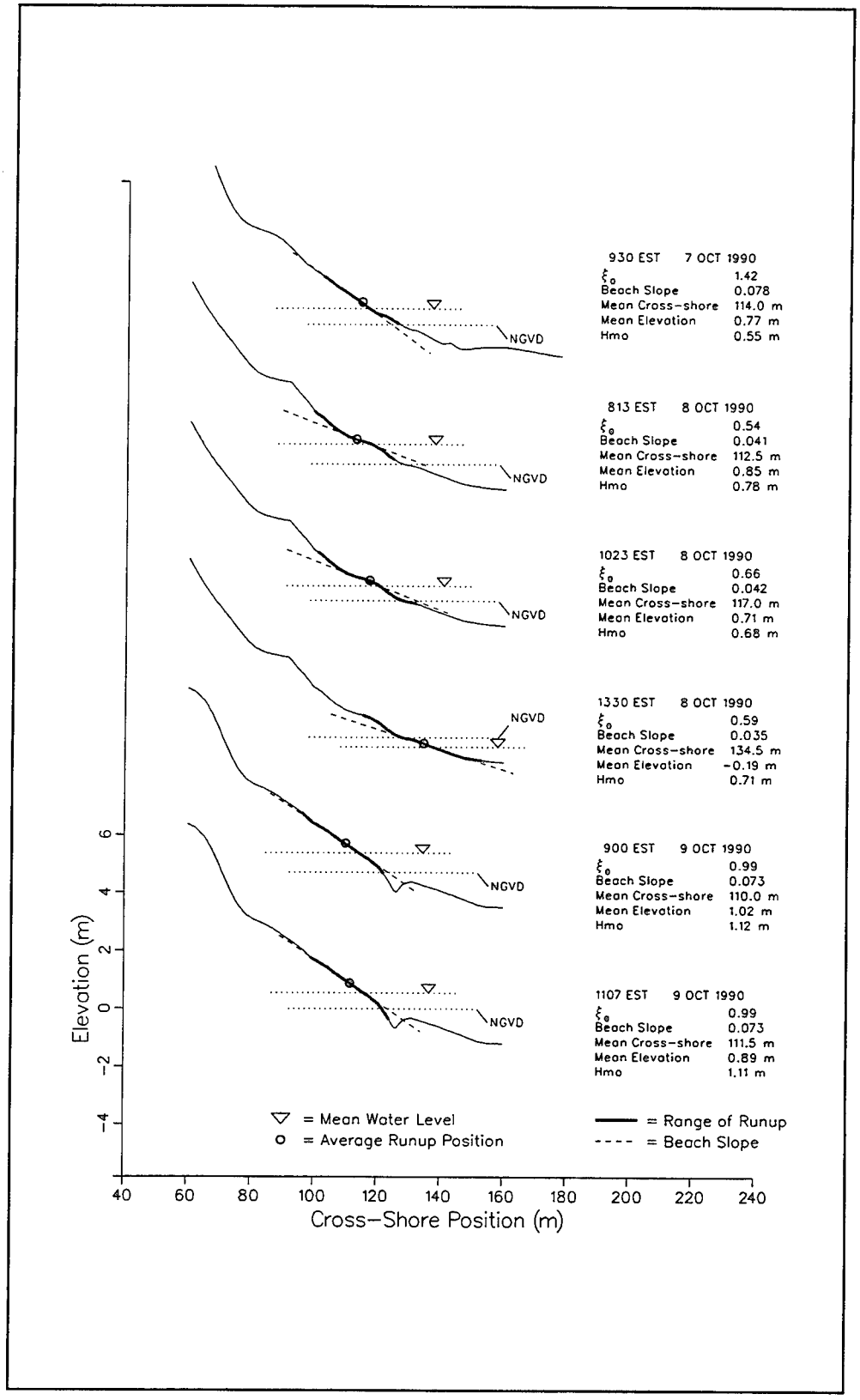

Figure B27. (Sheet 2 of 8)

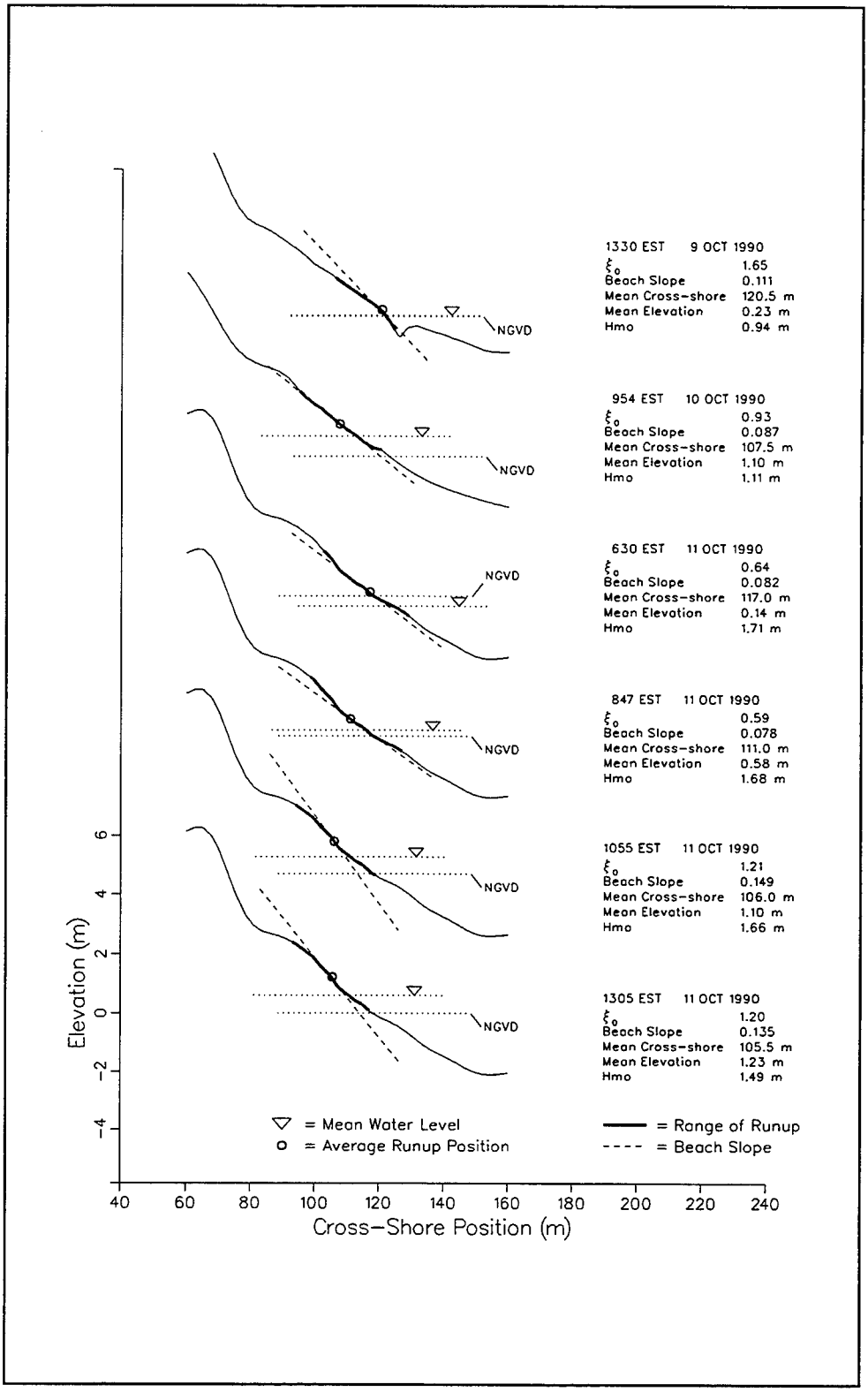

Figure B27. (Sheet 3 of 8)

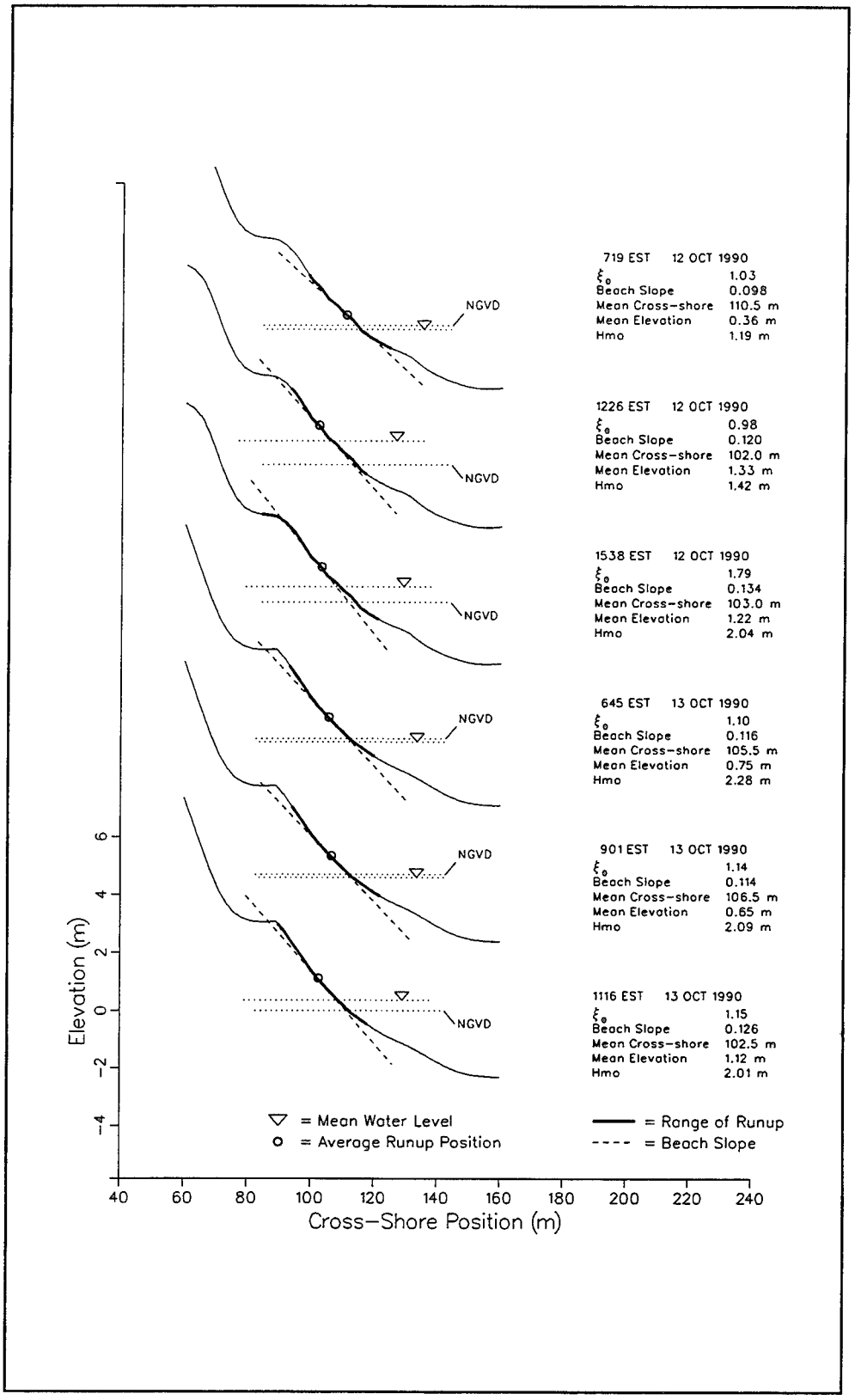

Figure B27. (Sheet 4 of 8)

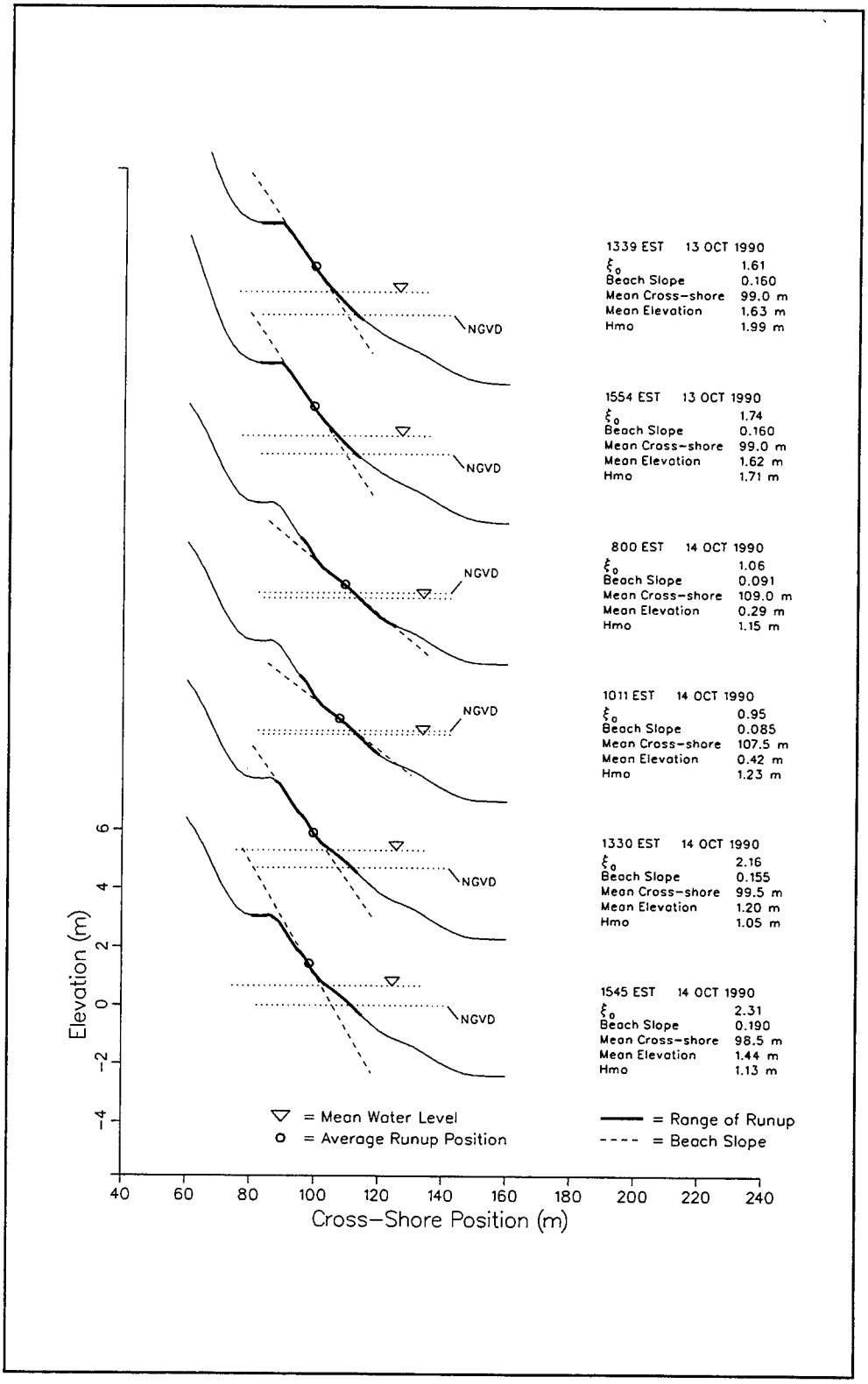

Figure B27. (Sheet 5 of 8)

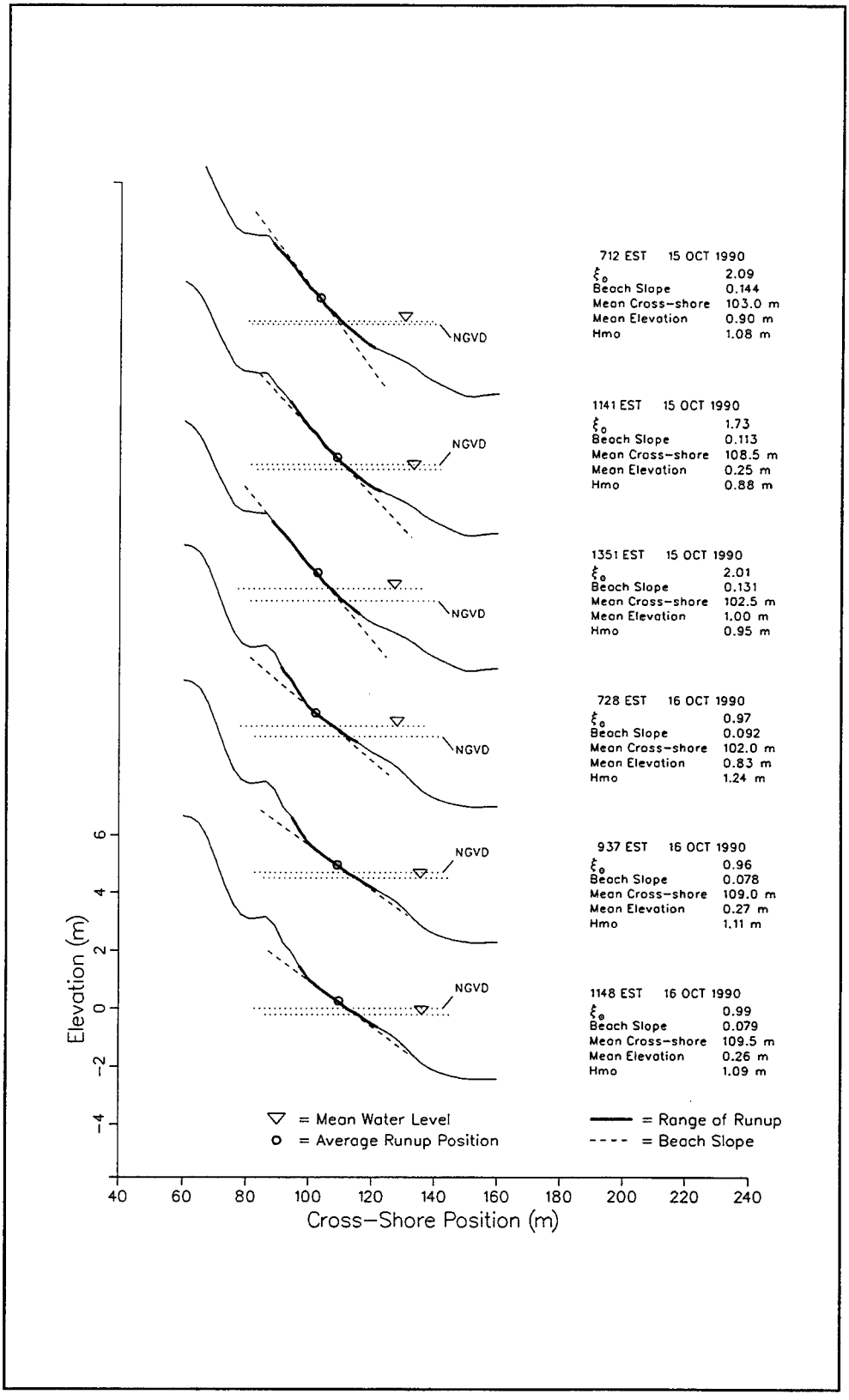

Figure B27. (Sheet 6 of 8)

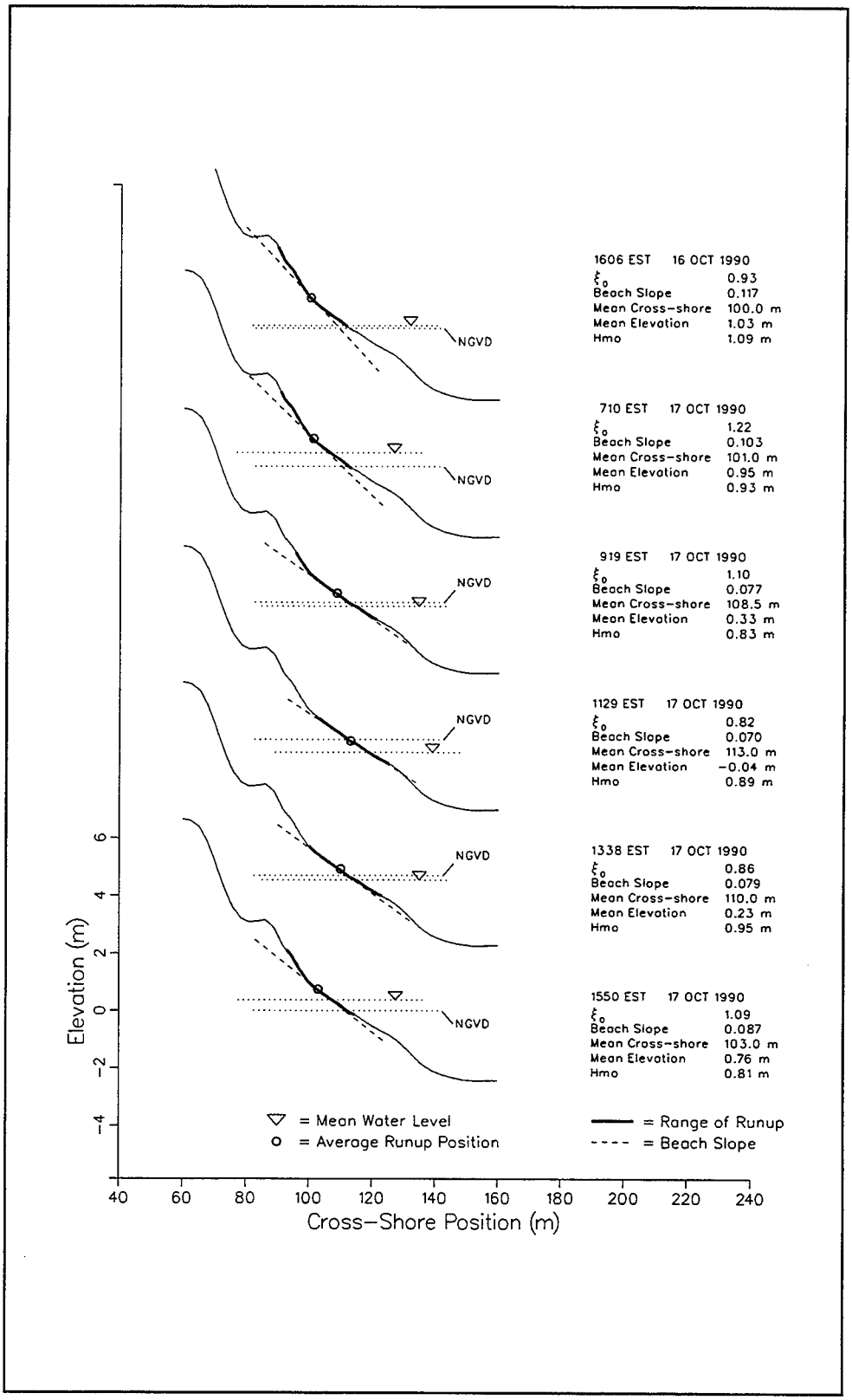

Figure B27. (Sheet 7 of 8)

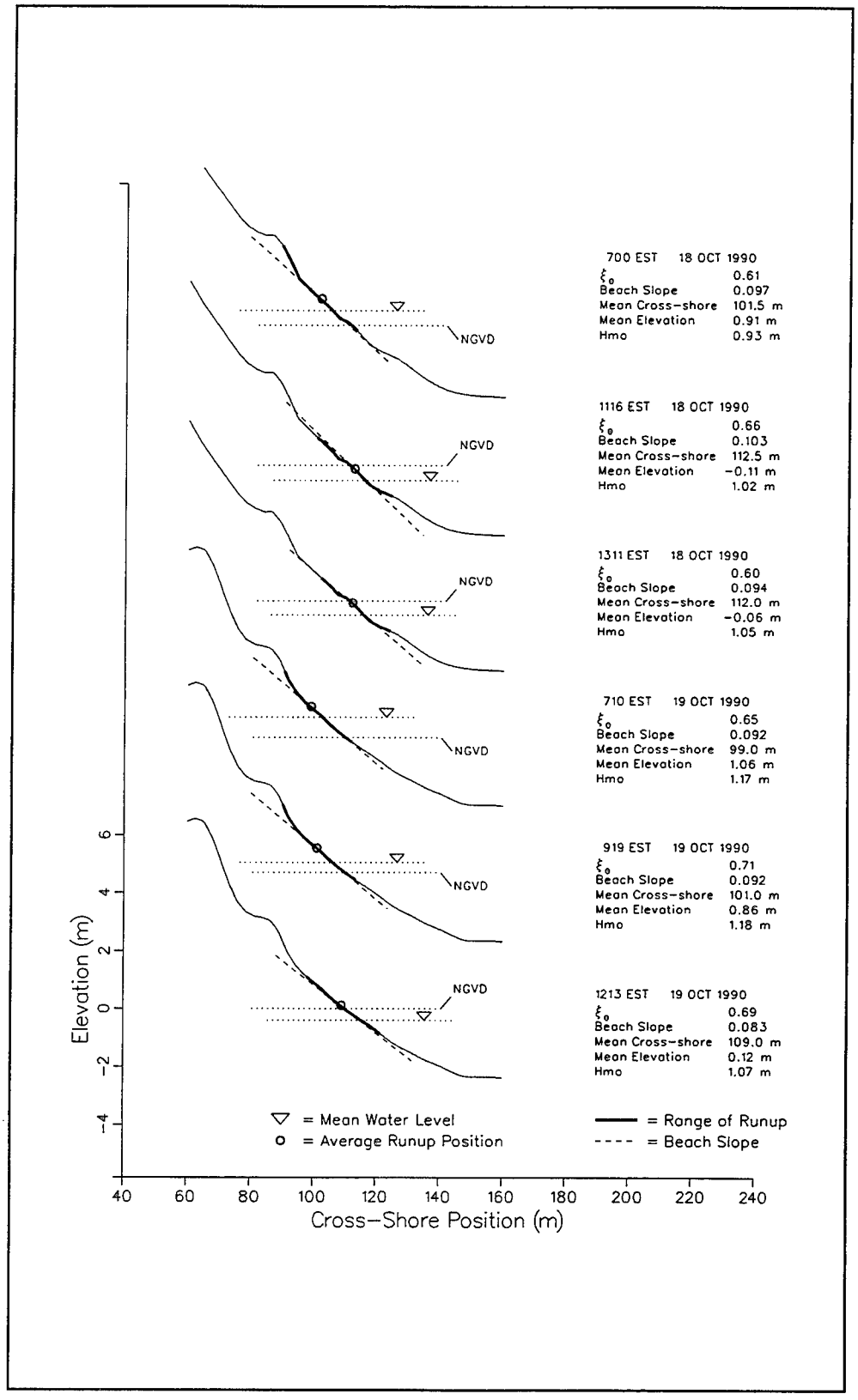

Figure B27. (Sheet 8 of 8)

Appendix C
Sediments

Nineteen sediment samples were collected along profile line 230 on 15 October 1990. Beach samples were scraped from the top layer of the beach face. Offshore samples were collected with a clamshell grab sampler by a person atop the Coastal Research Amphibious Buggy (CRAB) deck. The samples were then washed, dried, split, and sieved for analysis of grain size and sorting. The sieving was done with a *sonic sifter*, which sorts the sediments through small diameter sieves using high-frequency vibrations.

The size distribution of each sample, along with its relative position along the profile, are shown in Figure C1. The overall nature of the cross-shore size distribution is typical of sediments at the Field Research Facility with a wide range in sediment size on the beach face and in the inner bar/trough region. Seaward of the inner bar, the sediment is composed of fine, well-sorted sediments. Detailed tables and plots describing each sample are shown in Figures C2 through C20.

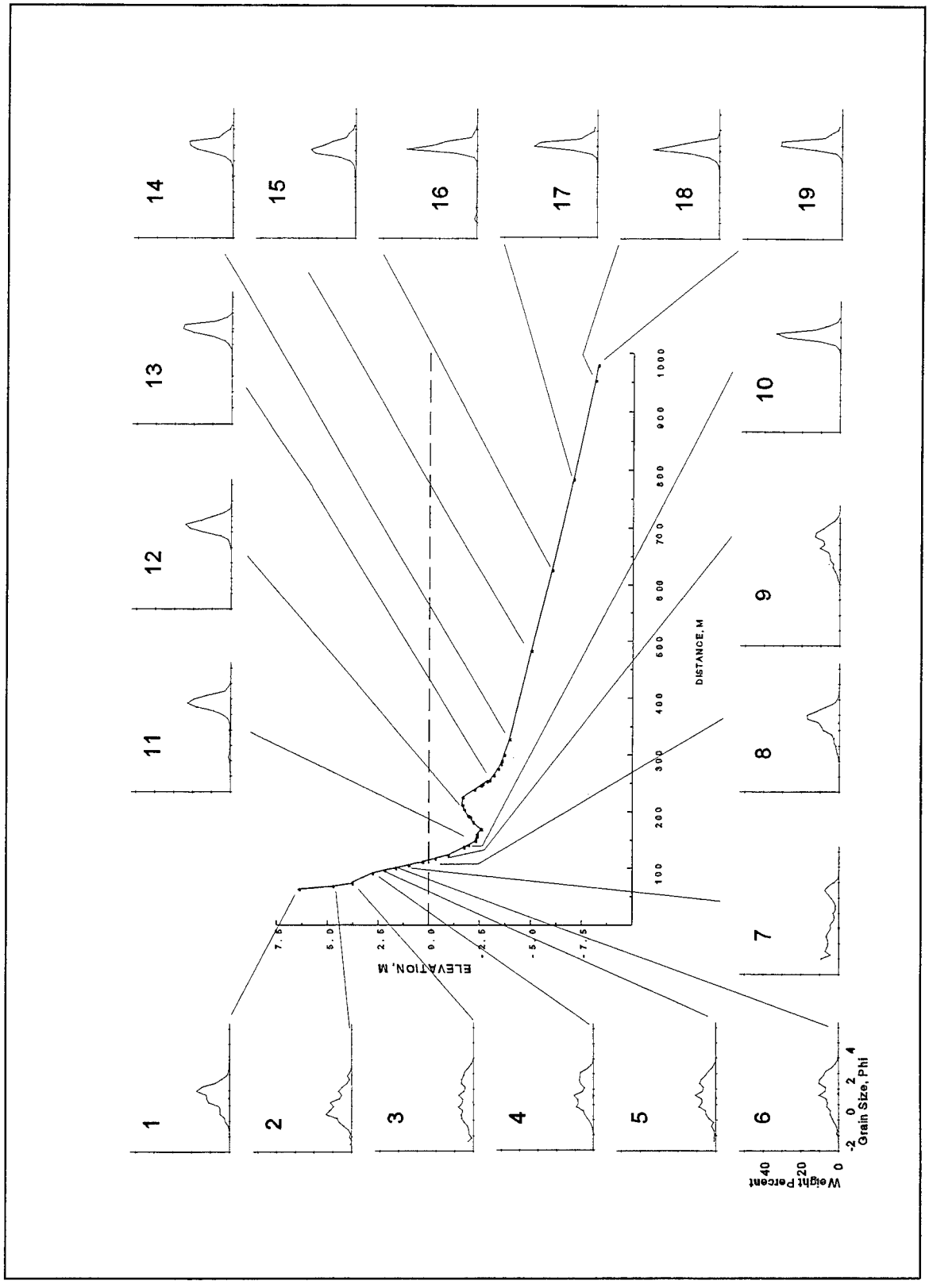

Figure C1. Schematic plot of cross-shore sediment size by sample number on profile line 230, 15 October 1990

DELILAH Sediment Sample - 1

Location: Longshore = 1005.8 m, Cross-shore = 44.6 m, Depth = 5.85 m

SIZE CLASSIFICATION: (By Weight Percent)	Gravel	Sand			Silt	Clay
		Coarse	Medium	Fine		
Wentworth	0.02	30.97	55.88	13.10	0.02	0.00
Unified	0.00	0.02	42.96	56.98	0.03	0.00

STANDARD STATISTICS:	Method of Moments	Folk Graphic Measures	Grain Size
Median Diameter		1.40 phi	0.380 mm
Mean Diameter	1.29 phi	1.30 phi	0.408 mm
Standard Deviation	0.70 phi	0.69 phi	
Skewness	-0.47	-0.21	
Kurtosis	2.94	1.01	

Diam. (phi)	Weight (%)	Diam. (phi)	Weight (%)	Diam. (phi)	Weight (%)	Diam. (phi)	Weight (%)	Diam. (phi)	Weight (%)
-1.50	0.000	-1.25	0.023	-1.00	0.000	-0.75	0.057	-0.50	0.540
-0.25	1.905	0.00	2.513	0.25	4.811	0.50	4.792	0.75	5.358
1.00	10.995	1.25	11.995	1.50	12.074	1.75	17.440	2.00	14.376
2.25	7.410	2.50	3.924	2.75	1.200	3.00	0.423	3.25	0.098
3.5	0.026	3.75	0.008	4.00	0.015	4.25	0.019		

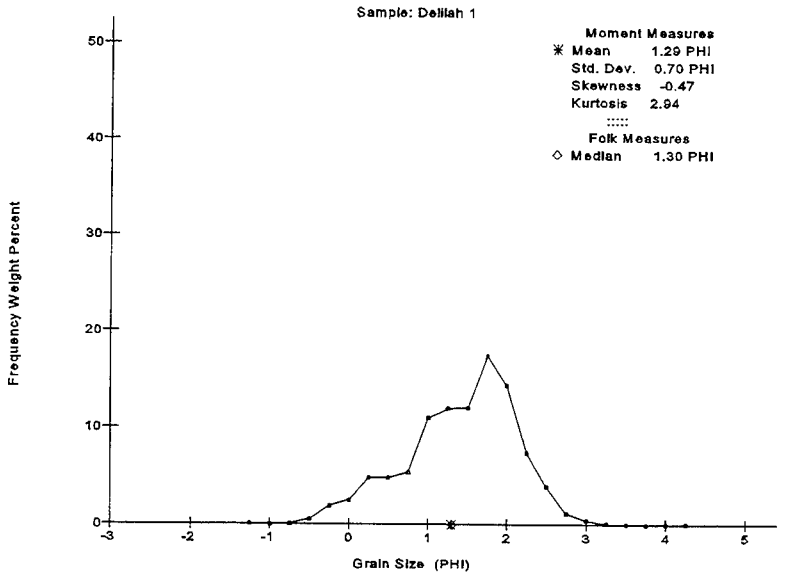

Figure C2. Grain size distribution for sediment sample 1, 15 October 1990

DELILAH Sediment Sample - 2

Location: Longshore = 1005.8 m, Cross-shore = 52.3 m, Depth = 7.51 m

SIZE CLASSIFICATION: (By Weight Percent)	Gravel	Sand			Silt	Clay
		Coarse	Medium	Fine		
Wentworth	2.16	67.08	23.88	6.81	0.06	0.00
Unified	0.00	2.16	73.80	23.98	0.06	0.00

STANDARD STATISTICS:	Method of Moments	Folk Graphic Measures	Grain Size
Median Diameter		0.55 phi	0.685 mm
Mean Diameter	0.64 phi	0.64 phi	0.644 mm
Standard Deviation	0.89 phi	0.89 phi	
Skewness	0.25	0.15	
Kurtosis	3.04	1.00	

Diam. (phi)	Weight (%)	Diam. (phi)	Weight (%)	Diam. (phi)	Weight (%)	Diam. (phi)	Weight (%)	Diam. (phi)	Weight (%)
-2.00	0.000	-1.75	0.617	-1.50	0.000	-1.25	1.040	-1.00	0.502
-0.75	1.753	-0.50	4.274	-0.25	6.692	0.00	7.774	0.25	13.819
0.50	11.782	0.75	9.654	1.00	11.335	1.25	6.716	1.50	5.217
1.75	6.958	2.00	4.993	2.25	2.527	2.50	1.064	2.75	2.231
3.00	0.762	3.25	0.181	3.5	0.048	3.75	0.000	4.00	0.000
4.25	0.060								

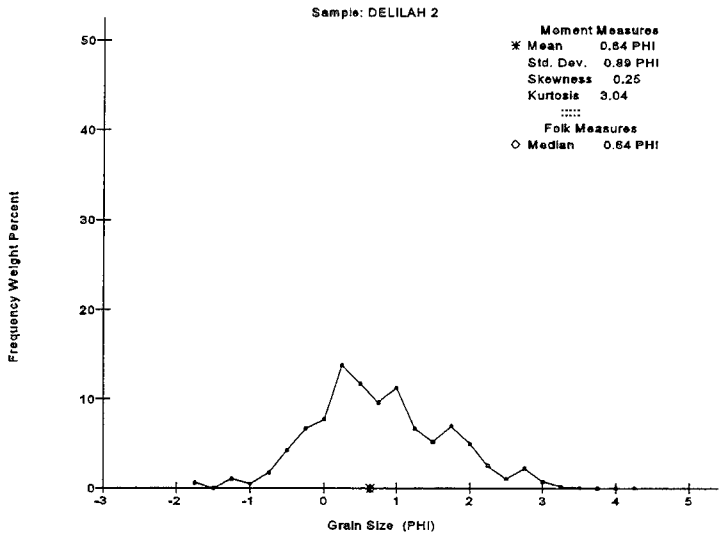

Figure C3. Grain size distribution for sediment sample 2, 15 October 1990

DELILAH Sediment Sample - 3

Location: Longshore = 1011.97 m, Cross-shore = 91.41 m, Depth = 2.86 m

SIZE CLASSIFICATION: (By Weight Percent)	Gravel	Sand			Silt	Clay
		Coarse	Medium	Fine		
Wentworth	11.96	51.28	22.37	14.39	0.00	0.00
Unified	0.00	11.96	56.39	31.65	0.00	0.00

STANDARD STATISTICS:	Method of Moments	Folk Graphic Measures	Grain Size
Median Diameter		0.52 phi	0.696 mm
Mean Diameter	0.52 phi	0.55 phi	0.697 mm
Standard Deviation	1.26 phi	1.31 phi	
Skewness	-0.12	-0.01	
Kurtosis	2.19	0.83	

Diam. (phi)	Weight (%)	Diam. (phi)	Weight (%)	Diam. (phi)	Weight (%)	Diam. (phi)	Weight (%)	Diam. (phi)	Weight (%)
-2.25	0.000	-2.00	3.014	-1.75	0.917	-1.50	2.448	-1.25	2.492
-1.00	3.090	-0.75	4.992	-0.50	6.280	-0.25	6.623	0.00	5.766
0.25	7.895	0.50	5.953	0.75	5.829	1.00	7.947	1.25	5.104
1.50	4.438	1.75	6.491	2.00	6.336	2.25	5.399	2.50	4.649
2.75	2.739	3.00	1.264	3.25	0.291	3.5	0.044		

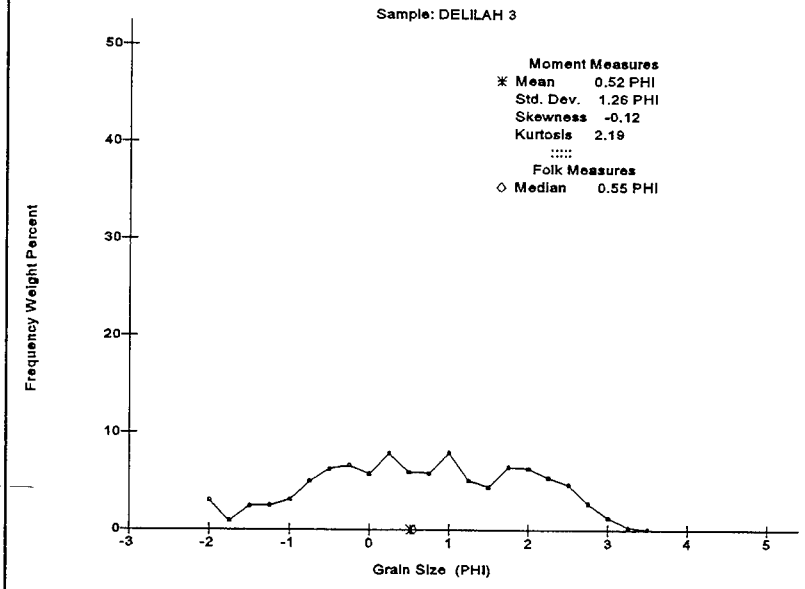

Figure C4. Grain size distribution for sediment sample 3, 15 October 1990

DELILAH Sediment Sample - 4

Location: Longshore = 1011.05 m, Cross-shore = 96.46 m, Depth = 2.18 m

SIZE CLASSIFICATION: (By Weight Percent)	Gravel -------	Sand -------			Silt	Clay
		Coarse	Medium	Fine		
Wentworth	1.34	52.82	26.02	19.79	0.02	0.00
Unified	0.00	1.34	58.92	39.72	0.02	0.00

STANDARD STATISTICS:	Method of Moments	Folk Graphic Measures	Grain Size
Median Diameter		0.90 phi	0.534 mm
Mean Diameter	0.98 phi	1.00 phi	0.505 mm
Standard Deviation	0.99 phi	1.02 phi	
Skewness	-0.01	0.08	
Kurtosis	2.13	0.79	

Diam. (phi)	Weight (%)	Diam. (phi)	Weight (%)	Diam. (phi)	Weight (%)	Diam. (phi)	Weight (%)	Diam. (phi)	Weight (%)
-1.75	0.000	-1.50	0.005	-1.25	0.393	-1.00	0.942	-0.75	1.811
-0.50	3.262	-0.25	4.915	0.00	5.622	0.25	9.313	0.50	8.399
0.75	8.607	1.00	10.893	1.25	6.094	1.50	5.031	1.75	7.045
2.00	7.854	2.25	7.429	2.50	7.184	2.75	3.520	3.00	1.326
3.25	0.254	3.5	0.060	3.75	0.018	4.00	0.000	4.25	0.023

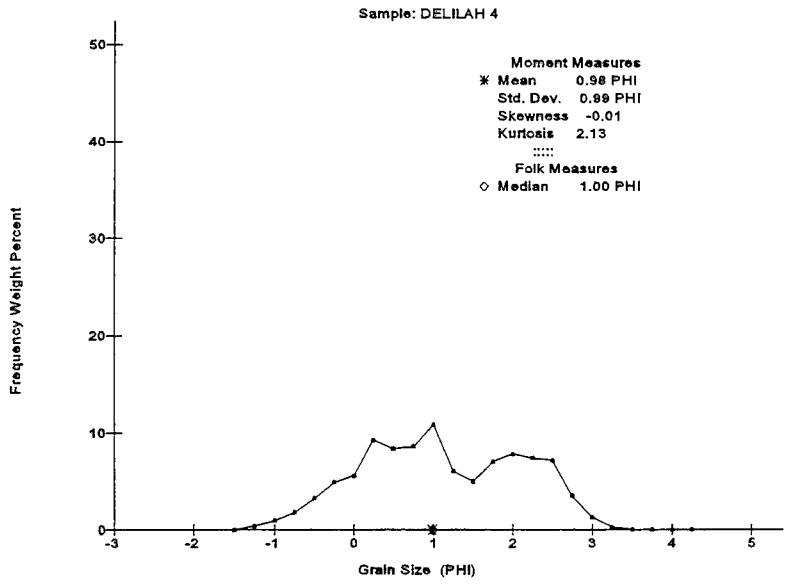

Figure C5. Grain size distribution for sediment sample 4, 15 October 1990

DELILAH Sediment Sample - 5

Location: Longshore = 1010.83 m, Cross-shore = 100.48 m, Depth = 1.66 m

SIZE CLASSIFICATION: (By Weight Percent)	Gravel	Sand			Silt	Clay
		Coarse	Medium	Fine		
Wentworth	5.99	50.71	30.11	13.18	0.00	0.00
Unified	0.00	5.99	57.93	36.08	0.00	0.00

STANDARD STATISTICS:	Method of Moments	Folk Graphic Measures	Grain Size
Median Diameter		0.85 phi	0.556 mm
Mean Diameter	0.80 phi	0.83 phi	0.575 mm
Standard Deviation	1.06 phi	1.07 phi	
Skewness	-0.36	-0.07	
Kurtosis	2.77	0.93	

Diam. (phi)	Weight (%)	Diam. (phi)	Weight (%)	Diam. (phi)	Weight (%)	Diam. (phi)	Weight (%)	Diam. (phi)	Weight (%)
-2.25	0.000	-2.00	1.021	-1.75	0.945	-1.50	0.684	-1.25	1.057
-1.00	2.282	-0.75	1.338	-0.50	3.702	-0.25	5.198	0.00	5.459
0.25	9.069	0.50	7.506	0.75	7.455	1.00	10.983	1.25	7.220
1.50	6.556	1.75	8.532	2.00	7.802	2.25	5.678	2.50	4.141
2.75	2.165	3.00	0.975	3.25	0.209	3.5	0.015		

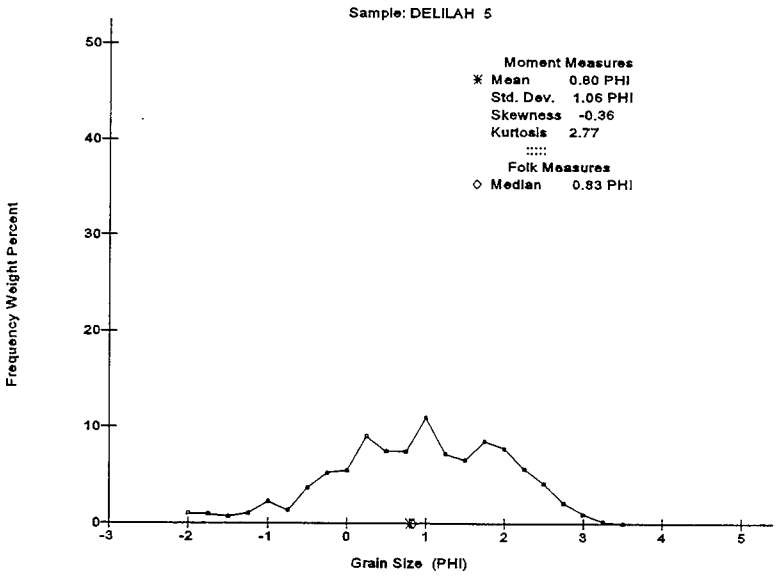

Figure C6. Grain size distribution for sediment sample 5, 15 October 1990

DELILAH Sediment Sample - 6

Location: Longshore = 1009.99 m, Cross-shore = 105.69 m, Depth = 1.02 m

SIZE CLASSIFICATION: (By Weight Percent)	Gravel	Sand			Silt	Clay
		Coarse	Medium	Fine		
Wentworth	2.42	42.79	33.96	20.82	0.00	0.00
Unified	0.00	2.42	49.84	47.74	0.00	0.00

STANDARD STATISTICS:	Method of Moments	Folk Graphic Measures	Grain Size
Median Diameter		1.17 phi	0.444 mm
Mean Diameter	1.09 phi	1.10 phi	0.471 mm
Standard Deviation	1.03 phi	1.05 phi	
Skewness	-0.37	-0.13	
Kurtosis	2.44	0.88	

Diam. (phi)	Weight (%)	Diam. (phi)	Weight (%)	Diam. (phi)	Weight (%)	Diam. (phi)	Weight (%)	Diam. (phi)	Weight (%)
-2.25	0.000	-2.00	0.012	-1.75	0.000	-1.50	0.784	-1.25	0.555
-1.00	1.067	-0.75	2.388	-0.50	3.208	-0.25	4.387	0.00	4.158
0.25	6.145	0.50	5.812	0.75	6.355	1.00	10.334	1.25	7.052
1.50	6.904	1.75	10.155	2.00	9.853	2.25	7.953	2.50	6.904
2.75	3.714	3.00	1.734	3.25	0.401	3.5	0.099	3.75	0.019

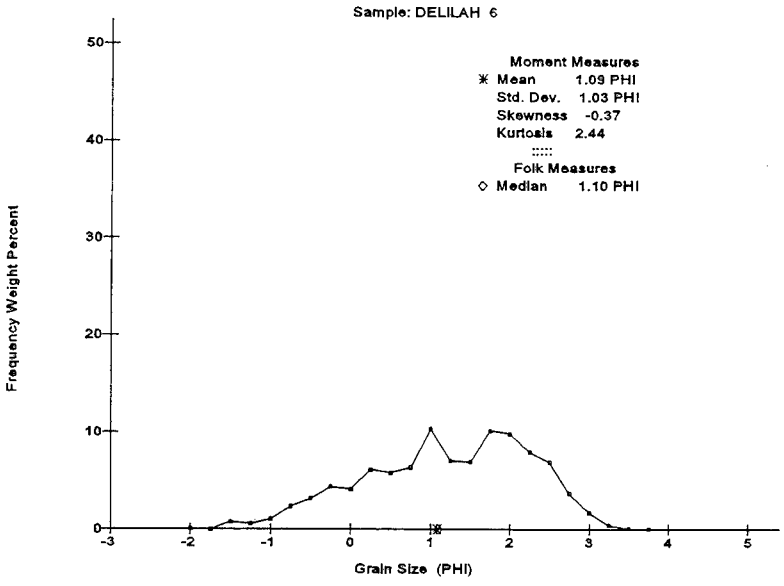

Figure C7. Grain size distribution for sediment sample 6, 15 October 1990

DELILAH Sediment Sample - 7

Location: Longshore = 1008.98 m, Cross-shore = 111.20 m, Depth = 0.34 m

SIZE CLASSIFICATION: (By Weight Percent)	Gravel	Sand			Silt	Clay
		Coarse	Medium	Fine		
Wentworth	32.76	35.11	10.19	21.94	0.00	0.00
Unified	0.00	32.76	36.88	30.36	0.00	0.00

STANDARD STATISTICS:	Method of Moments	Folk Graphic Measures	Grain Size
Median Diameter		-0.29 phi	1.219 mm
Mean Diameter	0.09 phi	0.10 phi	0.937 mm
Standard Deviation	1.63 phi	1.70 phi	
Skewness	0.30	0.26	
Kurtosis	1.69	0.62	

Diam. (phi)	Weight (%)	Diam. (phi)	Weight (%)	Diam. (phi)	Weight (%)	Diam. (phi)	Weight (%)	Diam. (phi)	Weight (%)
-2.25	0.000	-2.00	9.342	-1.75	4.259	-1.50	7.211	-1.25	6.226
-1.00	5.721	-0.75	5.842	-0.50	6.581	-0.25	5.612	0.00	4.239
0.25	4.510	0.50	2.891	0.75	2.418	1.00	3.016	1.25	1.776
1.50	1.688	1.75	2.705	2.00	4.025	2.25	5.773	2.50	7.517
2.75	5.600	3.00	2.527	3.25	0.444	3.5	0.065	3.75	0.012

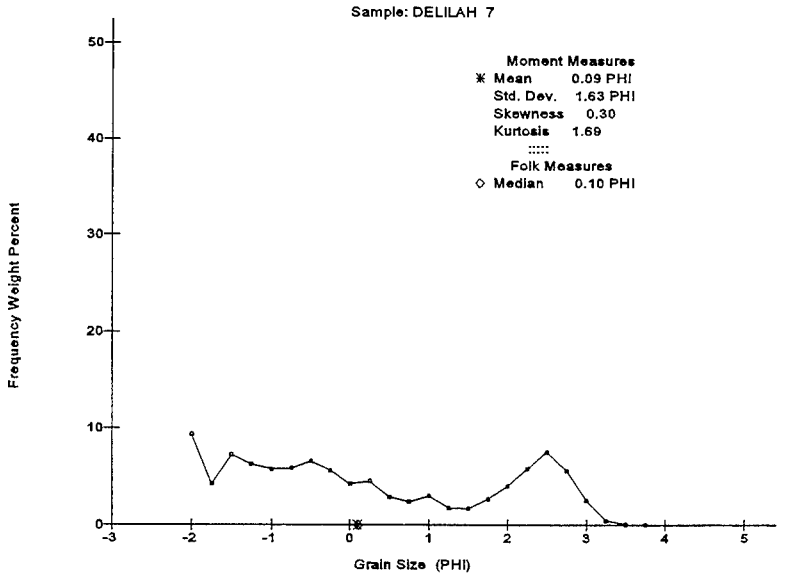

Figure C8. Grain size distribution for sediment sample 7, 15 October 1990

DELILAH Sediment Sample - 8

Location: Longshore = 1007.53 m, Cross-shore = 117.32 m, Depth = -0.29 m

SIZE CLASSIFICATION: (By Weight Percent)	Gravel	Sand			Silt	Clay
		Coarse	Medium	Fine		
Wentworth	0.17	22.58	53.73	23.52	0.00	0.00
Unified	0.00	0.17	31.87	67.96	0.00	0.00

STANDARD STATISTICS:	Method of Moments	Folk Graphic Measures	Grain Size
Median Diameter		1.61 phi	0.328 mm
Mean Diameter	1.48 phi	1.52 phi	0.358 mm
Standard Deviation	0.73 phi	0.71 phi	
Skewness	-0.75	-0.24	
Kurtosis	3.56	1.09	

Diam. (phi)	Weight (%)	Diam. (phi)	Weight (%)	Diam. (phi)	Weight (%)	Diam. (phi)	Weight (%)	Diam. (phi)	Weight (%)
-1.25	0.000	-1.00	0.166	-0.75	0.266	-0.50	0.973	-0.25	1.456
0.00	1.741	0.25	2.884	0.50	2.842	0.75	3.933	1.00	8.487
1.25	9.289	1.50	10.816	1.75	16.747	2.00	16.879	2.25	11.727
2.50	7.467	2.75	2.908	3.00	1.015	3.25	0.289	3.5	0.085
3.75	0.024								

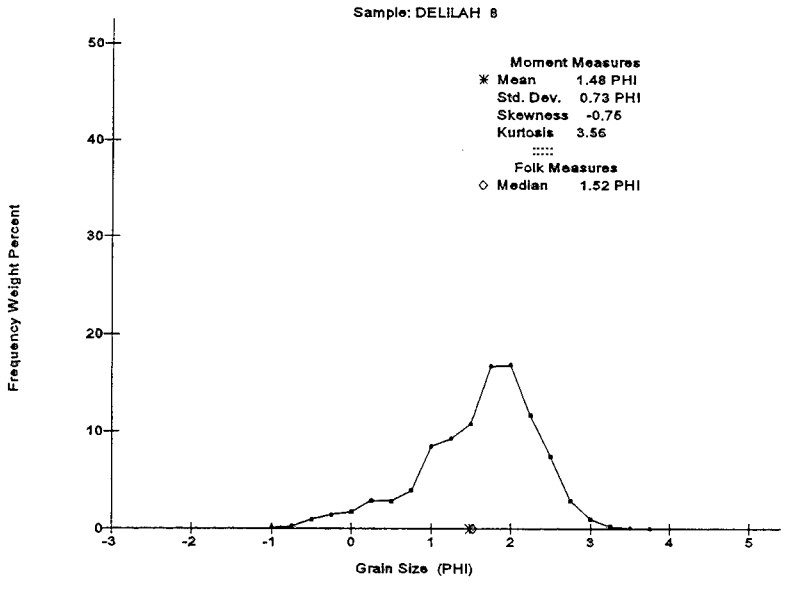

Figure C9. Grain size distribution for sediment sample 8, 15 October 1990

DELILAH Sediment Sample - 9

Location: Longshore = 1006.15 m, Cross-shore = 123.63 m, Depth = -0.93 m

SIZE CLASSIFICATION: (By Weight Percent)	Gravel	Sand			Silt	Clay
		Coarse	Medium	Fine		
Wentworth	1.17	37.19	42.28	19.36	0.00	0.00
Unified	0.00	1.17	45.27	53.56	0.00	0.00

STANDARD STATISTICS:	Method of Moments	Folk Graphic Measures	Grain Size
Median Diameter		1.35 phi	0.392 mm
Mean Diameter	1.20 phi	1.22 phi	0.434 mm
Standard Deviation	0.91 phi	0.92 phi	
Skewness	-0.51	-0.23	
Kurtosis	2.65	0.97	

Diam. (phi)	Weight (%)	Diam. (phi)	Weight (%)	Diam. (phi)	Weight (%)	Diam. (phi)	Weight (%)	Diam. (phi)	Weight (%)
-2.25	0.000	-2.00	0.005	-1.75	0.020	-1.50	0.000	-1.25	0.121
-1.00	1.025	-0.75	1.278	-0.50	2.541	-0.25	3.531	0.00	3.313
0.25	5.066	0.50	5.147	0.75	5.854	1.00	10.456	1.25	8.082
1.50	8.662	1.75	13.042	2.00	12.491	2.25	9.001	2.50	6.076
2.75	2.859	3.00	1.136	3.25	0.247	3.5	0.035	3.75	0.005

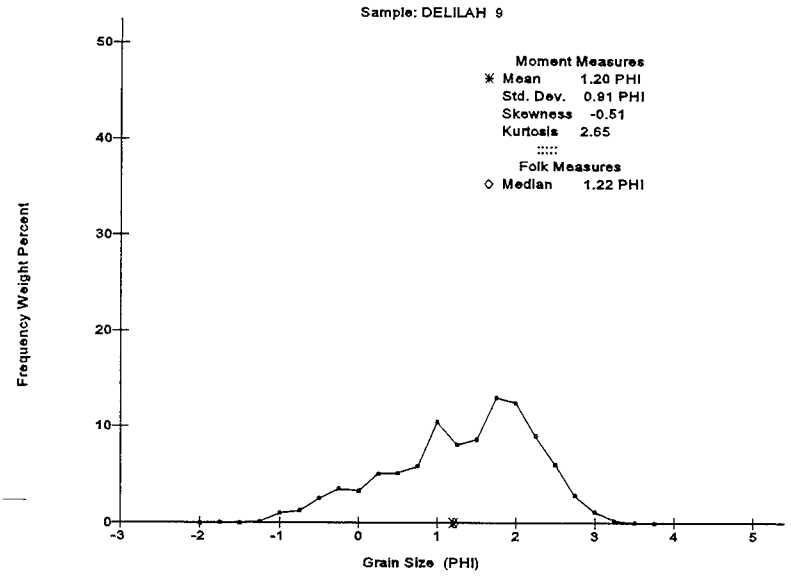

Figure C10. Grain size distribution for sediment sample 9, 15 October 1990

DELILAH Sediment Sample - 10

Location: Longshore = 1006.25 m, Cross-shore = 137.57 m, Depth = -1.7 m

SIZE CLASSIFICATION: (By Weight Percent)	Gravel	Sand			Silt	Clay
		Coarse	Medium	Fine		
Wentworth	0.12	0.24	0.34	98.75	0.56	0.00
Unified	0.00	0.12	0.28	97.31	2.29	0.00

STANDARD STATISTICS:	Method of Moments	Folk Graphic Measures	Grain Size
Median Diameter		3.05 phi	0.121 mm
Mean Diameter	3.04 phi	3.06 phi	0.122 mm
Standard Deviation	0.39 phi	0.32 phi	
Skewness	-2.78	0.06	
Kurtosis	31.98	1.17	

Diam. (phi)	Weight (%)	Diam. (phi)	Weight (%)	Diam. (phi)	Weight (%)	Diam. (phi)	Weight (%)	Diam. (phi)	Weight (%)
-2.25	0.000	-2.00	0.013	-1.75	0.000	-1.50	0.000	-1.25	0.058
-1.00	0.045	-0.75	0.051	-0.50	0.032	-0.25	0.000	0.00	0.006
0.25	0.000	0.50	0.032	0.75	0.038	1.00	0.083	1.25	0.038
1.50	0.045	1.75	0.077	2.00	0.179	2.25	0.563	2.50	2.520
2.75	11.015	3.00	28.900	3.25	34.114	3.5	13.529	3.75	6.371
4.00	1.734	4.25	0.557						

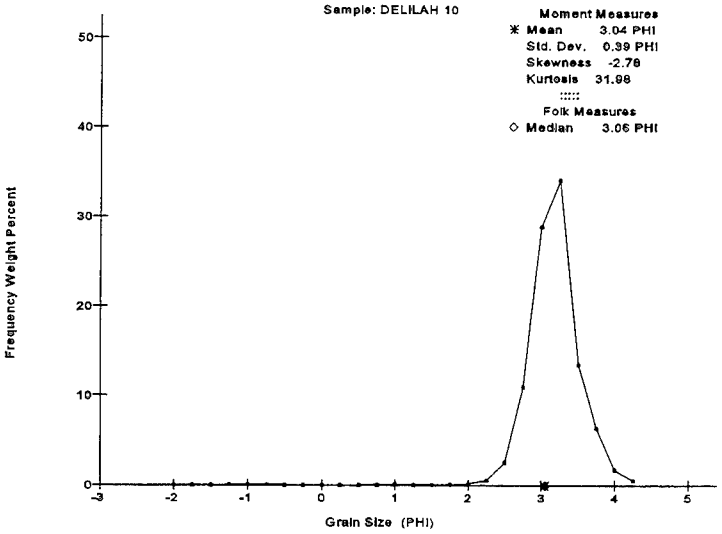

Figure C11. Grain size distribution for sediment sample 10, 15 October 1990

DELILAH Sediment Sample - 11

Location: Longshore = 1006.64 m, Cross-shore = 148.91 m, Depth = -2.29 m

SIZE CLASSIFICATION: (By Weight Percent)	Gravel	Sand			Silt	Clay
		Coarse	Medium	Fine		
Wentworth	1.26	4.09	7.22	87.37	0.06	0.00
Unified	0.00	1.26	4.57	93.81	0.36	0.00

STANDARD STATISTICS:	Method of Moments	Folk Graphic Measures	Grain Size
Median Diameter		2.61 phi	0.164 mm
Mean Diameter	2.46 phi	2.58 phi	0.182 mm
Standard Deviation	0.82 phi	0.59 phi	
Skewness	-2.64	-0.28	
Kurtosis	11.72	1.59	

Diam. (phi)	Weight (%)	Diam. (phi)	Weight (%)	Diam. (phi)	Weight (%)	Diam. (phi)	Weight (%)	Diam. (phi)	Weight (%)
-2.25	0.000	-2.00	0.021	-1.75	0.000	-1.50	0.360	-1.25	0.360
-1.00	0.524	-0.75	0.946	-0.50	0.637	-0.25	0.406	0.00	0.262
0.25	0.386	0.50	0.288	0.75	0.406	1.00	0.756	1.25	0.483
1.50	0.699	1.75	1.707	2.00	4.328	2.25	9.197	2.50	18.331
2.75	22.942	3.00	19.575	3.25	12.517	3.5	3.131	3.75	1.378
4.00	0.303	4.25	0.057						

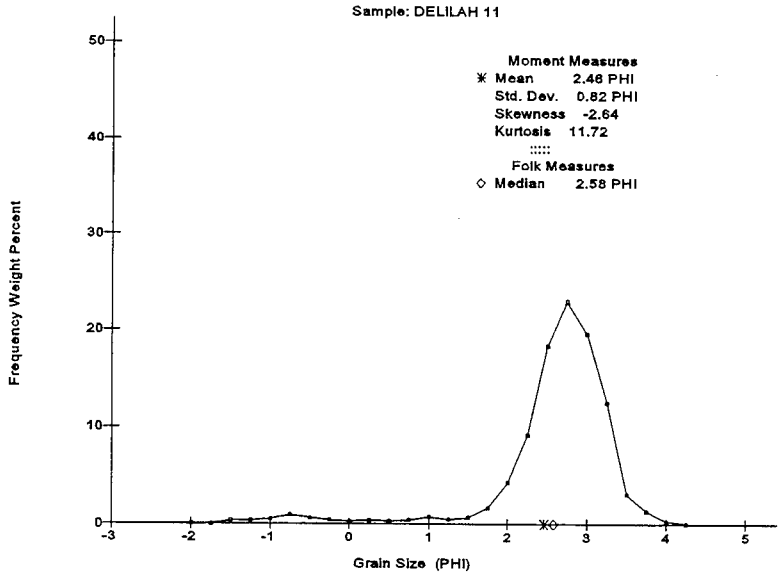

Figure C12. Grain size distribution for sediment sample 11, 15 October 1990

DELILAH Sediment Sample - 12

Location: Longshore = 1007.65 m, Cross-shore = 192.47 m, Depth = -1.94 m

SIZE CLASSIFICATION: (By Weight Percent)	Gravel	Sand			Silt	Clay
		Coarse	Medium	Fine		
Wentworth	0.11	0.94	22.36	76.57	0.02	0.00
Unified	0.00	0.11	1.73	98.12	0.04	0.00

STANDARD STATISTICS:	Method of Moments	Folk Graphic Measures	Grain Size
Median Diameter		2.30 phi	0.203 mm
Mean Diameter	2.29 phi	2.30 phi	0.205 mm
Standard Deviation	0.47 phi	0.43 phi	
Skewness	-1.15	-0.01	
Kurtosis	9.73	1.02	

Diam. (phi)	Weight (%)	Diam. (phi)	Weight (%)	Diam. (phi)	Weight (%)	Diam. (phi)	Weight (%)	Diam. (phi)	Weight (%)
-2.00	0.000	-1.75	0.011	-1.50	0.000	-1.25	0.005	-1.00	0.091
-0.75	0.080	-0.50	0.128	-0.25	0.027	0.00	0.000	0.25	0.037
0.50	0.091	0.75	0.101	1.00	0.480	1.25	0.785	1.50	1.516
1.75	5.486	2.00	14.575	2.25	21.711	2.50	24.262	2.75	15.734
3.00	9.852	3.25	4.072	3.5	0.742	3.75	0.171	4.00	0.027
4.25	0.016								

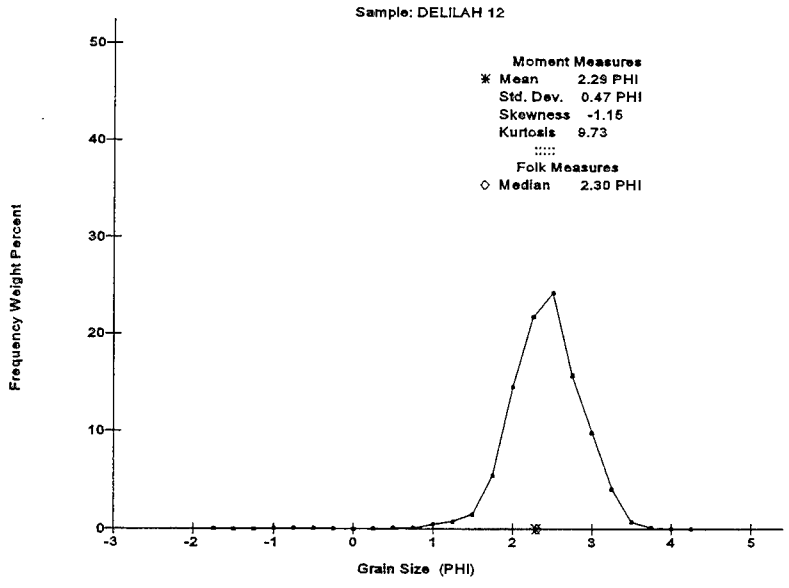

Figure C13. Grain size distribution for sediment sample 12, 15 October 1990

DELILAH Sediment Sample - 13

Location: Longshore = 1007.39 m, Cross-shore = 255.69 m, Depth = -2.95 m

SIZE CLASSIFICATION: (By Weight Percent)	Gravel	Sand			Silt	Clay
		Coarse	Medium	Fine		
Wentworth	0.10	1.43	2.66	95.69	0.11	0.00
Unified	0.00	0.10	1.67	97.85	0.39	0.00

STANDARD STATISTICS:	Method of Moments	Folk Graphic Measures	Grain Size
Median Diameter		2.87 phi	0.137 mm
Mean Diameter	2.80 phi	2.84 phi	0.143 mm
Standard Deviation	0.52 phi	0.39 phi	
Skewness	-2.72	-0.14	
Kurtosis	17.37	1.09	

Diam. (phi)	Weight (%)	Diam. (phi)	Weight (%)	Diam. (phi)	Weight (%)	Diam. (phi)	Weight (%)	Diam. (phi)	Weight (%)
-2.25	0.000	-2.00	0.006	-1.75	0.000	-1.50	0.017	-1.25	0.062
-1.00	0.011	-0.75	0.028	-0.50	0.238	-0.25	0.102	0.00	0.142
0.25	0.249	0.50	0.187	0.75	0.170	1.00	0.318	1.25	0.232
1.50	0.187	1.75	0.533	2.00	1.712	2.25	3.714	2.50	9.508
2.75	20.122	3.00	25.979	3.25	25.412	3.5	8.114	3.75	2.563
4.00	0.278	4.25	0.113						

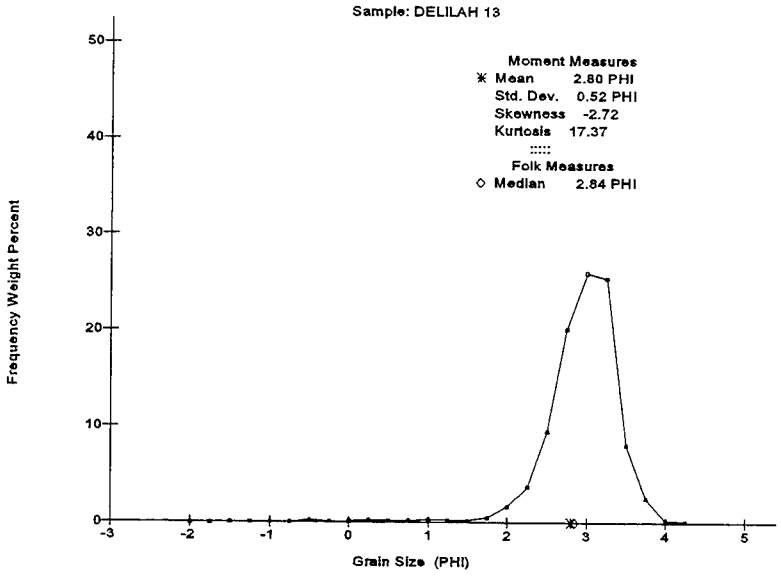

Figure C14. Grain size distribution for sediment sample 13, 15 October 1990

DELILAH Sediment Sample - 14

Location: Longshore = 1007.30 m, Cross-shore = 328.36 m, Depth = -3.95 m

SIZE CLASSIFICATION: (By Weight Percent)	Gravel -------	Sand -------			Silt	Clay
		Coarse	Medium	Fine		
Wentworth	0.09	1.83	3.01	94.28	0.80	0.00
Unified	0.00	0.09	2.19	95.06	2.65	0.00

STANDARD STATISTICS:	Method of Moments	Folk Graphic Measures	Grain Size
Median Diameter		2.87 phi	0.136 mm
Mean Diameter	2.82 phi	2.84 phi	0.142 mm
Standard Deviation	0.58 phi	0.45 phi	
Skewness	-1.98	-0.09	
Kurtosis	12.43	1.16	

Diam. (phi)	Weight (%)	Diam. (phi)	Weight (%)	Diam. (phi)	Weight (%)	Diam. (phi)	Weight (%)	Diam. (phi)	Weight (%)
-2.00	0.000	-1.75	0.061	-1.50	0.000	-1.25	0.000	-1.00	0.028
-0.75	0.083	-0.50	0.039	-0.25	0.266	0.00	0.116	0.25	0.139
0.50	0.233	0.75	0.377	1.00	0.576	1.25	0.366	1.50	0.371
1.75	0.742	2.00	1.529	2.25	4.078	2.50	10.682	2.75	19.098
3.00	22.688	3.25	23.170	3.5	7.469	3.75	5.236	4.00	1.856
4.25	0.798								

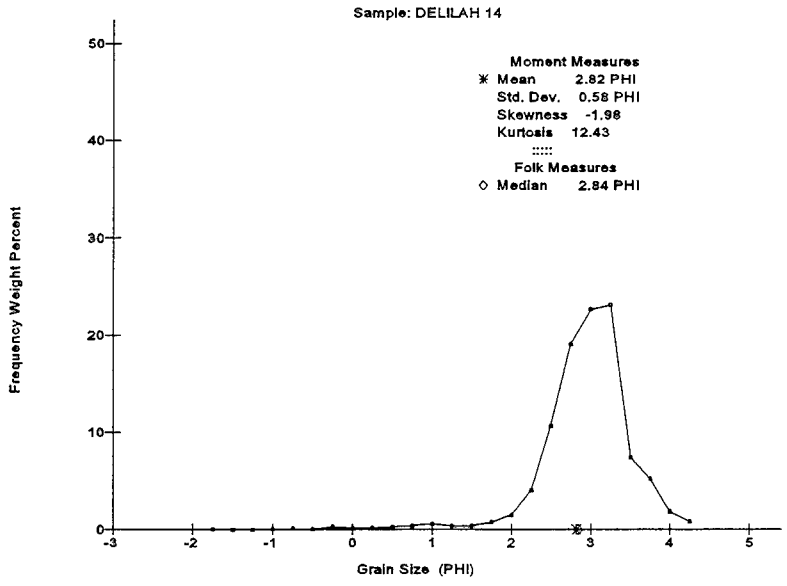

Figure C15. Grain size distribution for sediment sample 14, 15 October 1990

DELILAH Sediment Sample - 15

Location: Longshore = 1004.68 m, Cross-shore = 483.59 m, Depth = -5.00 m

SIZE CLASSIFICATION: (By Weight Percent)	Gravel	Sand			Silt	Clay
		Coarse	Medium	Fine		
Wentworth	0.07	1.34	4.69	93.29	0.62	0.00
Unified	0.00	0.07	1.68	96.31	1.94	0.00

STANDARD STATISTICS:	Method of Moments	Folk Graphic Measures	Grain Size
Median Diameter		2.64 phi	0.160 mm
Mean Diameter	2.66 phi	2.68 phi	0.158 mm
Standard Deviation	0.54 phi	0.47 phi	
Skewness	-1.04	0.12	
Kurtosis	9.02	1.12	

Diam. (phi)	Weight (%)	Diam. (phi)	Weight (%)	Diam. (phi)	Weight (%)	Diam. (phi)	Weight (%)	Diam. (phi)	Weight (%)
-1.50	0.000	-1.25	0.065	-1.00	0.006	-0.75	0.029	-0.50	0.082
-0.25	0.024	0.00	0.053	0.25	0.206	0.50	0.224	0.75	0.235
1.00	0.483	1.25	0.341	1.50	0.394	1.75	0.971	2.00	2.979
2.25	8.825	2.50	21.376	2.75	23.678	3.00	17.197	3.25	12.028
3.5	5.104	3.75	3.756	4.00	1.325	4.25	0.618		

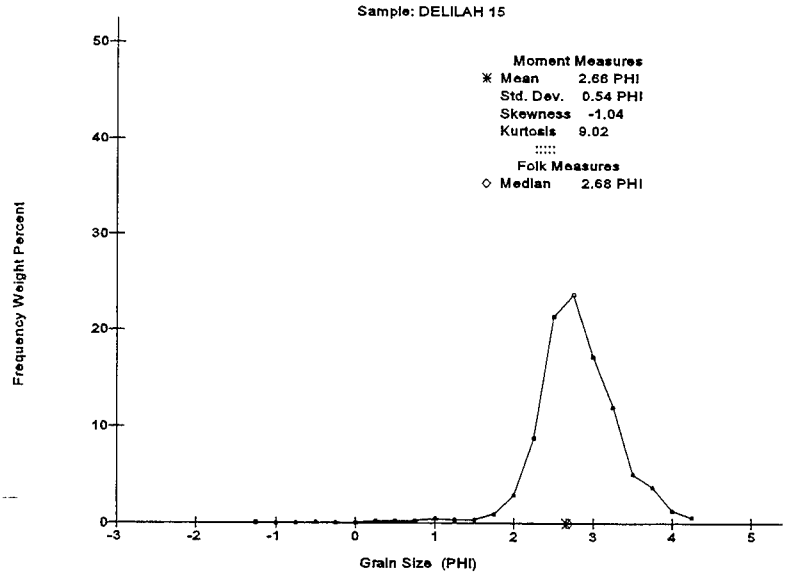

Figure C16. Grain size distribution for sediment sample 15, 15 October 1990

DELILAH Sediment Sample - 16

Location: Longshore = 1004.85 m, Cross-shore = 626.29 m, Depth = -6.04 m

SIZE CLASSIFICATION: (By Weight Percent)	Gravel	Sand			Silt	Clay
		Coarse	Medium	Fine		
Wentworth	2.49	0.25	0.33	96.52	0.42	0.00
Unified	0.00	2.49	0.25	96.13	1.14	0.00

STANDARD STATISTICS:	Method of Moments	Folk Graphic Measures	Grain Size
Median Diameter		2.72 phi	0.152 mm
Mean Diameter	2.67 phi	2.77 phi	0.157 mm
Standard Deviation	0.78 phi	0.32 phi	
Skewness	-4.34	0.19	
Kurtosis	25.09	1.09	

Diam. (phi)	Weight (%)	Diam. (phi)	Weight (%)	Diam. (phi)	Weight (%)	Diam. (phi)	Weight (%)	Diam. (phi)	Weight (%)
-2.25	0.000	-2.00	0.012	-1.75	1.407	-1.50	0.583	-1.25	0.000
-1.00	0.484	-0.75	0.075	-0.50	0.069	-0.25	0.023	0.00	0.023
0.25	0.035	0.50	0.000	0.75	0.000	1.00	0.023	1.25	0.000
1.50	0.000	1.75	0.063	2.00	0.271	2.25	1.886	2.50	11.662
2.75	37.519	3.00	23.301	3.25	16.092	3.5	3.265	3.75	2.071
4.00	0.721	4.25	0.415						

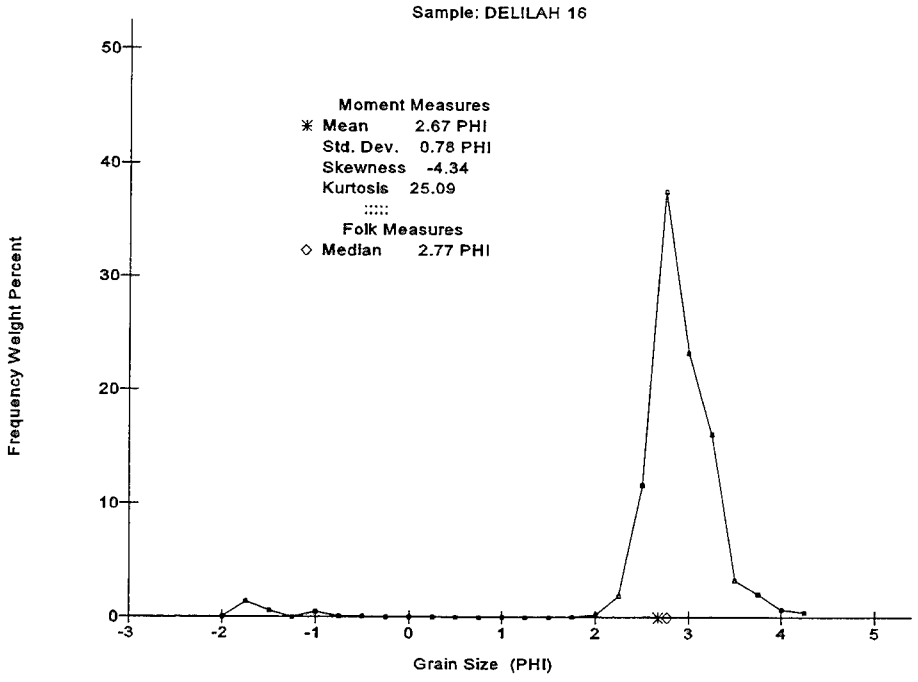

Figure C17. Grain size distribution for sediment sample 16, 15 October 1990

DELILAH Sediment Sample - 17

Location: Longshore = 1004.98 m, Cross-shore = 784.70 m, Depth = -7.07 m

SIZE CLASSIFICATION: (By Weight Percent)	Gravel	------- Sand -------			Silt	Clay
		Coarse	Medium	Fine		
Wentworth	0.01	0.10	0.07	98.39	1.43	0.00
Unified	0.00	0.01	0.10	96.73	3.16	0.00

STANDARD STATISTICS:	Method of Moments	Folk Graphic Measures	Grain Size
Median Diameter		2.99 phi	0.126 mm
Mean Diameter	3.02 phi	3.01 phi	0.124 mm
Standard Deviation	0.35 phi	0.32 phi	
Skewness	-0.61	0.13	
Kurtosis	15.72	1.22	

Diam. (phi)	Weight (%)	Diam. (phi)	Weight (%)	Diam. (phi)	Weight (%)	Diam. (phi)	Weight (%)	Diam. (phi)	Weight (%)
-1.25	0.000	-1.00	0.006	-0.75	0.023	-0.50	0.063	-0.25	0.000
0.00	0.000	0.25	0.017	0.50	0.000	0.75	0.000	1.00	0.000
1.25	0.000	1.50	0.000	1.75	0.000	2.00	0.075	2.25	0.513
2.50	3.076	2.75	13.339	3.00	34.245	3.25	30.859	3.5	9.203
3.75	5.425	4.00	1.728	4.25	1.428				

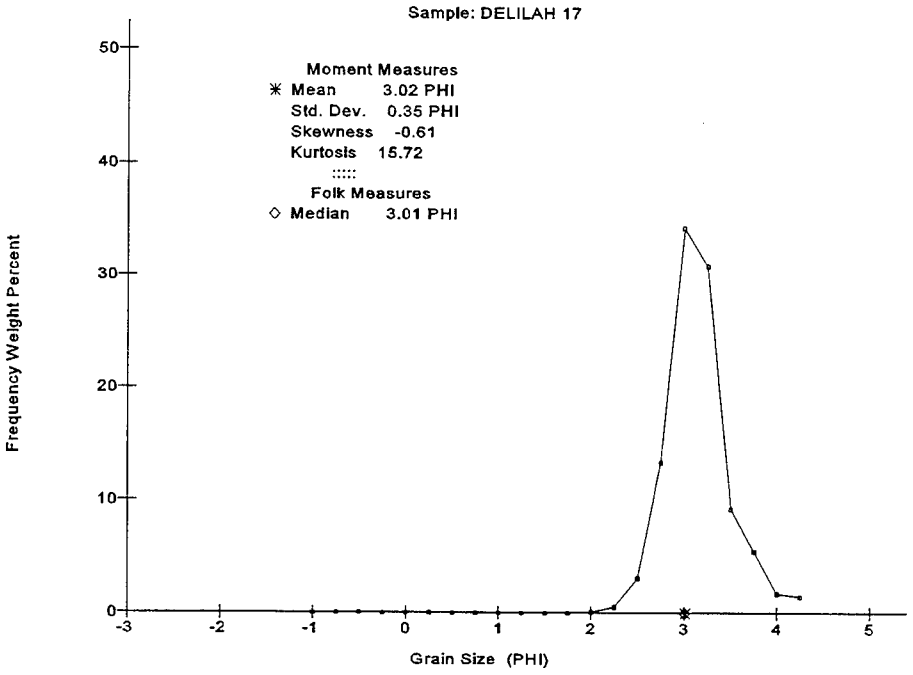

Figure C18. Grain size distribution for sediment sample 17, 15 October 1990

DELILAH Sediment Sample - 18

Location: Longshore = 1006.06 m, Cross-shore = 953.62 m, Depth = -8.13 m

SIZE CLASSIFICATION: (By Weight Percent)	Gravel -------	Sand -------			Silt	Clay
		Coarse	Medium	Fine		
Wentworth	0.28	1.08	3.15	95.49	0.00	0.00
Unified	0.00	0.28	1.22	98.43	0.06	0.00

STANDARD STATISTICS:	Method of Moments	Folk Graphic Measures	Grain Size
Median Diameter		2.67 phi	0.157 mm
Mean Diameter	2.63 phi	2.67 phi	0.161 mm
Standard Deviation	0.48 phi	0.34 phi	
Skewness	-3.61	-0.06	
Kurtosis	26.36	1.17	

Diam. (phi)	Weight (%)	Diam. (phi)	Weight (%)	Diam. (phi)	Weight (%)	Diam. (phi)	Weight (%)	Diam. (phi)	Weight (%)
-2.25	0.000	-2.00	0.005	-1.75	0.000	-1.50	0.010	-1.25	0.155
-1.00	0.109	-0.75	0.098	-0.50	0.258	-0.25	0.109	0.00	0.041
0.25	0.078	0.50	0.072	0.75	0.217	1.00	0.207	1.25	0.140
1.50	0.264	1.75	0.677	2.00	2.068	2.25	5.593	2.50	15.881
2.75	35.174	3.00	23.935	3.25	13.038	3.5	1.391	3.75	0.414
4.00	0.062								

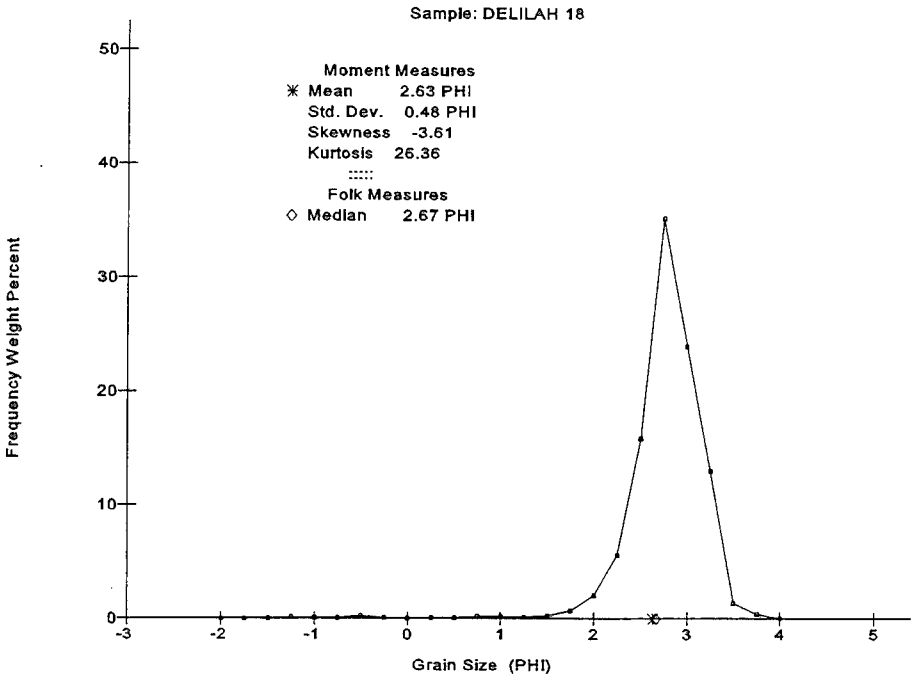

Figure C19. Grain size distribution for sediment sample 18, 15 October 1990

DELILAH Sediment Sample - 19

Location: Longshore = 1005.82 m, Cross-shore = 979.55 m, Depth = -8.27 m

SIZE CLASSIFICATION: (By Weight Percent)	Gravel	Sand			Silt	Clay
		Coarse	Medium	Fine		
Wentworth	0.04	0.26	0.30	98.19	1.21	0.00
Unified	0.00	0.04	0.28	96.47	3.21	0.00

STANDARD STATISTICS:	Method of Moments	Folk Graphic Measures	Grain Size
Median Diameter		3.00 phi	0.125 mm
Mean Diameter	3.01 phi	3.01 phi	0.124 mm
Standard Deviation	0.39 phi	0.32 phi	
Skewness	-1.88	0.10	
Kurtosis	25.50	1.21	

Diam. (phi)	Weight (%)	Diam. (phi)	Weight (%)	Diam. (phi)	Weight (%)	Diam. (phi)	Weight (%)	Diam. (phi)	Weight (%)
-2.25	0.000	-2.00	0.024	-1.75	0.010	-1.50	0.000	-1.25	0.000
-1.00	0.005	-0.75	0.082	-0.50	0.005	-0.25	0.005	0.00	0.014
0.25	0.043	0.50	0.043	0.75	0.019	1.00	0.048	1.25	0.019
1.50	0.029	1.75	0.087	2.00	0.169	2.25	0.700	2.50	2.825
2.75	13.769	3.00	32.121	3.25	31.822	3.5	9.123	3.75	5.829
4.00	1.999	4.25	1.207						

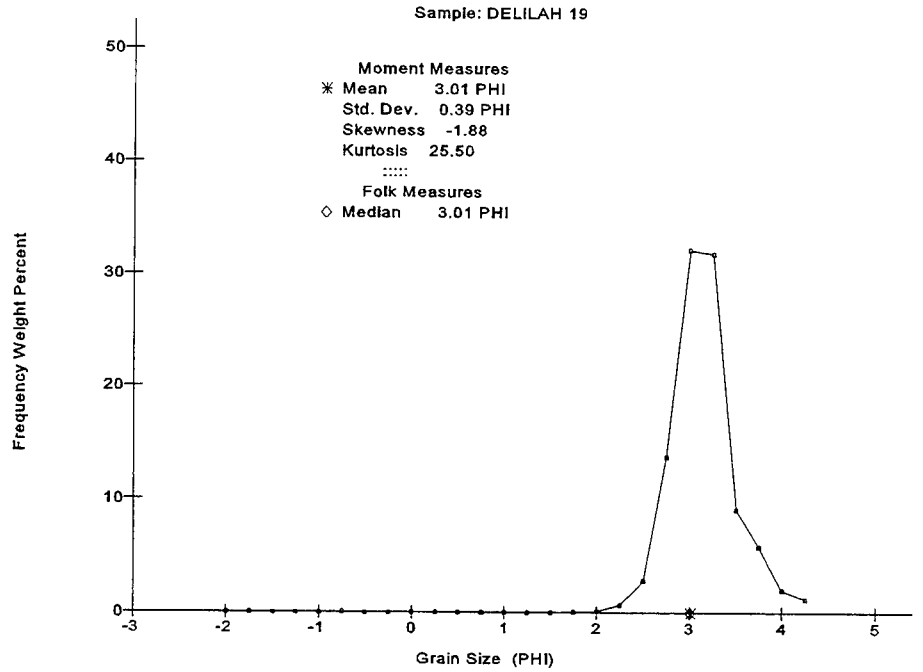

Figure C20. Grain size distribution for sediment sample 19, 15 October 1990

Appendix D
Current Meter Calibrations

Two types of electromagnetic current meters were used in the DELILAH array, Marsh-McBirney 551's (Figure 4 in the main text) and Scripps Institution of Oceanography "open frame" sensors (Figure D1). All of the current meters were calibrated in a constant flow tank by the Naval Oceanographic Office in Bay St. Louis, MS. Each instrument was calibrated at five speeds ranging from 0.0 to 1.91 m/s and four probe orientations ($\pm$ X, $\pm$Y). All instruments deployed during the experiment were also postcalibrated. Because of the biological growth that developed on the open frame current meters, they were post-calibrated with and without the growth. Although the growth had decayed somewhat by the time the instruments were recalibrated, the results give some indication of their performance under fouled conditions. The calibration results, including pre- and postcalibration gains and bias values, and computed changes between the calibrations, are listed in Tables D1 and D2.

Pre- and postcalibrations were used to adjust the collected time series data. In general, the precalibration was used unless the postcalibration was significantly different. Then, either the postcalibration was used or the pre- and postcalibrations were averaged. The decision to use only the postcalibration was based primarily on a comparison with nearby gauges during a time of high flow over linear bathymetry. In most cases, the current meter offsets were determined using the calibration curve for each channel of a given gauge and applied as a bias in volts (Figures D2 through D33). After plotting the time series in engineering units, however, further offsets of the velocities from zero were obvious for open frame channels 2711, 2731, and 2741 in the crest subarray, and for Marsh-McBirney channels 2701 and 2901 in the primary cross-shore subarray. These channels all measured cross-shore currents. The offsets appeared to be systematic throughout the duration of each time series, suggesting that a constant value applied to these data would be a satisfactory adjustment. To correct for these offsets, current velocities taken from these channels during a calm period (6-10 October) were correlated against data from channels which did not appear to require further offsets. The y-intercept of the regression curve for each channel was the offset applied in meters per second to the current velocities. Correlation coefficient (r^2) values

for these regressions ranged from 0.77 m/sec to 0.90 m/s. The greatest offset of -0.231 m/s was applied to channel 2741. New biases were computed from the changed offset using the following equation:

$$bias_{new} = bias_{orig.} + (\Delta offset / gain_{orig.}). \quad (1)$$

The open frame electromagnetic current meters posed a particular problem because of unanticipated biological fouling. Normally, the offset can be field determined by comparing data collected at orientations of 0 deg and 180 deg. However, the high wave activity during the last 2 weeks of the experiment prevented this check from being accomplished. An analysis performed on the current meter data from the crest and trough subarrays indicates an increase in the gains of the open frame sensors from the beginning to end of the experiment. This analysis is described in detail in the "Data Processing" section of Appendix E.

Comparison calibration plots for the open frame current meters and the Marsh-McBirney sensors, where the post-calibration differed from the pre-calibration, are shown in Figures D2 through D33.

Table D1
Calibration Data for Open Frame Electromagnetic Current Meters

Serial Number		Gauge Number	Pre-Cal. Gain (m/s)/V	Pre-Cal. Bias V	Cleaned Post-Cal. Gain (m/s)/V	Cleaned Post-Cal. Bias V	Post to Pre-Cal. Gain % Diff.	Post to Pre-Cal. Offset Diff. m/s	Post-Cal w/growth Gain (m/s)/V	Post-Cal w/growth Bias V	Calibration Used
OF6	X	2541	1.087	-0.022	1.084	-0.070	-0.276	0.052	1.374	-0.120	Pre-cal.
	Y	2542	1.083	0.071	1.076	-0.433	-0.646	0.543	1.366	-0.335	Pre-cal.
OF7	X	2711	1.051	-0.051	1.053	-0.172	0.190	0.127	1.396	-0.103	Offset
	Y	2712	1.075	0.131	1.072	0.401	-0.279	-0.289	1.416	0.347	Post-cal
OF9	X	2741	1.029	0.076	1.035	-1.081	0.583	1.197	1.393	-1.619	Offset.
	Y	2742	1.052	0.120	0.960	3.283	-8.745	-3.026	1.189	4.816	Pre-cal.
OF10	X	2721	1.085	0.091	1.079	0.070	-0.553	0.024	1.573	0.090	Pre-cal.
	Y	2722	1.058	-0.102	1.049	-0.021	-0.851	-0.086	1.581	-0.018	Pre-cal.
OF16	X	2731	1.062	0.192	1.068	0.359	0.565	-0.179	1.437	0.450	Offset.
	Y	2732	1.079	0.078	1.087	0.167	0.741	-0.098	1.576	0.098	Pre-cal.

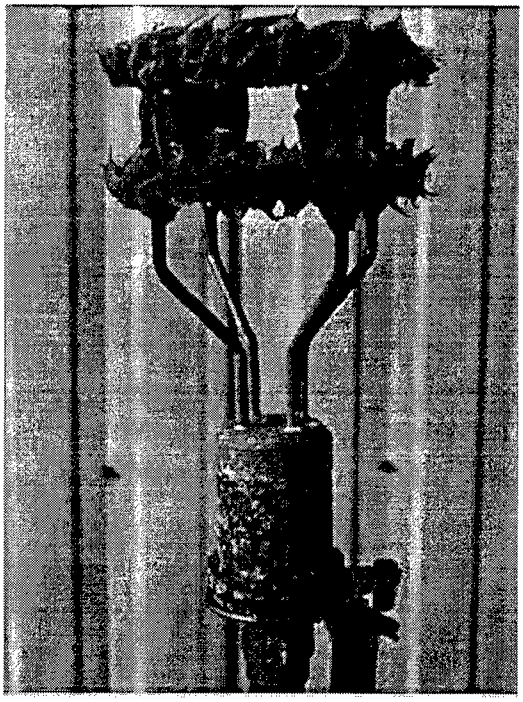

Figure D1. The Scripps' open frame current meter. The image was taken shortly after removal (note the biofouling)

Table D2
Calibration Data for Marsh-McBirney, Inc. Electromagnetic Current Meters

Serial Number	Gauge Number	Pre-cal.		Post-cal.		Post to Pre-cal.		Avg. Cal		Cal. Used
		Gain (m/s)/V	Bias V	Gain (m/)/V	Bias V	Gain % Diff.	Offset Diff (m/s)	Gain (m/s)/V	Bias V	
S385 X	2321	0.823	0.009	0.907	0.009	10.207	-0.001	0.865	1.084	Average
Y	2322	1.038	0.008	1.139	0.008	9.730	-0.001	1.089	0.008	Average
S476 X	2331	1.125	-0.132	suspect						Pre-cal.
Y	2332	1.253	-0.006	calibration						Pre-cal.
S760 X	2341	1.267	-0.013	1.290	-0.012	1.815	-0.001			Pre-cal.
Y	2342	1.086	-0.015	1.095	-0.016	0.829	0.002			Pre-cal.
S761 X	2351	1.583	0.032	switch						Pre-cal.
Y	2352	1.581	0.012	to S762						Pre-cal.
S762 X	2351	1.099	-0.051	1.122	-0.013	2.093	-0.041			Pre-cal.
Y	2352	1.120	0.013	1.121	-0.004	0.089	0.019			Pre-cal.
S765 X	sled	1.154	0.023	1.177	-0.029	1.993	0.060			Pre-cal.
Y		1.335	0.046	1.356	0.067	1.573	-0.029			Pre-cal.
S766 X	sled	1.123	0.051	1.147	0.051	2.137	-0.002			Pre-cal.
Y		1.089	0.037	1.053	0.127	-3.306	-0.094			Pre-cal.
S837 X	sled	0.941	0.029	1.230	0.007	30.712	0.018			Post-cal.
Y		0.949	0.025	1.064	0.000	12.118	0.024			Post-cal.
S892 X	2311	1.277	-0.023	1.283	-0.015	0.470	-0.011			Pre-cal.
Y	2312	1.150	0.039	1.143	0.040	-0.609	-0.001			Pre-cal.
S972 X	2401	0.877	-0.299	1.064	-0.029	21.323	-0.231			Pre-cal.
Y	2402	1.048	-0.069	1.075	-0.032	2.576	-0.038	1.062	-0.050	Average
S1050 X	sled	0.652	-0.014	0.650	-0.006	-0.307	-0.005			Pre-cal.
Y		0.650	-0.014	0.649	-0.006	-0.154	-0.005			Pre-cal.
S1080 X	sled			1.093	-0.009					Post-cal.
Y				1.069	0.006					Post-cal.
S1013 X	2501	1.055	-0.001	1.054	0.026	-0.095	-0.028			Pre-cal.
Y	2502	1.080	0.031	1.033	0.030	-4.352	0.003	1.057	0.031	Average
S1015 X	2801	1.036	-0.023	suspect						Pre-cal.
Y	2802	1.056	-0.004	calibration						Pre-cal.
S1081 X	2301	1.000	0.002	1.010	0.000	1.000	0.002			Pre-cal.
Y	2302	1.029	0.001	1.039	0.015	0.972	-0.015			Pre-cal.
S1082 X	2201	1.013	-0.005	1.012	-0.003	-0.099	-0.002			Pre-cal.
Y	2202	1.072	-0.193	1.065	-0.133	-0.653	-0.065			Pre-cal.
S1083 X	2101	1.023	-0.013	1.018	-0.008	-0.489	-0.005			Pre-cal.
Y	2102	1.083	-0.012	1.053	-0.010	-2.770	-0.003			Pre-cal.
S1084 X	2901	1.013	-0.011							Offset
Y	2902	1.028	-0.052	1.040	-0.033	1.167	-0.019			Pre-cal.
S1012 X	2701	1.044	-0.029	1.049	-0.038	0.479	-0.010			Offset
Y	2702	1.089	-0.017	1.091	-0.021	0.184	-0.003			Pre-cal.
S1011 X	2601	1.045	0.037	gauge						Pre-cal.
Y	2602	1.051	0.052	destroyed						Pre-cal.

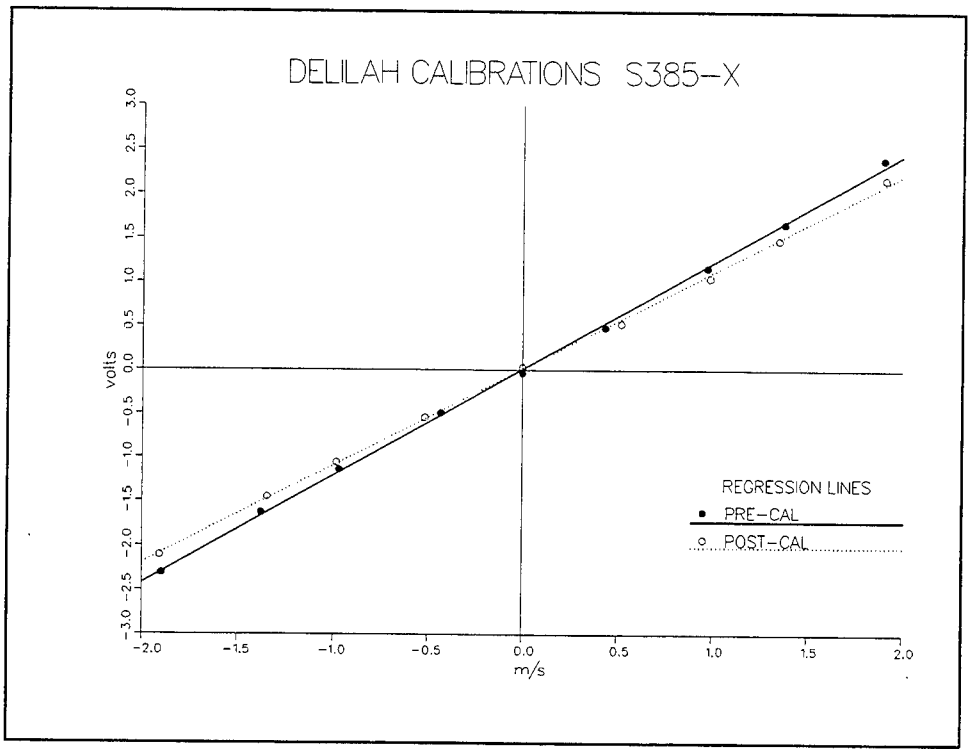

Figure D2. Calibration data for S385-X. Average calibration used

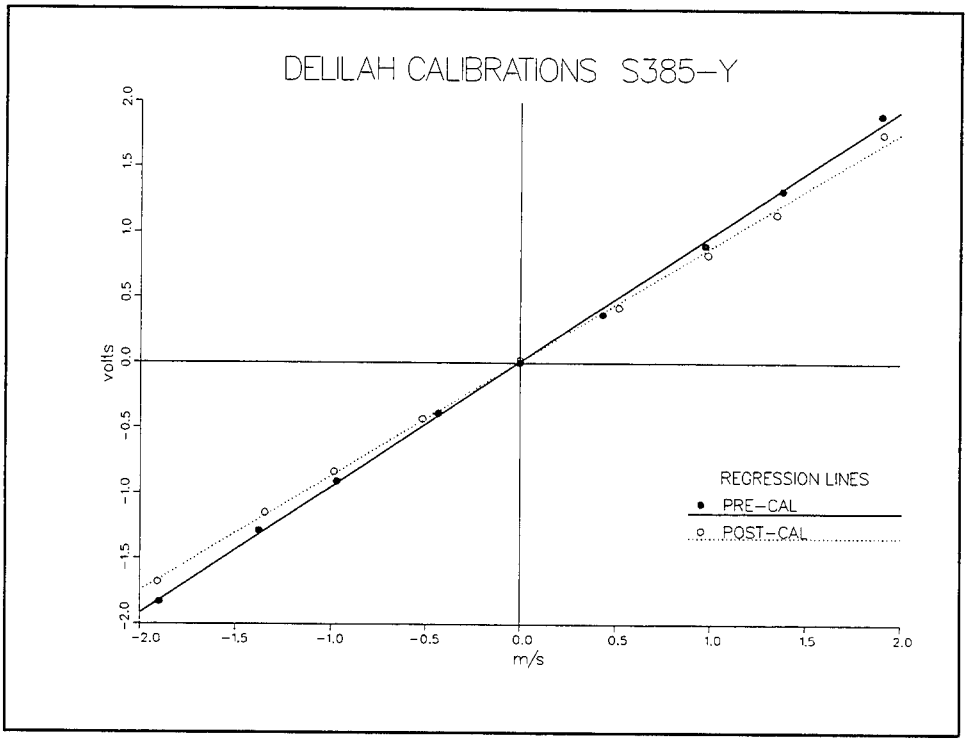

Figure D3. Calibration data for S385-Y. Average calibration used

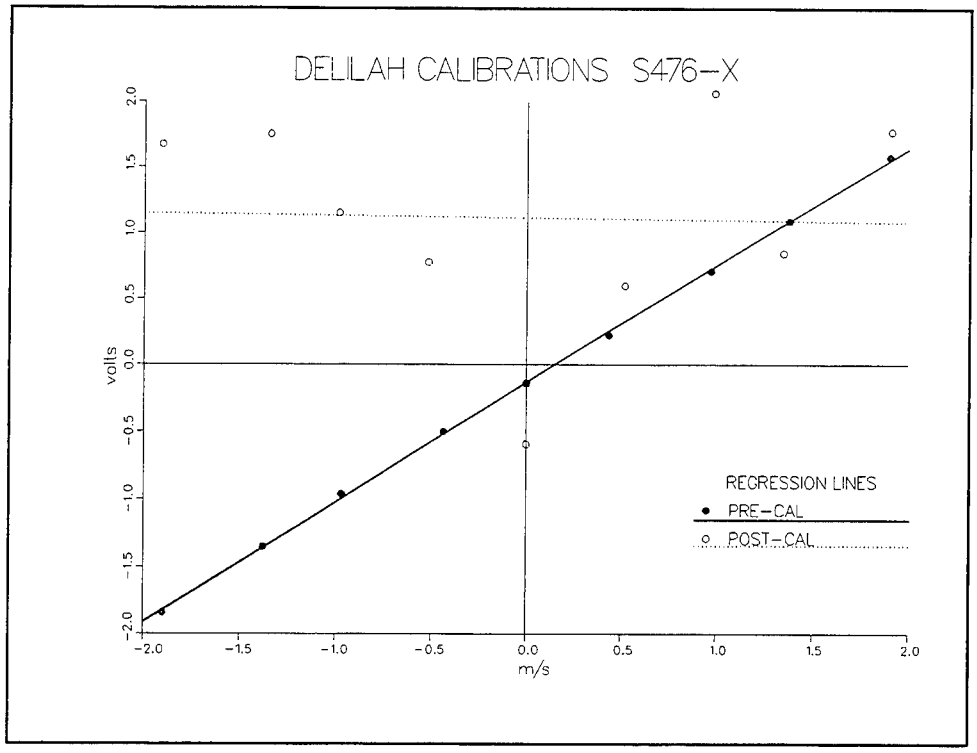

Figure D4. Calibration data for S476-X. Pre-calibration used

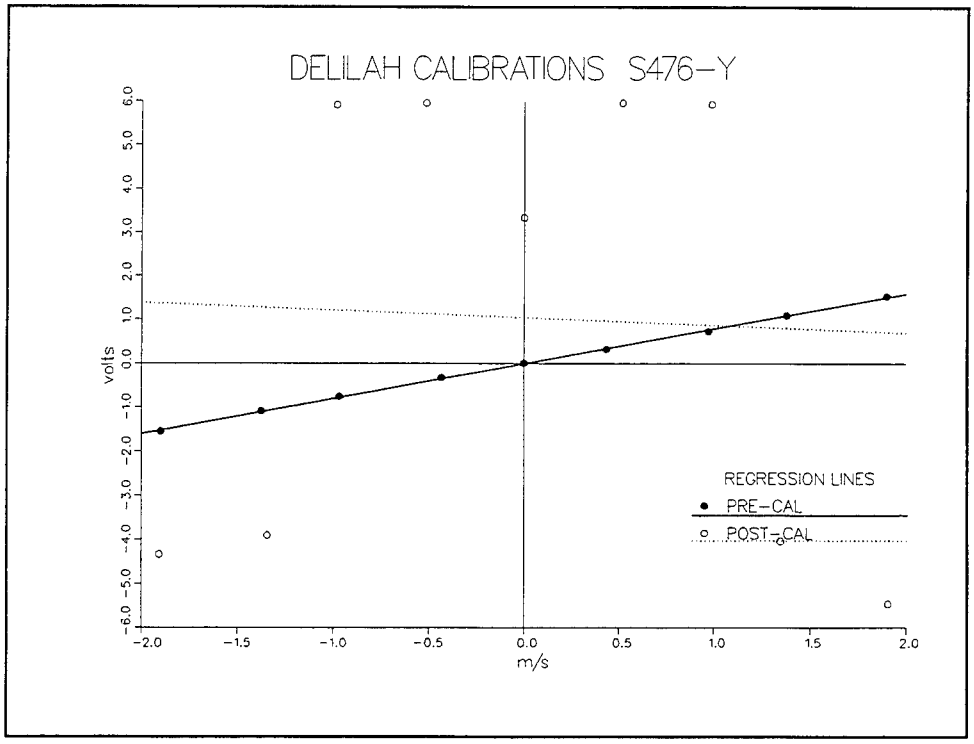

Figure D5. Calibration data for S476-Y. Pre-calibration used

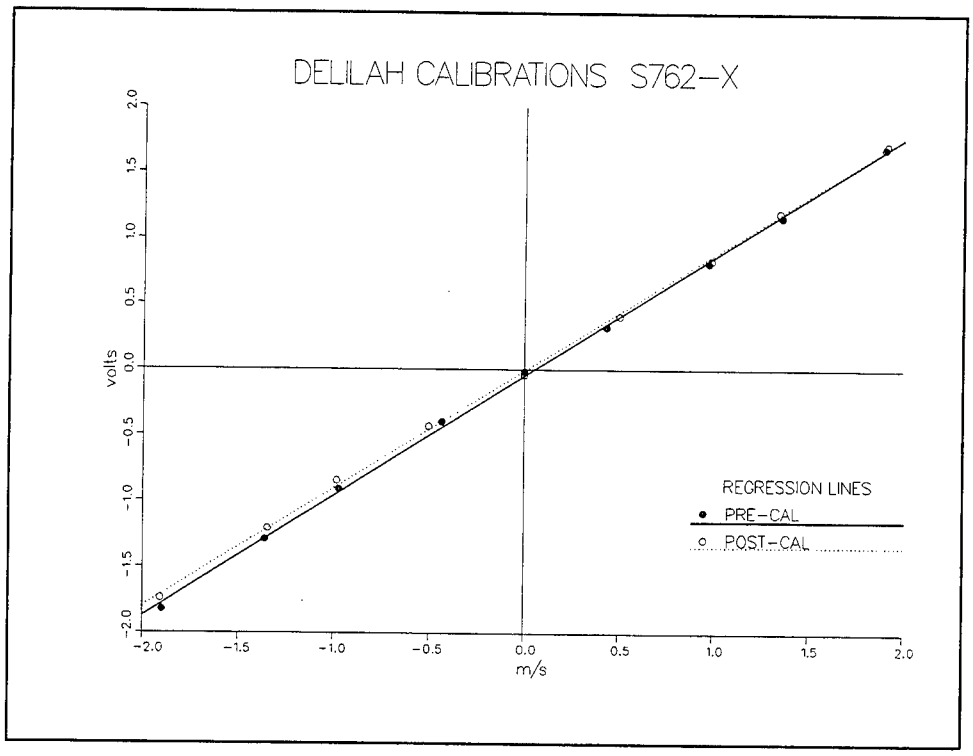

Figure D6. Calibration data for S762-X. Pre-calibration used

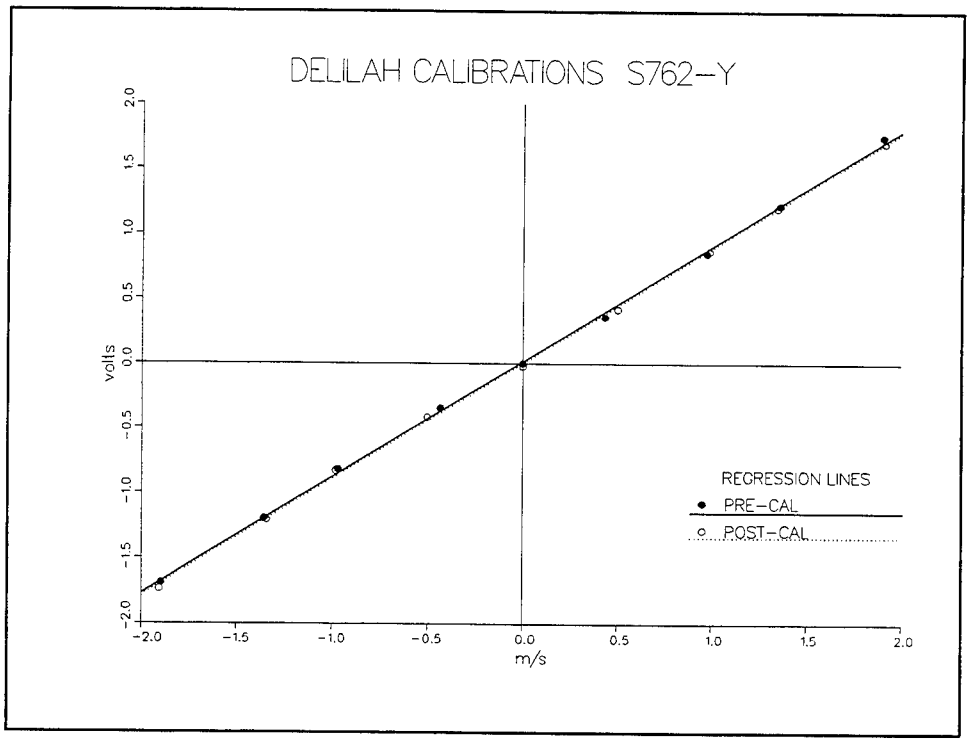

Figure D7. Calibration data for S762-Y. Pre-calibration used

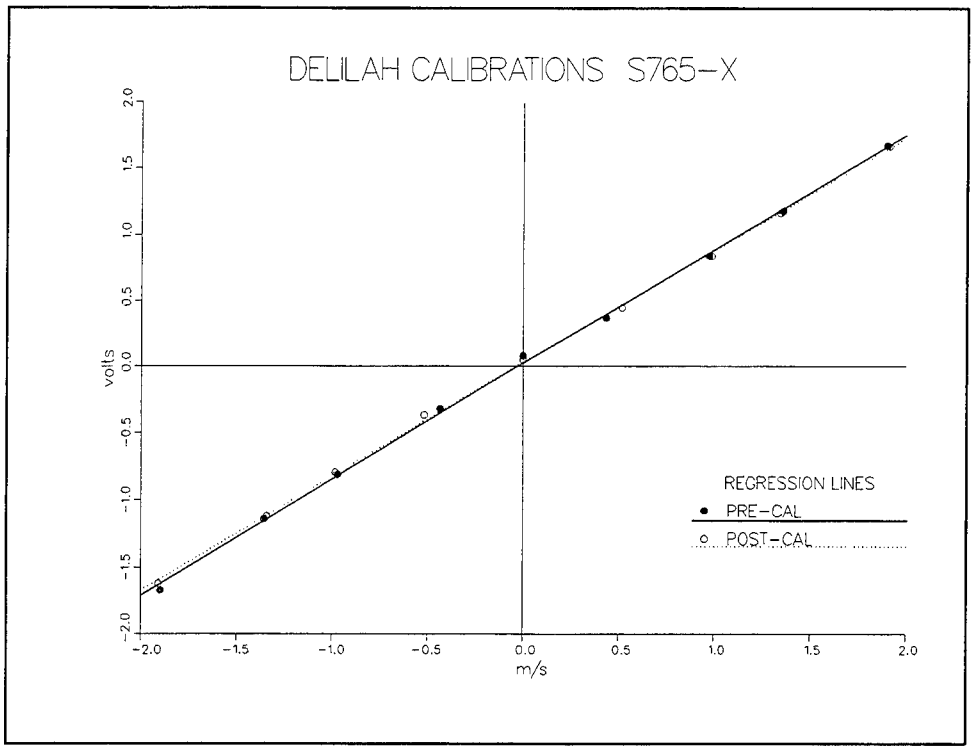

Figure D8. Calibration data for S765-X. Pre-calibration used

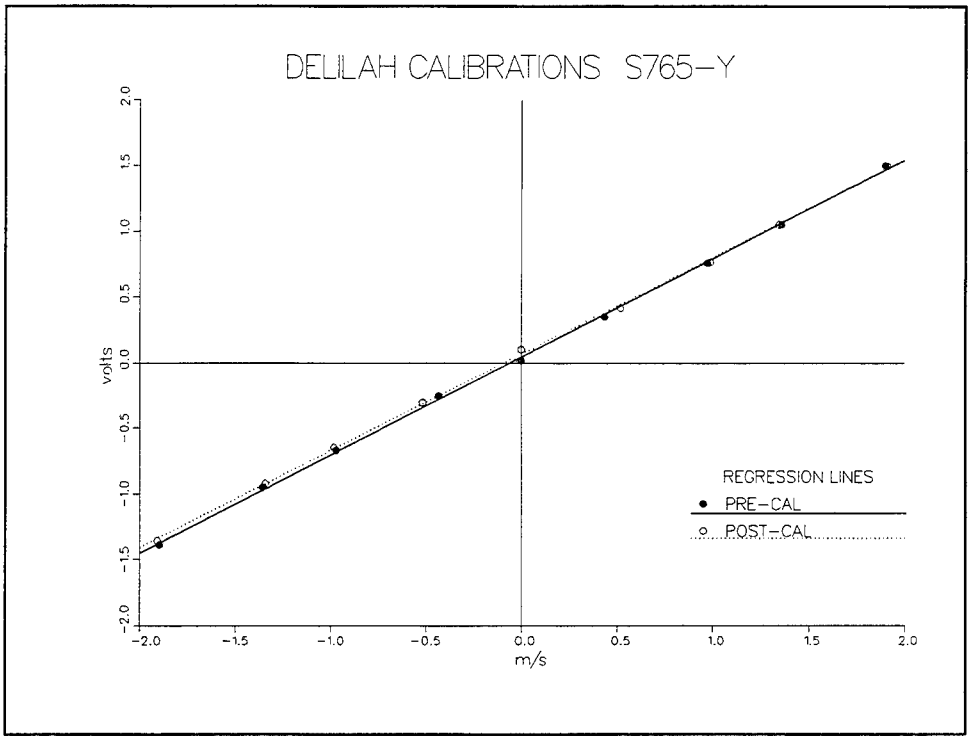

Figure D9. Calibration data for S765-Y. Pre-calibration used

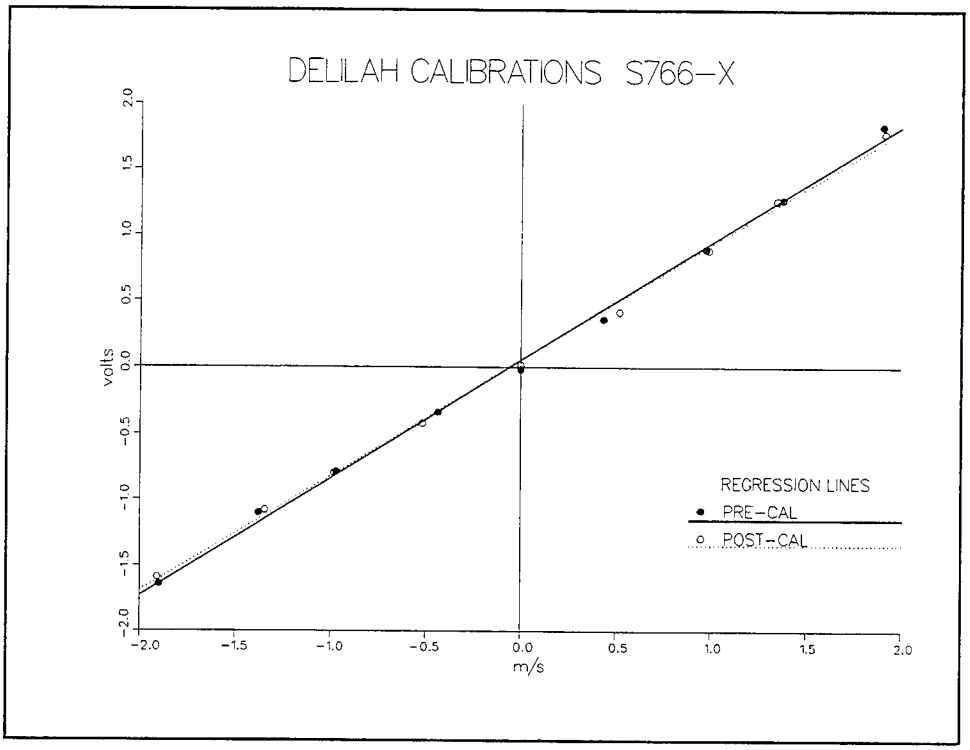

Figure D10. Calibration data for S766-X. Pre-calibration used

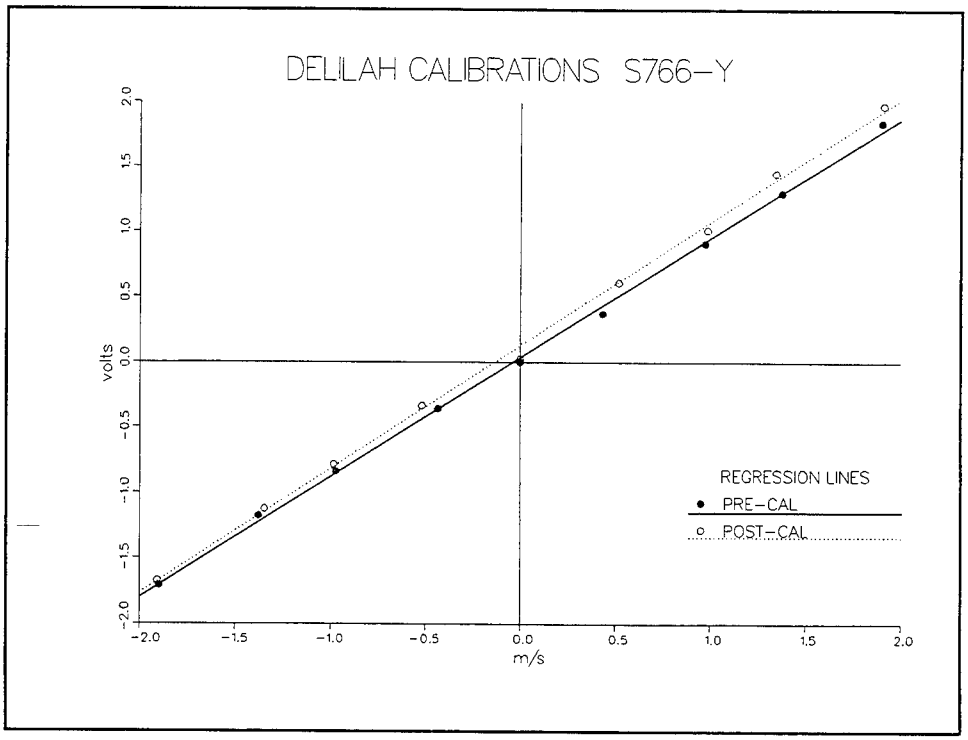

Figure D11. Calibration data for S766-Y. Pre-calibration used

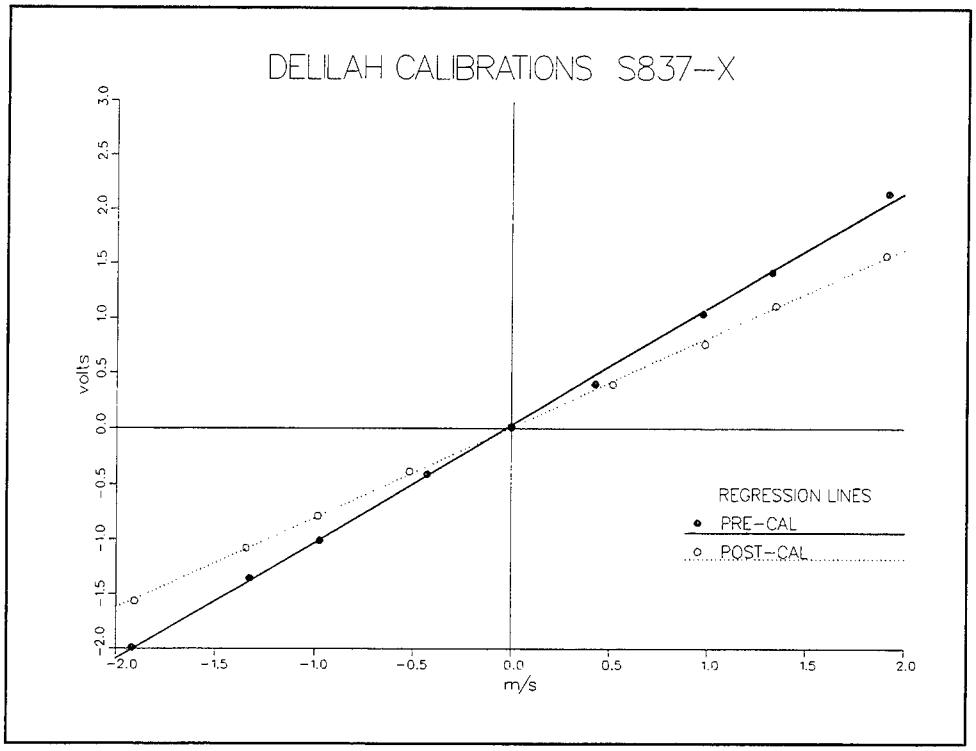

Figure D12. Calibration data for S837-X. Post-calibration used

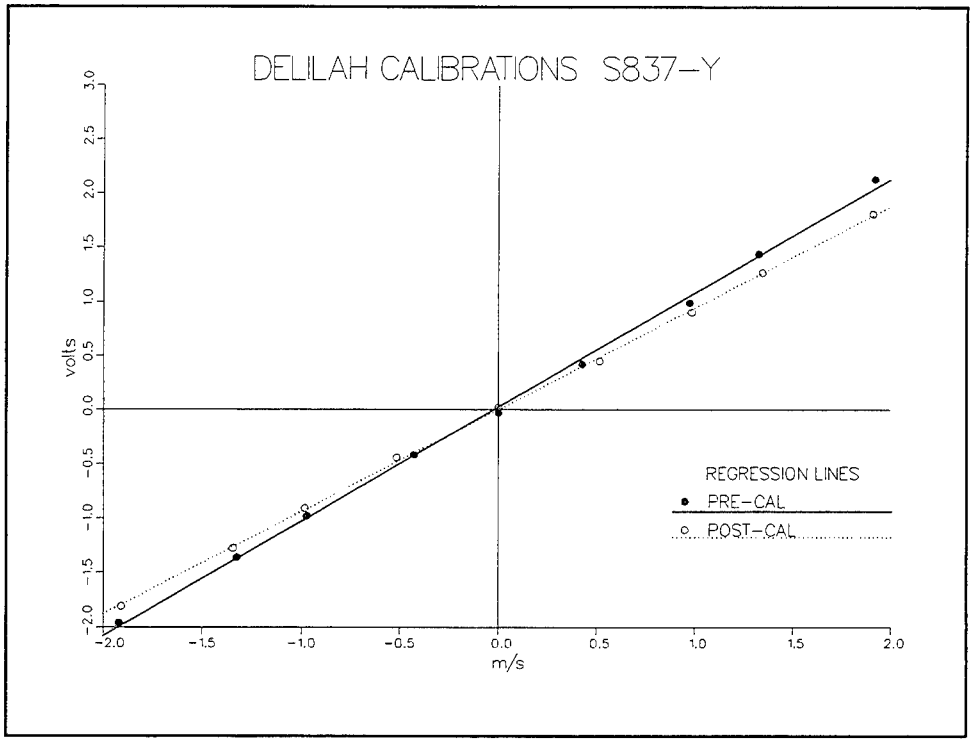

Figure D13. Calibration data for S837-Y. Post-calibration used

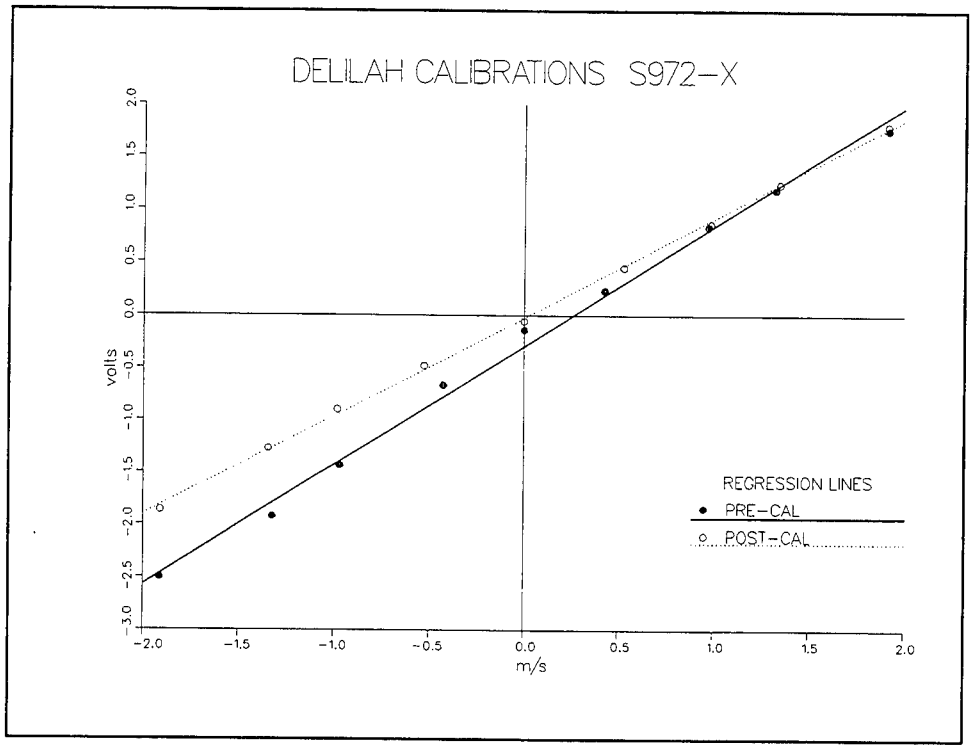

Figure D14. Calibration data for S972-X. Post-calibration used

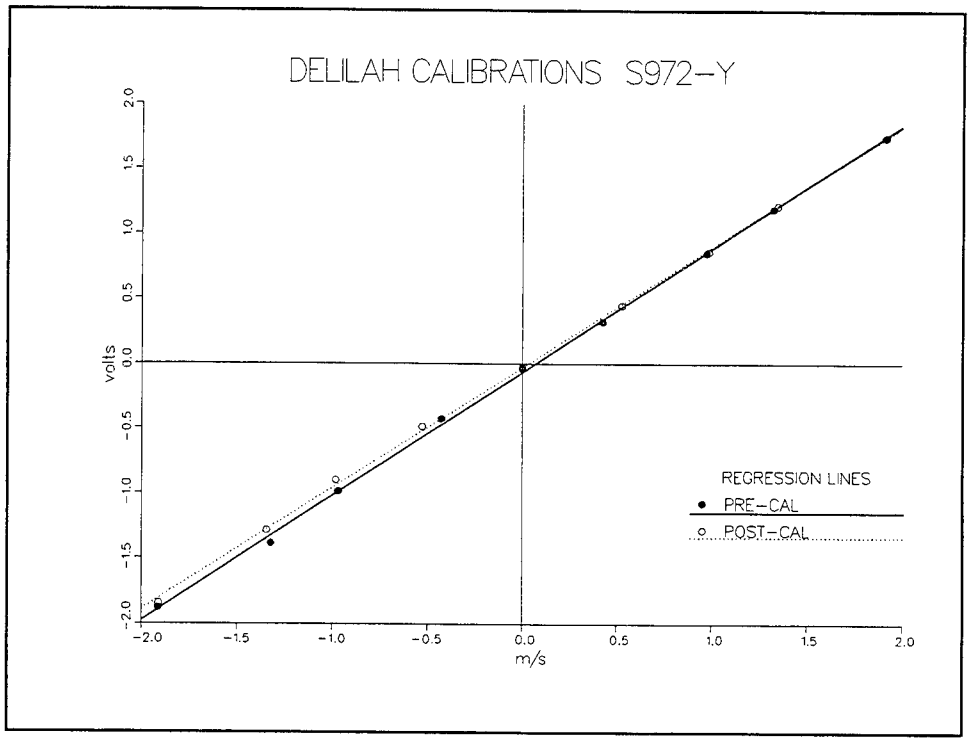

Figure D15. Calibration data for S972-Y. Average calibration used

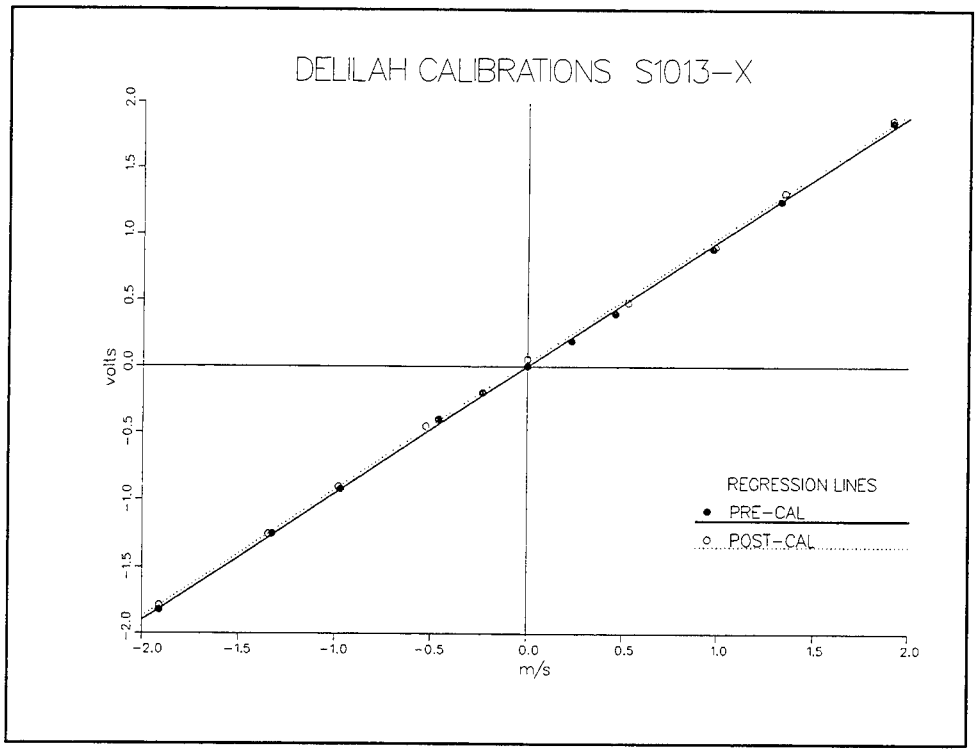

Figure D16. Calibration data for S1013-x. Pre-calibration used

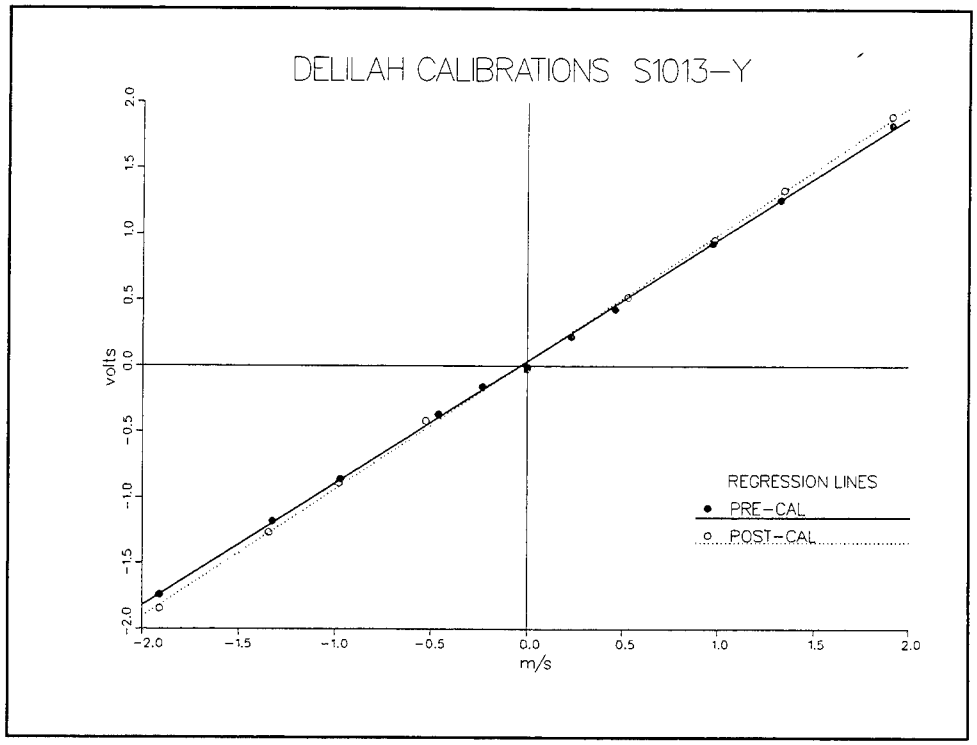

Figure D17. Calibration data for S1013-Y. Average calibration used

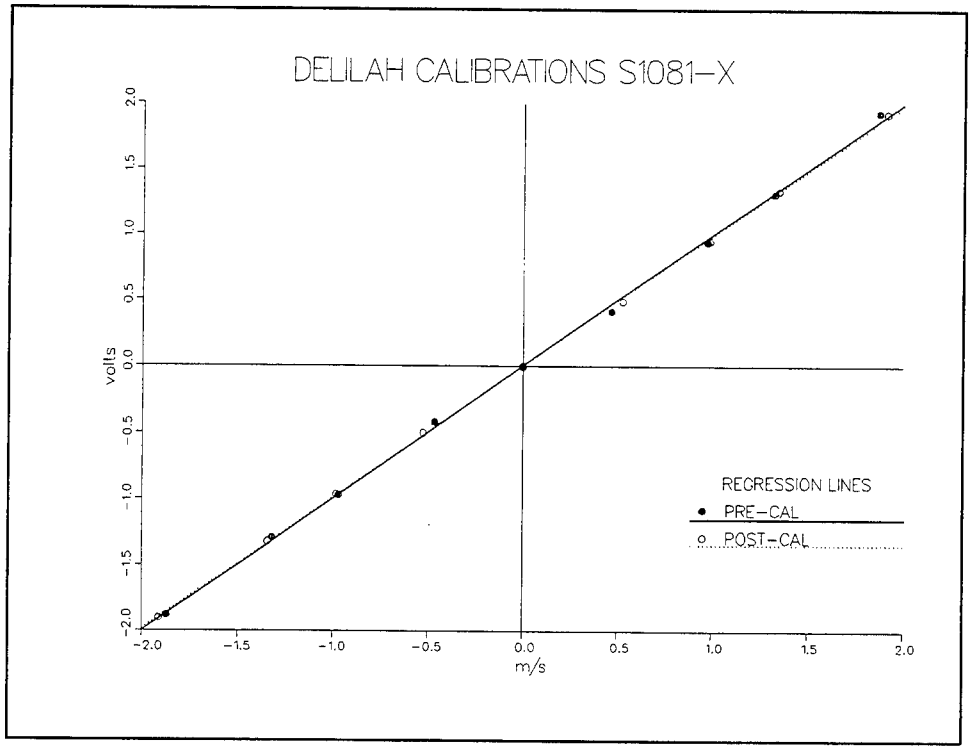

Figure D18. Calibration data for S1081-X. Pre-calibration used

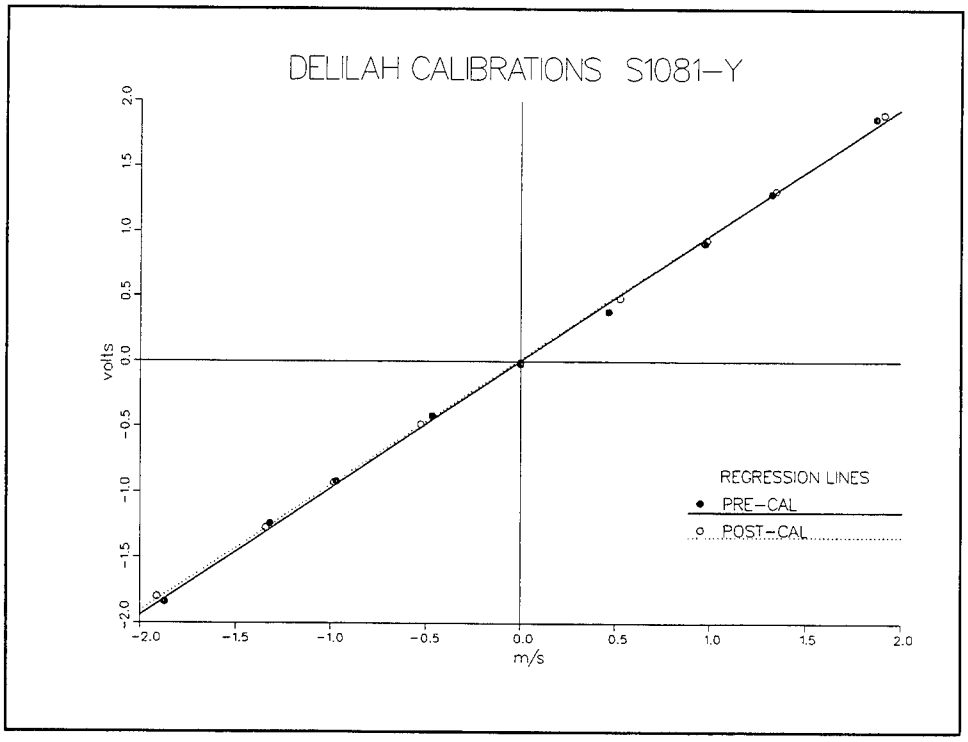

Figure D19. Calibration data for S1081-Y. Pre-calibration used

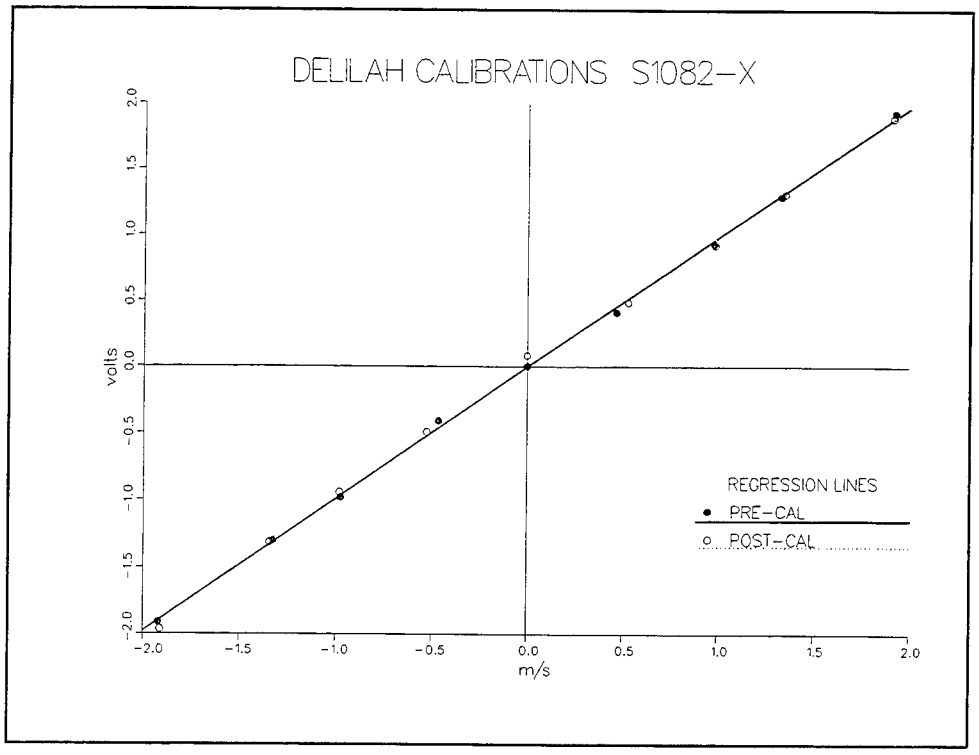

Figure D20. Calibration data for S1082-X. Pre-calibration used

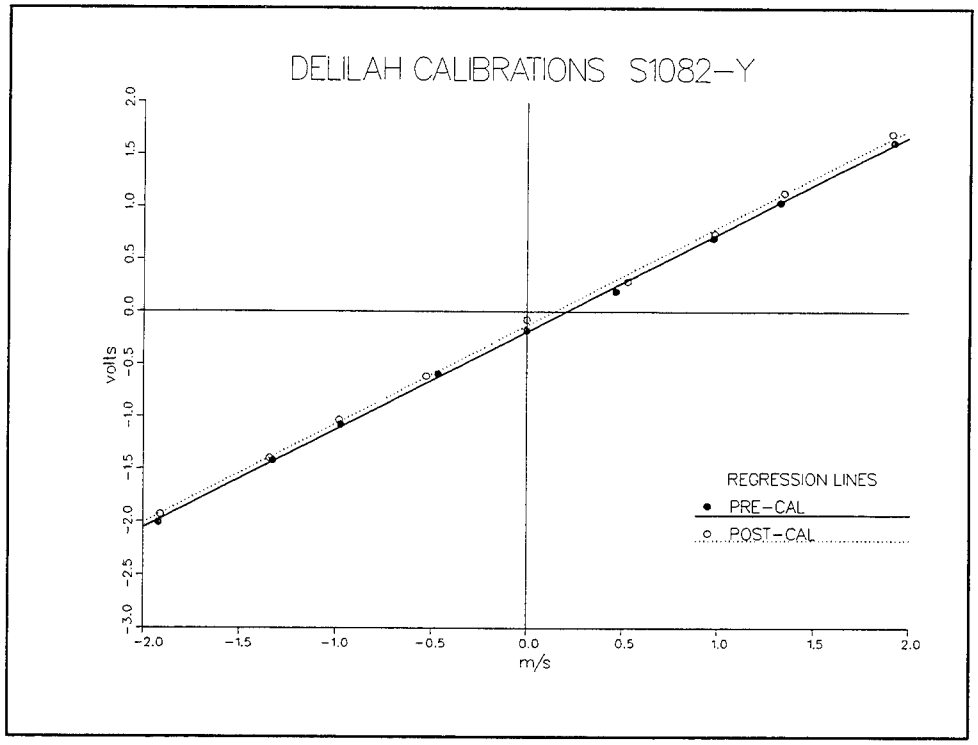

Figure D21. Calibration data for S1082-Y. Pre-calibration used

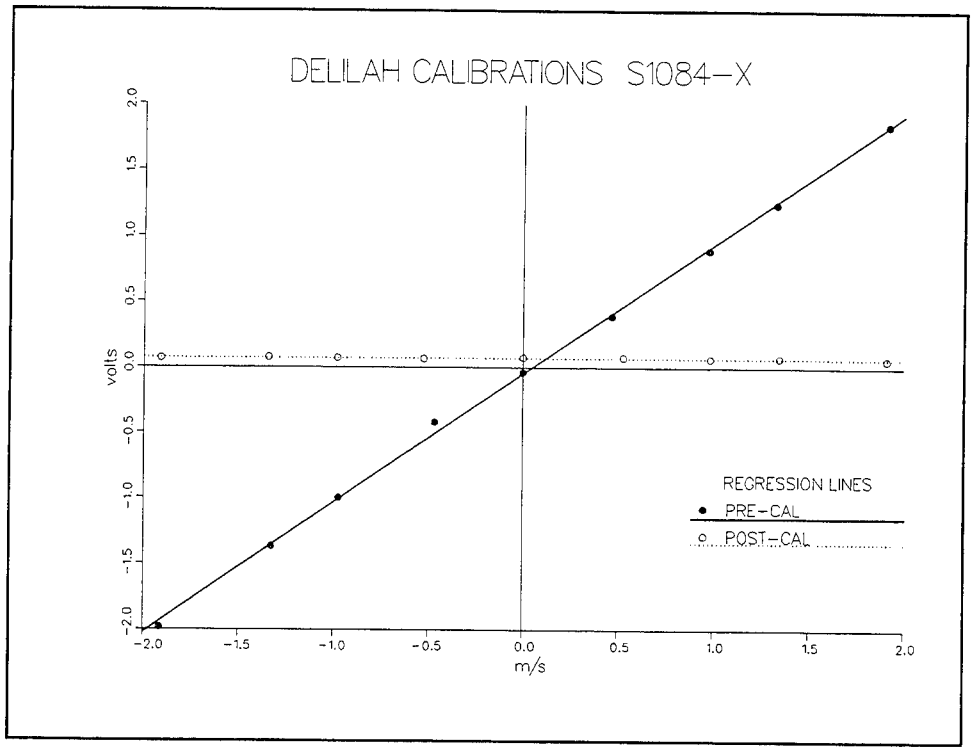

Figure D22. Calibration data for S1084-X. Pre-calibration used

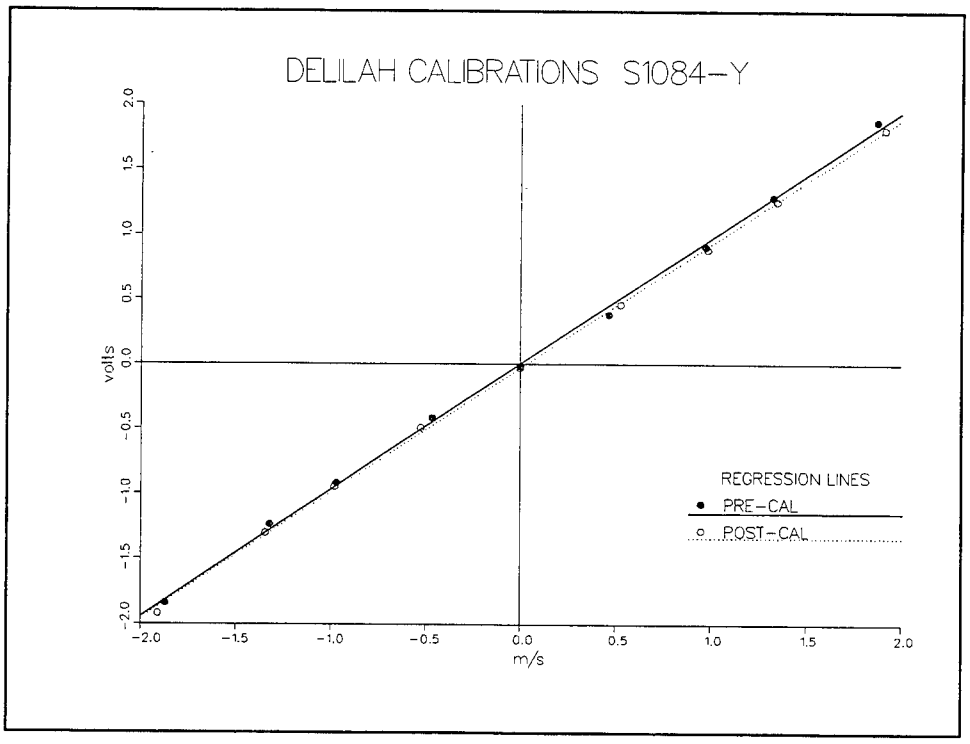

Figure D23. Calibration data for S1084-Y. Pre-calibration used

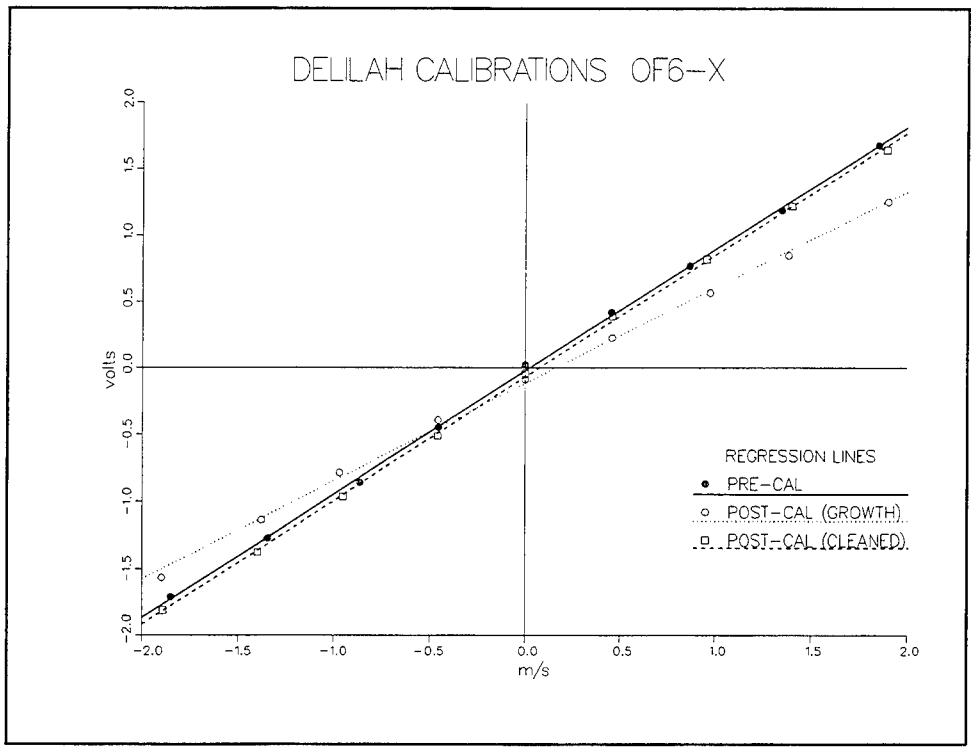

Figure D24. Calibration data for OF6-X. Pre-calibration used

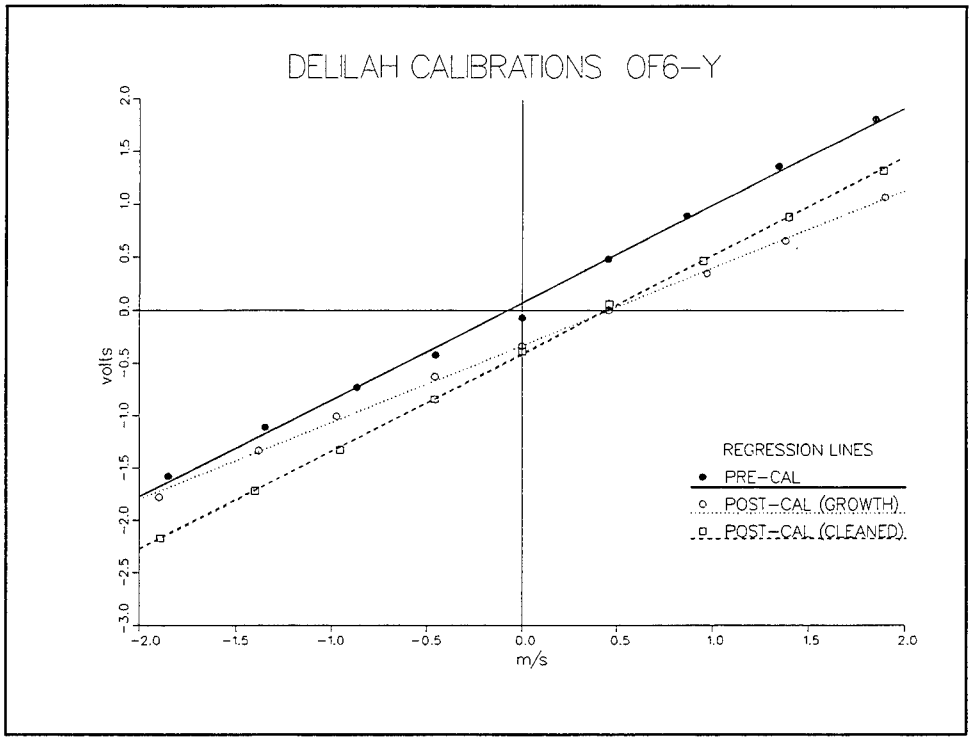

Figure D25. Calibration data for OF6-Y. Pre-calibration used

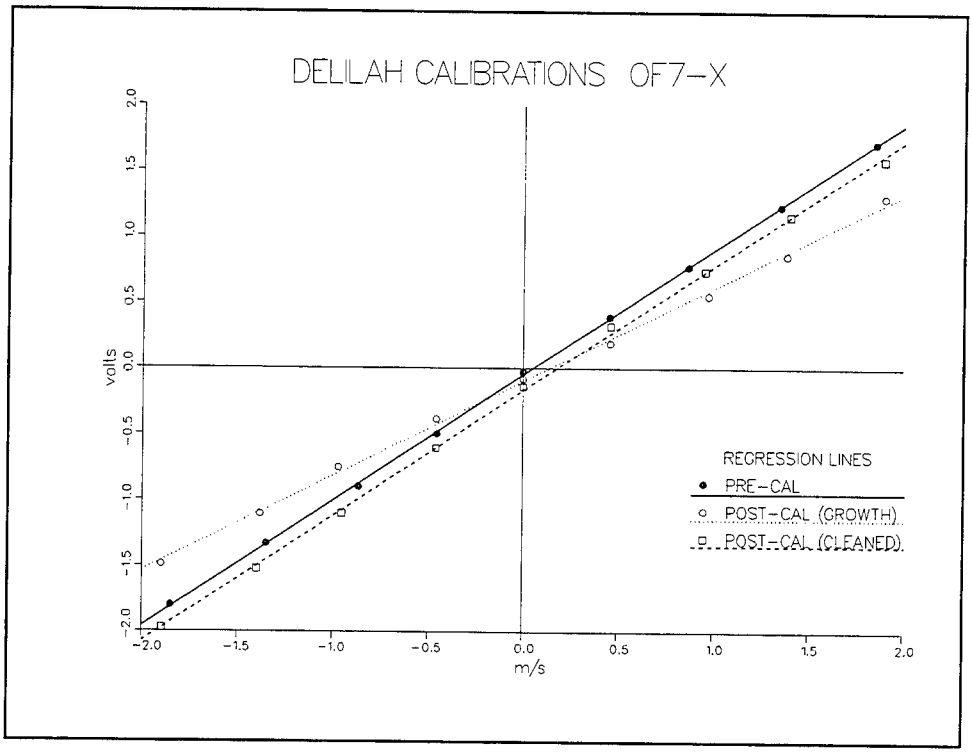

Figure D26. Calibration data for OF7-X. Pre-calibration used

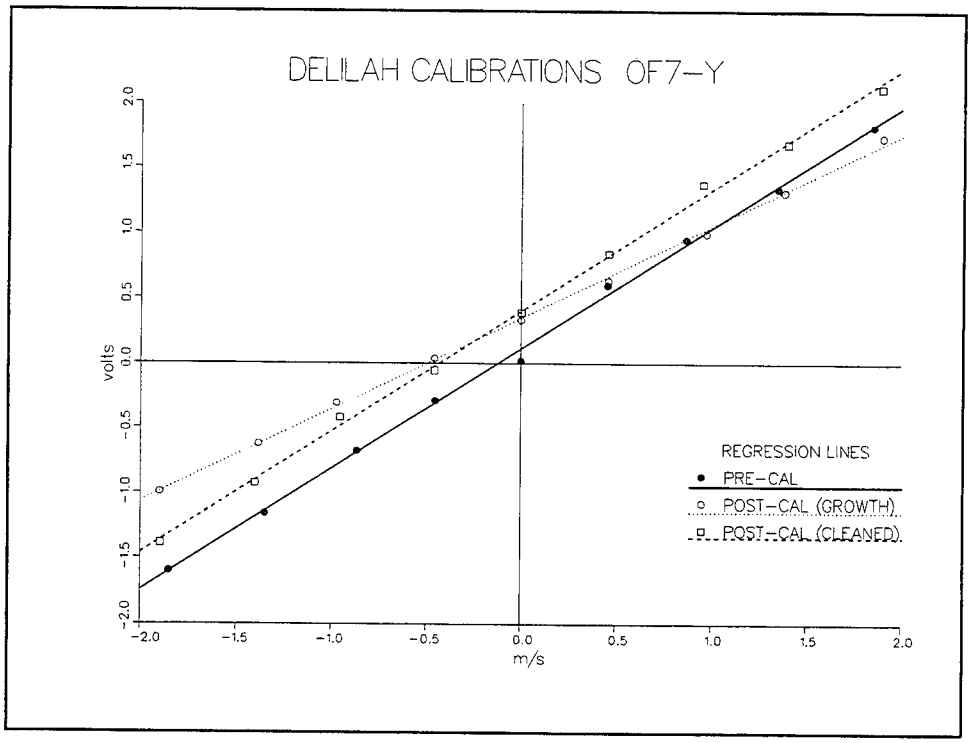

Figure D27. Calibration data for OF7-Y. CLEANED post-calibration used

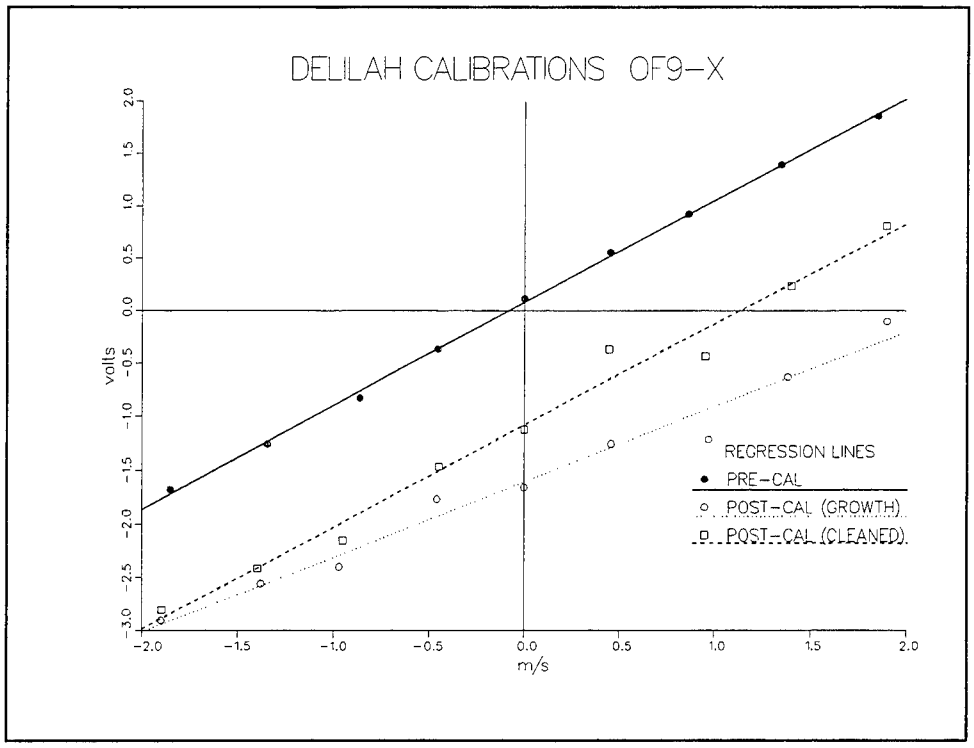

Figure D28. Calibration data for OF9-X. Pre-calibration used

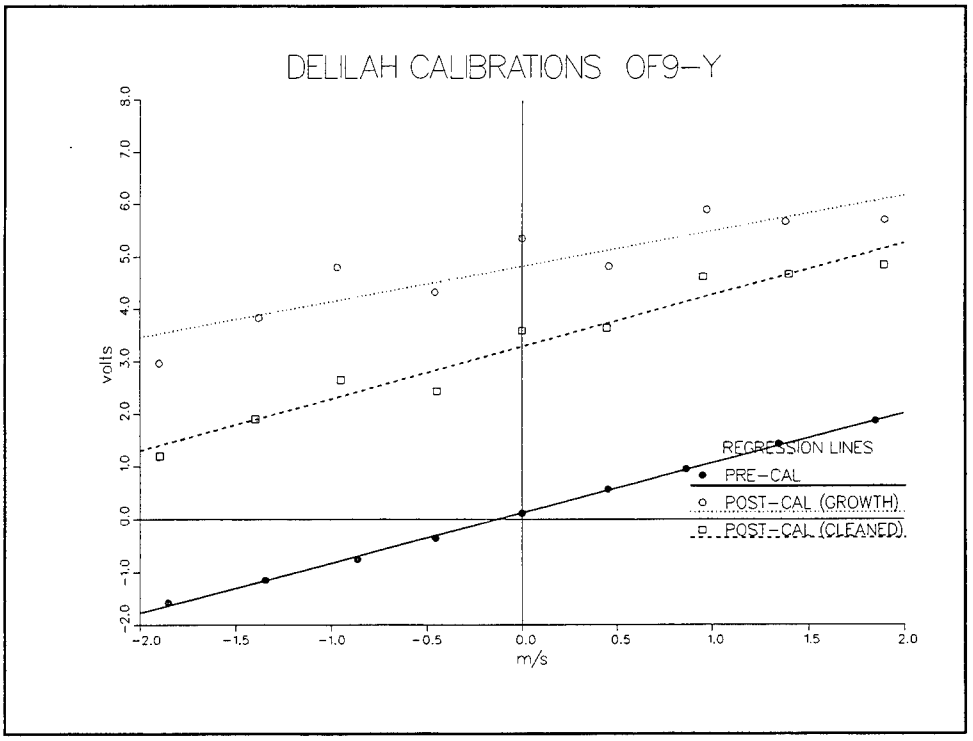

Figure D29. Calibration data for OF9-Y. Pre-calibration used

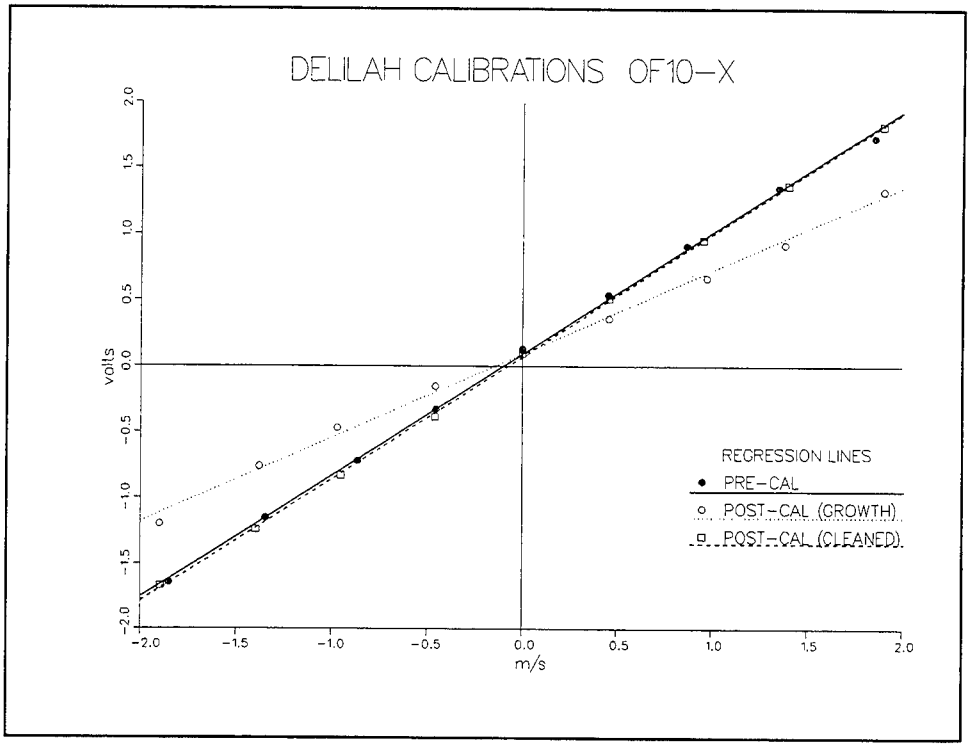

Figure D30. Calibration data for OF10-X. Pre-calibration used

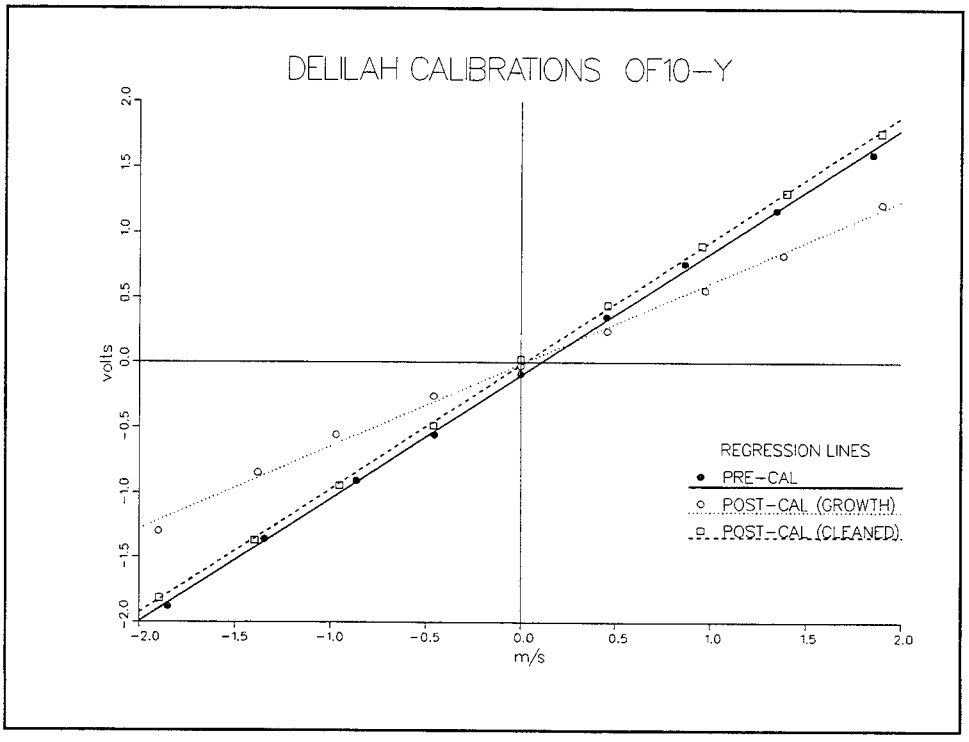

Figure D31. Calibration data for OF10-Y. Pre-calibration used

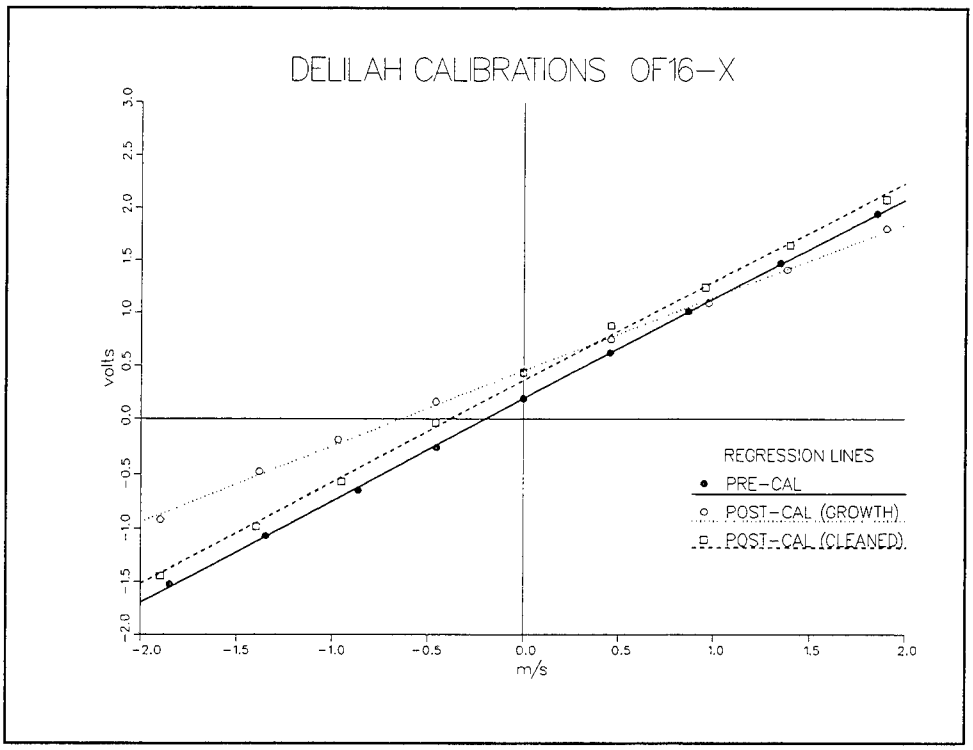

Figure D32. Calibration data for OF16-X. Pre-calibration used

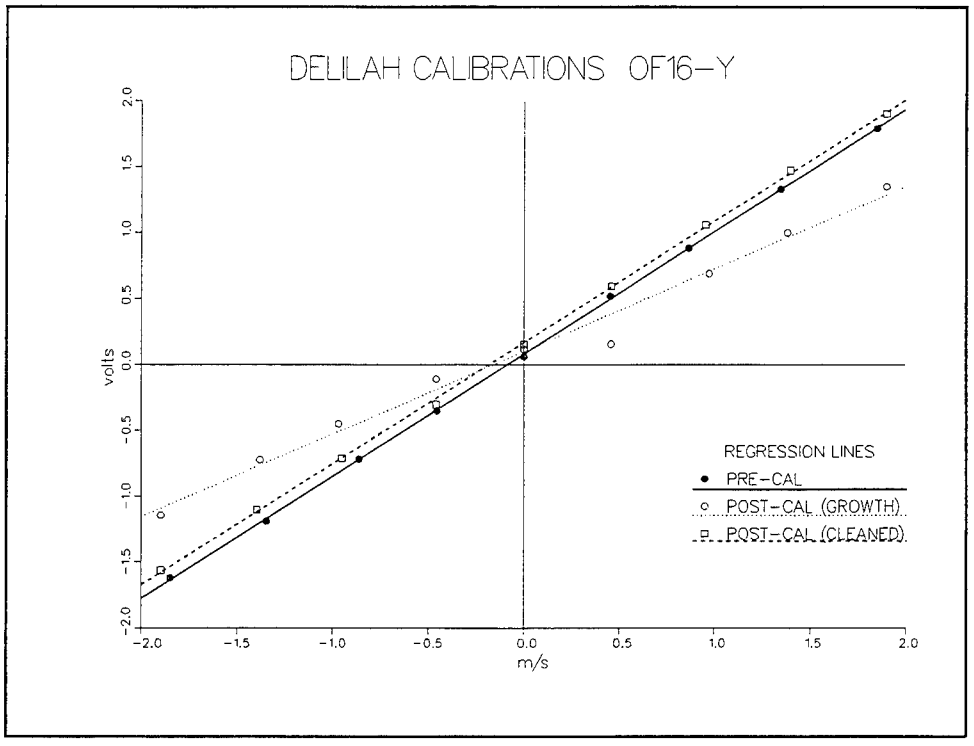

Figure D33. Calibration data for OF16-Y. Pre-calibration used

Appendix E
Stationary Instrument Data

This appendix includes information about the mounting, positioning, and naming of the DELILAH array instruments. It also provides details on the basic measurements taken at the Field Research Facility (FRF), and a methodology for processing the data. Day-by-day sensor status reports (changes in instrument height, orientation, etc.) were included based on the experiment notes of Dr. Peter Howd and Dr. Edward Thornton. Other factors such as biological growth, bent sensor mounts, or changing local depths have not been included. Data from the surf zone arrays were collected continuously except for the time required to change tapes.

DELILAH Array

Instruments

The 19 instruments of the DELILAH array are shown in Figure E1. Nine instrument packages form the primary cross-shore array of the DELILAH array (indicated by squares in Figure E1). These nine gauges were provided by the Naval Postgraduate School. Ten additional current meters, provided by Scripps Institute of Oceanography, were installed to form three subarrays (indicated by circles in Figure E1). One longshore subarray located in the trough consisted of six current meters. The second longshore subarray was formed by five current meters seaward of the bar crest, labeled the crest subarray. The third subarray was a three-gauge cross-shore array over the bar, between the two longshore subarrays.

Each primary cross-shore subarray instrument package included a small ball (Model 512) Marsh-McBirney electromagnetic current meter, a Paroscientific pressure gauge (except instrument package 80), and a Setra strain-gauge pressure sensor. The Paroscientific gauge was connected to a thin copper tube that was buried in the bottom in order to isolate the orifice from the current flow. The Paroscientific gauge was designed to measure wave-induced setup while the strain gauge pressure sensors measured wave energy. After considerable analysis at the Naval Postgraduate School, it was decided

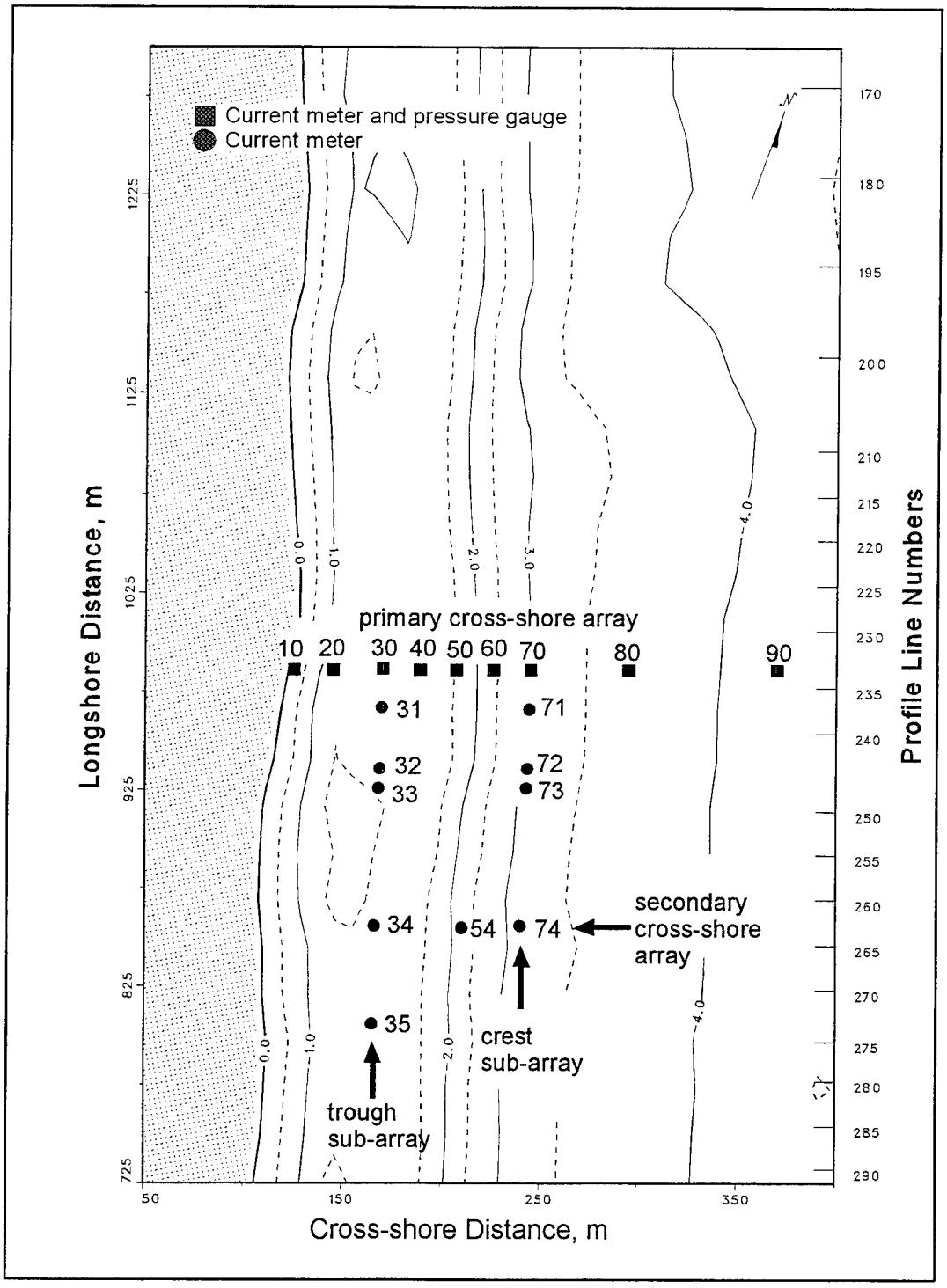

Figure E1. Location and numbering of the DELILAH array

that because of the uncertainty in sensor height and other factors, the Paroscientific sensors could not be used to measure setup[1]. Data from all sensors (four channels) were internally converted to a digital signal and transmitted as a serial data stream back to shore. Each instrument package was connected to a data collection system using four-conductor, double armor, lightweight cable. Each electronics package was hose-clamped to the support pipes and connected to the cable with four-pin Brantner underwater connectors.

Except for the two seawardmost instruments (80 and 90), the current meter probes for the primary cross-shore array were mounted on a separate line of pipes placed 1.5 m northeast of the instrument package/pressure gauge pipe (Figure 6 in the main text). At the five innermost positions (10 to 50), the current meter stinger was mounted downward, 30 cm away from the mounting pipe. All other stingers were mounted upright. Some of the downward-mounted stingers were adjusted during the experiment to keep them either above the sand or in the water.

A second data acquisition system was used to sample the analog output from the 10 current meters in the three subarrays. Five Scripps open frame electromagnetic current meters mounted upward were used in the Crest sub-array. Five Marsh-McBirney current meters with their sensors mounted downward were used in the trough subarray. A single upward-mounted open frame (54) completed the secondary three-element cross-shore subarray. Each of these current meters was wired back to the base of the duneline using seven-conductor double armor cable. The cables were wired into watertight "Hoffman" boxes. Power to the Hoffman boxes was isolated through the use of DC-to-DC converters as a preventative measure to reduce potential ground loops.

Figure E2 shows the location of the cross-shore instruments, including the initial position of the current meters relative to the changing bottom and water surface. Note the nearness of some sensors to the water's surface. This was taken into account when processing the data from these sensors and is discussed in the data analysis section that follows.

Current meter orientations were determined with an underwater digital compass mounted on a long nonmagnetic pipe so that it was not affected by the steel in the sensor mount. For Marsh-McBirney current meters (Nos. 2101-2352) the compass was read with the meters aligned to the direction of -y flow of the sensor ball. For the open frame meters, the compass was read with the meter aligned in the direction of +x flow. At the time of the DELILAH experiment, it was believed that the pier axis was 70 deg east of true north, and the current meters were aligned relative to the pier. More recent measures have computed the pier orientation at 71.8 deg. Current meter orientations are listed in Table E1.

---

[1] Personal Communication, 29 April 1997, Dr. Edward Thornton, Dept of Oceanography, Naval Postgraduate School, Monterey CA

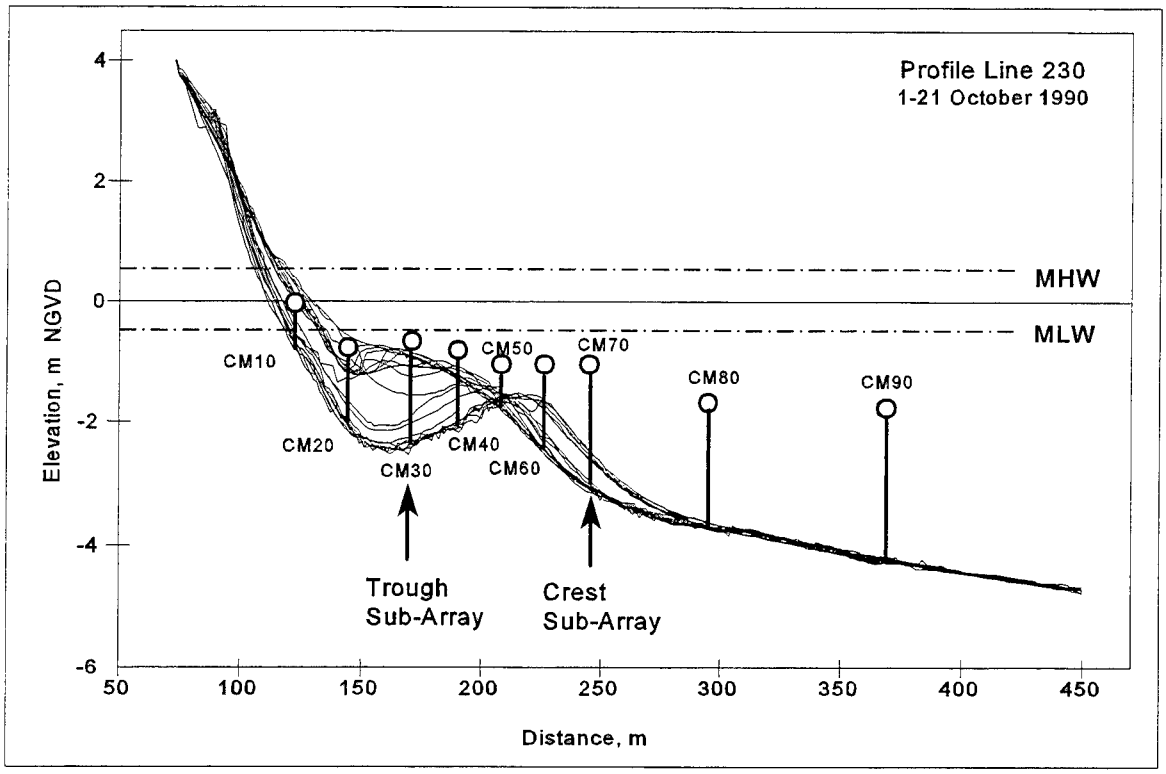

Figure E2. Location of the cross-shore current meters at the start of DELILAH along with the profile changes. Vertical arrows mark the two longshore subarrays

A Met One anemometer was mounted on the top of the pipe at position 35. The anemometer was hit by high waves and failed on October 13.

DELILAH array gauge numbering

The following tables list the DELILAH instruments by gauge number and name. The gauge number is a four-digit number uniquely identifying the gauge, while the gauge name is a short alphanumeric string that identifies both the type of instrument and the location. Both were required to collect and process data at the FRF.

Included in both labels is the location numbering scheme (Figure E1) which uses a two digit-number to locate every surf zone instrument. The first digit (1-9) refers to the cross-shore locations starting at the shoreline and moving offshore. The second digit numbers the longshore location starting with 0 at the primary cross-shore array and increasing to 5 at the southernmost gauge location.

The gauge number is stored in the header of the FRF's time series data (along with other information such as the gauge depth, gain, and bias). It is composed of four digits. The first digit, always a 2, identifies the gauge as a

DELILAH instrument. The middle two digits refer to the location code described above. The last digit identifies the sensor (or channel) at that particular location. The sensors used were:

a. Current speed in the X direction.
b. Current speed in the Y direction.
c. Paroscientific pressure gauge.
d. Strain gauge pressure sensor.

Thus, a gauge number of 2503 is a DELILAH instrument, located at the 50 position, the fifth offshore gauge on the primary cross shore subarray, and is the Paroscientific pressure gauge (type 3).

The Gauge Name is used only to describe the particular gauge. It is not stored with either the raw time series or the FRF's summary statistics file. The following conventions are used:

CM - Current meter (Either open-frame or Marsh-McBirney).
PD - Pressure gauge to measure water Depth. This refers to the buried Paroscientific pressure sensors designed to measure setup.
PW - Pressure gauge to measure Waves. Refers to the strain gauge pressure sensors to be placed on the cross-shore array.
Y - Current measurement, positive to the south (also known as U).
X - Current measurement, positive offshore (also known as V).
SLED - This word precedes the names of instruments mounted on the sled.

Current meters and pressure gauges used in DELILAH are listed in Tables E1 and E2, respectively. The tables include gauge name, gauge number, serial number plots, gain, bias, and coordinates relative to the FRF coordinate system. The signs of the gains may differ from those listed in Appendix D. The signs have been adjusted to compensate for instruments being mounted downward. A negative gain flips the data of the channel so that they correspond to the conventions of:

+Y - a southward-moving longshore current.
+X - an offshore-moving cross-shore current.

DELILAH array data collection

Data were sampled at 8 Hz except for the Paroscientific sensors, which were sampled at 1 Hz. The primary cross-shore array had an unanticipated 4 to 8-sec gap in the data which occurred approximately every 20 min as a result of the microprocessors used. The 10 current meters in the three subarrays did not have these data gaps. These gaps in the time series were filled with values of -9999 so they are easily identified. There was no way to eliminate these gaps.

Table E1
DELILAH Array Current Meter Locations and Gauge Numbering

Gauge Name	Gauge Number	Serial Number	FRF Coordinate System [1]			Gauge Depth[2] m	Direction from true N deg
			Longshore m	Cross-shore m	Depth[2] m		
CM10 X	2101	90990/S1083	985.95	125.06	-0.28	0.07	162.3
Y	2102						
CM20 X	2201	9089/S1082	985.94	144.99	-1.39	-0.77	162.3
Y	2202						
CM30 X	2301	90988/S1081	985.61	169.97	-0.87	-0.66	162.3
Y	2302						
CM40 X	2401	81161/S9721	985.95	188.94	-1.32	-0.82	162.3
Y	2402						
CM50 X	2501	81455/S1013	985.88	207.41	-1.88	-0.98	160.9
Y	2502						163.7
CM60 X	2601	81453/S1011	986.08	226.25	-2.33	-1.02	162.3
Y	2602						
CM70 X	2701	81454/S1012	985.91	245.00	-3.03	-1.05	162.3
Y	2702						
CM80 X	2801	81456/S1015	985.97	295.21	-3.68	-1.66	162.3
Y	2802						
CM90 X	2901	90991/S1084	986.11	370.12	-4.25	-1.68	162.3
Y	2902						
CM31 X	2311	MM S892	967.22	169.57	-0.94	-0.82	160.9
Y	2312						163.7
CM32 X	2321	MM S385	936.44	168.68	-1.86	-0.78	162.3
Y	2322						
CM33 X	2331	MM S476	926.17	168.21	-1.88	-1.67	162.3
Y	2332						
CM34 X	2341	MM S760	856.09	166.06	-1.60	-0.82	161.6
Y	2342						
CM35 X	2351	MM S761	806.37	164.87	-1.58	-0.92	160.9
Y	2352						
X	2351	MM S762	Replaced MM S761 at 1251, 3 Oct 91				
Y	2352						
CM54 X	2541	Open Frame 6	855.87	210.37	-2.09	-1.02	252.3
Y	2542						
CM71 X	2711	Open Frame 7	966.04	244.36	-3.02	-0.93	252.3
Y	2712						
CM72 X	2721	Open Frame 10	936.08	243.65	-3.07	-1.01	252.3
Y	2722						
CM73 X	2731	Open Frame 16	926.06	243.16	-3.11	-1.04	252.3
Y	2732						
CM74 X	2741	Open Frame 9	856.05	240.88	-3.21	-1.27	252.3
Y	2742						

[1] Coordinates are relative to the FRF coordinate system which is orthogonal to the research pier. The origin of this system is on the southern property line, behind the dune crest.
[2] Depths relative to NGVD at start of DELILAH.

TABLE E2
DELILAH Array Pressure Gauge Locations and Numbering

Gauge Name	Gauge Number	Serial Number	Gain[3] (m/s)/V	Bias[3] V	FRF Coordinate System[1] Longshore m	Cross-shore m	Depth[3] m	Gauge Depth[3] m
Paroscientific Pressure Gauges (Water Depth Measurement)								
PD10	2103	32089	1.0	0	984.41	124.86	-0.28	-0.07
PD20	2203	29439	1.0	0	984.75	145.03	-1.39	-0.69
PD30	2303	32088	1.0	0	984.99	169.78	-0.87	-0.55
PD40	2403	30735	1.0	0	985.01	188.60	-1.32	-0.67
PD50	2503	30566	1.0	0	984.88	207.54	-1.88	-0.78
PD60	2603	30344	1.0	0	985.29	226.46	-2.33	-0.81
PD70	2703	30564	1.0	0	985.07	245.02	-3.03	-1.00
PD90	2903	30565	1.0	0	986.11	370.12	-4.25	-3.26
Strain Gauges (Wave Measurement)								
PW10	2104	#2	1.0	0	984.41	124.86	-0.28	-0.65
PW20	2204	#3	1.0	0	984.75	145.03	-1.39	-0.86
PW30	2304	#4	1.0	0	984.99	169.78	-0.87	-0.75
PW40	2404	#5	1.0	0	985.01	188.60	-1.32	-0.86
PW50	2504	#6	1.0	0	984.88	207.54	-1.88	-0.98
PW60	2604	#7	1.0	0	985.29	226.46	-2.33	-1.22
PW70	2704	#8	1.0	0	985.07	245.02	-3.03	-1.20
PW80	2804	#9	1.0	0	985.97	295.21	-3.68	-3.04
PW90	2904	#1	1.0	0	986.11	370.12	-4.25	-3.06

[1]Coordinates are relative to the FRF coordinate system which is orthogonal to the research pier. The origin of this system is on the southern property line, behind the dune crest.
[2] The gain and bias values for these sensors were already adjusted for prior to the data being written.
[3] Depths relative to NGVD at start of DELILAH.

Gains and biases applied can be found in the data file headers of each time series. Several of the gauges (CM73 at 0939 on 20 October, CM71 at 1030 on 20 October, and CM50 at 1358 on 4 October) were rotated 180°during the experiment, noted as a change in the sign of the gains, in order to conform to other Marsh McBirney current meter orientations. Other orientation changes that occurred and must be noted include: gauge CM31 rotated 20° clockwise (visually estimated) at 1330 on 15 October, gauge CM10 rotated 2° clockwise between the beginning of collection at 0834 and end of collection at 1455 on 11 October and also re-aligned 17.6° clockwise between 0624 and 1330 on 18 October, and a re-alignment of gauge CM20 rotated 28.1° counter-clockwise between 0624 and 1330 on 18 October. In addition, a 10° landward bend from vertical in Gauge CM73 was corrected at 0939 on 20 October. These rotations

were noted in the time series headers.

Throughout the experiment, two current meters, CM10 and CM20, were in a zone that experienced large bathymetric change. This necessitated moving the gauges up and down in order to ensure that they remained submerged in the water but were sufficiently far above the sediment surface. Gauge CM10 was moved up on 7 and 8 October and down on 9,11, and 18 October. Gauge CM20 was moved up on 7 and 8 October. Measurements of how far up or down these gauges were moved were recorded and the time series headers were modified.

The electronics package at position 60 (Figure E1) was lost during the high waves of Hurricane Lili at approximately 0700 on October 11. The sensors at position 30 stopped functioning a few days later.

DELILAH array data analysis

Although several of the current meters were vertically adjusted to maintain submergence and to remain above the bottom, several of the shallower gauges would occasionally became exposed in the wave troughs, particulary during low tide. A technique for determining when the current meters were exposed is presented, and was used to mark time series headers with a data quality parameter for exposed sensors. Several methods for estimating gauge exposure could be envisioned, the one presented here was used since it was fairly simple to employ. This technique finds the lowest trough elevation in each pressure gauge record (Setra gauges), then determines if the position of the corresponding current meter is above the lowest trough. This was a reasonable approach, particularly for the primary cross-shore array, since the current meters and pressure sensors were only separated by 1.5 m. The 10 current meters in the sub-arrays did not have co-located pressure gauges, so comparisons were made with primary cross-shore array pressure gages at the same cross-shore coordinate. Longshore homogeneity of the wave field was assumed.

DELILAH array pressure gauges recorded offsets and daily variations which were corrected by comparison to the Paroscientific pressure gauge LA33 (gauge number 231) in the FRF's permanent 8-m array. Gaps sometimes occurred in the data from gauge 231. If the gaps were less than 30 minutes in length, interpolation was used to attain water levels for those times. On 20 October, 1990 gauge 231 stopped functioning, from that time forward, the tide gauge located at the end of the pier was used for water level comparisons (Gauge 1, Figure E3). The tide gauge was not used for correcting water levels through the entire experiment because the signal from this gauge is typically not as accurate as the signal from the Paroscientific gauge. It samples a single point every six minutes which results in a noisier signal. This method

does not take into account any potential wave setup between the 8-m array and the nearshore DELILAH array. The changes in the water levels for the current meters resulting from this analysis are presented in Figure E4.

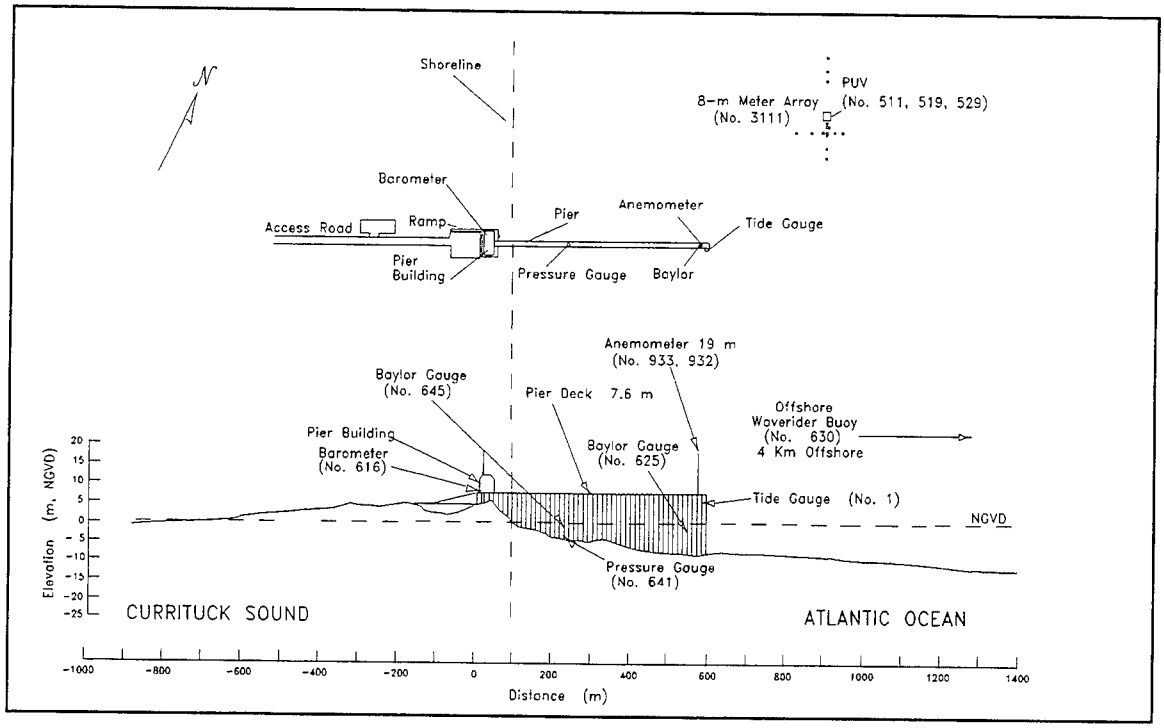

Figure E3. Schematic showing position of FRF's stationary instrumentation

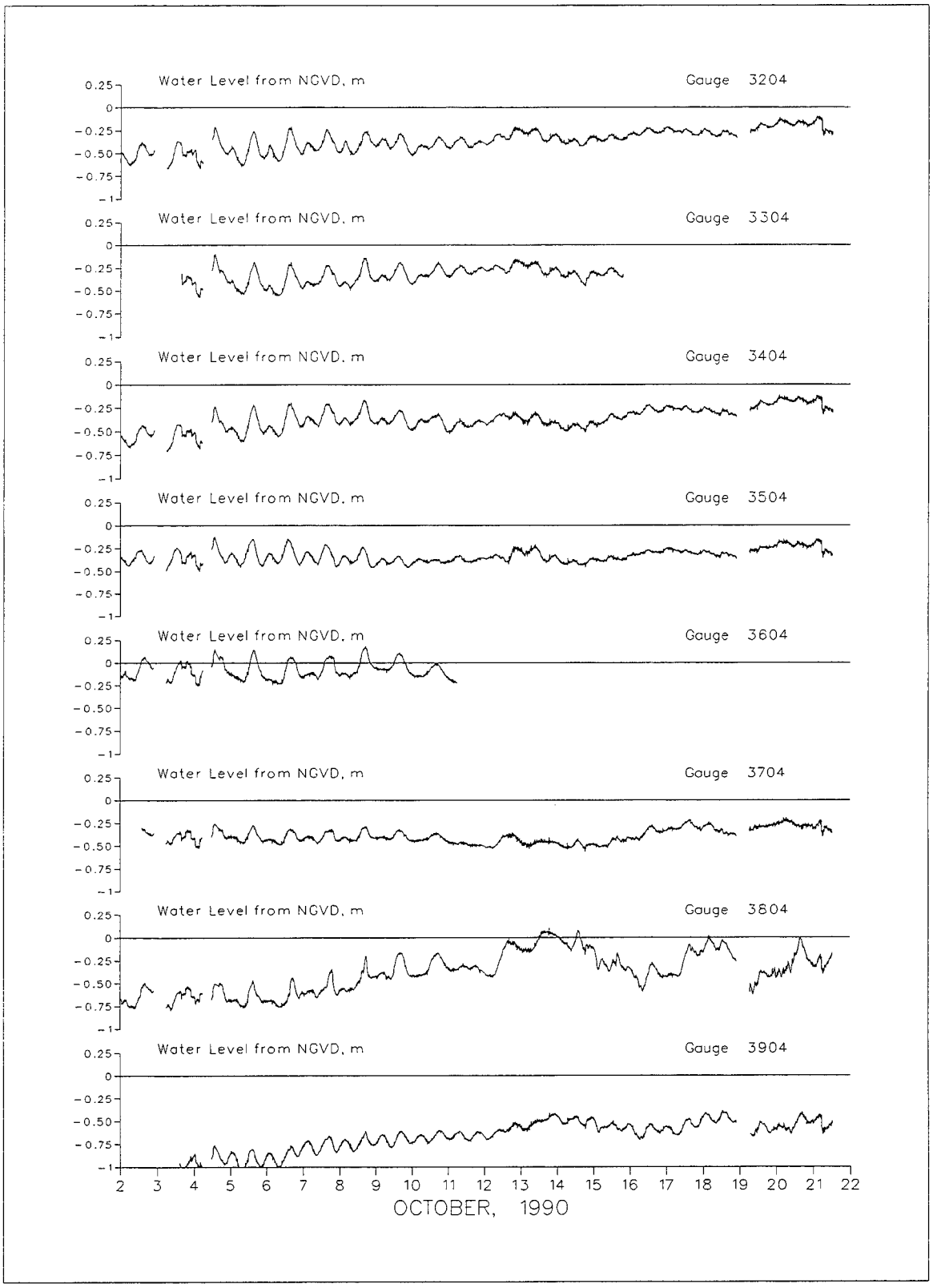

Figure E4. Changes in water levels for current meters resulting from comparison to 8-m array Paroscientific pressure gauge 231

An additional data quality analysis was performed on each current meter record to determine the effect of biofouling on signal attenuation. This procedure, referred to as the *PUV-test*, Z(σ), used a ratio of surface wave H_{mo} computed from pressure gauges and current meters, to estimate a gain correction for the current meters. The method to calculate the PUV-test follows.

Pressure gauge data (in units of meters of sea water) were surface normalized by the pressure response function $K(z,d,k) = \cosh k(z+d)/\cosh kd$, where z is gauge depth from (ensemble) mean sea level, d is total water depth, and k is radian wavenumber (related to radian frequency σ by the dispersion relation $\sigma^2 = gk\tanh kd$) immediately after Fourier transformation, by dividing the complex Fourier coefficients at frequencies σ by $K(z,d,k)$. Current meter data were surface normalized in a similar fashion except that the Fourier coefficients were divided by $\frac{gk}{\sigma}K(z,d,k)$. In linearized wave theory, the auto-spectrum from surface normalized pressure $C_{pp}(\sigma)$ is equal to the sum of the auto-spectra from the two surface normalized velocity components $C_{uu}(\sigma)$ and $C_{vv}(\sigma)$ for u and v, respectively. A routine check on data quality for co-located pressure and current meter data , the *PUV-test*, is to compute the function ,$Z^2(\sigma) = C_{pp}(\sigma)/[C_{uu}(\sigma) + C_{vv}(\sigma)]$,which was expected to be unity in the wind-wave pass band of frequencies in regions where linear theory applies.

The PUV-test analysis used the same gauge pairs as the exposed current meter analysis, current meters without colocated pressure gauges were matched with primary array pressure gauges at the same cross-shore coordinate. Again, longshore homogeneity was assumed. An average PUV-test is calculated for each current meter record over a select frequency range of the Z(σ). This PUV-test is averaged over the half-power bandwidth in the pressure gauge energy spectra, for the spectral peak that lies in the wind-wave band (0.4 to 0.05 Hz). These PUV-test values are used as a multiplier to adjust the mean current amplitudes. Inherent in this treatment is the assumption of uniform fouling between both axes of each current meter. Corrected and uncorrected current velocities, and PUV-test values are recorded in the DELILAH statistics database. Plots of the PUV-test values are presented in Figures E5 and E6. These data are noisy because averages are taken over short time segments. PUV-test plots for current meters that are not colocated to pressure gauges are especially noisy. The noisiness increases with the distance between current meter and pressure gauge. Plots CM71, CM72, CM73 and CM74 demonstrate this spatial inhomogeneity. The consistent PUV-test value of less than one for gauge CM90 indicates the pressure gauge was either lower in the water than believed or the current meter was higher.

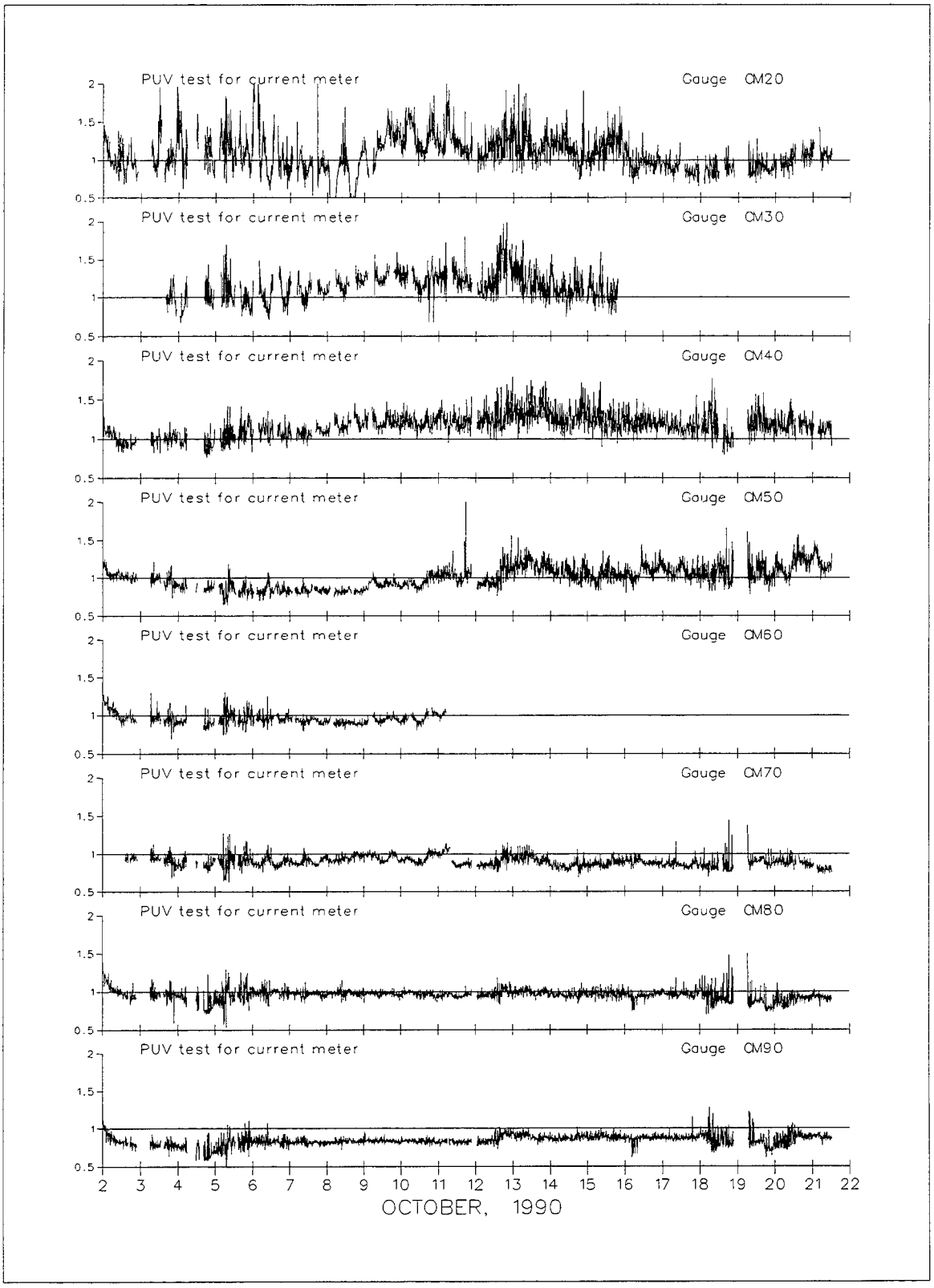

Figure E5. PUV-test values for gauges in the primary cross-shore subarray

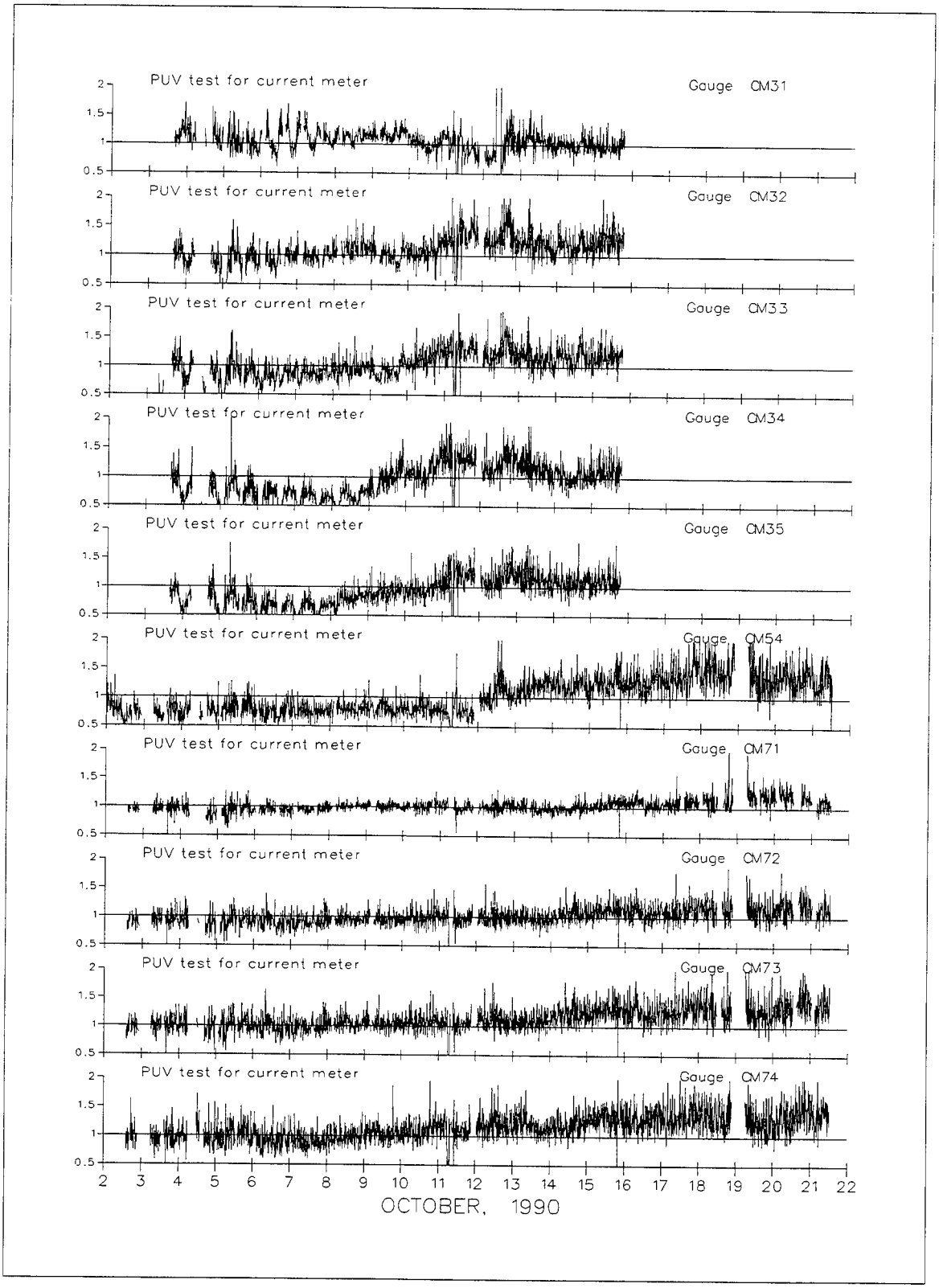

Figure E6. PUV-test values for gauges in the secondary cross-shore, trough and crest subarrays

Data from each instrument in the primary cross-shore subarray, the trough array, and crest array are plotted in Figures E7 through E12. Gauge 1 in these plots is a primary National Oceanic and Atmospheric Administration tide gauge located at the end of the FRF pier. These plots have been processed to handle data gaps, establish gauge depths relative to mean sea surface, and eliminate gauges that became exposed at low tide. Analysis has indicated the data set is of highest quality between 6 and 16 October. In the first few days of the experiment problems existed in the collection system and gauge elevations and orientation were being adjusted. After the 16 October biofouling of current meters had significantly attenuated the sensor response, this was especially true for the Scripps Open Frame gauges. For these Open Frame gauges, there appears to be three identifiable portions of the experiment where three separate gains can appropriately be applied to each Open Frame current meter. The PUV-test values remained fairly constant during the first portion of the experiment, from 1 October through 8 October, then increased from 9 October through 13 October, and stabilized again from 14 October through 19 October. When these PUV-test multipliers are applied to the data, differences in the current velocity as great as 0.24 m/sec (27.5 % change in velocity) can result. For these reasons DATA COLLECTED USING OPEN FRAME SENSORS SHOULD BE USED WITH CAUTION.

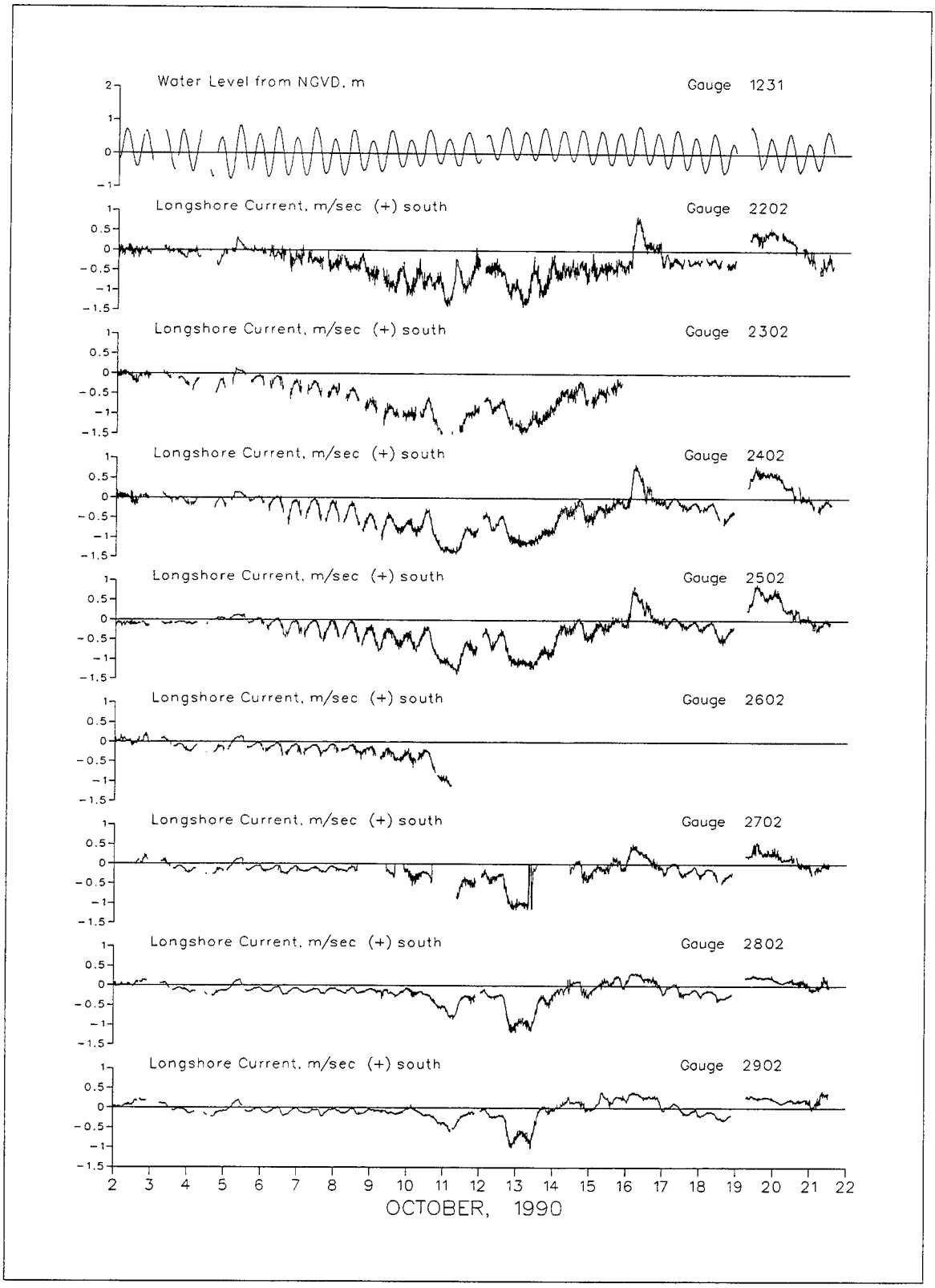

Figure E7. Longshore Currents, primary cross-shore subarray

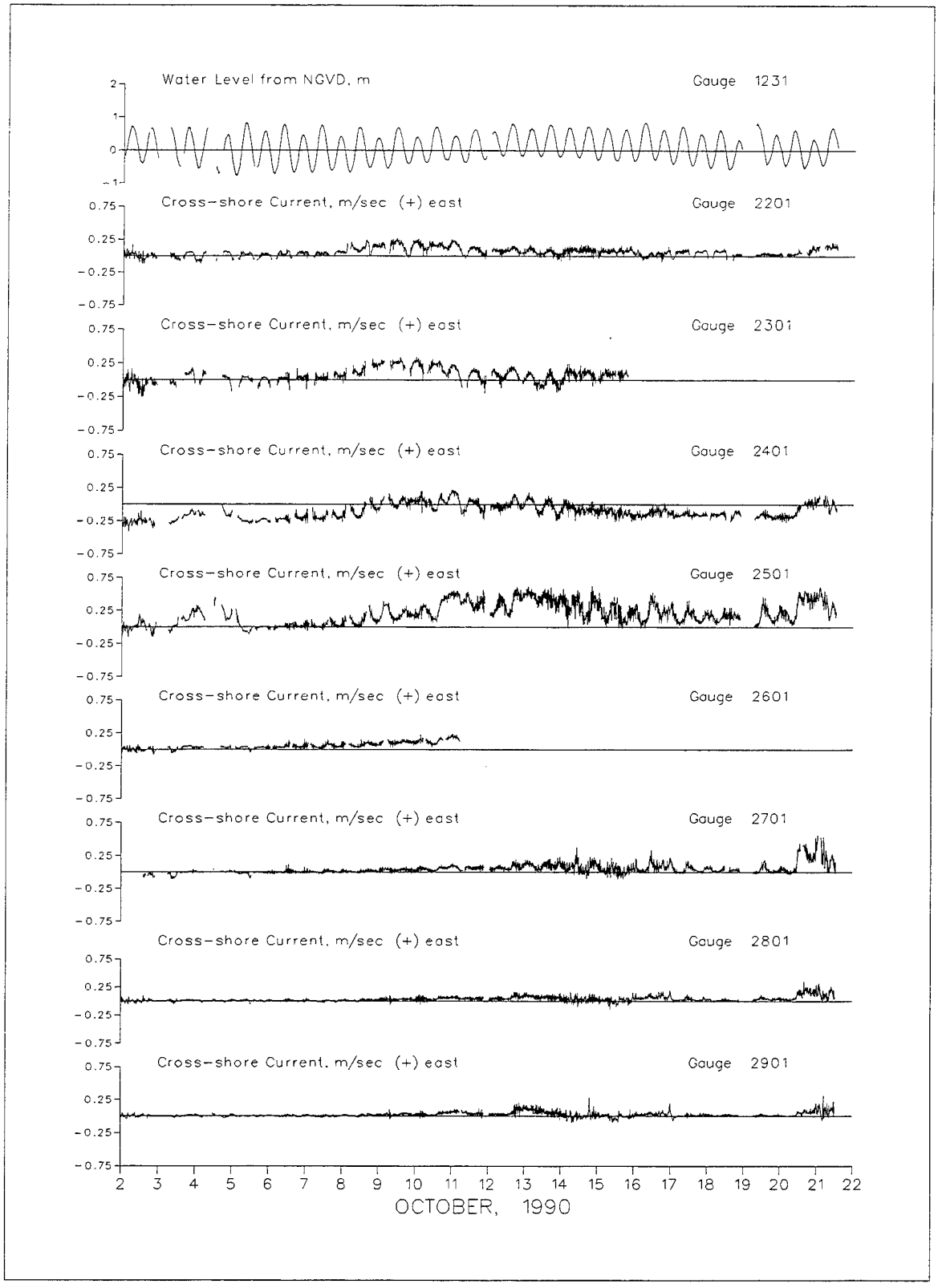

Figure E8. Cross-shore currents, primary cross-shore subarray

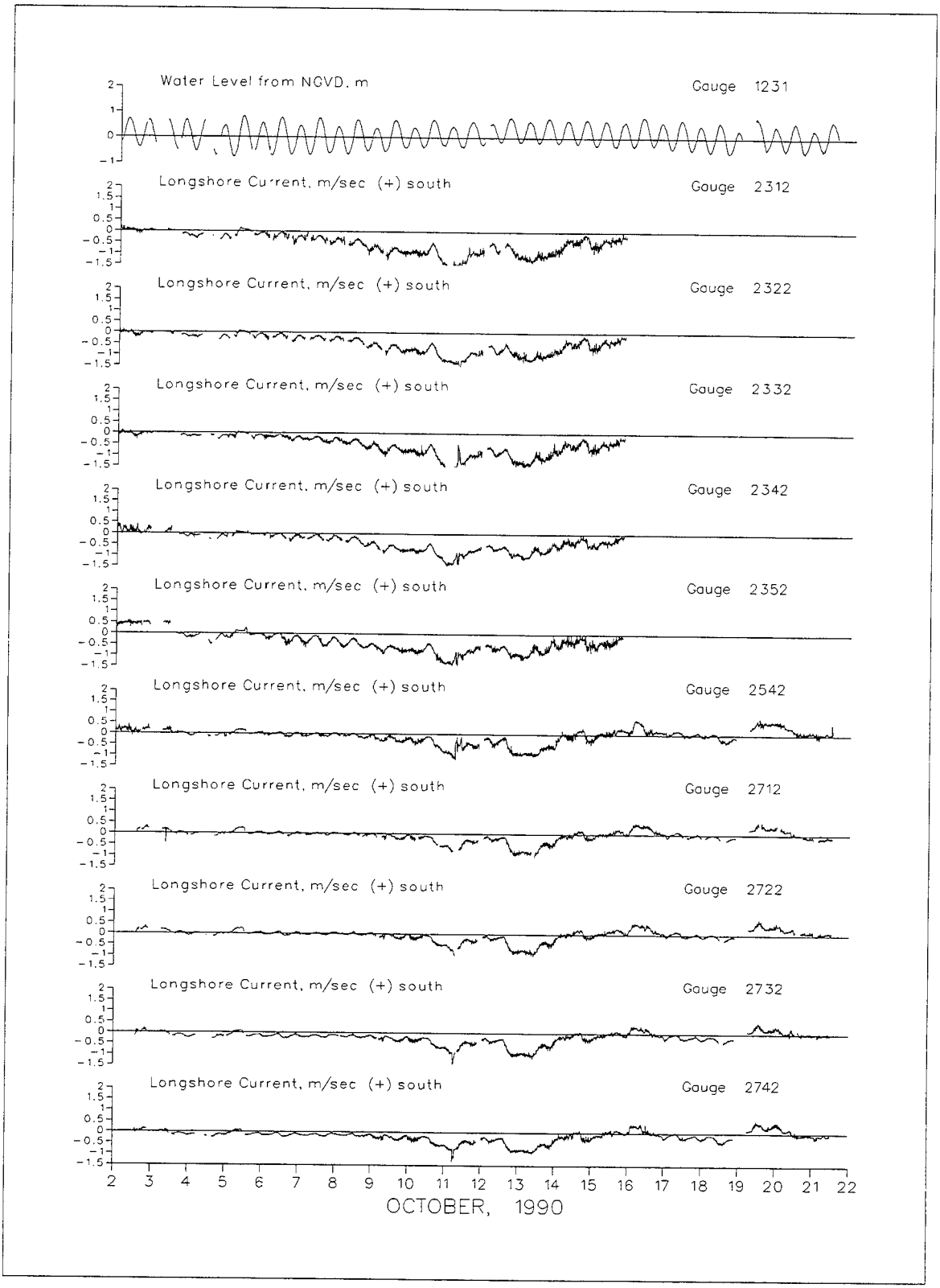

Figure E9. Long shore currents, trough and crest subarrays

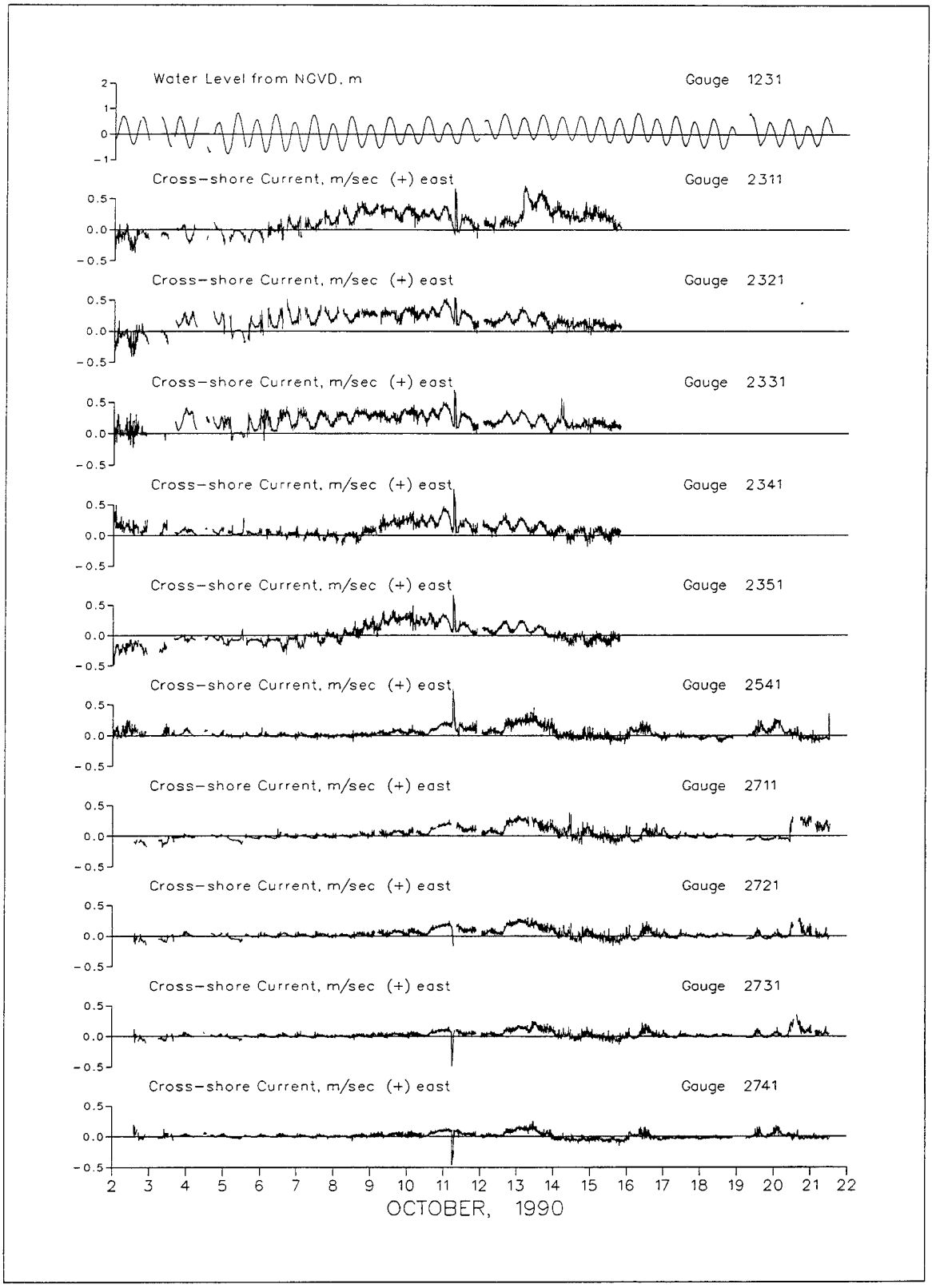

Figure E10. Cross-shore currents, trough and crest subarrays

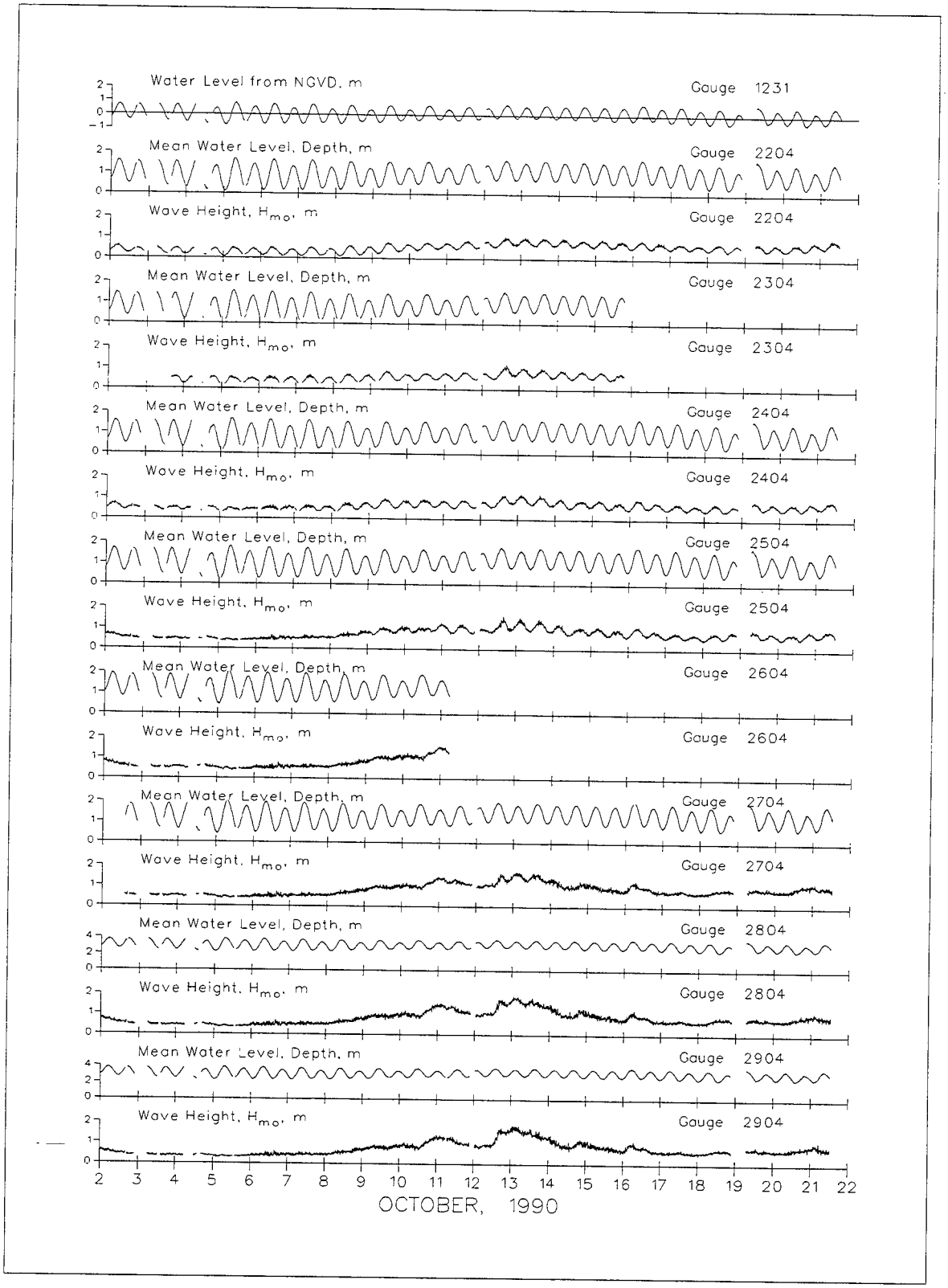

Figure E11. Wave heights and water levels, cross-shore pressure strain gauges

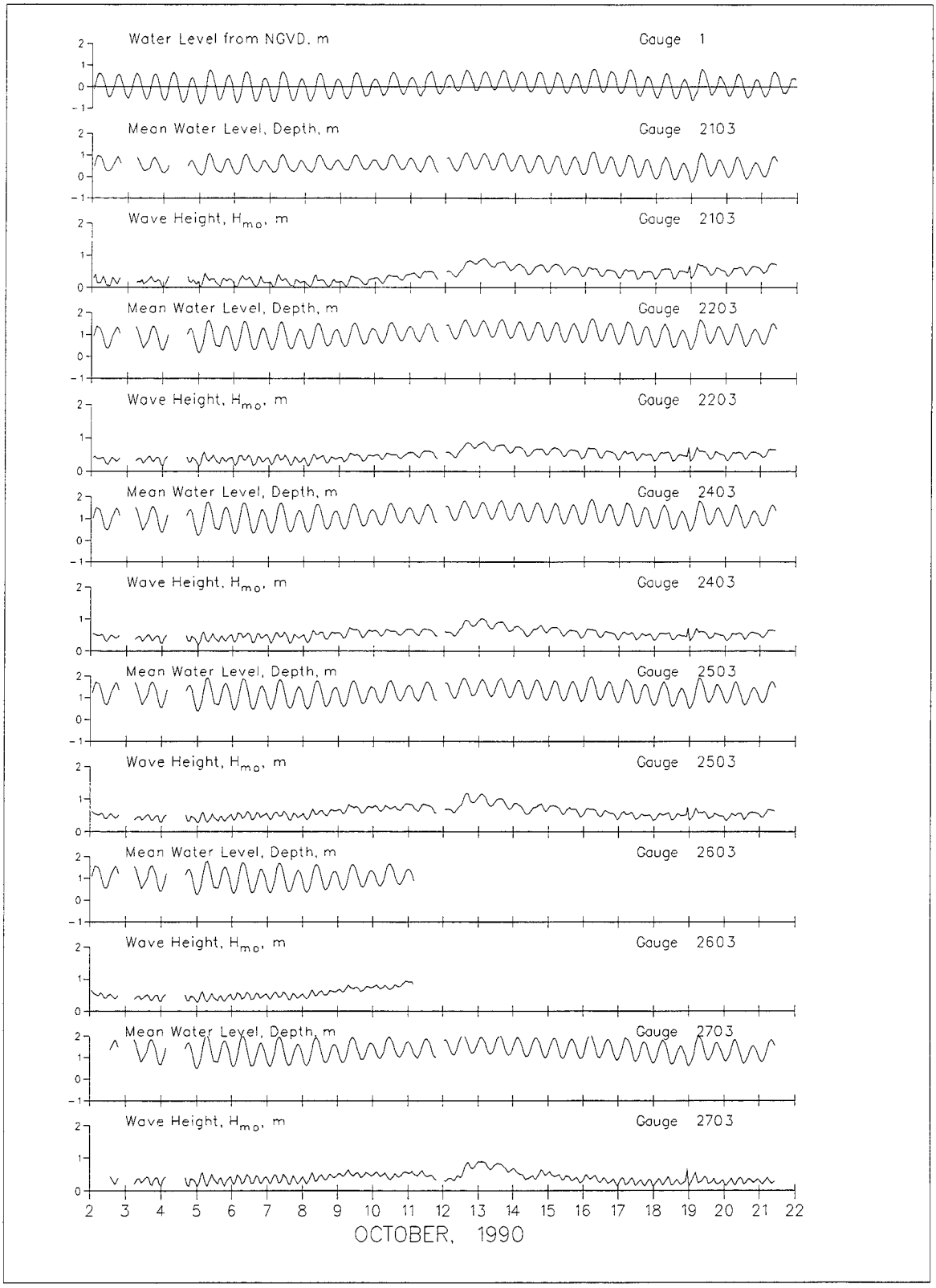

Figure E12. Wave heights and water levels, cross-shore Paroscientific pressure gauges

FRF Permanent Instrumentation

A group of instruments that is permanently installed at the FRF allows for the continuous collection of oceanographic and meteorologic data. During large cooperative experiments, such as DELILAH, these instruments not only provide researchers with information on conditions during the experiment, but also with an invaluable archive of data from which to compare and interpret trends. The permanent instrumentation includes the 8-m array; Baylor wave gauges; waverider buoy; and gauges for wind speed, wind direction, tide, atmospheric pressure, and temperature. Table E3 lists the FRF permanent instruments by name and number and includes gain, bias, coordinates relative to the FRF coordinate system, and gauge depth. Figure E3 is a schematic depicting the location of these instruments.

An additional numbering convention for FRF permanent instrumentation is used to refer to combinations of gauges. This is a four digit gauge number that associates a name with the results of a multi-sensor data analysis. Among these four-digit combination gauges are 3111, which is the pressure sensors in the 8-m array; 3519, which is the vector averaged currents of the PUV gauge in the 8-m array; and 3932, which is the vector averaged wind speed and direction. Statistics from these and other gauges show the basic climatology during DELILAH in Figure E13.

8-m Array

The 8-m array is composed of a linear longshore array of ten pressure sensors (Nos. 101-191), a cross-shore array of five pressure sensors (Nos. 211-251), and a combination pressure/current meter (PUV) (Nos. 511, 519, and 529) within the array. The fifteen pressure gauges are mounted approximately 0.5 m off the bottom in the vicinity of the 8-m isobath. The array employs pressure sensors, manufactured by Senso-Metrics Inc., with a range of 0-25 psir (pounds per square inch relative to 1 atm). Each sensor was statically calibrated prior to deployment and mounted on a 2-in.-diam pipe jetted into the ocean bottom. A complete analysis of the data results in a three-dimensional directional spectra as illustrated in Figures E14 through E24. Characteristic wave heights from spectral observation are most frequently given as H_{mo}, which is four times the standard deviation of sea-surface displacement. It can be determined from the volume under the frequency-direction spectrum by the equation:

$$H_{mo}^2 = 16 \sum_{n=1}^{N} \sum_{m=1}^{M} S(f_n, \theta_m)\, df\, d\theta \qquad (1)$$

It can also be found from the integrated frequency spectrum by:

$$H_{mo}^2 = 16 \sum_{n=1}^{N} S(f_n)\, df \tag{2}$$

which is its more conventional definition, or from the integrated direction spectrum (Equation 3) by:

$$H_{mo}^2 = 16 \sum_{m=1}^{M} S(\theta_m)\, d\theta \tag{3}$$

Peak wave period (T_p) and peak direction (θ_p), can be determined by integrating the data in both direction and frequency as shown by the graphs on the vertical panels in Figures E12-E22. Note that as defined, the peak direction does not necessarily correspond to the waves which occurred at the peak period (i.e. peak energy). The PUV directional wave gauge consists of a Marsh-McBirney electromagnetic current meter and a Senso-Metrics Co., Inc. pressure sensor. It is mounted on a tripod located within the linear array. Wave direction is measured in degrees relative to true North and indicates the direction the waves are coming from. A detailed discussion of the data processing required to transform measured time series to estimates of frequency-direction spectra may be found in Long and Atmadja (1994)[1].

Surface Wave Gauges

The Baylor gauges and the waverider buoy are two different types of gauges used to collect wave information. The Baylor gauges (nos. 625 and 645) are surface piercing inductance staff gauges mounted on the pier at the locations indicated in Table E3 and Figure E3. The waverider (no. 630) is an accelerometer buoy located four kilometer offshore. Data analysis is similar for the two gauge types. Data were collected in 34 min records, which consisted of 4,096 data values (representing the voltage output of the sensor) sampled at 2 Hz. After the voltages were converted to engineering units using the sensor calibration factors, the time series were edited to eliminate erroneous jumps and spikes.

Wind Gauge

Measurements of the wind speed (no. 933) and direction (no. 932) were made at the seaward end of the research pier using a Qualimetrics Corporation Skyvane Model 2101 anemometer. Wind directions are reported relative to

---

[1] Long, Charles E., and Atmadja, Juliana. (1994). "Index and Bulk Parameters for Frequency-Direction Spectra Measured at CERC Field Research Facility, September 1990 to August 1991," Miscellaneous Paper CERC-94-5, U.S. Army Engineer Waterways Experiment Station, Vicksburg, MS.

true North with onshore winds having a direction of 71.8°. Summary statistics of 34 minute mean values of these data are presented as the wind vector plot in Figure E11.

Tide Gauge

Water level data were collected by a National Oceanic and Atmospheric Administration (NOAA) tide gage located at the seaward end of the research pier (Gage 1). A 6 minute mean value from the tide gauge, computed once per hour, is plotted as water level from NGVD in Figures E7 through E13.

Barometer and Thermometer

Atmospheric pressure (gauge 616) and air temperature (gauge 624) were measured by Yellow Springs Instrument Co. sensors installed at the FRF building. Summary statistics of 34 minute mean values of atmospheric pressure is included in Figure E13.

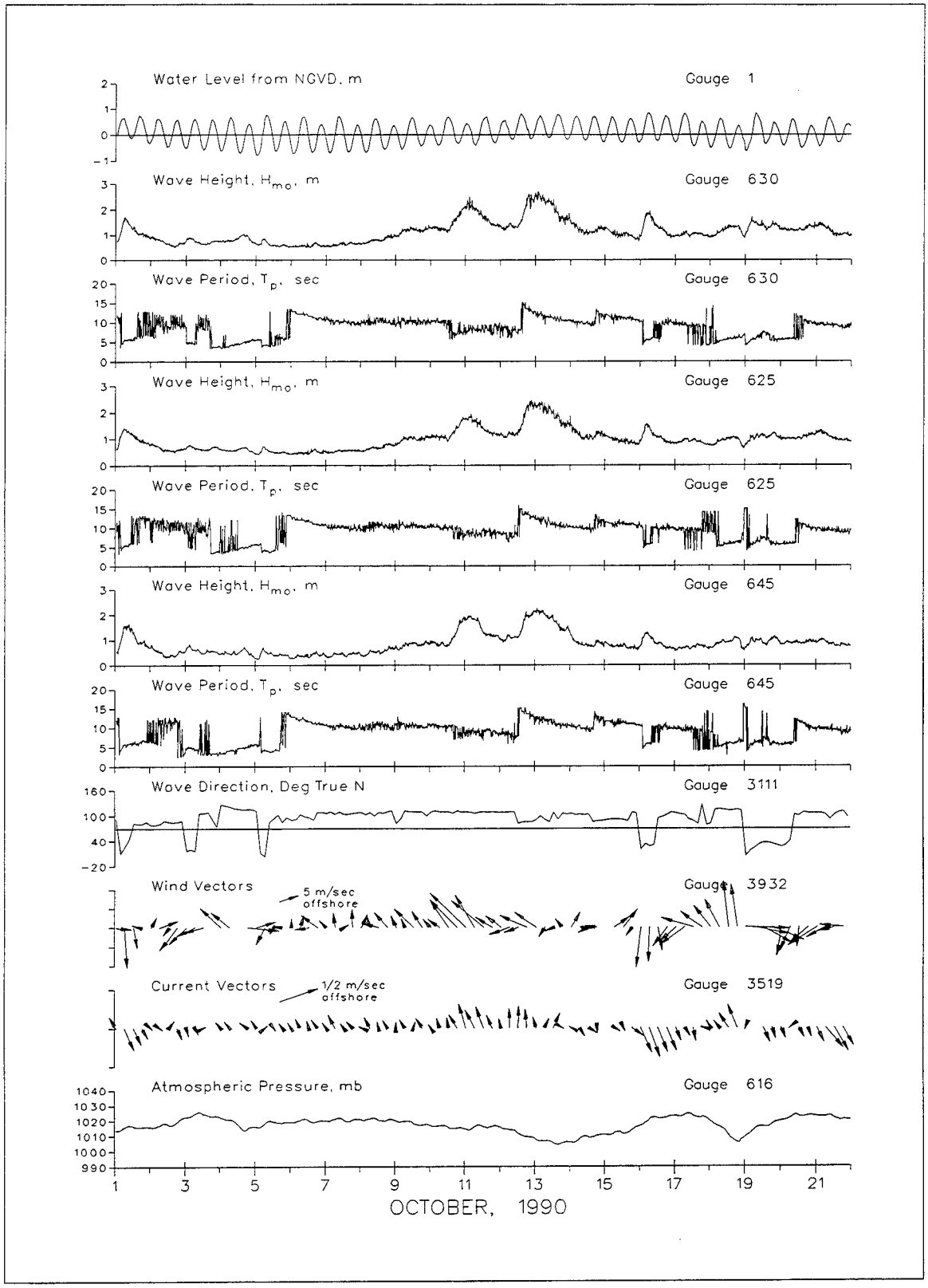

Figure E13. FRF instrumentation

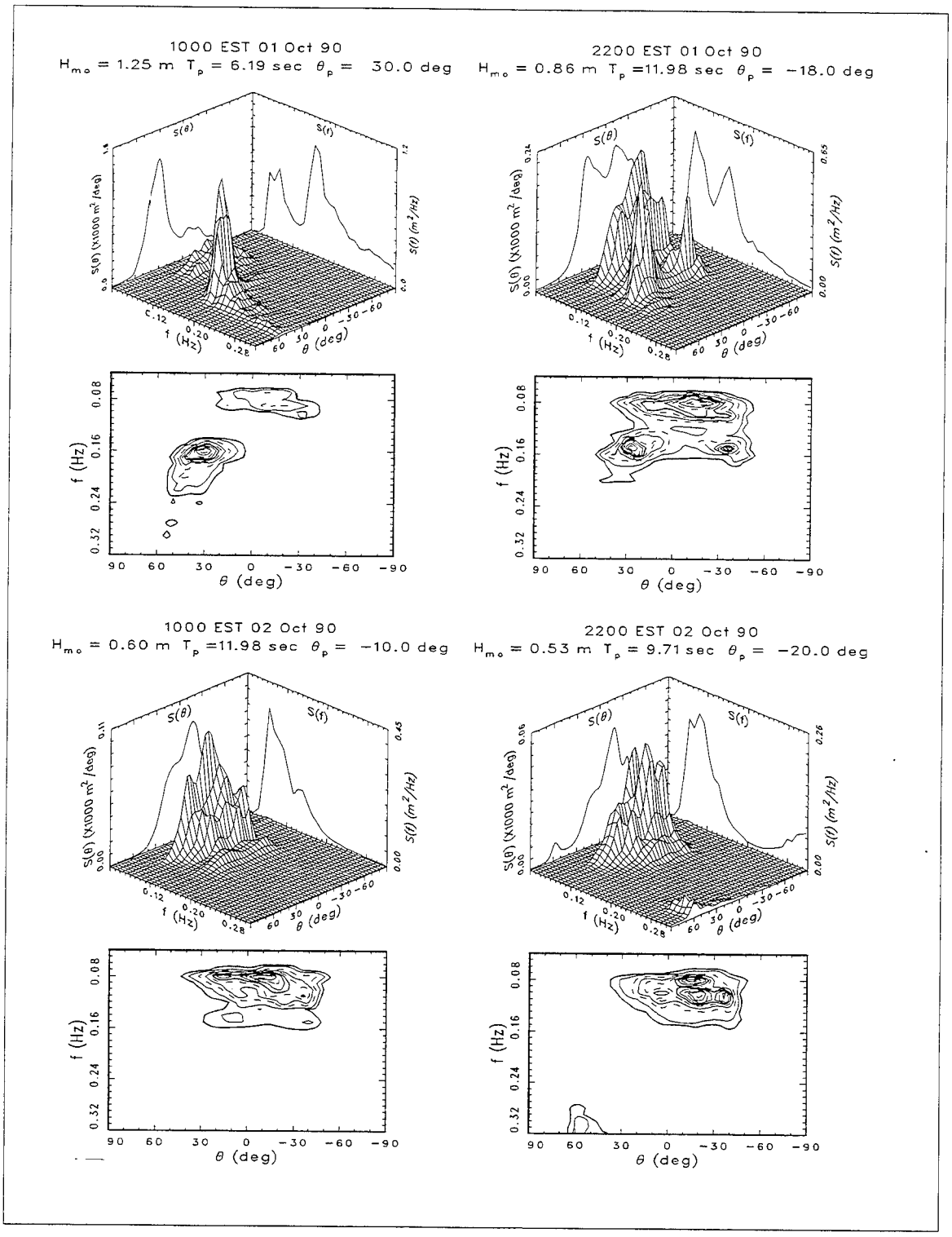

Figure E14. Representative frequency-direction spectra from 8-m array for 1 and 2 October 1990

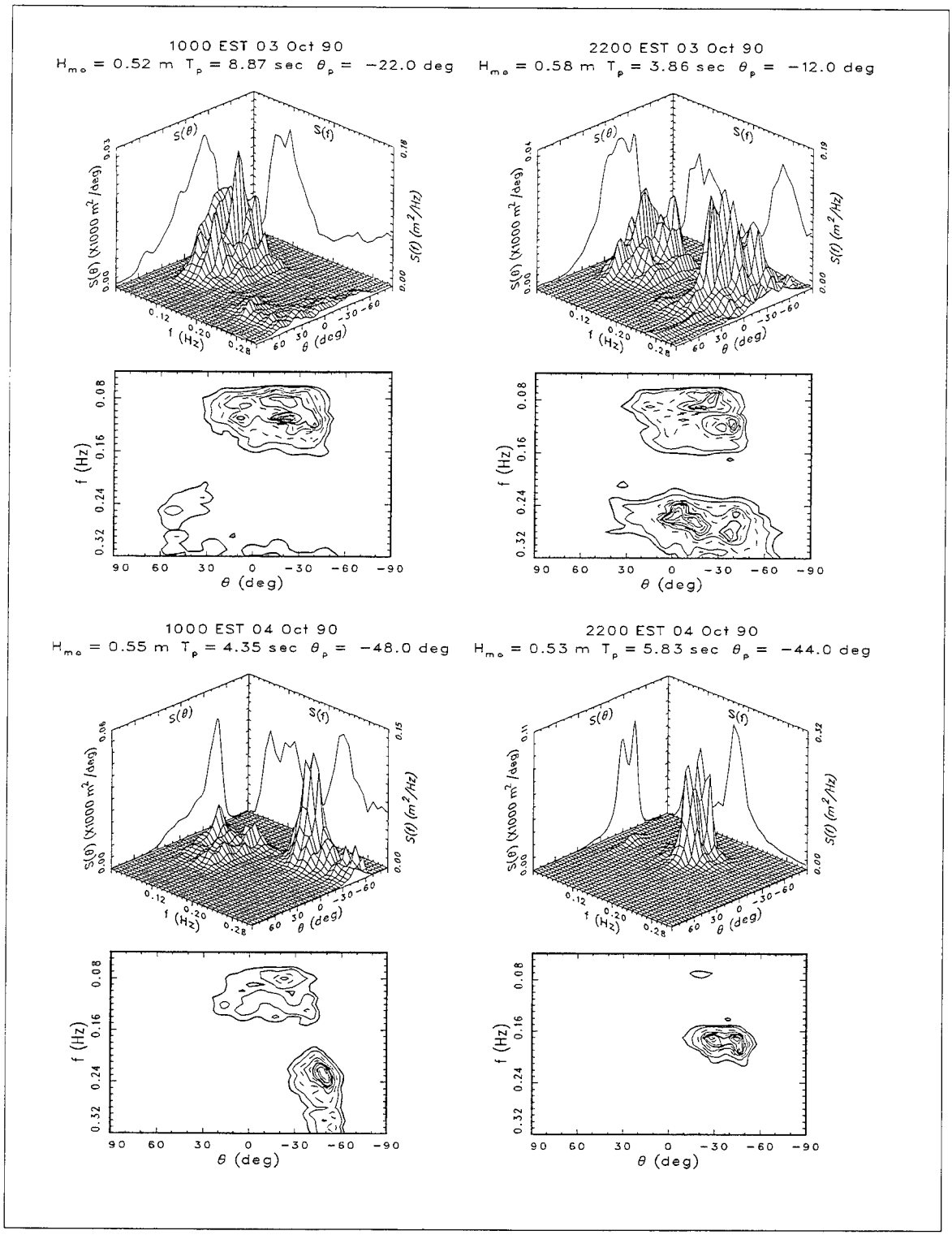

Figure E15. Representative frequency-direction spectra from 8-m array for 3 and 4 October 1990

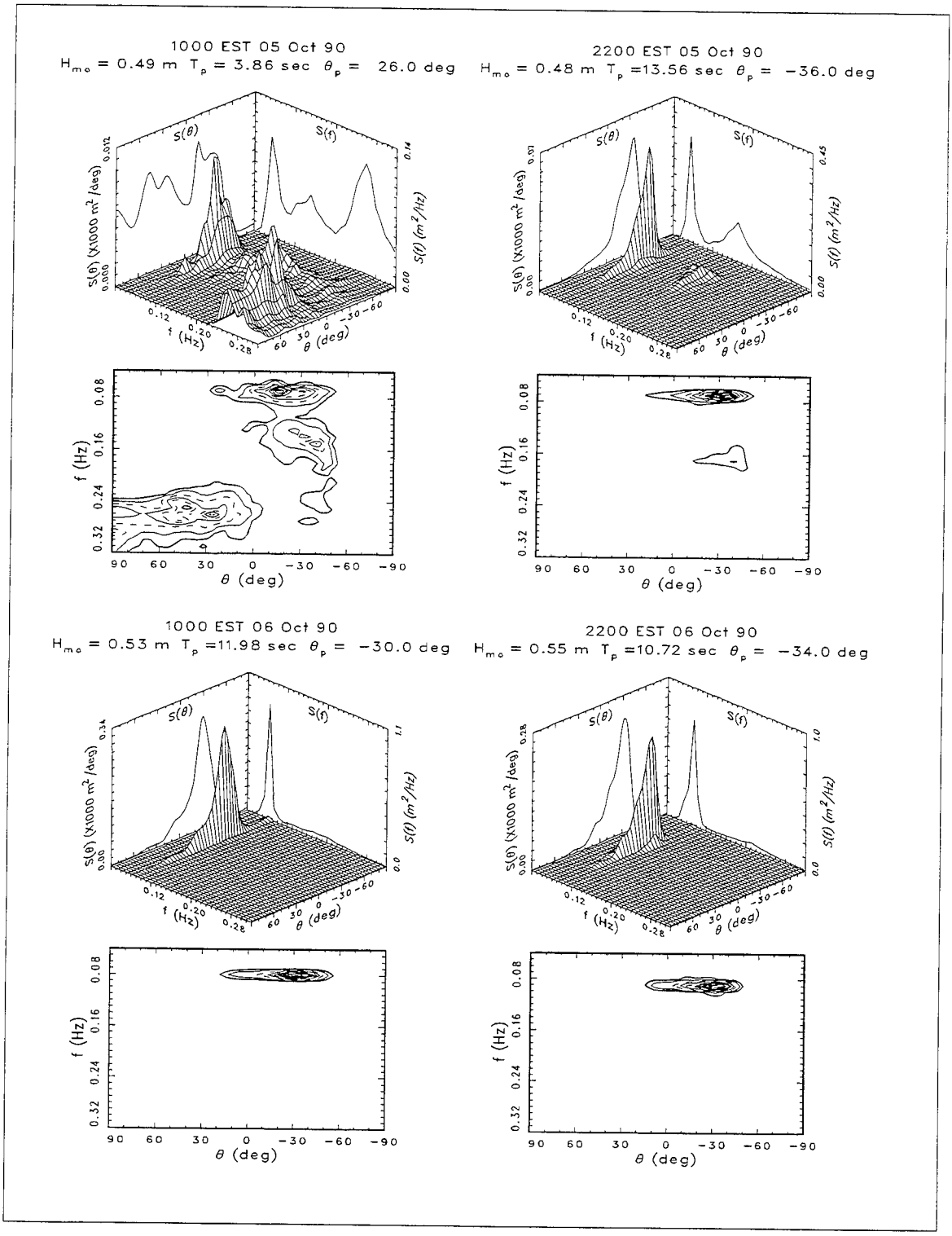

Figure E16. Representative frequency-direction spectra from 8-m array for 5 and 6 October 1990

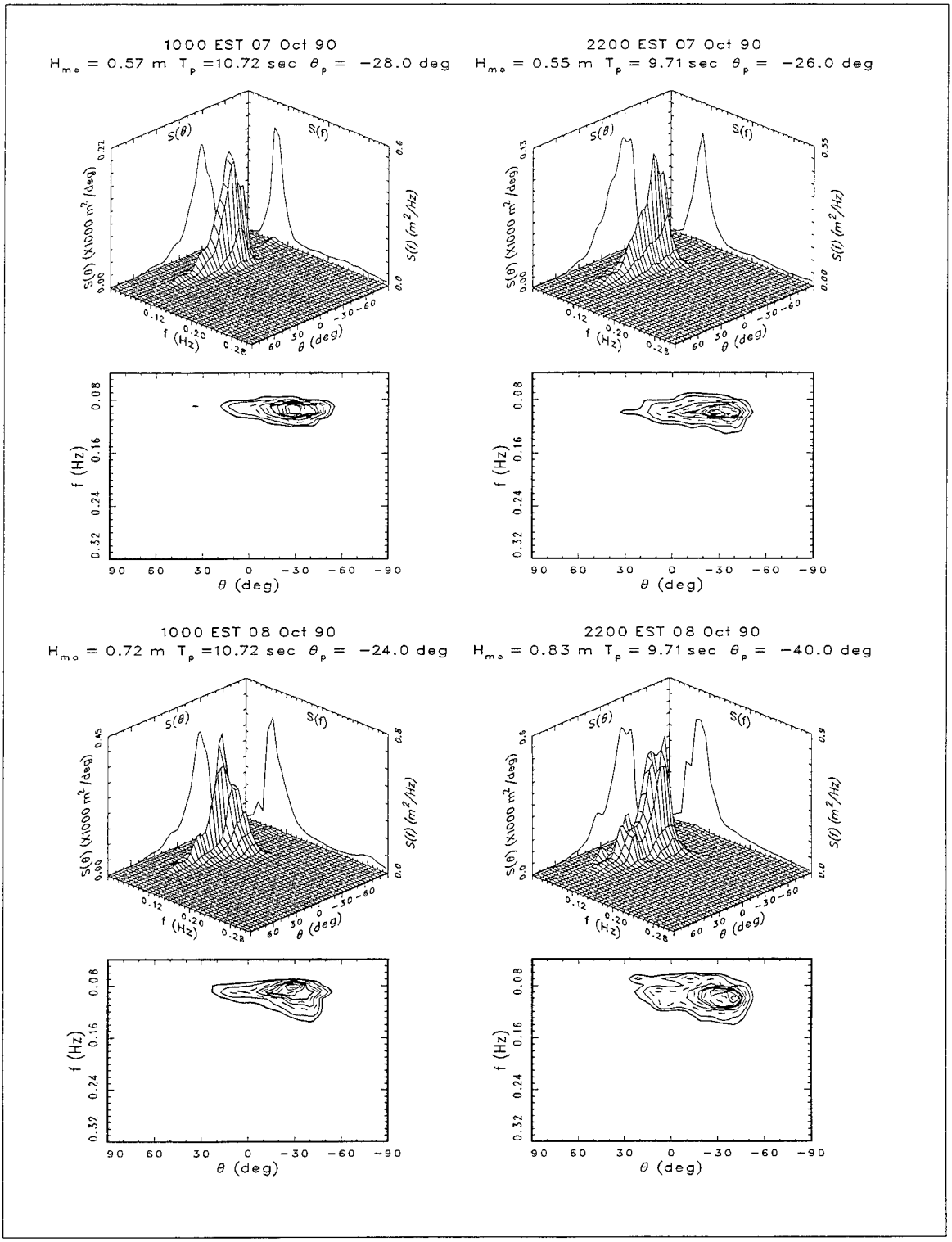

Figure E17. Representative frequency-direction spectra from 8-m array for 7 and 8 October 1990

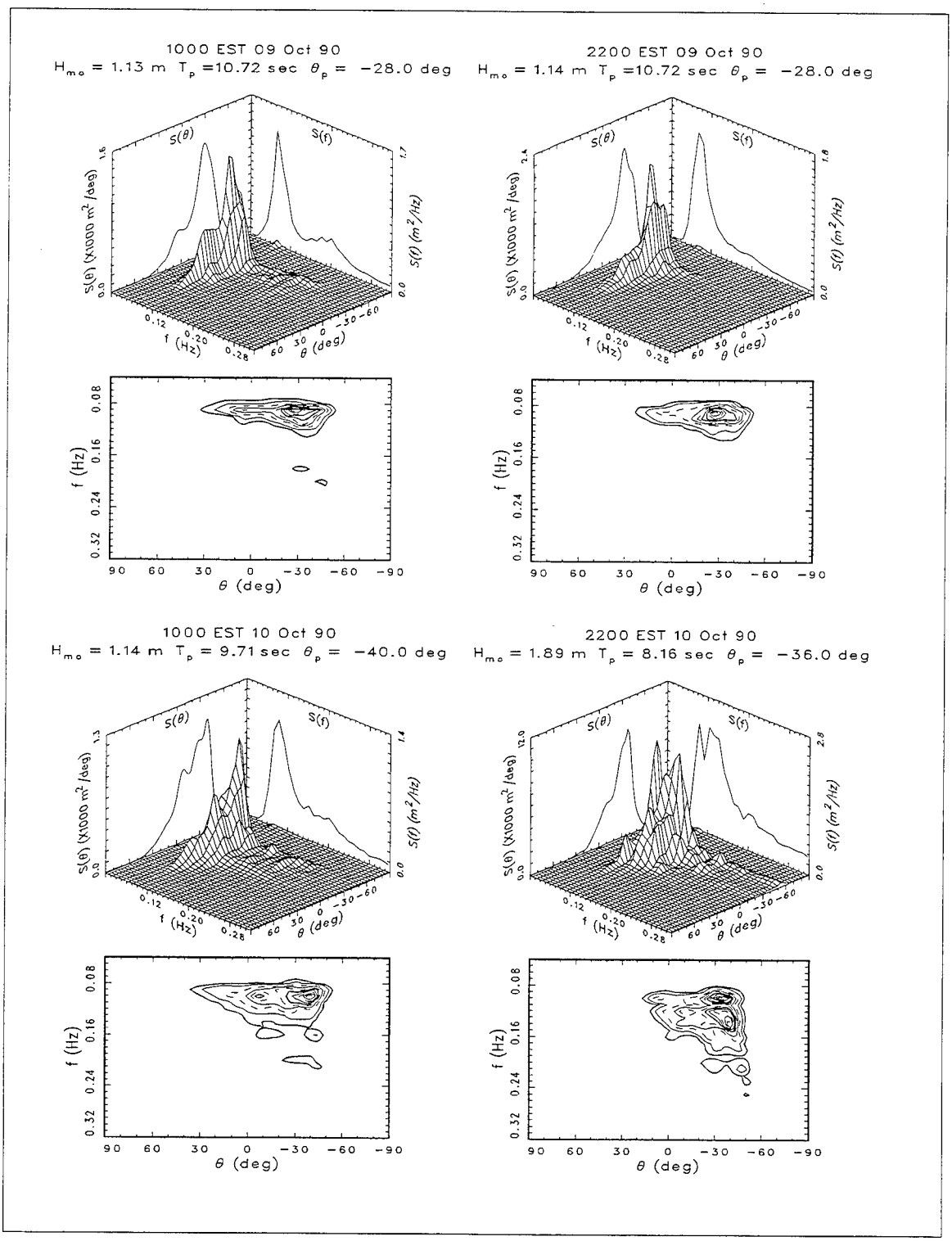

Figure E18. Representative frequency-direction spectra from 8-m array for 9 and 10 October 1990

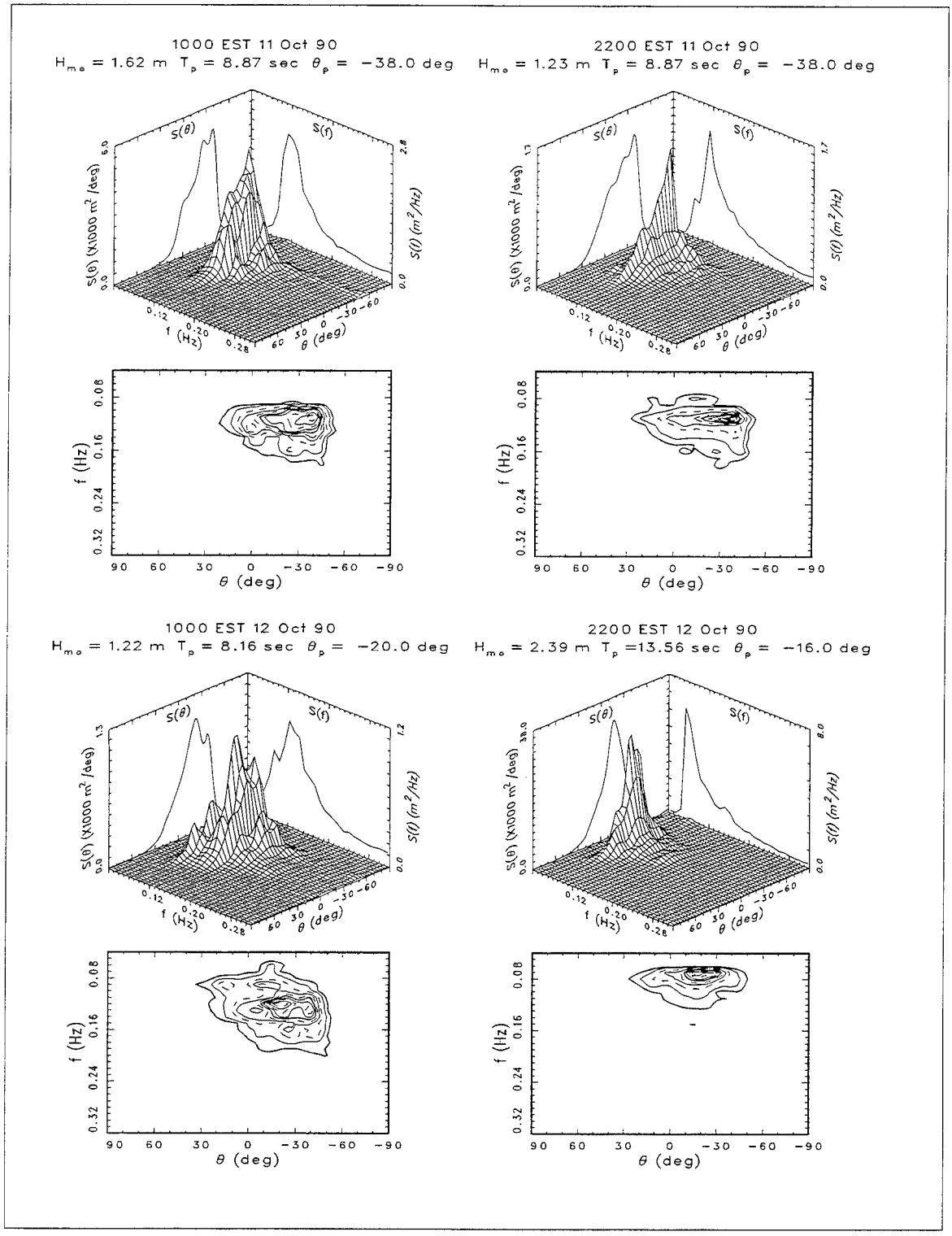

Figure E19. Representative frequency-direction spectra from 8-m array for 11 and 12 October 1990

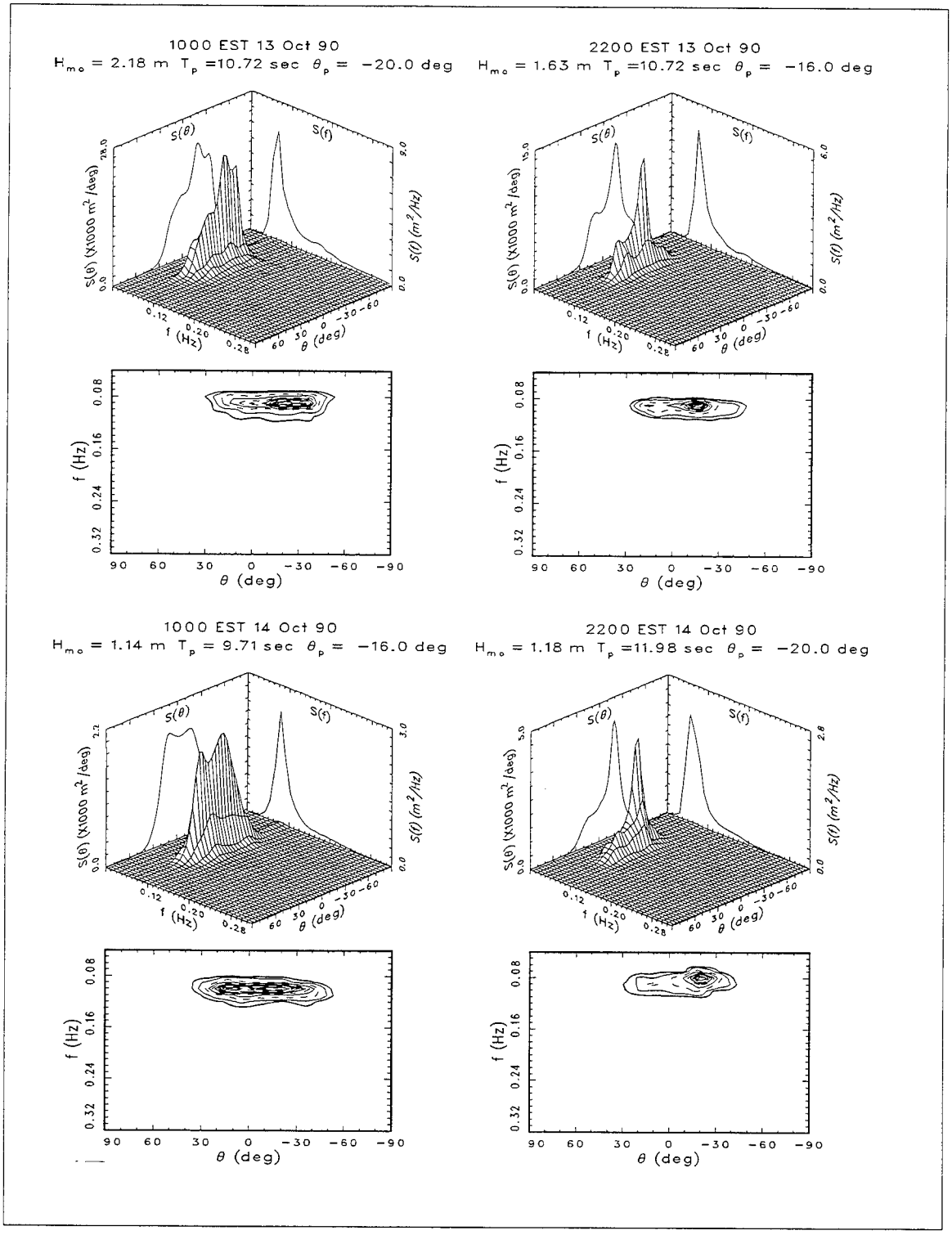

Figure E20. Representative frequency-direction spectra from 8-m array for 13 and 14 October 1990

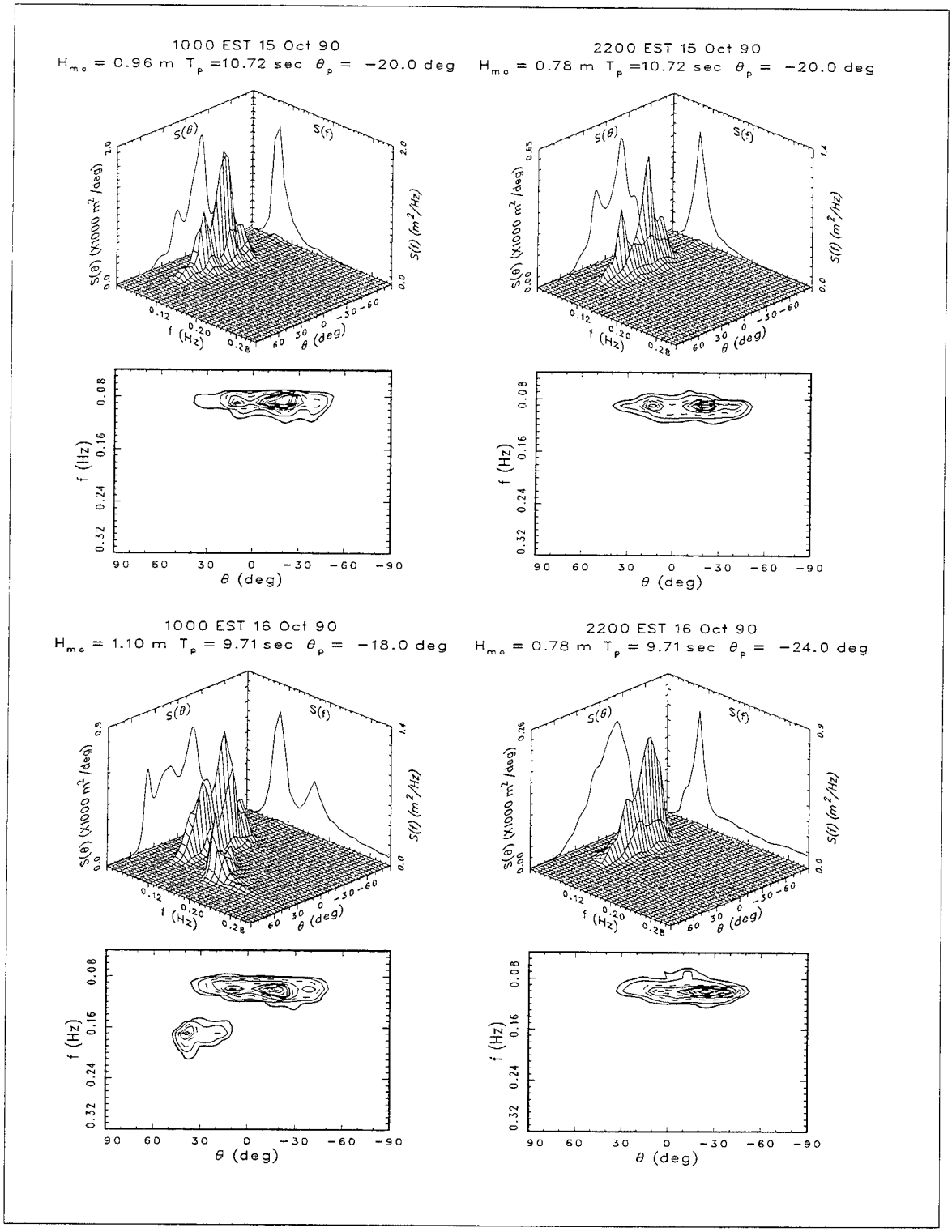

Figure E21. Representative frequency-direction spectra from 8-m array for 15 and 16 October 1990

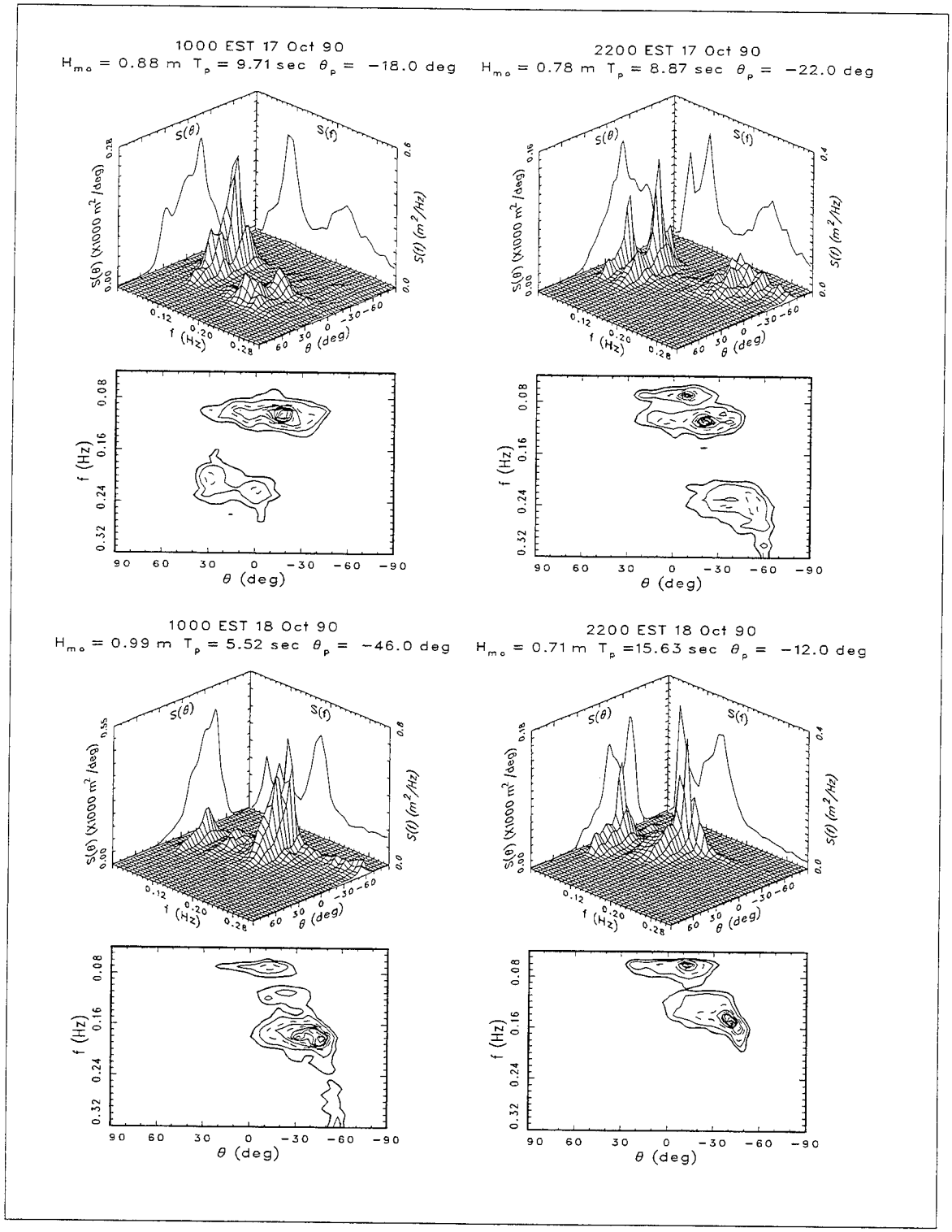

Figure E22. Representative frequency-direction spectra from 8-m array for 17 and 18 October 1990

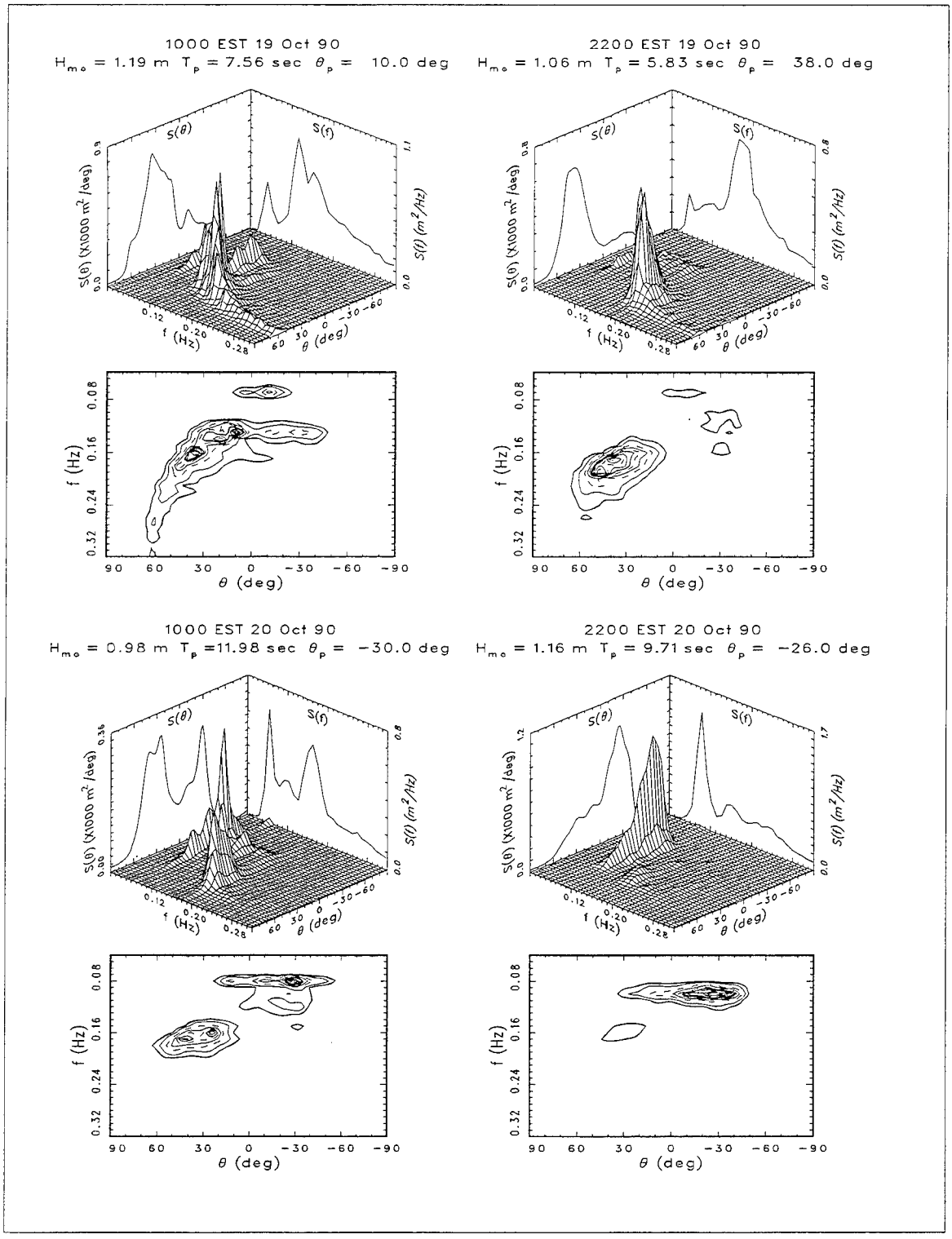

Figure E23. Representative frequency-direction spectra from 8-m array for 19 and 20 October 1990

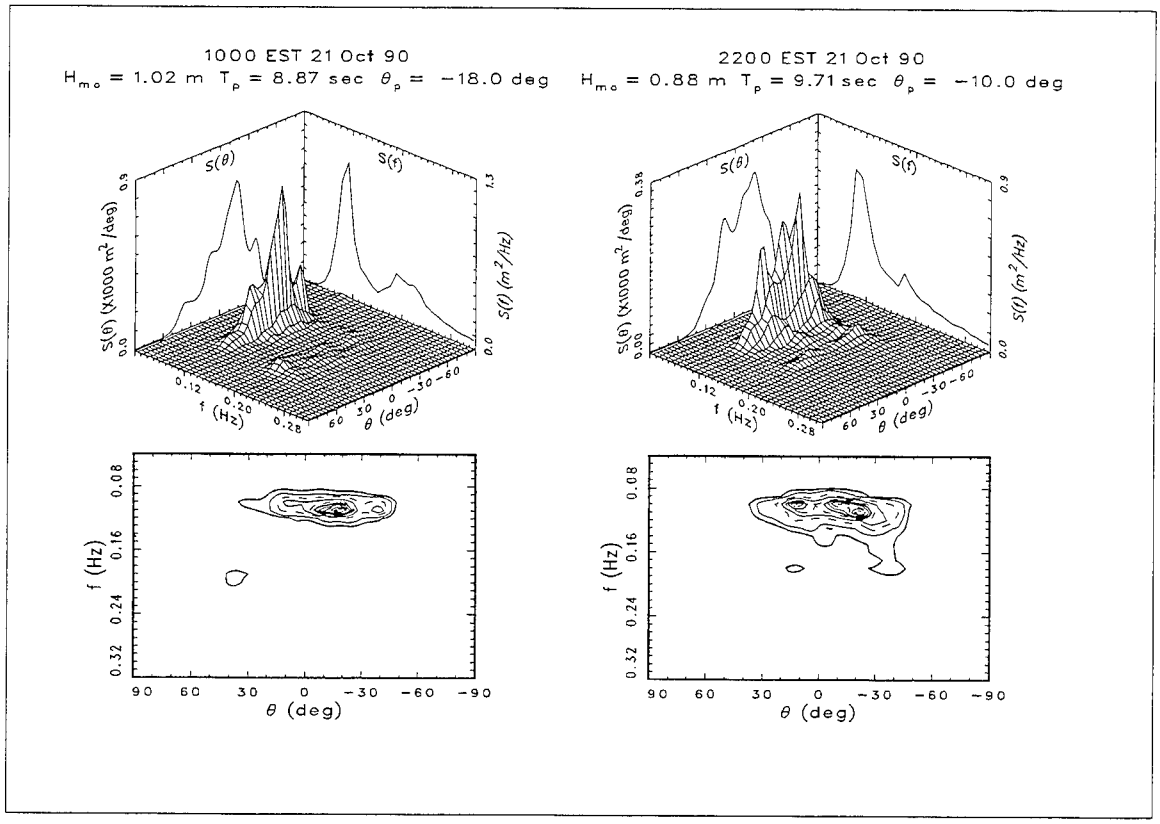

Figure E24. Representative frequency-direction spectra from 8-m array for 21 October, 1990

Longshore Subarray Directional Wave Measurements

The following discussion describes one approach to processing some of the data collected during DELILAH. It is not the only acceptable processing method, but it is described here in detail to demonstrate one way of handling the data complexities. A preliminary analysis of the wind-wave directional spectra from the two longshore subarrays during DELILAH was performed by Dr. Charles Long. The arrays were not ideal for wind-wave analysis, consequently simplifying assumptions as well as some modifications to the data were applied. Some of the data processing techniques described here may also be useful for other than wind-wave analysis.

Basic assumptions

The following assumptions were made:

Linear theory is valid throughout.

The wave field is stationary for durations of 2 hr 16 min (the total lengths of records analyzed).

The wave field is uniform over the longshore length of each array.

Mean currents have no effect on the observations.

Gauge selection

The two longshore subarrays are used in the analysis. The crest subarray, seaward of the nearshore bar crest, consisted of the pressure gauge 2704, and five two-axis (x/y) current meters: Marsh-McBirney 2701/2702, and the Scripps Open Frame current meters 2711/2712, 2721/2722, 2731/2732, and 2741/2742. The set comprises an 11-element array with each current meter representing two elements.

The trough subarray was generally on the trough side of the nearshore bar crest. It used pressure gauge 2304, and five Marsh-McBirney two-axis current meters 2301/2302, 2311/2312, 2321/2322, 2331/2332, and 2341/2342. This set also constitutes an 11-element array.

Data selection

The intent was to compare nearshore results with spectra from the FRF 8-m array. 8-m array frequency-direction spectra were computed from records of 2 hr 16 min duration (16,384 data points at 2 Hz, or 8,192 sec) for each gauge, with collection times at 3-hr intervals, starting daily at 0100, 0400, 0700, 1000, 1300, 1600, 1900, and 2200 Eastern Standard Time. To compare data of the same duration and collection start times required finding 16 contiguous

records from the crest and trough subarrays that began at about (± 4 minutes) the same times as the FRF collections. Because of the logistics involved with changing tapes, not all FRF collections had a matching crest or trough collection, so some cases are missing from the analyzed set.

Data gaps

To deal with the gaps, and make maximum use of available data, processing occurred as follows:

The pressure gauge from each array (2704 for crest, or 2304 for trough) was processed first. The 8-Hz data were subsampled at 2 Hz by taking every fourth point, starting with the first point in the first of the 16 contiguous records to be processed, and storing the points in a single long array of 16,384 points. The long array was then broken into 31 half-lapped ensembles of 512-sec duration (1,024 points), and each ensemble was searched for data gaps.

If no gaps were detected, an ensemble record was accepted as it was. If a gap occurred in the second half of any ensemble record except the first, the bounding indices of the ensemble record were shifted to earlier times so that the last point in the ensemble record was the last good data point before the gap. If a gap occurred in the second half of the first ensemble record, that record was not used in analysis. The ensemble bounding indices from the long array were stored for later use with current meter data.

If a gap occurred in the first half of any ensemble record except for the final one, the bounding indices of the ensemble record were shifted to later times so that the first point in the ensemble record was the first good data point after the gap. If a gap occurred in the first half of the last ensemble record, that record was not used in analysis. Again, the ensemble bounding indices from the long array were stored for later use with current meter data.

This procedure resulted in occasional redundancy of the ensemble records, and occasional loss of one ensemble record (or half an ensemble's worth of data points), so that there were only 30 ensembles instead of 31. However, this method retained most of the useful data and none of the gapped data.

After the pressure gauge data had been analyzed for gaps, the current meter data were processed. Current meter data were also decimated to 2 Hz from 8 Hz and written into long arrays. To ensure no offsets in time, the ensemble record bounding indices from the pressure gauge were used to define the current meter ensemble records. Consequently, a given ensemble spanned the same period of time from all gauges in an array, so that relative phasing was preserved for all ensembles. In this way, a working database of ensemble records for each collection was created.

Modifications to pressure data

To establish realistic gauge depths relative to the (collection) mean sea surface, the barometric (gauge 616) mean value (in meters of water) was subtracted from the pressure gauge mean value (in meters of water). When the (positive) gauge depth relative to NGVD was added to the barometrically corrected gauge mean, the record should have reflected the tide plus any setup or setdown from wind or radiation stresses. However, this was not what was observed. Mean pressures from both gauges 2704 and 2304 seemed low. High tide didn't get very high above NGVD, and low tide was much lower.

This was further pursued in an effort to determine an accurate estimate of gauge depths by comparing means from gauge 2704, from the 2703 pressure gauge, and from predicted tides. Figure E25 shows some results from 3-21 October 1990. In the relatively quiescent days of 3-7 October, the 2703 gauge appears to read high relative to predicted tides by about 0.10 m, and gauge 2304 reads considerably lower. The difference between the means is also plotted in Figure E25b and appears to fluctuate around 0.40 m.

As there was not a clear pattern to explain the differences, a bias of 0.40 m was added to the means of both gauges 2704 and 2304 for all runs. Where this is incorrect, it will have a strong effect on results because all gauge depths are keyed on the pressure gauges; pressure and current meter wave signals were surface corrected using these depths, and cross spectra were normalized with the surface-corrected pressure auto-spectra.

Modifications to current meter data

In data processing, current meter data records were read in pairs, and the component velocities were rotated from the orientations given in the time series data headers into the FRF coordinate system. Additionally, the signs of the rotated signals were adjusted so that the cross-shore velocity (U) was positive in the onshore direction, and the longshore velocity (V) was positive in the southerly direction. Due to the change in the coordinate system mentioned earlier, this is the reverse of the previous convention.

Because of the biofouling on the Scripps open frame current meters (2711/ 2712, 2721/2722, 2731/2732, and 2741/2742), the current meter gains for all current meters were adjusted to be consistent with sea surface displacement variance frequency spectra derived from the pressure gauge (2704 for the crest array, 2304 for the trough array). To do this, the PUV-test, (described in the "DELILAH array data analysis" section earlier in Appendix E) was used.

To adjust the current meter gains, the mean value of the $Z(\sigma)$ over the range of (cyclic) frequencies 0.006 to 0.338 Hz was computed, and then the gains listed in the header records were amplified or reduced until this mean value was unity. Identical gain amplifications were applied equally to both

channels of a two-axis current meter under the assumption that the biofouling or other signal degradation was horizontally isotropic, and because a way to determine gain adjustments on individual current meter channels is not known. This assumption is important because overcorrecting one current meter channel relative to another changes the apparent wave direction at that current meter, and degrades the directional estimator.

To illustrate the temporal behavior of the gains, the time series of the gains for each subarray have been plotted. Figure E26 shows the gains from the trough subarray, and Figure E27 shows the gains from the crest subarray. The results make qualitative sense in that the Marsh-McBirney current meters (station 70 in the crest subarray, and all stations in the trough subarray) had gains that generally remained within 20 percent of unity, while the Scripps open frames (stations 71-74 in the crest subarray) had gains near unity early in the experiment, but drifted high as time evolved, suggesting the influence of fouling. Note that all of the gain adjustments were keyed to the spectra from the pressure gauges, and, because the pressure gauge depths were modified, some noise may have been introduced in the current meter gain adjustments. For instance, there appears to be a diel variation in the gains from the trough array that is reminiscent of the pressure gauge differences shown in Figure E25b. There may be a relationship between these phenomena, but what that relationship is, remains uncertain.

Total water depths

In an earlier pass through the data, the total water depth, as listed for each gauge location, was assumed constant. However, the depths were not constant throughout the experiment, and erratic changes in depth occurred after the energetic events beginning on 10 October. Subsequently, total water depths for each gauge site were established by interpolating the bathymetric minigrid surveys in both time and space, to obtain a more correct total water depth for each gauge location and for each collection. Water depths found in this manner are used in analysis and are plotted as time series in Figure E28 (trough subarray) and Figure E29(crest subarray). When the bar moved offshore during the energetic events, shoaling occurred under the crest subarray, and deepening occurred under the trough subarray. More consistent results overall were obtained when changing depths were used in the analysis.

Exposed gauges

Despite efforts to position the gauges so that they remained within the water at all tide stages, at some low tide stages, some of the gauges became exposed. Because such events add unacceptable noise to the cross-spectral matrix, all such cases were eliminated from analysis. These were identified using a method similar to that described in the "DELILAH array data analysis" section earlier in this appendix. The one difference in this analysis was the use of a 0.40-m bias in the gauge depth adjustment, and the other analysis determining a bias from correlating water levels with a tide gauge (gauge 1). This analysis

was done by saving the minimum instantaneous water level from the raw pressure signal and comparing it to the depth of the shallowest gauge in the array being analyzed. If it appeared that the shallowest gauge was at or out of the water surface in the trough of any wave passing the pressure gauge, the analysis was aborted. This may have been a liberal treatment because it nominally allowed the Marsh-McBirney current meters to function within several ball diameters of the free surface for a few seconds in some runs, which is generally considered unacceptable. The time series of velocity and pressure from some of the marginal runs were visually inspected and it was not always obvious that the signal was degraded. A more conservative constraint may be appropriate if further analysis is pursued.

Data checking

A check on data quality was performed by overlaying the frequency spectra plots from all gauges for each run that survived the exposure test. Figure E30 is an example of this. Some features which may not be obvious include:

a. The main graph shows the frequency spectra (in log coordinates) from all gauges plotted out to the Nyquist frequency (1 Hz for the 2-Hz subsample frequency) so that background noise floors can be seen.

b. The pressure spectrum is offset downward by three orders of magnitude to isolate its shape from spectral curves from the other gauges. Spectra from longshore currents are offset downward by one order of magnitude to isolate that group of spectra. Spectra from cross-shore currents are plotted with no offset.

c. Raw spectra are shown throughout *except in the low-frequency (including wind-wave) pass band* of 0.006 to 0.338 Hz. In the low-frequency band, the spectra have been surface normalized as described above under "Modifications current meter data." This helps to determine how much surface correction is done even for these shallow gauges, and indicates if noise is amplified or reduced in surface normalization.

d. Modified current meter gains have been applied to the current meter spectra in these plots to see if modified spectra form tight groupings for each type of gauge.

e. Curves near the part of the main graph ordinate labeled 'Z' are the $Z(\sigma)$ function described above (actually $Z(f)$ is used) *after* its mean value is forced to unity. These functions are plotted on a linear scale. These curves are informative in that if they are reasonably flat, the surface normalization and gain modification might be considered satisfactory. The example shown is reasonably clean. Visual inspection of the plot shows some degradation of these curves in time. In some high-energy conditions, there is considerable chatter at the lower

frequencies, due possibly in some part to shear waves, which have a stronger velocity signal than pressure signal.

f. Also shown in the upper right corner of Figure E30 are numbers representing a possible modified pressure gauge gain (which should be 1.0 for all cases in these runs).

Data quality plots were used to identify cases with data that were clearly bad. Surface-corrected velocity spectra should cluster together, with one grouping each for alongshore and cross-shore velocities. Barring other sources of noise, these spectra should follow a chi-square error distribution. For the nominal 160 degrees of freedom with which these spectra were computed, the 95-percent confidence interval extends from about 21-percent below to about 2-percent above the true value of each spectrum, or a range of about 4-percent. Though the true values are not known, members of a group of spectra were considered satisfactory if the range of spectral densities agrees to within about 44 percent at each of the discrete frequencies in the nominal wind wave pass band of 0.04 to 0.32 Hz. Pressure data were considered satisfactory if $Z(f)$ was reasonably uniform through the wind-wave pass band of frequencies, indicating consistent frequency dependence of velocity and pressure data. Excepting high-energy, low-frequency conditions, where shear waves may be influential, the nominal acceptable range of PUV-test results is $0.8 < Z(f) < 1.2$. Data acceptance criteria given here served as rough guidelines. Minor exceptions were tolerated in this analysis in an effort to maximize the amount of data considered to be useable.

The mean current data contained either severe, persistent nonuniformity or some yet-to-be understood bias. It remains unclear what the source of the problem was or how to circumvent it . Consequently, any effects from mean currents were ignored, though the wind-wave parts of the current meter records seemed acceptable. Data that passed the quality control constraints were used.

Final data sets

Processed data satisfied three constraints: (a) start times and durations had to match FRF collections,(b) there were no exposed gauges, and (c) pass band frequency spectra satisfactorily met the constraints of the data quality plots. Table E4 lists the cases from the trough and crest subarrays that satisfied these constraints. More exposed gauges occurred in the trough subarray, and the current meter at station 30 was lost sometime on 15 October. Therefore, the total set of cases for the trough subarray is small.

Table E4
DELILAH Collection Times that are Concurrent with FRF Collection Times and Pass the Quality Control Standards

Date	FRF Collection Time							
	0100	0400	0700	1000	1300	1600	1900	2200
Trough subarray								
10/03/90						1557	1856	
10/04/90							1902	
10/05/90			0659	0959		1558	1857	
10/06/90			0659			1600	1859	
10/07/90			0702	1001		1604		2201
10/08/90			0658	0957	1304			
10/09/90				1002				
10/10/90	0104	0403		0956				
10/11/90								
10/12/90								
10/13/90								
10/14/90				1004		1604	1903	2203
10/15/90	0103	0402		1001		1603		
10/16/90								
Crest subarray								
10/03/90			0700	1000		1557	1856	
10/04/90	0103						1902	
10/05/90			0659	0959		1558	1857	2206
10/06/90			0659			1600	1859	
10/07/90		0358	0702	1001		1604		2201
10/08/90		0400	0658	0957	1304			
10/09/90				1002				
10/10/90	0104			0956				
10/11/90								
10/12/90	0057	0356		1004	1303			
10/13/90	0058	0357						
10/14/90						1604	1903	
10/15/90	0103	0402		1001		1603		2205
10/16/90	0056	0404			1302			2158
10/17/90	0057	0356	0705	1004	1303	1600		2156
10/18/90	0104		0659			1600	1859	
10/19/90		0401	0701	1000		1602		2200
10/20/90	0100	0359	0657	0956			1901	2156
10/21/90		0403	0701					

Satisfactory data runs were processed for frequency-direction spectra following the basic premises for IMLE described by Davis and Regier[1], and Pawka.[2] Figures E31 through E38 are examples of trough subarray spectra and Figures E39 through E47 are examples of crest subarray spectra. When possible, two representative spectra for each sampling day are presented. As summarized in Table E5, all gauges were used for the lowest frequencies, but only the pressure gauge and two current meters were used for the highest frequencies. Figures E48 and E49 summarize the directional data from the trough and crest subarrays respectively.

Table E5
DELILAH Gauges Used in Directional Spectral Estimation

Frequency Range (Hz)	Crest Subarray Gauges										
	2704	2701	2702	2711	2712	2721	2722	2731	2732	2741	2742
0.04<r≤0.10	✔	✔	✔	✔	✔	✔	✔	✔	✔	✔	✔
0.10<r≤0.18	✔	✔	✔	✔	✔	✔	✔	✔	✔	✔	
0.18<r≤0.32	✔	✔	✔	✔	✔						
	Trough Subarray Gauges										
	2304	2301	2302	2311	2312	2321	2322	2331	2332	2341	2342
0.04<r≤0.10	✔	✔	✔	✔	✔	✔	✔	✔	✔	✔	✔
0.10<r≤0.18	✔	✔	✔	✔	✔	✔	✔	✔	✔	✔	
0.18<r≤0.32	✔	✔	✔	✔	✔						

[1] Davis, R. E., and Regier, L. A. (1977). "Methods for estimating directional wave spectra from multi-element arrays," *Journal of Marine Research* 35, 453-77.
[2] Pawka, S. S. (1983). "Island shadows in wave directional spectra," *Journal of Geophysical Research* 88, 2579-91.

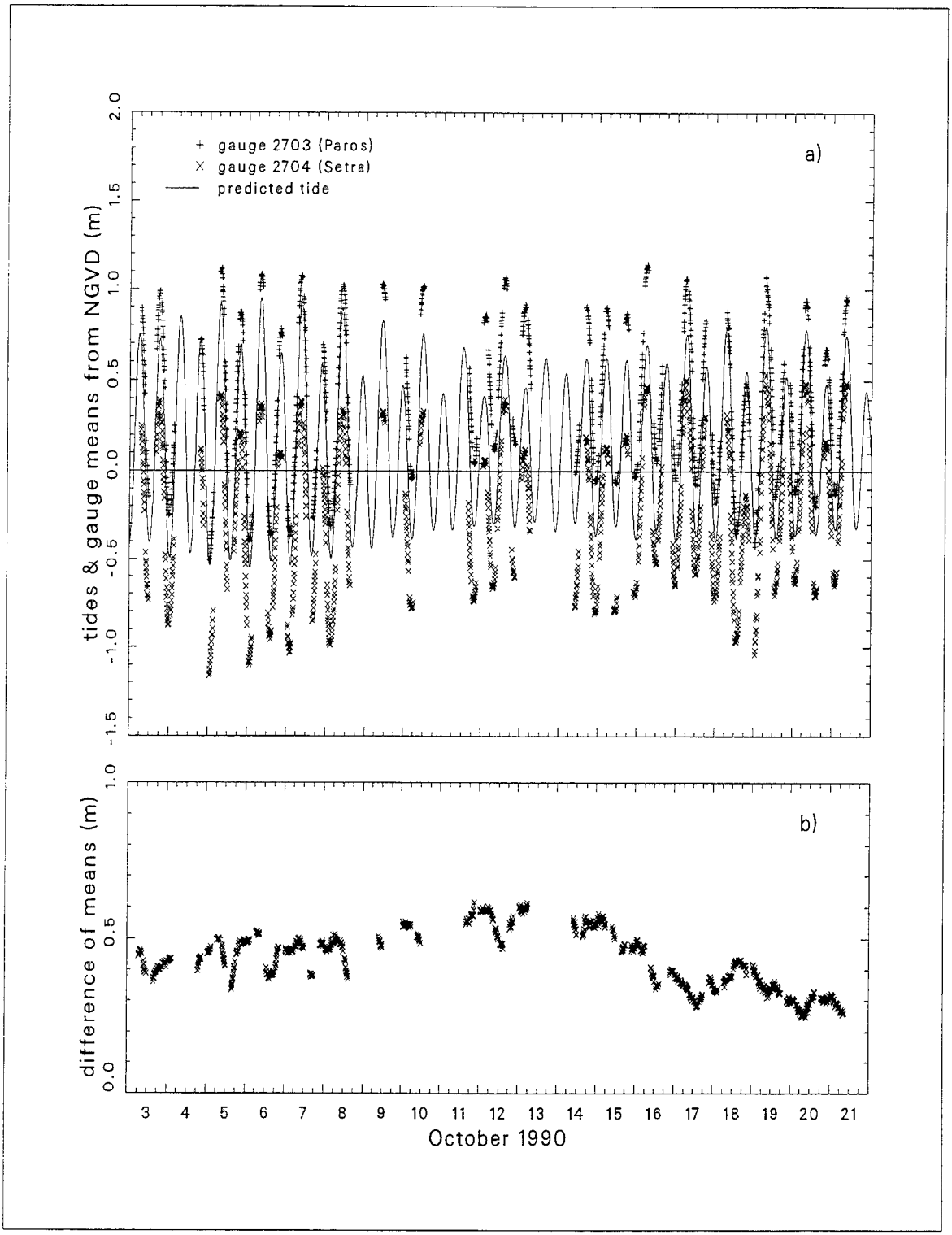

Figure E25. Time series of a) pressure gauge means at station 70 compared to predicted tide, and b) pressure gauge 2704 (Setra) subtracted from pressure gauge 2703 (Paroscientific)

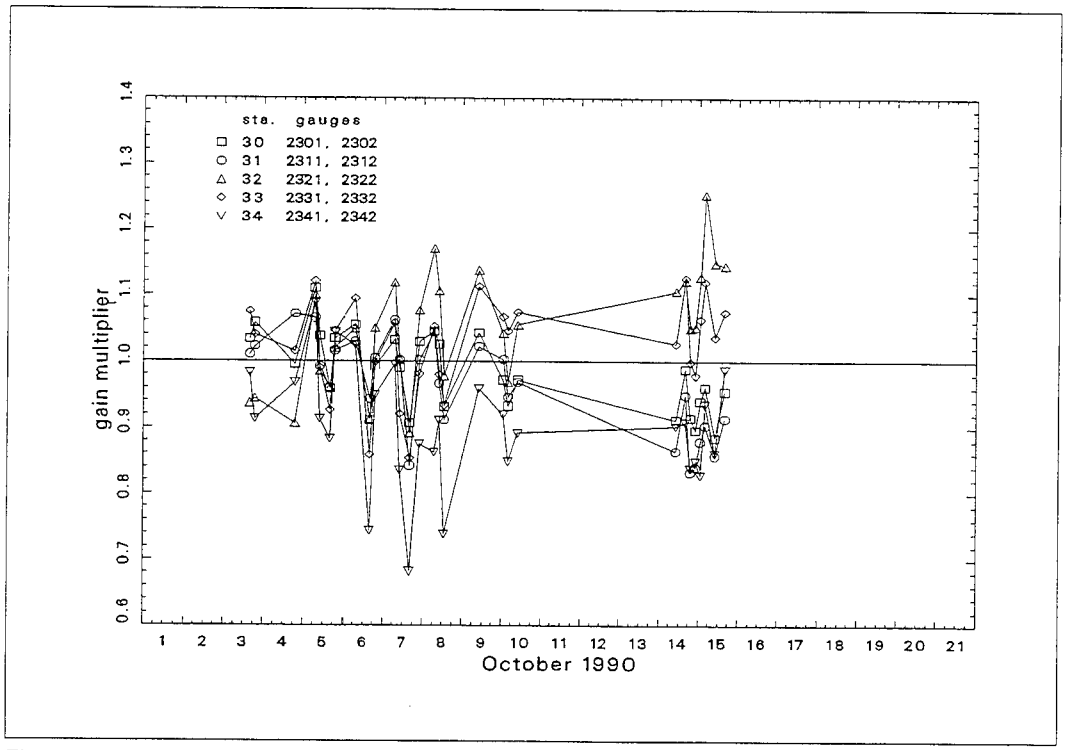

Figure E26. Gain multipliers for trough subarray current meters deduced from PUV-test

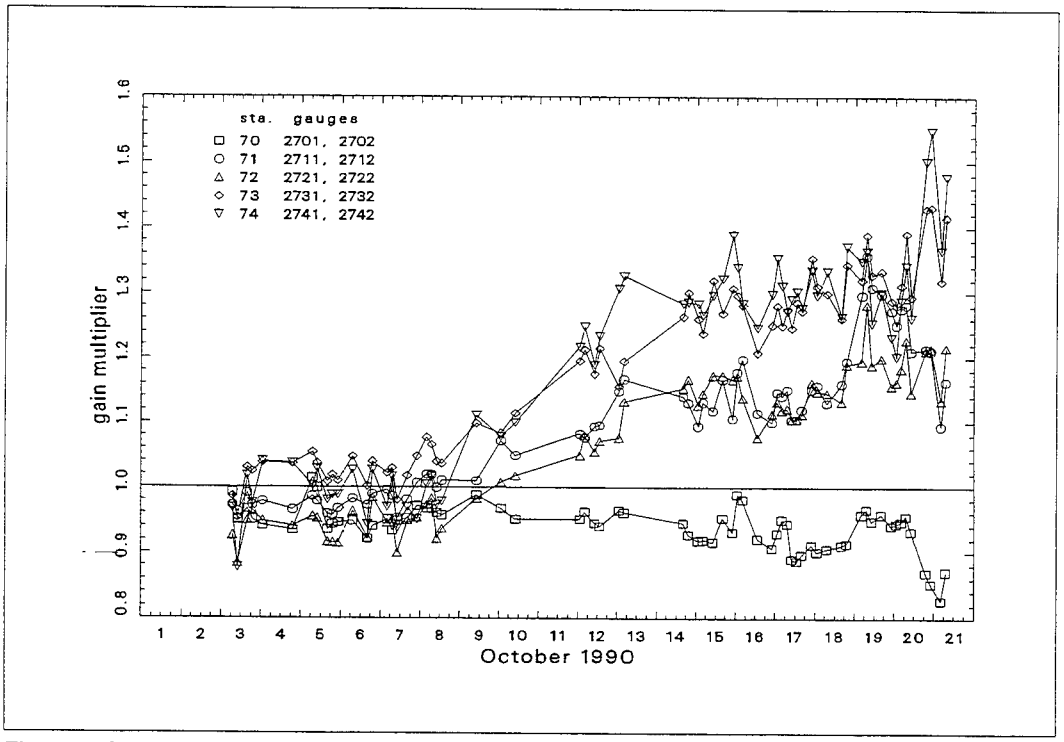

Figure E27. Gain multipliers for crest subarray current meters deduced from PUV-test

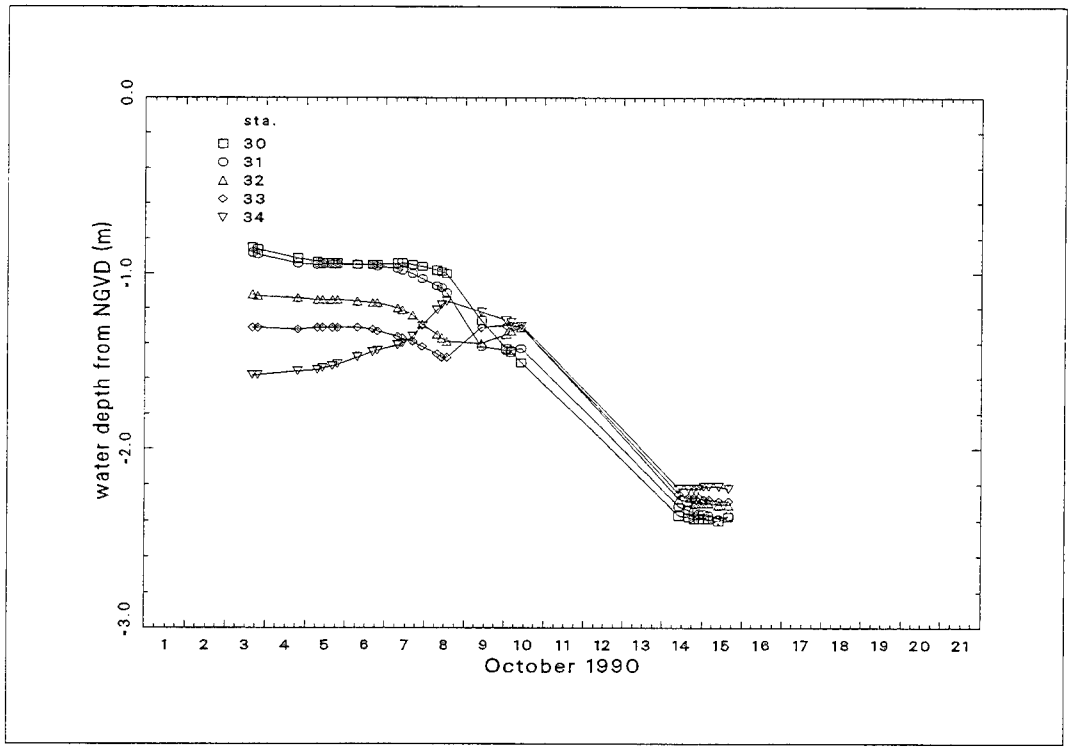

Figure E28. Water depths at trough subarray stations deduced from minigrid surveys

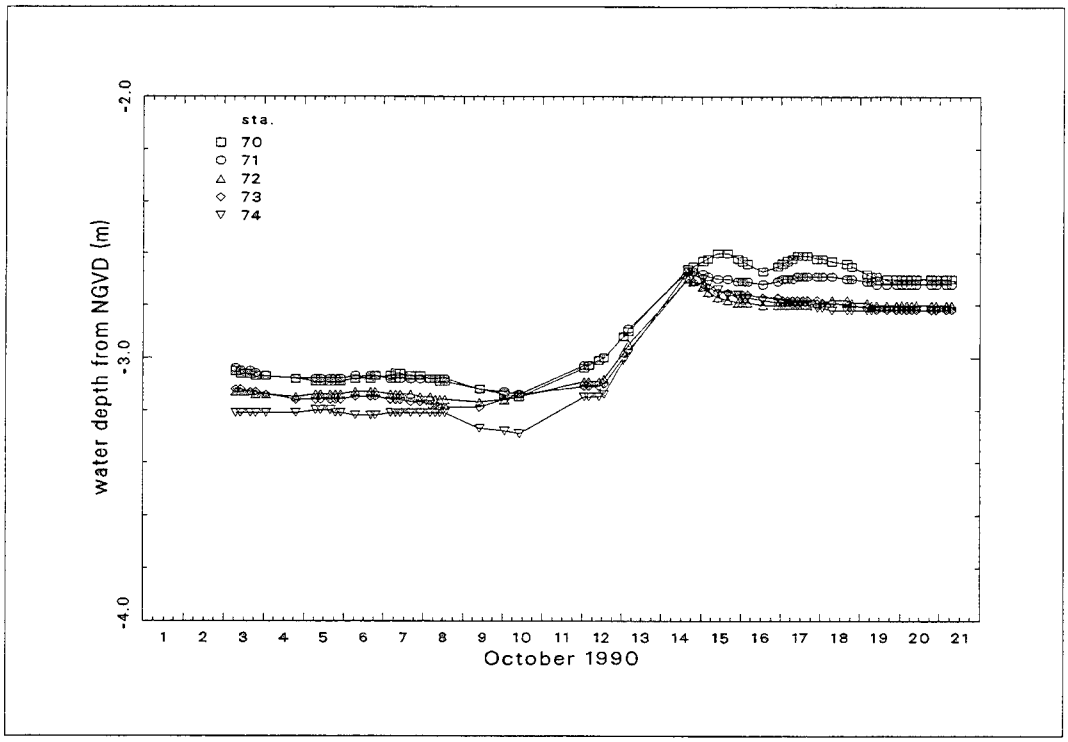

Figure E29. Water depths at crest subarray stations deduced from minigrid surveys

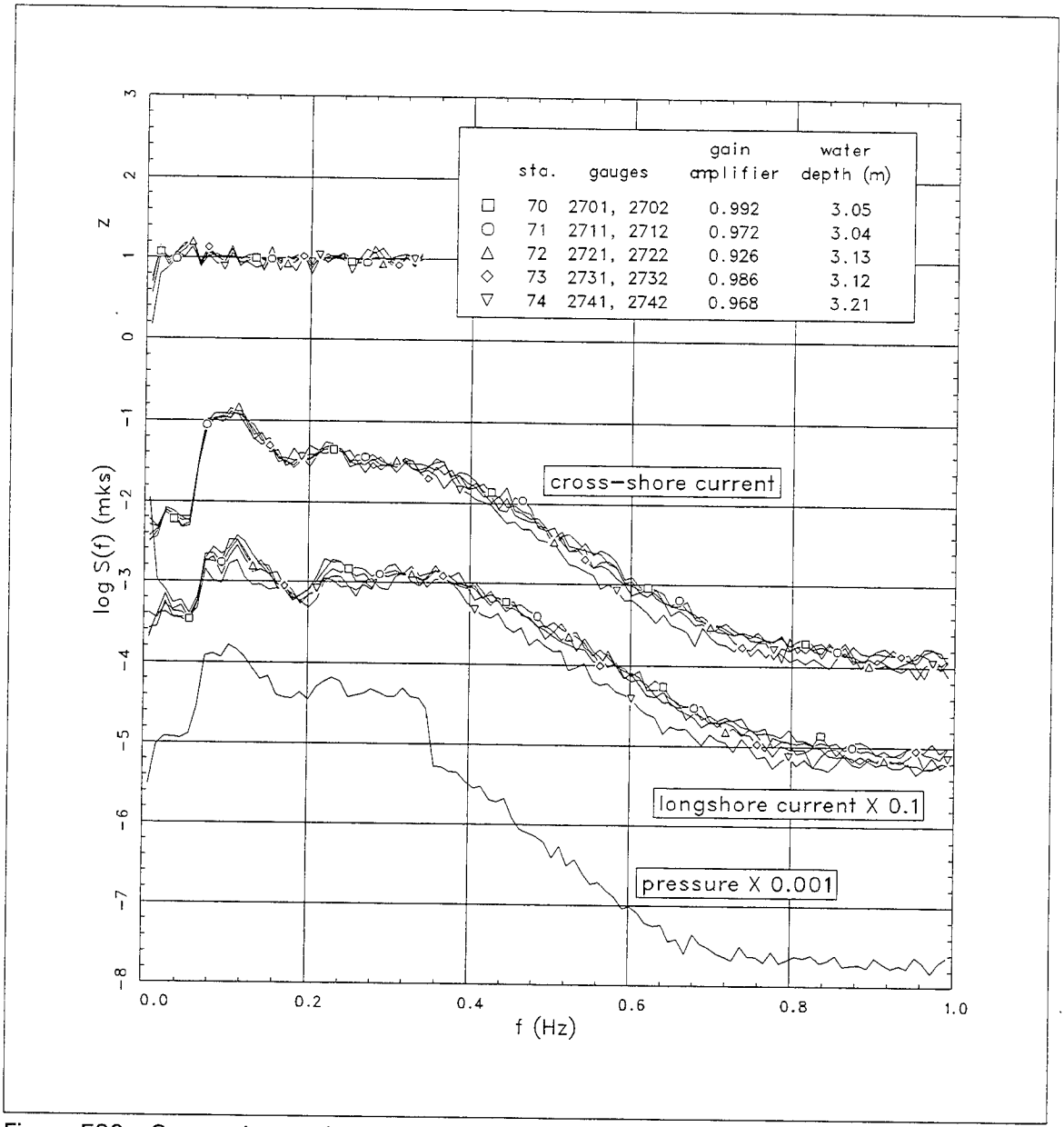

Figure E30. Crest subarray frequency spectra and PUV-test results for the 0700 run on 3 October 1990

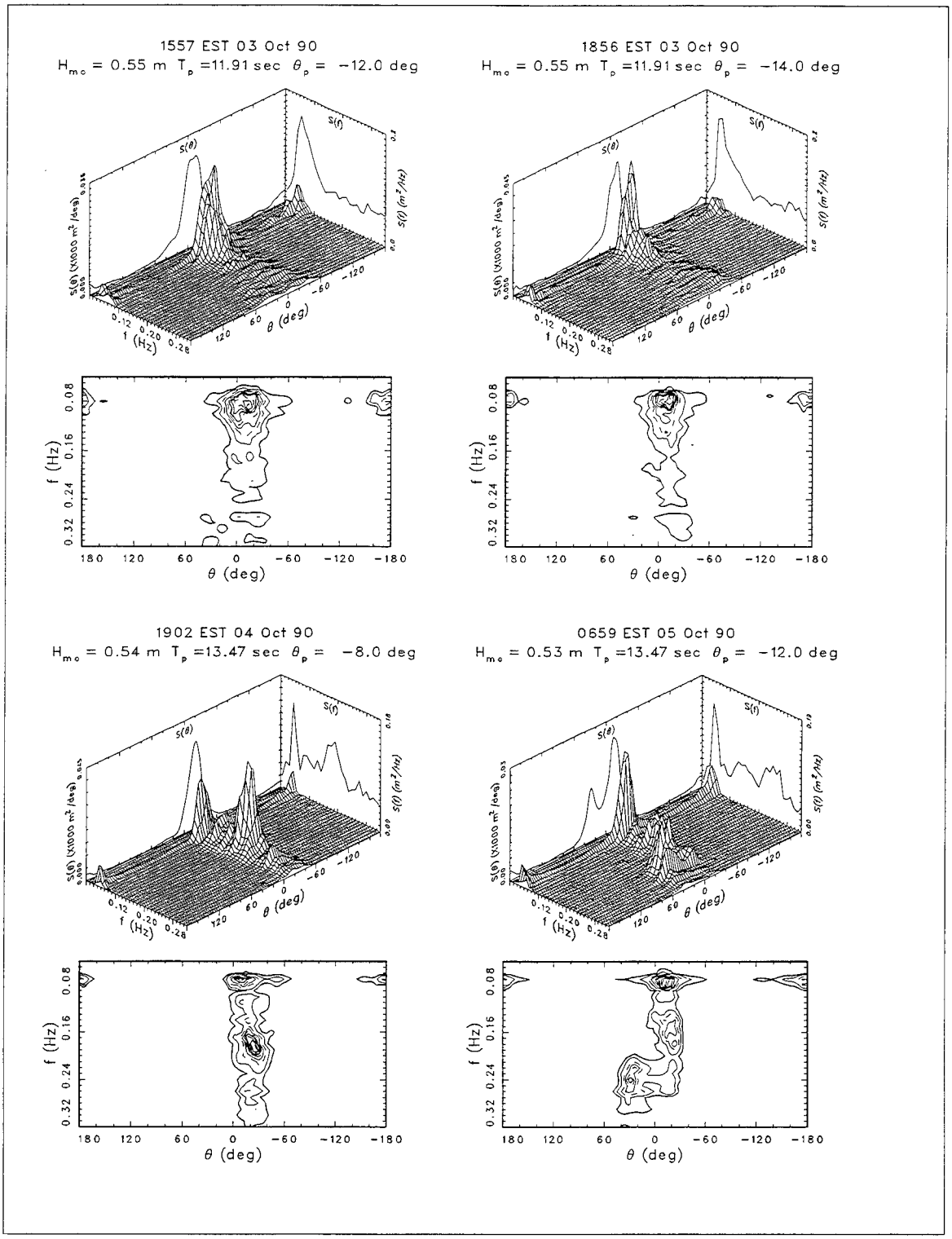

Figure E31. Representative frequency-direction spectra from trough subarray for 3, 4, and 5 October 1990

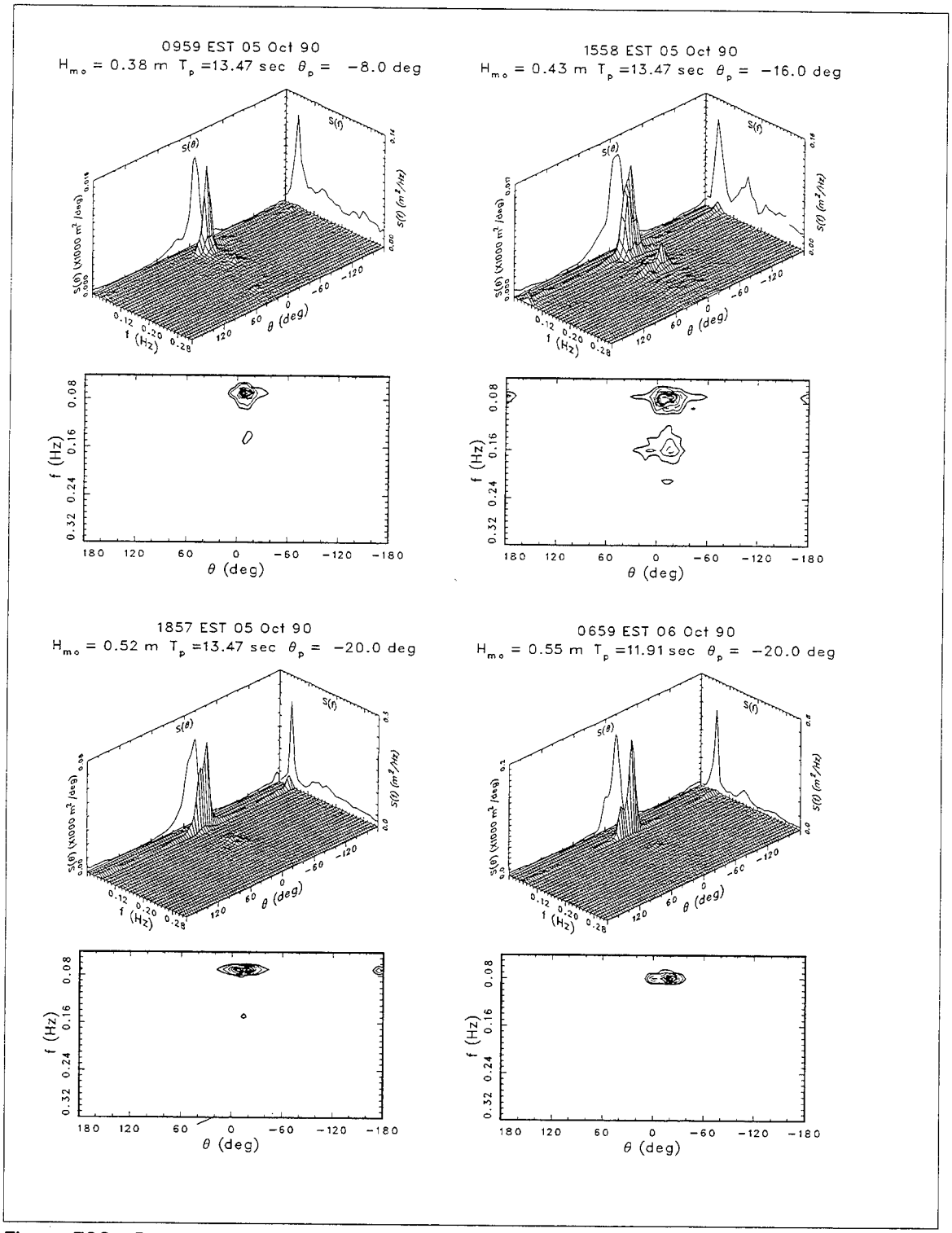

Figure E32. Representative frequency-direction spectra from trough subarray for 5 and 6 October 1990

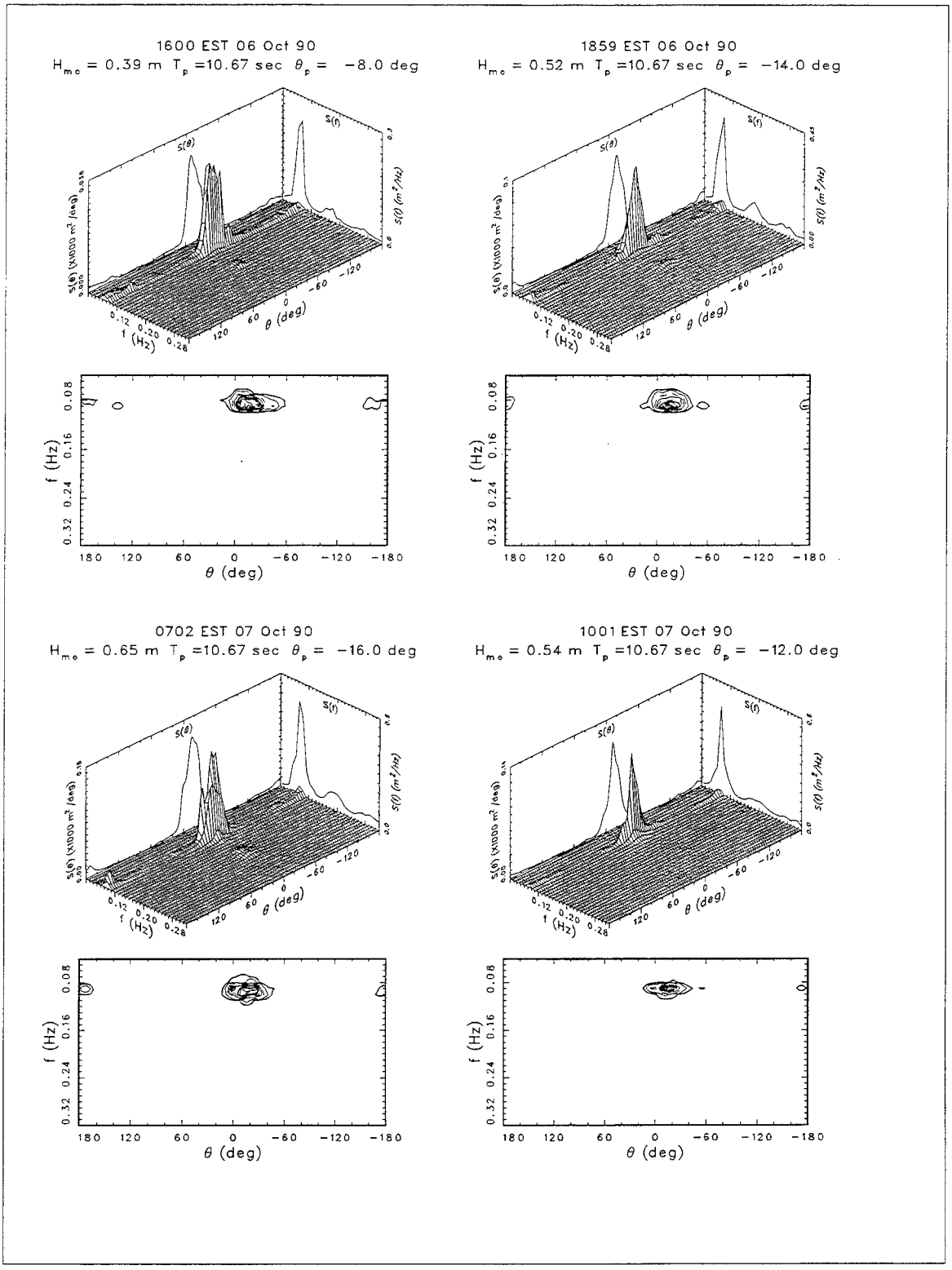

Figure E33. Representative frequency-direction spectra from trough subarray for 6 and 7 October 1990

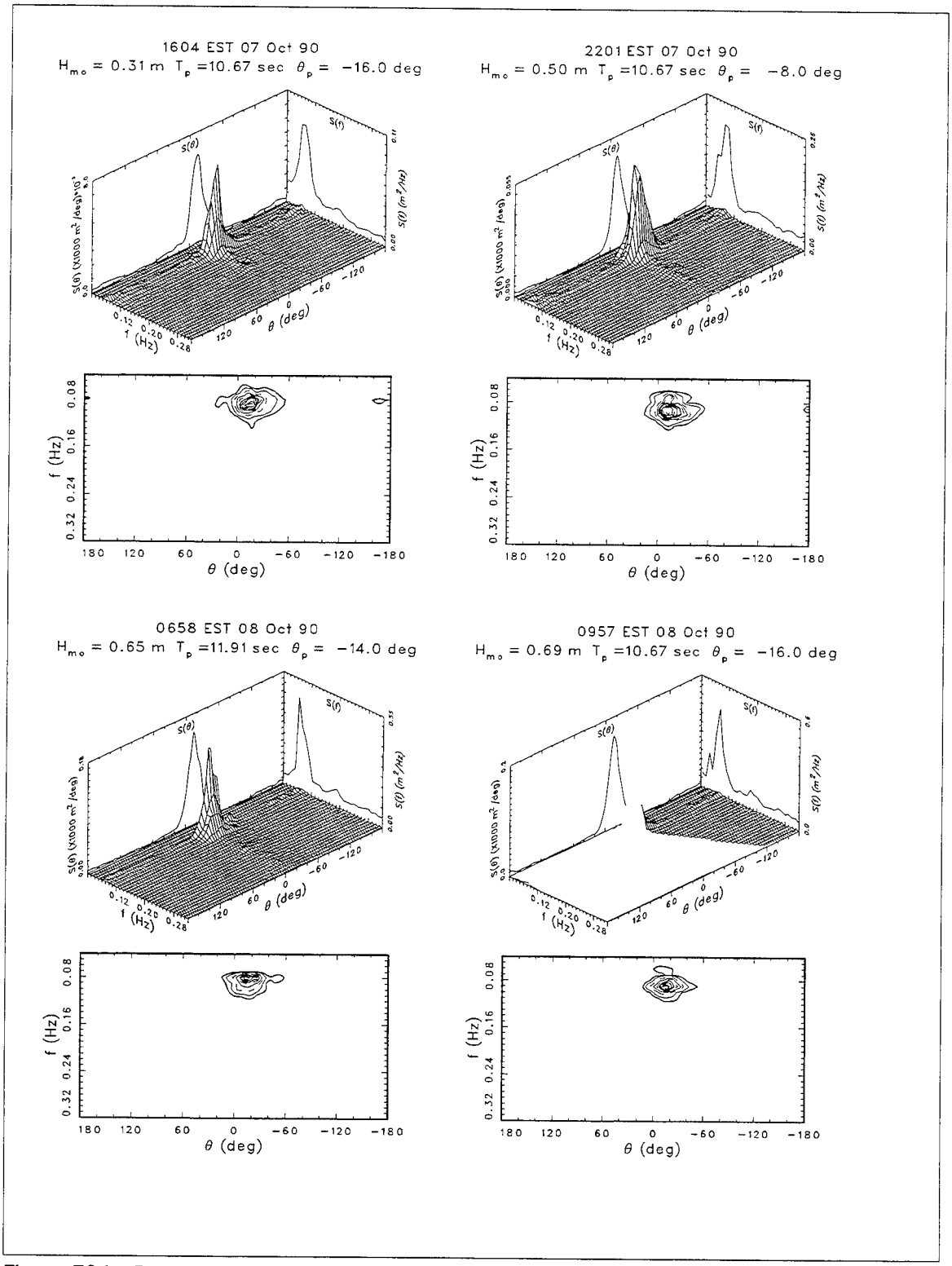

Figure E34. Representative frequency-direction spectra from trough subarray for 7 and 8 October 1990

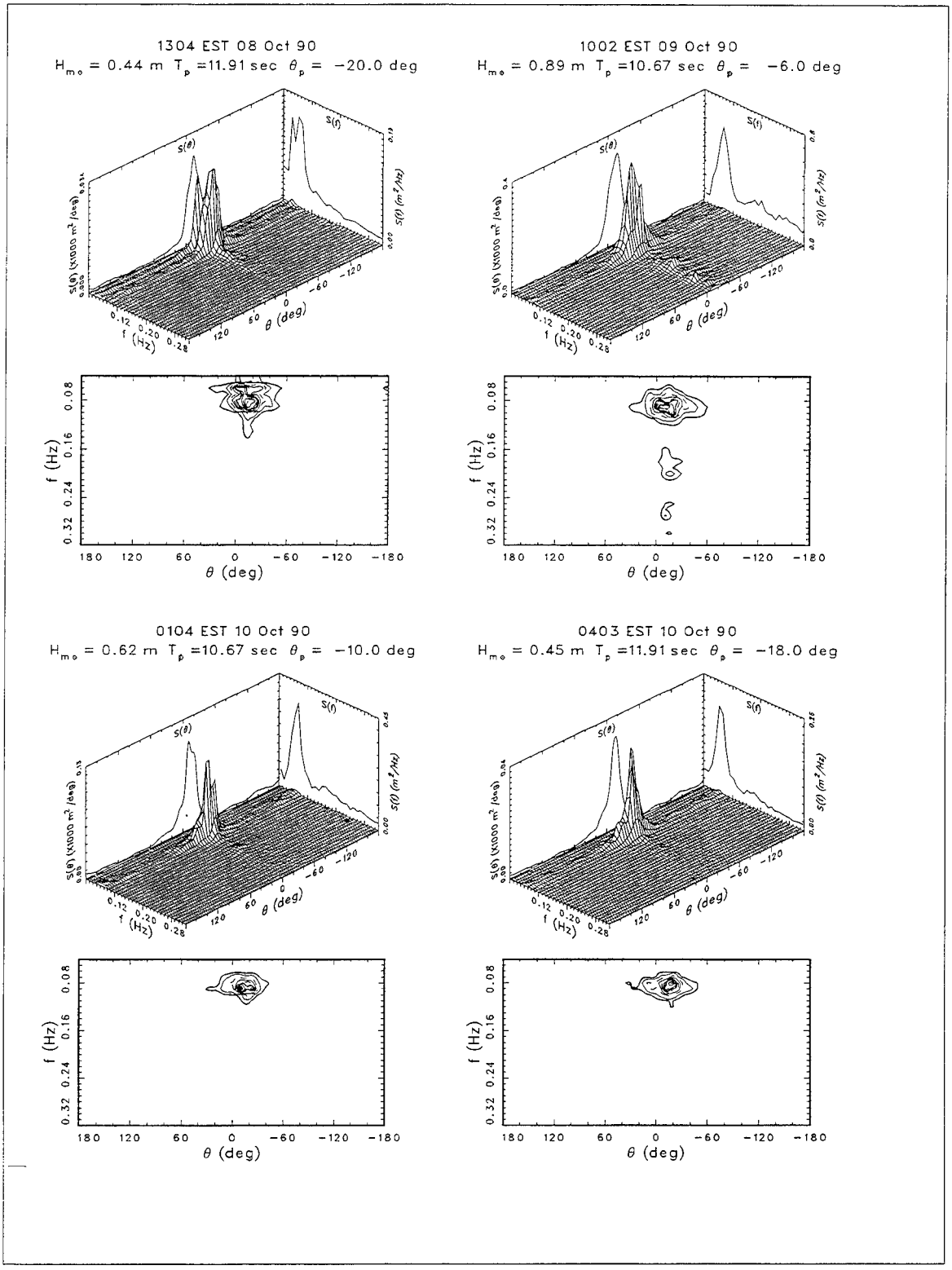

Figure E35. Representative frequency-direction spectra from trough subarray for 8, 9, and 10 October 1990

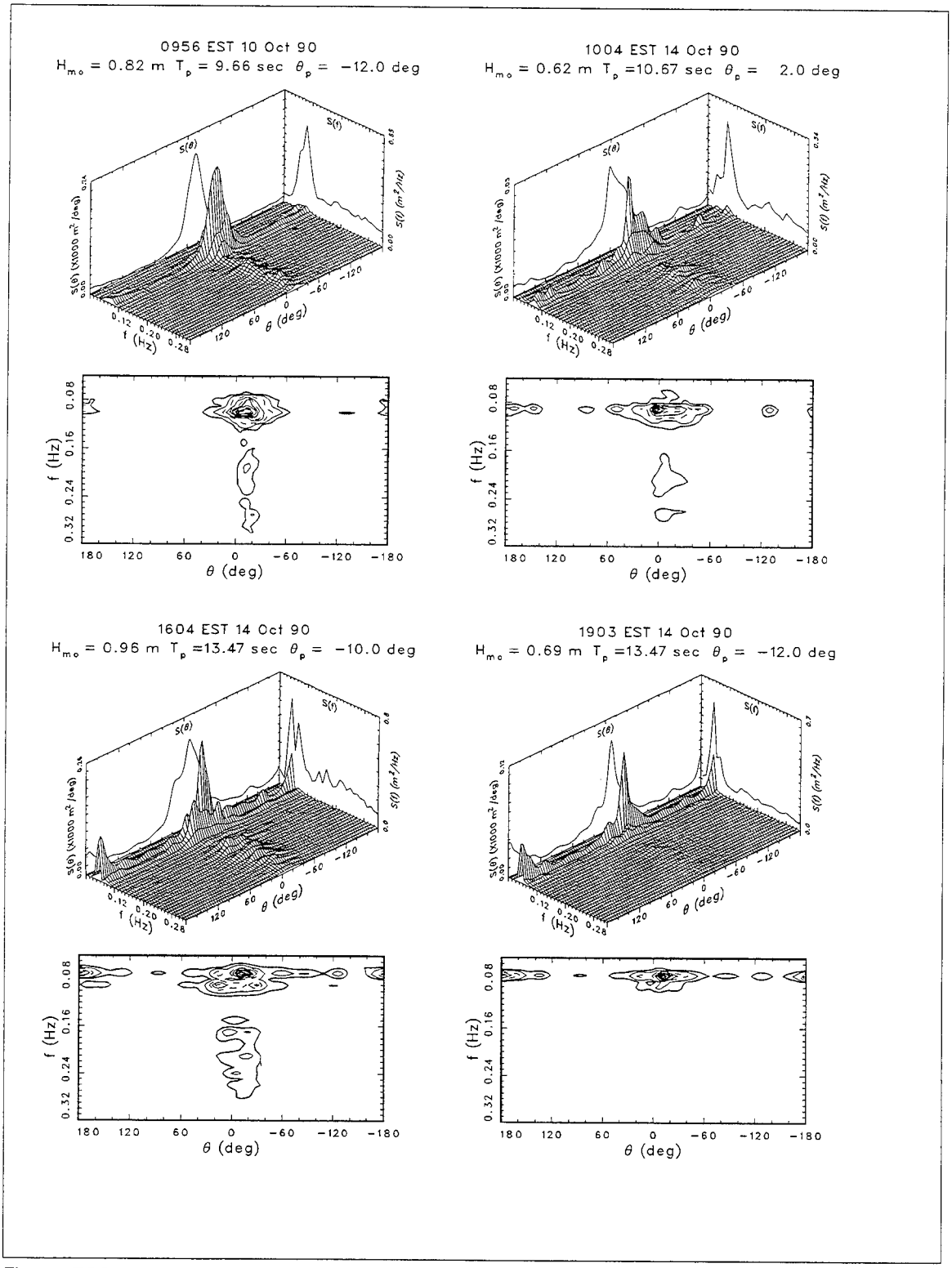

Figure E36. Representative frequency-direction spectra from trough subarray for 10 and 14 October 1990

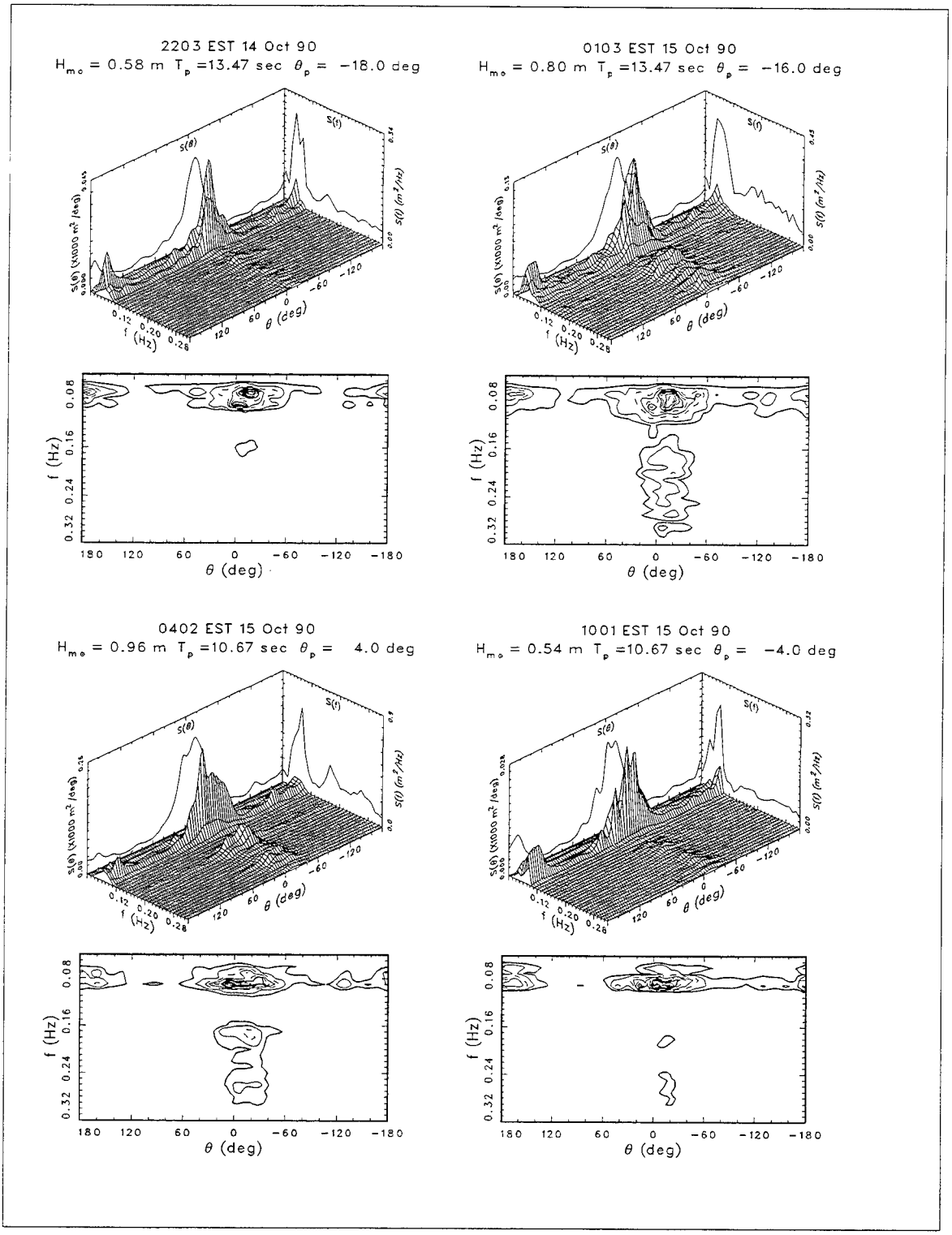

Figure E37. Representative frequency-direction spectra from trough subarray for 14 and 15 October 1990

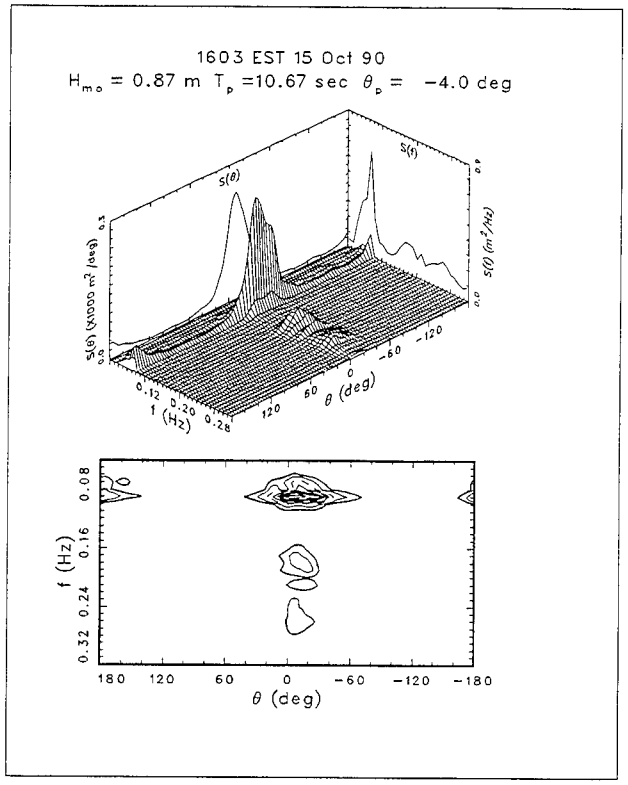

Figure E38. Representative frequency-direction spectra from trough subarray for 15 October 1990

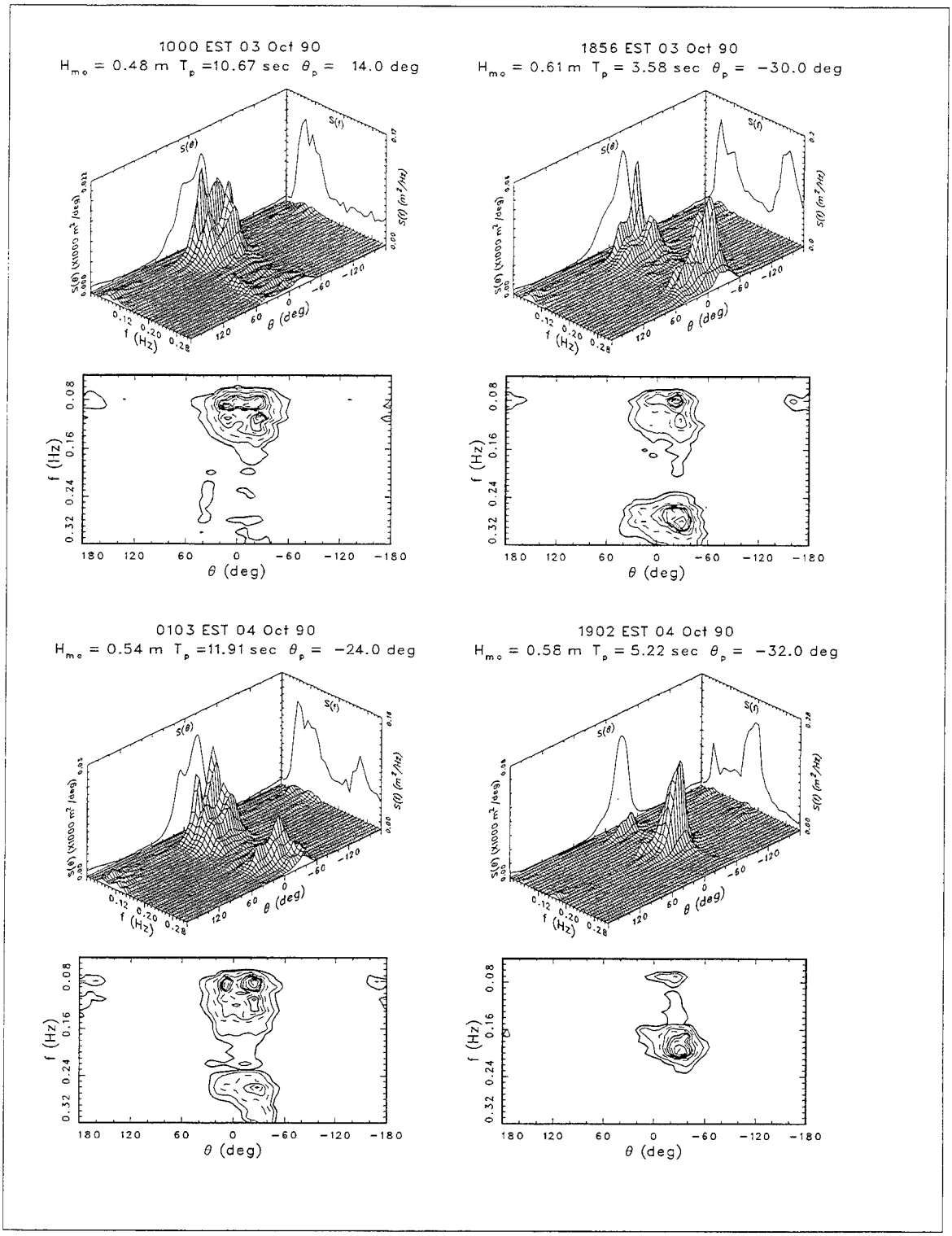

Figure E39. Representative frequency-direction spectra from crest subarray for 3 and 4 October 1990

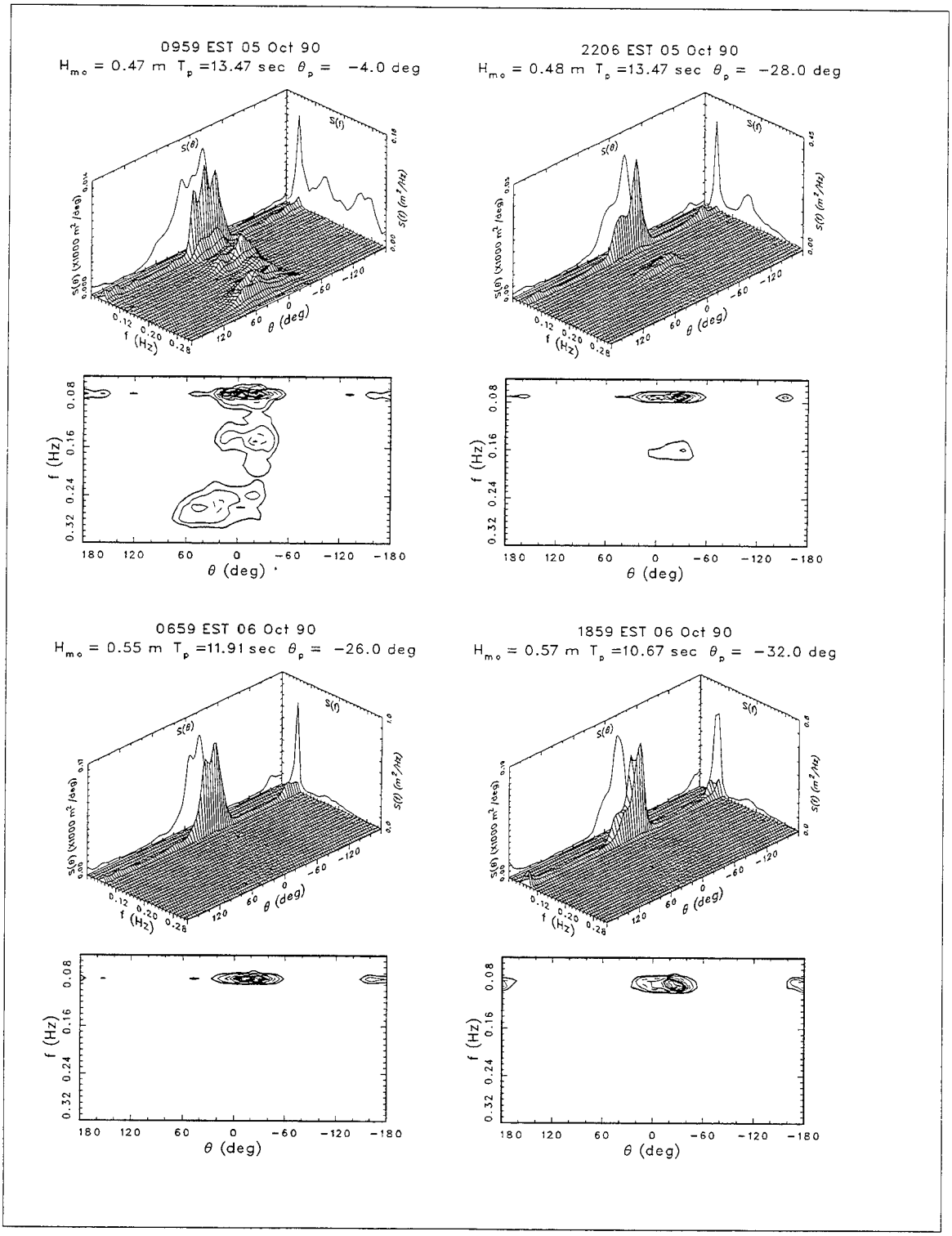

Figure E40. Representative frequency-direction spectra from crest subarray for 5 and 6 October 1990

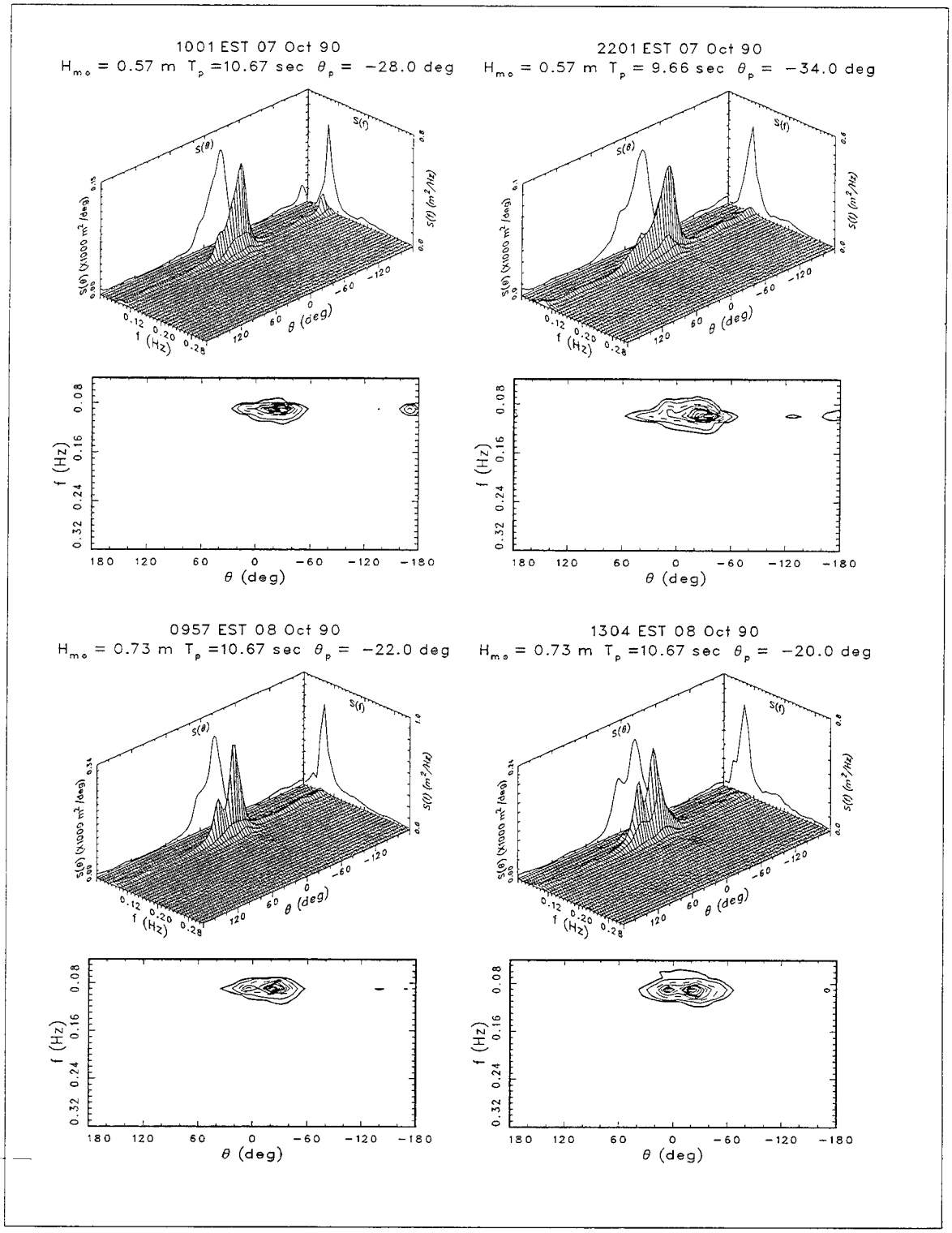

Figure E41. Representative frequency-direction spectra from crest subarray for 7 and 8 Ocober 1990

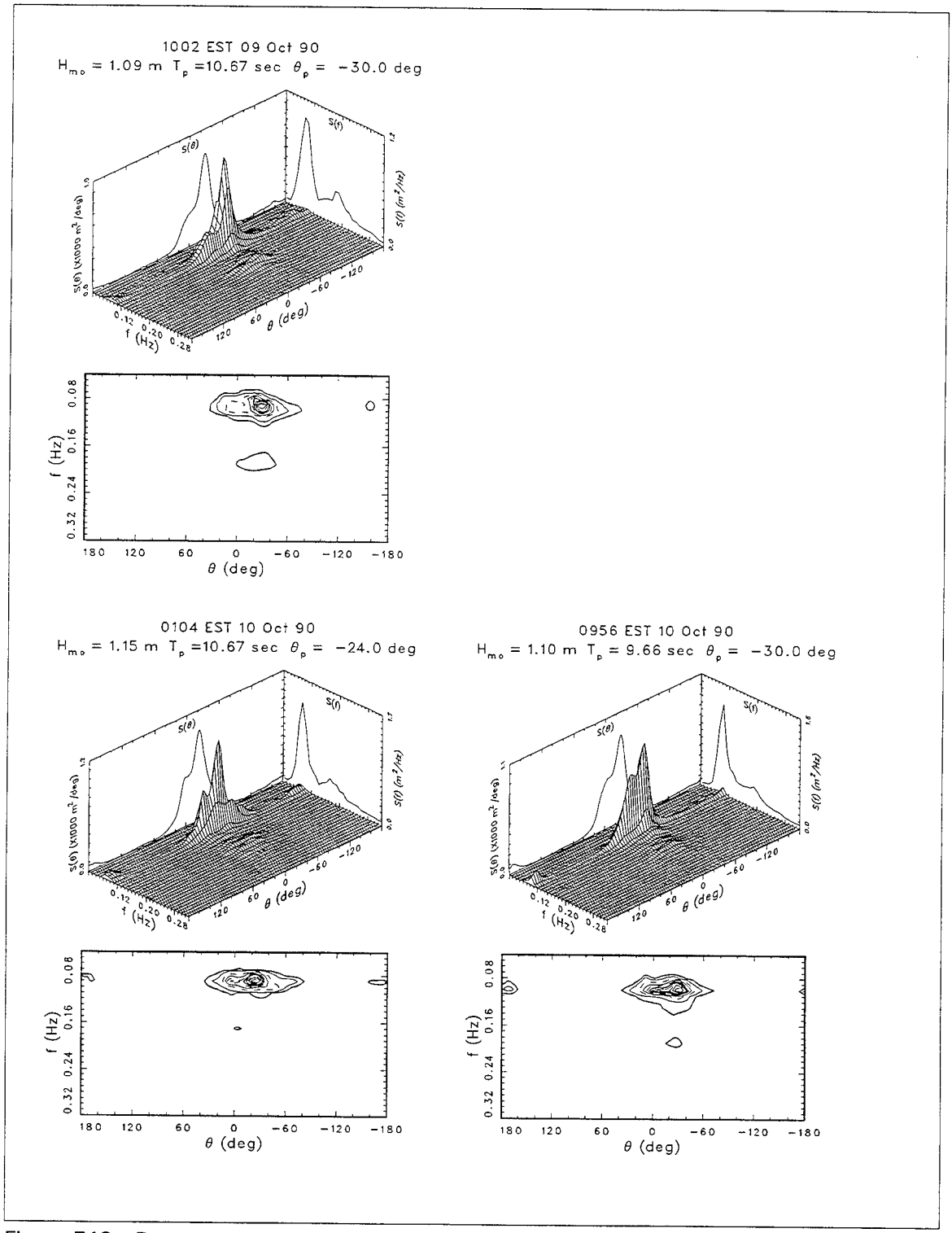

Figure E42. Representative frequency-direction spectra from crest subarray for 9 and 10 October 1990

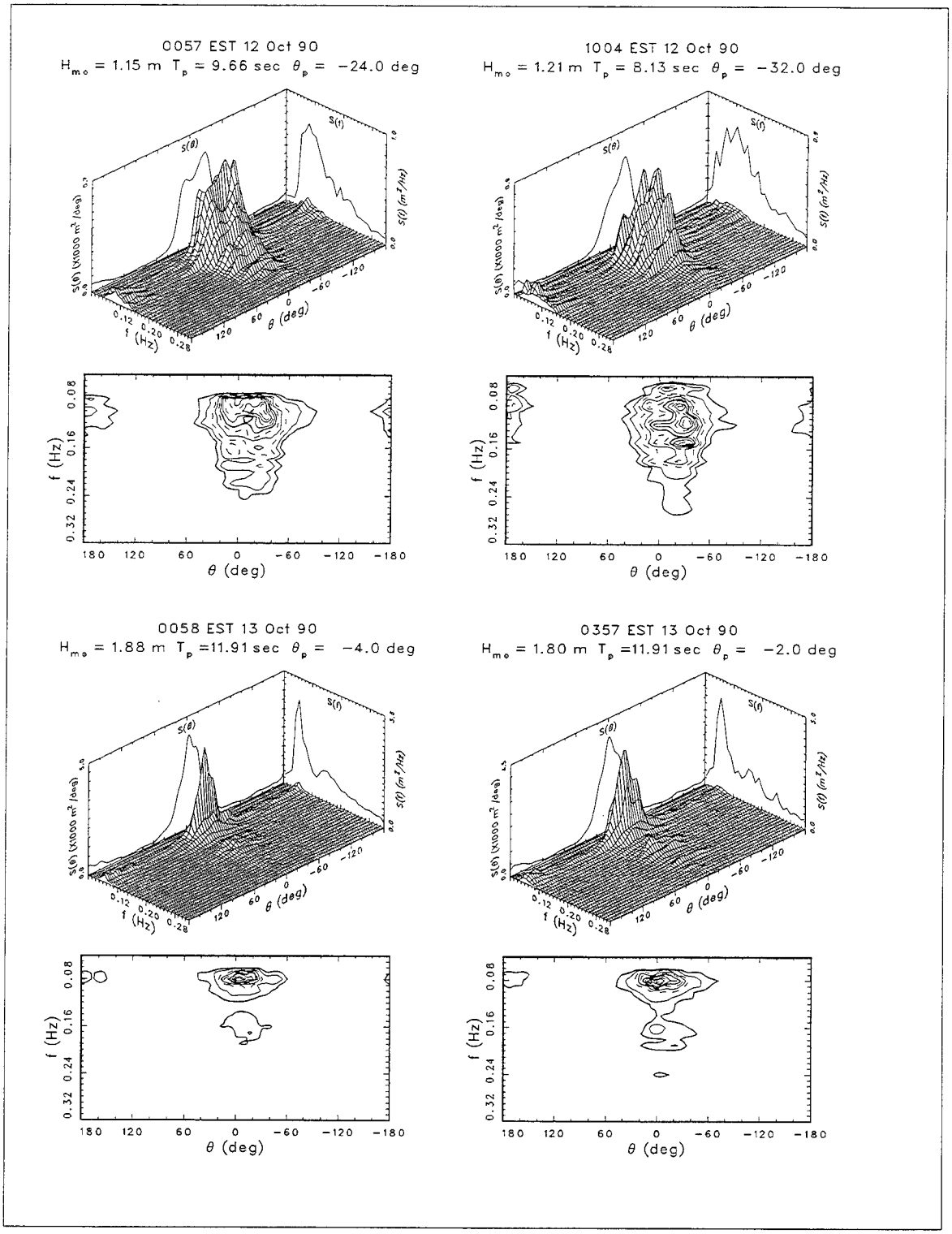

Figure E43. Representative frequency-direction spectra from crest subarray for 12 and 13 October 1990

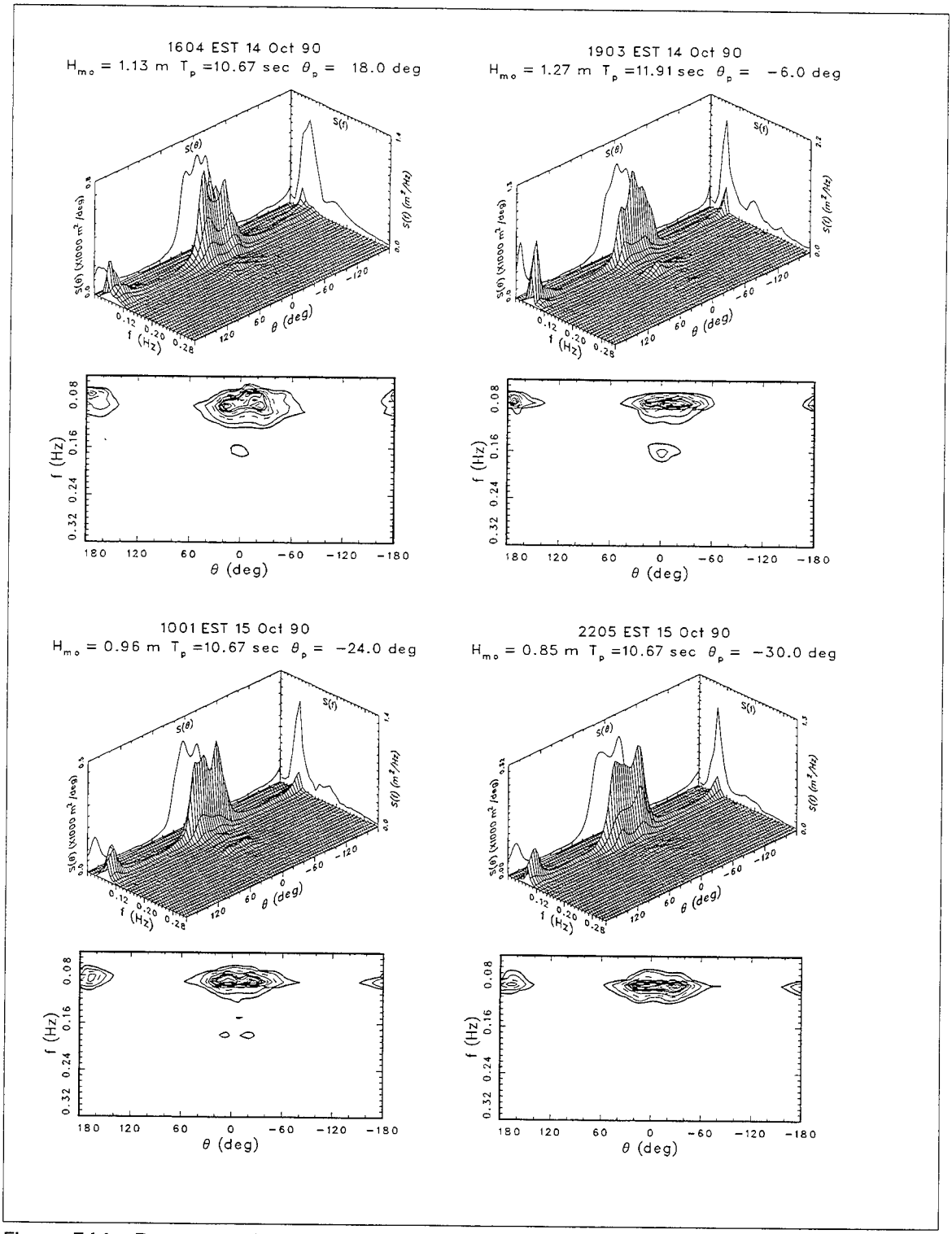

Figure E44. Representative frequency-direction spectra from crest subarray for 14 and 15 October 1990

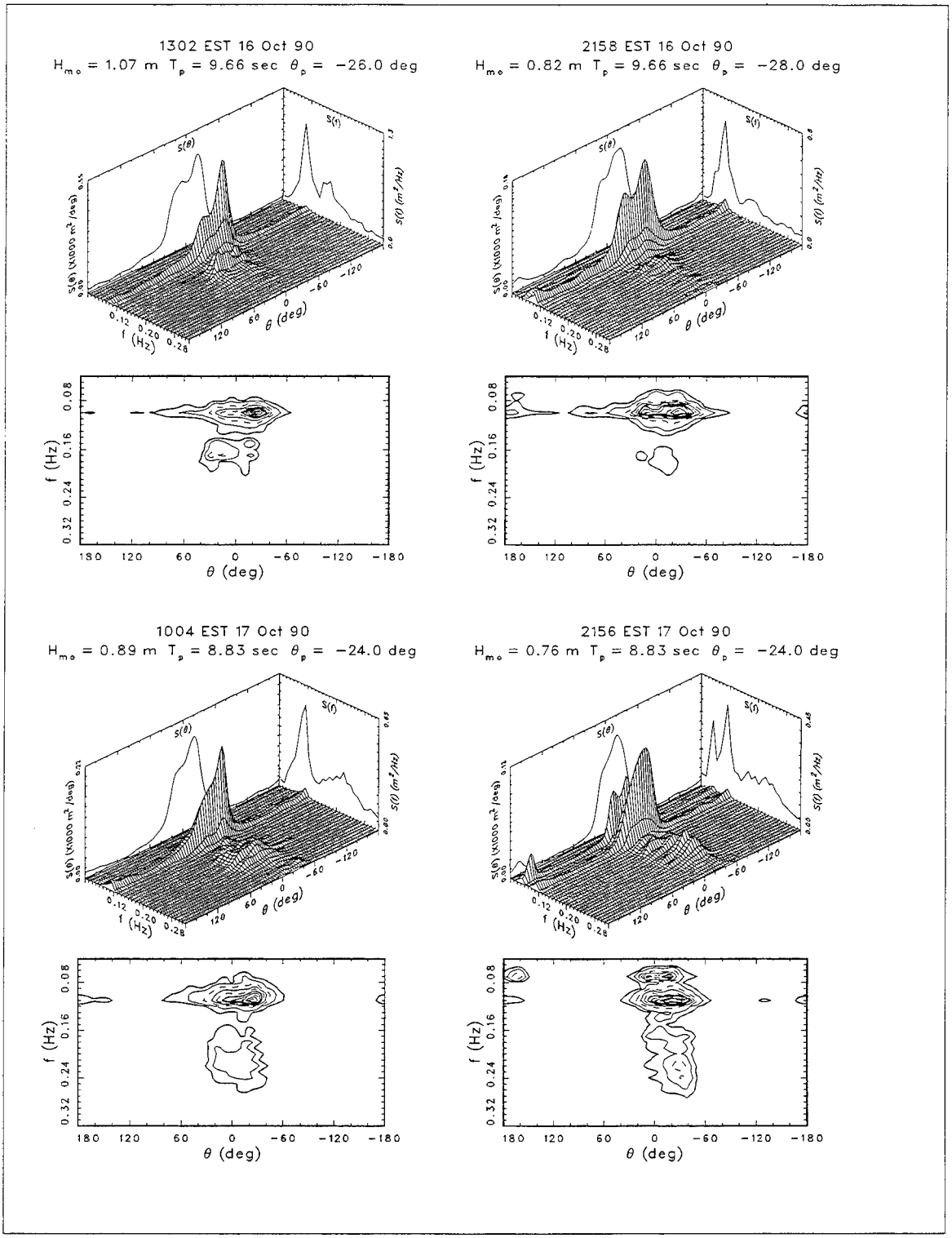

Figure E45. Representative frequency-direction spectra from crest subarray for 16 and 17 October, 1990

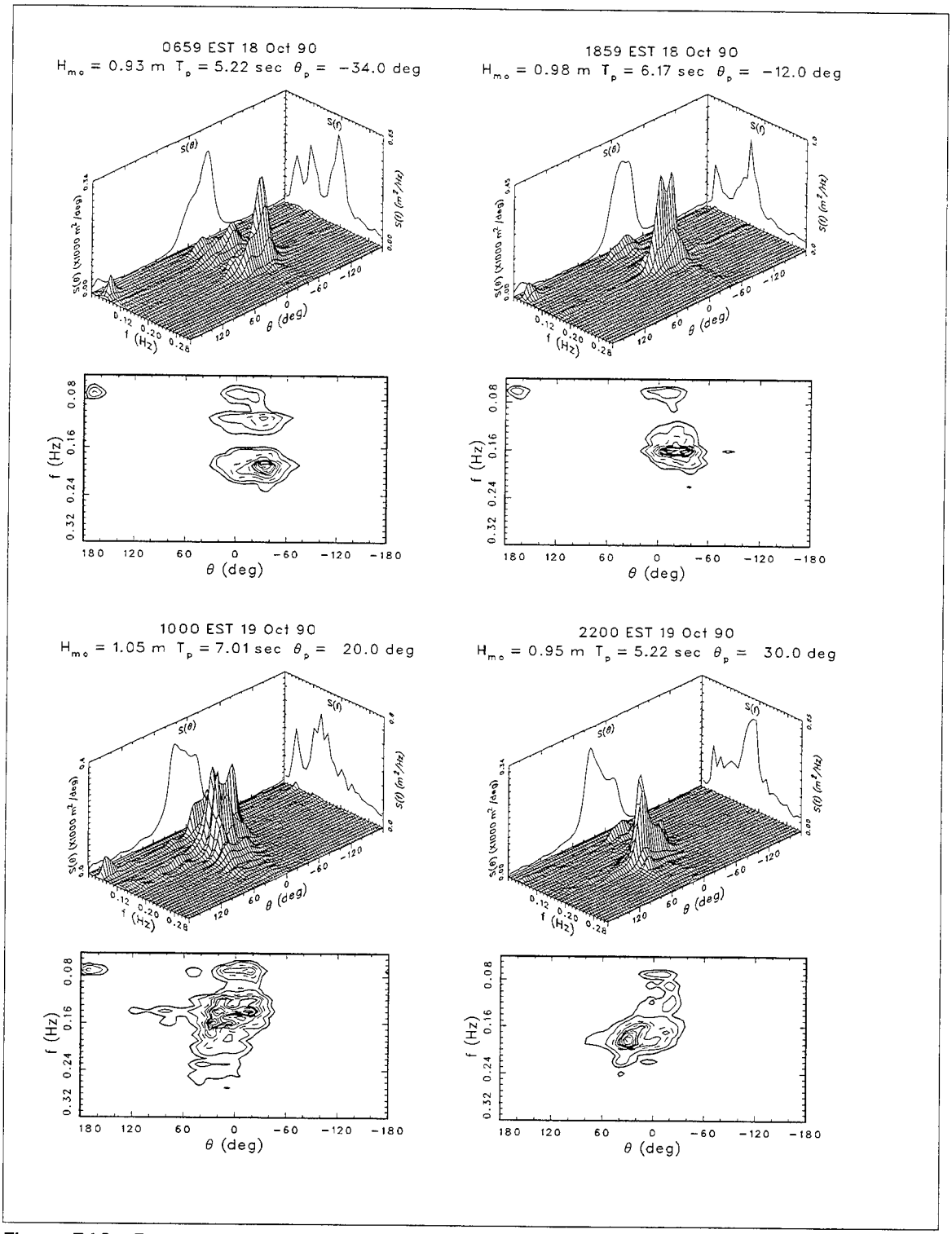

Figure E46. Representative frequency-direction spectra from crest subarray for 18 and 19 October 1990

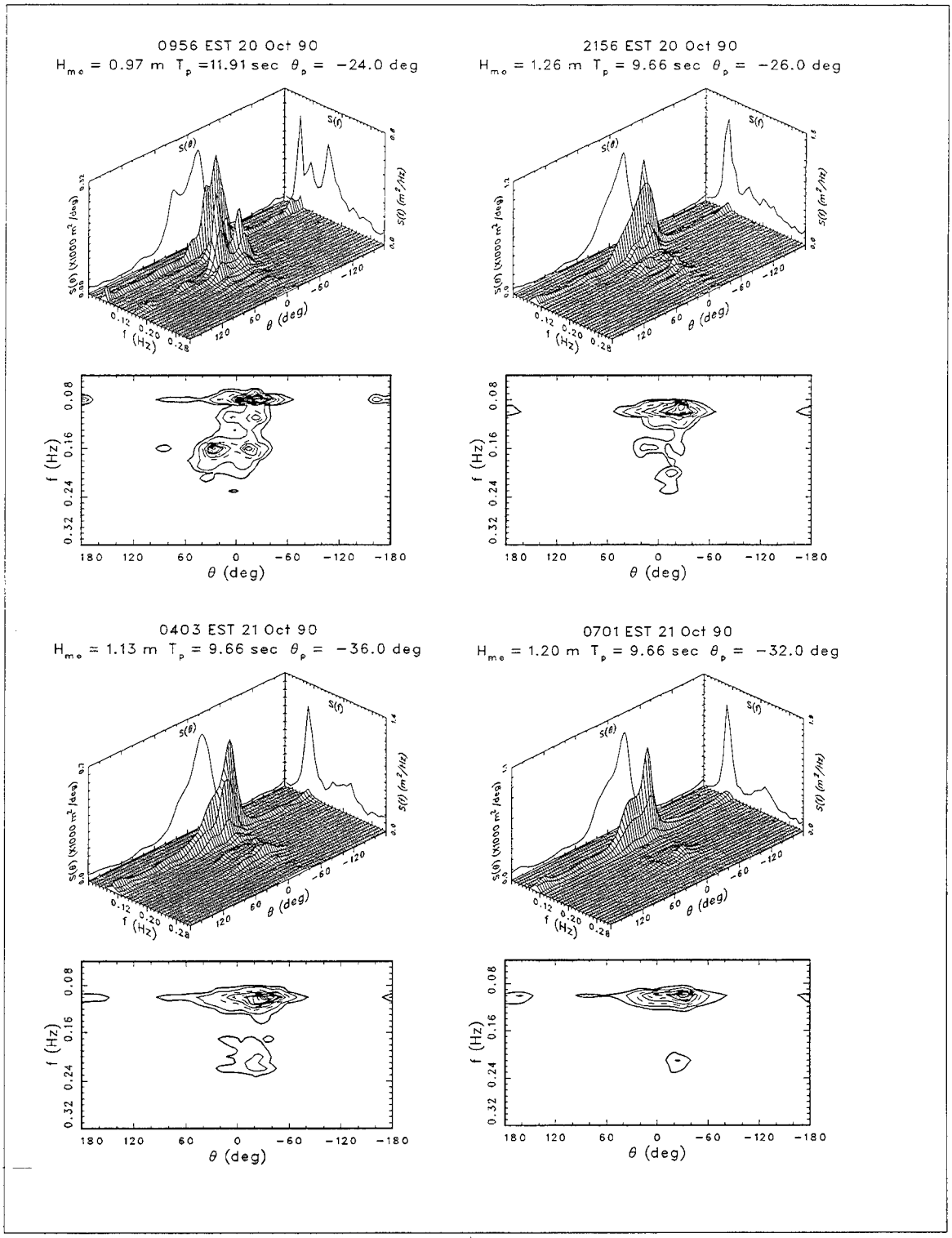

Figure E47. Representative frequency-direction spectra from crest subarray for 20 and 21 October 1990

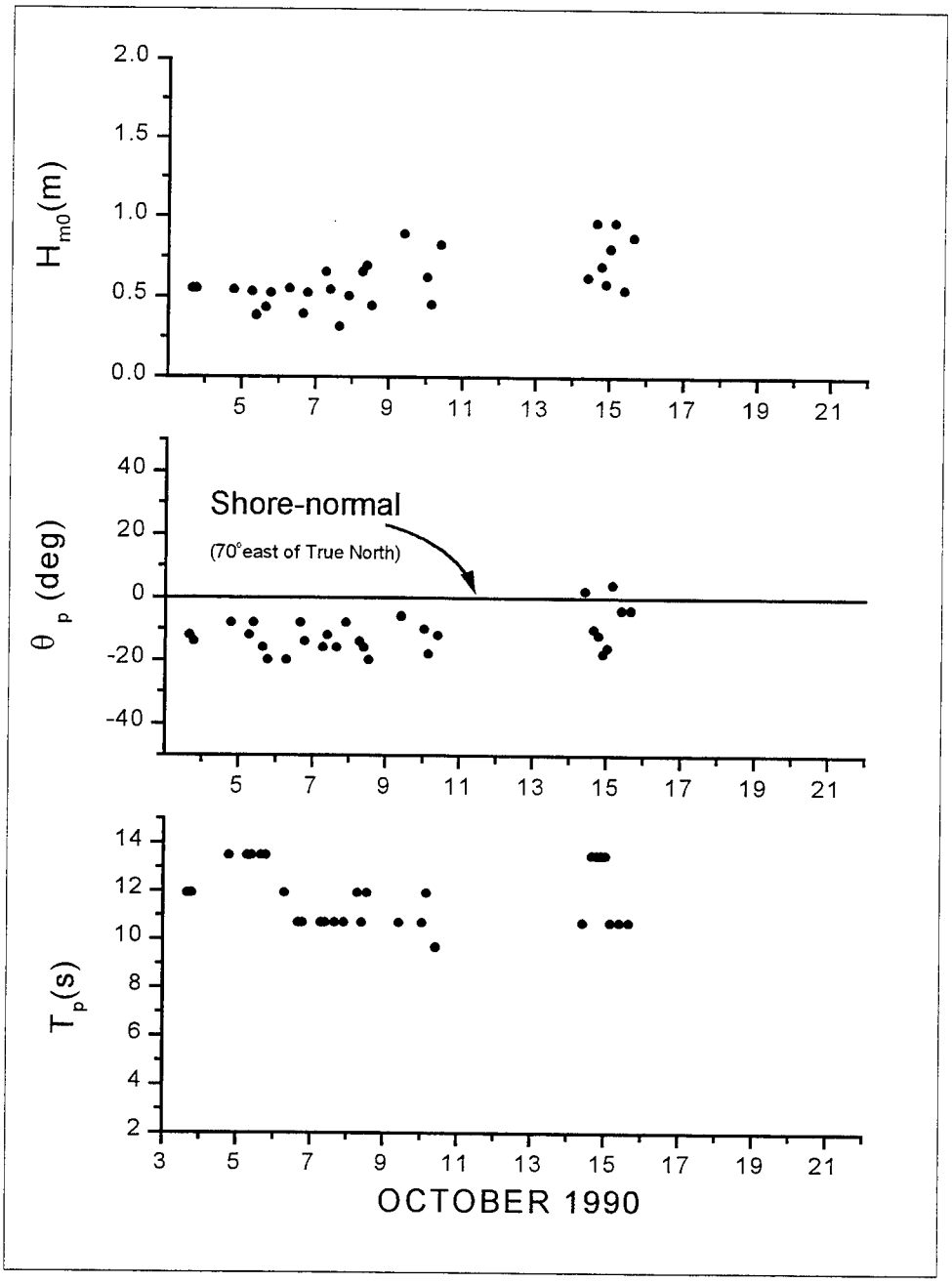

Figure E48. Wave height, direction, and period derived from frequency-direction spectra of trough subarray

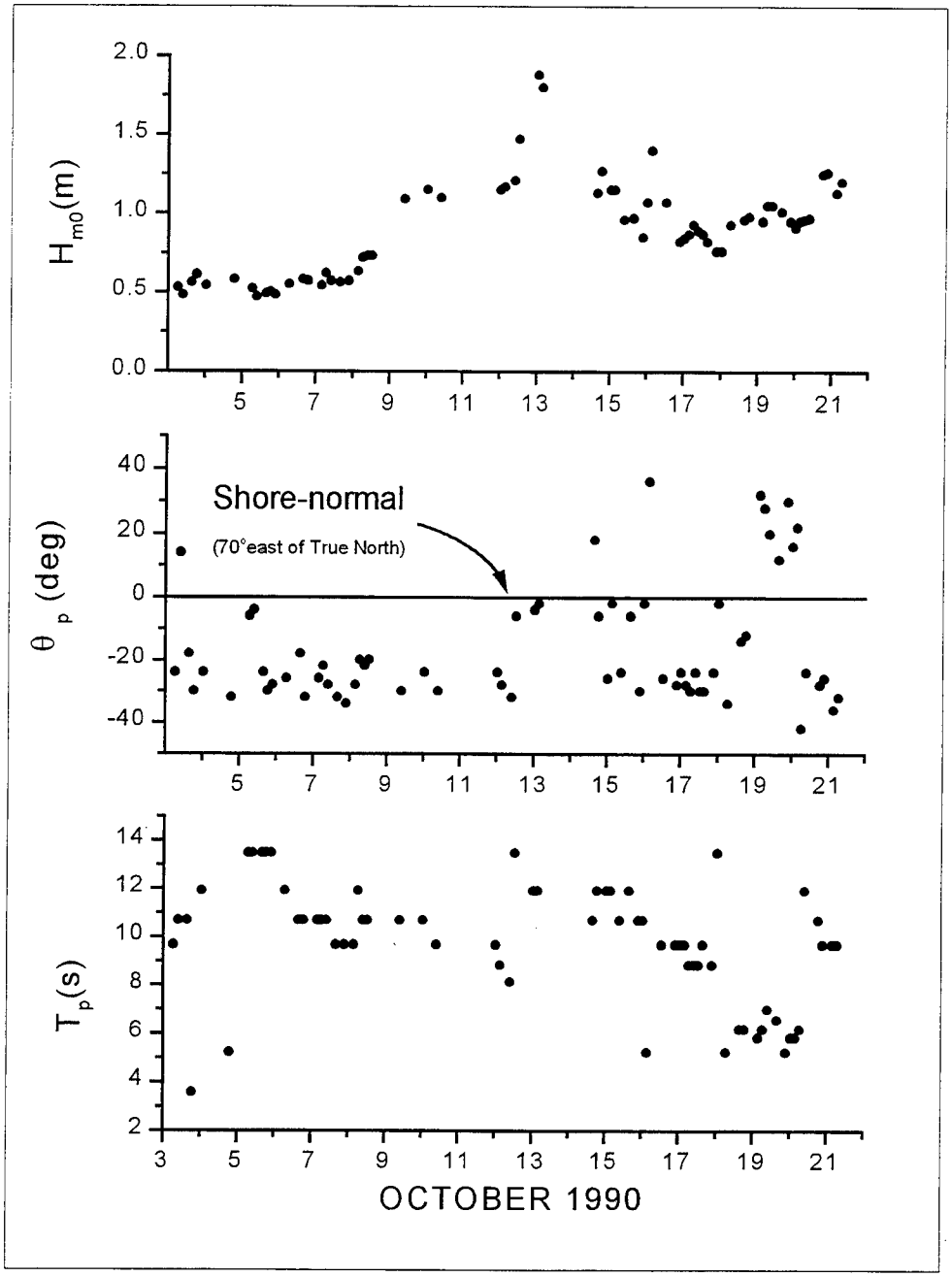

Figure E49. Wave height, direction, and period derived from frequency-direction spectra of crest subarray.

Appendix F
Instrumented Sled

The instrumented sled was equipped with a 0- to 25- psir (psi relative to one atmosphere) Senso-Metrics pressure gauge, a resistance wire wave gauge, and five current meters arranged vertically. The current meters were mounted at elevations 0.35, 0.60, 1.00, 1.35, and 1.75 m above the bed on a diagonally sloping beam (Figure 7 of the Introduction section). The beam was parallel to the shoreline, so the meters were aligned at approximately the same cross-shore coordinate. The meters were spread over an alongshore distance of approximately 3.5 m. The sled was deployed so that the lower end of the beam was in the up-drift direction of the longshore current to reduce flow interference, such that the current meters were up-drift of the beam. A common timing pulse was used for all current meters to reduce interference between instruments for this close proximity deployment. They were aligned to measure longshore and cross-shore components of the current when the sled was towed out normal to the shore. The sled was also instrumented with a digital compass for orientation measurement, and a Met One anemometer. The data were transmitted via radio modem to a personal computer located in a van on the FRF pier.

The sled was pulled offshore with the CRAB (Figure 8 of the Introduction section) and then incrementally retrieved, stopping at several cross-shore locations, with the FRF's forklift. The sled was towed offshore past the breaker zone to a depth of approximately 3 m, typically to a cross-shore coordinate of 245 m. The runs were along a line just north of the primary cross-shore array and the retrieval stops were made adjacent to an instrument in the array, with three to eight stops for each cross-shore transect. Locations of the sled and the start time for each run are given in Table F1. The position and orientation of the sled were recorded using an electronic total station which sighted two prisms located on the sled mast.

At each sled position, data were collected for 34 min (except for run #SL1910A which was only 8 minutes long due to low battery). The collection period of 34 min was selected to provide a balance between the time needed for stable statistics on each run and to maintain a short enough transect time to assume stationarity of the incident waves.

The DELILAH array gauges provide background data on the horizontal structure of the hydrodynamics and on the stationarity of the waves and currents. Sled measurements were made during the final six days of the DELILAH experiment, from 16 to 21 October. Incident waves during these days provided a variety of conditions with wave heights of 0.5 to 1.5 m, peak spectral periods of 5 to 15 sec, wind speeds of 5 to 15 m/s, and wave directions both north and south of shore-normal. The maximum time-averaged current velocities exceeded 0.5 m/sec during measurements with the sled.

Quality control checks during the experiment indicated that the middle current meter (elevation 1.0 m) had a large offset, relative to the pre-experiment calibration. Calibrations were performed in the field during three runs (SL1808A, SL1909A, and SL1916A) by rotating the current meters and comparing the measured data to a similar run without meter rotation.

In shallow depths one or more current meters were often out of the water. An estimate of when this occurred was done with the same procedure as described for the DELILAH array current meters in the DELILAH array data analysis section in Appendix E. A minimum water elevation for each wave trough was computed from the pressure gauge record, then the elevation of each current meter was checked to determine if it exceeded the lowest wave trough. A data quality flag was set in each time series header for current meters that were believed to be exposed. An additional quality check of the current meter gains was then done with the PUV-test procedure as described in Appendix E.

Table F1
Summary of DELILAH Sled Runs

Run#	Date	Time	FRF Coordinates			Dir	Comments
			Longshore, m	Cross-shore, m	Depth, m		
SL1610A	16OCT	10:27	1018	245	2.2	S	
SL1610B	16OCT	11:11	1016	226	1.2	S	
SL1610C	16OCT	11:50	1015	207	1.2	S	
SL1610D	16OCT	12:29	1013	185	1.7	S	
SL1610E	16OCT	13:08	1012	171	2.0	S	
SL1610F	16OCT	13:47	1011	145	1.7	S	
SL1610H	16OCT	15:06	1011	132	1.2	S	
SL1708A	17OCT	08:42	1021	208	2.0	S	
SL1710A	17OCT	10:04	1019	248	2.5	N	
SL1710B	17OCT	10:46	1020	233	1.4	N	
SL1710C	17OCT	11:25	1021	214	1.4	N	
SL1710D	17OCT	12:05	1020	195	1.6	N	
SL1710E	17OCT	12:44	1021	175	2.0	N	
SL1710F	17OCT	13:23	1021	149	1.6	N	
SL1714A	17OCT	14:21	1021	214	1.6	N	
SL1714B	17OCT	15:03	1022	194	1.9	N	
SL1714C	17OCT	15:42	1022	176	2.4	N	
SL1714D	17OCT	16:23	1022	152	2.5	N	
SL1808A	18OCT	08:37	1014	244	2.9	N	Meters rotated 180° for cal.
SL1810A	18OCT	10:55	1019	241	2.1	N	
SL1810B	18OCT	11:38	1017	224	1.2	N	
SL1810C	18OCT	12:19	1016	206	1.1	N	
SL1810D	18OCT	13:00	1017	189	1.4	N	
SL1810E	18OCT	13:41	1017	170	1.7	N	
SL1810F	18OCT	14:22	1019	145	1.5	N	
SL1815A	18OCT	15:20	1019	209	1.1	N	
SL1815B	18OCT	16:00	1019	189	3.5	N	
SL1815C	18OCT	16:40	1019	169	1.9	N	
SL1909A	19OCT	09:29	1014	145	1.3	S	Meters rotated 180° for cal.
SL1910A	19OCT	10:32	1010	145	0.8	S	battery low, 8-min run
SL1912A	19OCT	12:33	1012	244	2.3	S	
SL1912B	19OCT	13:18	1013	226	1.4	S	
SL1912C	19OCT	13:58	1014	208	1.4	S	
SL1912D	19OCT	14:38	1013	189	1.9	S	
SL1912E	19OCT	15:19	1013	165	2.2	S	
SL1912F	19OCT	15:58	1014	144	2.1	S	
SL1916A	19OCT	16:53	1012	146	2.3	S	Meters rotated 180° for cal. (except 0.6 m)
SL2011A	20OCT	11:09	1008	243	2.7	S	
SL2011B	20OCT	11:48	1009	226	1.7	S	
SL2011C	20OCT	12:29	1010	208	1.3	S	
SL2011D	20OCT	13:08	1010	189	1.7	S	
SL2011E	20OCT	13:48	1011	170	1.9	S	
SL2011F	20OCT	14:29	1012	145	2.0	S	
SL2011G	20OCT	15:08	1014	131	1.2	S	
SL2011H	20OCT	15:45	1014	131	1.3	S	
SL2109A	21OCT	08:55	1018	246	3.0	S	
SL2109B	21OCT	09:37	1016	226	2.7	S	
SL2109C	21OCT	10:18	1016	207	2.4	S	
SL2109D	21OCT	11:00	1016	189	2.5	S	
SL2109E	21OCT	11:39	1015	170	2.5	S	

Dir: S - sled oriented for currents flowing South
N - sled oriented for currents flowing North

Current meter elevations above bottom: 1.75 m, 1.35 m, 1.0 m, 0.6 m, 0.35 m

Appendix G
Participant Addresses & Publications

This appendix includes lists of the DELILAH investigators and of completed publications as of the date of publication.

Participant Addresses

Mr. William A. Birkemeier
USACE Waterways Experiment Station
Field Research Facility
1261 Duck Rd.
Kitty Hawk, NC 27949

Phone: 919-261-3511
Fax: 919-261-4432
Internet: w.birkemeier@cerc.wes.army.mil

Dr. Steve Elgar
Department of Electrical Engineering
and Computer Science
Washington State University
Pullman, WA 99164-2752

Phone: 509-335-6602
Fax: 509-335-3818
Internet: elgar@eecs.wsu.edu

Dr. Robert Guza
Center for Coastal Studies
Scripps Institution of Oceanography
University of California, San Diego
La Jolla, CA 92093-0209

Phone: 619-534-0585
Fax: 619-534-0300
Internet: rtg@coast.ucsd.edu

Mr. Kent K. Hathaway
USACE Waterways Experiment Station
Field Research Facility
1261 Duck Rd.
Kitty Hawk, NC 27949

Phone: 919-261-3511
Fax: 919-261-4432
Internet: k.hathaway@cerc.wes.army.mil

Dr. Thomas H. Herbers
Department of Oceanography,
Code OC/He
Naval Postgraduate School
Monterey, CA 93943-5100

Phone: 408-656-2917
Fax: 408-656-2712
Internet: herbers@oc.nps.navy.mil

Dr. Todd Holland
Naval Research Laboratory, Code 7442
Stennis Space Center, MS 39529

Phone: 601-688-5320
Fax: 601-688-4476
Internet: tholland@nrlssc.navy.mil

Dr. Rob A. Holman
College of Oceanography
Oregon State University
Oceanography Admin Bldg 104
Corvallis, OR 97331-5503

Phone: 503-737-2914
Fax: 503-737-2064
Internet: holman@oce.orst.edu

Dr. Peter Howd
Duke Marine Laboratory
111 Pivers Island Rd.
Beaufort, NC 28516

Phone: 919-504-7629
Fax: 919-504-7648
Internet: peter@metolius.ml.duke.edu

Dr. Nicholas Kraus
USACE Waterways Experiment Station
Attn: CEWES-CV-M
3909 Halls Ferry Rd.
Vicksburg, MS 39180-6199

Phone: 601-634-2016
Fax: 601-634-4253
Internet: n.kraus@cerc.wes.army.mil

Dr. Tom C. Lippmann
Center for Coastal Studies
Scripps Institution of Oceanography
University of California San Diego
La Jolla, CA 92093-0209

Phone: 619-822-0605
Fax: 619-534-0300
Internet: lippmann@coast.ucsd.edu

Dr. Joan Oltman-Shay
Northwest Research Associates
300 120th Av NE
Bldg 7, Suite 770
Bellevue, WA 98005

Phone: 206-453-8141 X 314
Fax: 206-646-9123
Internet: shay@ocean.washington.edu

Dr. Jane Smith
USACE Waterways Experiment Station
Attn: CEWES-CR-P
3909 Halls Ferry Rd.
Vicksburg, MS 39180-6199

Phone: 601-634-2079
Fax: 601-634-4314
Internet: jm.smith@cerc.wes.army.mil

Dr. Edward B. Thornton
Dept. of Oceanography
Naval Postgraduate School
Monterey, CA 93943-5100

Phone: 408-656-2847
Fax: 408-656-2712
Internet: thornton@oc.nps.navy.mil

Dr. Dennis Trizna
Radar Propagation & Scattering
Naval Research Laboratory
Code 5303
4555 Overlook Ave SW
Washington, DC 20375-5320

Phone: 202-404-7891
Fax: 202-404-3303
Internet: triznad@ccf.nrl.navy.mil

Publications

This listing of DELILAH and water-wave-related SAMSON publications was current as of May 1997. It is arranged by primary authorship. Interested readers may want to consult more up-to-date publication lists.

Birkemeier, W. A., Long, C. E., and Hathaway, K. K. (1997). "DELILAH, DUCK94 and SandyDuck: Three nearshore experiments." *Proceedings, 25th International Conference on Coastal Engineering,* American Society of Civil Engineers.

Bryan, K. R., and Bowen, A. J. "Bar-trapped edge waves and longshore currents," in review, *Journal of Geophysical Research.*

Bryan, K. R., Howd, P. A., and Bowen, A. J. "Field observations of bar-trapped edge waves," in review, *Journal of Geophysical Research.*

Chandran, V., Elgar, S., and Vanhoff, B. (1994). "Statistics of tricoherence," *IEEE Signal Processing* 42, 3430-3440.

Church, J. C., Thornton, E. B., and Oltman-Shay, J. (1992). "Mixing by shear instabilities of the longshore current, *Proceedings of the 23rd International Conference on Coastal Engineering*, American Society of Civil Engineers, 2999-3011.

Church, J. C. and Thornton, E. B. (1992). "Bottom stress modification by breaking waves within a longshore current model," *Proceedings of the 23rd International Conference on Coastal Engineering*, American Society of Civil Engineers, 3012-3025.

Church, J. C. and Thornton, E. B. (1993). "Effects of breaking wave induced turbulence within a longshore current model," *Coastal Engineering* 20, 1-28.

Church, J. C., Thornton, E. B. and Oltman-Shay, J. (1994). "Effects of shear instabilities on longshore current profiles," *Proceedings Coastal Dynamics '94.* American Society of Civil Engineers, 376-390.

Dodd, N. (1994). "On the destabilization of a longshore current on a plane beach: Bottom shear stress, critical conditions, and onset of instability," *Journal of Geophysical Research* 99 (C1), 811-824.

Elgar, S., Herbers, T.H.C., and Guza, R.T. (1994). "Reflection of ocean surface gravity waves from a natural beach," *Journal of Physical Oceanography* 24, 1503-1511.

Elgar, S., Herbers, T. H. C., Chandran, V., and Guza, R. T. (1995). "Observations of nonlinear ocean surface gravity waves," *Journal of Geophysical Research* 100, 4977-4983.

Elgar, S., Herbers, T. H. C., Chandran, V., and Guza, R. T. (1995). "Higher-order spectral analysis of nonlinear ocean surface gravity waves," *Journal of Geophysical Research* 100 (C3), 4977-4983.

Elgar, S., Herbers, T. H. C., Okihiro, M., Oltman-Shay, J., and Guza, R. T. (1992). "Observations of infragravity waves," *Journal of Geophysical Research* 97 (C10), 15,573-15,577.

Falaques, A., and Iranzo, V. (1994). "Numerical simulation of vorticity waves in the nearshore," *Journal of Geophysical Research* 99 (C1), 825-841.

Faria, A.F., (1995). "Quasi-3D Nearshore Circulation Model," M.S. Thesis, Naval Postgraduate School, Monterey, CA

Faria, A.F., E.B. Thornton and Stanton, T.P. (1995) A "A quasi-3D model of longshore currents," *Proceedings Coastal Dynamics '95*. American Society of Civil Engineers 389-400.

Gallagher, E., Boyd, B., Elgar, S., Guza, R. T., and Woodward, B. T. (1996). "Performance of a sonar altimeter in the nearshore," *Marine Geology* 133 (3-4), 241.

Herbers, T. H. C., and Guza, R. T. (1994). "Nonlinear wave interactions and high-frequency seafloor pressure," *Journal of Geophysical Research* 99 (C5), 10,035-10,048.

Herbers, T. H. C., Elgar, S., and Guza, R. T. (1994). "Infragravity-frequency (0.005-0.05 Hz) motions on the shelf; Part I: Local nonlinear forcing by surface waves," *Journal of Physical Oceanography* 24, 917-927.

_____(1995). "Generation and propagation of surf beat," *Journal of Geophysical Research* 100 (C12), 24,863-24,872.

Herbers, T. H. C., Elgar, S., Guza, R. T, and O'Reilly, W. C. (1995). "Infragravity-frequency (0.005-0.05 Hz) motions on the shelf; Part II: Free waves," *Journal of Physical Oceanography* 25, 1063-1079.

Holland, K. T., and Holman, R. A. (1993). "The statistical distribution of swash maxima on natural beaches," *Journal of Geophysical Research* 98 (C6), 10271-10278.

Holland, K. T., Valentine, C., and Holman, R. A. "Wavenumber-frequency structure of infragravity swash motions," in review, *Journal of Geophysical Research.*

Holman, R. A., and Sallenger, A. H. Jr. (1993). "Sand bar generation: A discussion of the Duck experiment series," *Journal of Coastal Research* SI(15), 76-92.

Howd, P. A., Bowen, A. J., and Holman, R. A. (1992a). "Edge waves in the presence of strong longshore currents," *Journal of Geophysical Research* 97 (C7), 11357-11371.

_____ (1992b). "Edge waves in the presence of strong longshore currents," *Journal of Geophysical Research* 97 (C7), 11,357-11,371.

Howd, P. A., Oltman-Shay, J., and Holman, R. A. (1991). "Wave variance partitioning in the trough of a barred beach," *Journal of Geophysical Research* 96 (C7), 12781-12795.

Larson, M. (1995). "Model for decay of random waves in surf zone," *Journal of Waterway, Port, Coastal, and Water Engineering,* American Society of Civil Engineers 121 (1), 1-12.

Lippmann, T. C., and Holman, R. A. (1991). " Phase speed and angle of breaking waves measured with video techniques", *Coastal Sediments '91*, 542-556, 1991

Lippmann, T. C., and Holman, R. A. (1993). "Wave group modulations in cross-shore breaking patterns," Proc. 23rd *International Conference on Coastal Engineering*, American Society of Civil Engineers, 918-931.

Lippmann, T. C. and Thornton, E. B. (1995) "Wave stress and longshore currents on barred profiles," *Proceedings Coastal Dynamics 95*. American Society of Civil Engineers

Lippmann, T. C., Thornton, E. B. and Reniers, A. J. H. M.(1995) "Wave stress and longshore current on barred profiles," *Proceedings Coastal Dynamics '95*. American Society of Civil Engineers, 401-412.

Lippmann, T. C., Brookins, A. H., and Thornton, E. B. (1996) "Wave energy transformation on natural profiles" *Coastal Engineering*, (27):1-20

Lippmann, T. C., Herbers, T. H. C. and Thornton, E. B. "Gravity and shear wave contributions to nearshore infragravity motions", in review, *Journal of Physical Oceanography*.

Lippmann, T. C., Herbers, T. H. C. and Thornton, E. B. "The cross-shore variation of infragravity wave pressure and velocities in shallow water", in press, *Proceedings Coastal Dynamics '97*, American Society of Civil Engineers.

Lippmann, T. C., Jorgensen, C. F. and Thornton, E. B. "Wave slopes and breaking distributions in the surf zone", in review,

Lippmann, T. C. and Thornton, E. B. "The spatial distribution of wave rollers and turbulent kinetic energy on a barred beach," in review, *Journal of Geophysical Research*

Lippmann, T. C., and Thornton, E. B. "The spatial distribution of wave breaking on a barred beach", in review, *Journal of Geophysical Research*

Lippmann, T., Thornton, E.B., and Brookins, H. "Breaking wave transformation using a roller model," in press, *Journal of Coastal Engineering*

Liu, Z., Elgar, S., and Guza, R. T. (1993). "Groups of ocean waves: comparisons between linear theory, approximations to linear theory, and observations," *ASCE Journal of Waterway, Port, Coastal, and Ocean Engineering* 119, 144-159.

Nye, T., and Yamamoto, T. (1994). "Concurrent measurements of the directional spectra of microseismic energy and surface gravity waves," *Journal of Geophysical Research* 99 (C7), 14,321-14,338.

Okihiro, M., and Guza, R. T. (1995). "Infragravity energy modulation by tides," *Journal of Geophysical Research* 100 (C8), 16,143-16,148.

Reniers, A. J. H. M., E. B. Thornton, and Lippmann, T. C. "Effects of alongshore non-uniformity's on longshore currents measured in the field," in review, *Journal of Geophysical Research.*

Reniers, A. J. H. M., E. B. Thornton, and Lippmann, T. C. (1995). Longshore currents over barred beaches, *Proceedings Coastal Dynamics 95.* American Society of Civil Engineers, New York, 413-424.

Scott, K. A., Thornton, E. B., and Birkemeier, W. A. (1991). "Mean currents and sediment transport at DELILAH," *Proceedings of Coastal Sediments 1991*, American Society of Civil Engineers, 477-488.

Smith, J. M., Larson, M., and Kraus, N. C. (1993). "Longshore current on a barred beach: Field measurements and calculation," *Journal of Geophysical Research* 98 (C12), 22,717-22,731.

Smith, J. M., Svendsen, I. A., and Putrevu, U. (1992). "Vertical structure of the nearshore current at DELILAH: Measured and modeled," *Proceedings of the 23rd International Conference on Coastal Engineering*, American Society of Civil Engineers, 2825-2838.

Thornton, E.B., and Lippman, T. (1994). "Longshore currents measured in the field" *Proceedings Coastal Dynamics '94*. American Society of Civil Engineers, 414-426

Thornton, E. B., Humiston, R. T., and Birkemeier, W. A. (1996). "Bar/trough generation on a natural beach," *Journal of Geophysical Research* 101 (C5), 12,097-12,110.

Thornton, E.B. and Kim, C.S., (1993). "Tidal modulation of wave heights and longshore currents inside the surf zone" *Journal of Geophysical Research* 98(C9)16,509-16,519

Wallerstein, G., and Elgar, S. (1992). "Shockwaves in stellar atmospheres and breaking waves on an ocean beach," *Science* 256, 1531-1536.

REPORT DOCUMENTATION PAGE

Form Approved
OMB No. 0704-0188

1. AGENCY USE ONLY *(Leave blank)*	2. REPORT DATE	3. REPORT TYPE AND DATES COVERED
	September 1997	Final report

4. TITLE AND SUBTITLE
1990 DELILAH Nearshore Experiment: Summary Report

5. FUNDING NUMBERS

6. AUTHOR(S)
William A. Birkemeier, Cinde Donoghue, Charles E. Long,
Kent K. Hathaway, Clifford F. Baron

7. PERFORMING ORGANIZATION NAME(S) AND ADDRESS(ES)
U.S. Army Engineer Waterways Experiment Station
3909 Halls Ferry Road, Vicksburg, MS 39180-6199

8. PERFORMING ORGANIZATION REPORT NUMBER
Technical Report CHL-97-24

9. SPONSORING/MONITORING AGENCY NAME(S) AND ADDRESS(ES)
U.S. Army Corps of Engineers
Washington, DC 20314-1000

10. SPONSORING/MONITORING AGENCY REPORT NUMBER

11. SUPPLEMENTARY NOTES
Available from National Technical Information Service, 5285 Port Royal Road, Springfield, VA 22161.

12a. DISTRIBUTION/AVAILABILITY STATEMENT
Approved for public release; distribution is unlimited.

12b. DISTRIBUTION CODE

13. ABSTRACT ***(Maximum 200 words)***

This report summarizes the primary data sets collected during the DELILAH nearshore experiment held in October 1990 at the Field Research Facility, Coastal and Hydraulics Laboratory, U.S. Army Engineer Waterways Experiment Station. DELILAH was designed to investigate the physics of the nearshore zone using a large array of stationary and mobile instruments, video cameras, radar systems, and precision surveys. This report was prepared to document and publicize the DELILAH data set. It complements a growing series of technical papers, reports, theses, dissertations, and other results based on DELILAH data. These data are available electronically on-line or via other media such as CD-ROM.

14. SUBJECT TERMS
Coastal research
DELILAH
Directional wave data
Nearshore currents
Nearshore zone

15. NUMBER OF PAGES
213

16. PRICE CODE

17. SECURITY CLASSIFICATION OF REPORT	18. SECURITY CLASSIFICATION OF THIS PAGE	19. SECURITY CLASSIFICATION OF ABSTRACT	20. LIMITATION OF ABSTRACT
UNCLASSIFIED	UNCLASSIFIED		